FINAL REPORT

Fundamental study on quantum nanojets

H.H. Chiu
Space Science and Technology Center
Institute of Aeronautics and Astronautics
National Cheng-Kung University
Tainan, Taiwan 70101

Project title: Fundamental study on quantum nanojets
Project number: AOARD-03-4039
Date: August 14 2003 ~ August 13 2004

Executive Summary

The objectives of the project were to develop basic quantum scientific foundation and technical know-how required for major breakthroughs and innovations in “nanojet technology, which will contribute to the technology developments and the preservation of a superior leadership of US Airforce in frontier quantum nanojet technologies.

Nanojets are the matter jets of nanosize, which serve as a unique method of transporting particles, emitted from a single or multiple jet nozzle of nanometer size to a target site at a designed flow rate, with design particle density and energy. The controlled transport and manipulation of the streams of particles offer potential applications in atom-molecular assembling, nanofabrication, single electron transistor, atom optics, atom lithography, atomic interferometer, drug delivery in biomedical application, nano-propulsion and energy sensors.

Nanojets are classified into two major categories depending on three primary factors: characteristic dimensions of the jets, the particle density and injection energy. In general, nanojets of the liquids of high molecules weight, operating at high injection energy exhibit classical jet like behavior which are predicted by molecular dynamics or classical Navier-Stokes type equation with analytical formulation based on lubrication theory, see for example, Moseler and Landman and Eggers. However, the jets of electrons or particles with sufficiently low atomic weights operating at low injection energy will exhibit quantum wave behavior, which are markedly different from the conventional liquid jets. Hence the classical models cease to apply. It is worthy of mention that in prior to the present study there had been little or no in-depth investigations of the nanojets, which operate in the region where the quantum effects play the dominant dynamic roles. Thus it was assessed that the key to the successful development of nanojet technology is to establish the fundamental knowledge of the quantum mechanical structures, dynamics and energetic of the nanojets operating in the ranges of interest in special classes of particle nanojets applications.

In order to achieve the goal of quantum nanojet technology described above, we developed a

Report Documentation Page

Form Approved
OMB No. 0704-0188

1. REPORT DATE	2. REPORT TYPE	3. DATES COVERED
02 FEB 2006		

4. TITLE AND SUBTITLE	5a. CONTRACT NUMBER
Fundamental study on quantum nanojets? structures, dynamics and energetic	**F6256203P0460**
	5b. GRANT NUMBER
	5c. PROGRAM ELEMENT NUMBER
6. AUTHOR(S)	5d. PROJECT NUMBER
Huei-huang Chiu	5e. TASK NUMBER
	5f. WORK UNIT NUMBER
7. PERFORMING ORGANIZATION NAME(S) AND ADDRESS(ES)	8. PERFORMING ORGANIZATION REPORT NUMBER
National Cheng Kung University,1, University Road,Tainan 701,Taiwan,TW,701	**AOARD-034039**
9. SPONSORING/MONITORING AGENCY NAME(S) AND ADDRESS(ES)	10. SPONSOR/MONITOR'S ACRONYM(S)
	11. SPONSOR/MONITOR'S REPORT NUMBER(S)

12. DISTRIBUTION/AVAILABILITY STATEMENT

Approved for public release; distribution unlimited.

13. SUPPLEMENTARY NOTES

14. ABSTRACT

The contractor shall investigate quantum fluid mechanics. Technical work plan Analytical formulations and exact solutions of planar and axi-symmetric nanojets of Schrodinger?s fluid in QM formalism. (QM-QDFD equivalence) Numerical simulation of planar and axi-symmetric nanojets of Schrodinger?s fluid in QDFD formalism. (QDFD-QM equivalence) Analytical formulations of planar and cylindrical shaped nanojets injector in QDFD formalism. Conservation equations of QDFD Canonical theoretic formulation of the axiomatic solutions of nanojet flows in an injector of planar and cylindrical configurations. Two types of axiomatic representations, dilatation based and diffusion kinetic energy based will be carried out to facilitate the prediction of nano-jet flows in injectors. Overall flow structures of nanojets will examine the overall nanojet flow configuration to assess the following characteristics: Exterior flow characteristics and their dependence on the injection conditions, Interior flow characteristics and their effects on the exterior jet configuration, Collective quantum behaviors on the spreading of the jets, particle separation, local flow rates, and jet penetration.

15. SUBJECT TERMS

16. SECURITY CLASSIFICATION OF:			17. LIMITATION OF ABSTRACT	18. NUMBER OF PAGES	19a. NAME OF RESPONSIBLE PERSON
a. REPORT	b. ABSTRACT	c. THIS PAGE			
unclassified	**unclassified**	**unclassified**		**172**	

fundamental analytical and numerical simulation research program focused on the jet fluid dynamics based on two *quantum mechanical* perspectives; Schrödinger's wave mechanics and quantum fluid dynamics based on Hamilton-Jacoby formalism. Each of the formalisms offers unique ontological and methodological advantages, which provided valuable complementary knowledge for the understanding of the structures, dynamics and energetic of quantum nanojets.

We accomplished the comprehensive research project in the following three major categories:

I. Quantum Theory of Nanojets:

Mathematical formulation, analytical solution methods and numerical simulations by modern computational schemes for Schrödinger's equation and quantum fluid dynamics, are developed. Principles of quantum mechanical equivalence between two formalisms are established.

.

1) Inverse Problems,

a). Schrödinger's wave mechanics are used to construct the analytical solution of wave fields from which the nanojet flow field structures are predicted.

References 2, 3, 4, 5, 6, 7, 8

b) Two-slit jet flow field structures are calculated in a broad jet operating range of *"quantum Reynolds number"*, defined by the ratio of the inertia force to the quantum force. This is the key parameter that affects the jet behaviors and structures quantum behavior, structures, dynamics and energetic.

References 2, 3, 4, 5, 6, 7, 8

c) Multi-slit electron jets, formed by periodically arranged array of nanojets nozzles, are analyzed in broad operating range of quantum Reynolds number.

References 8

2). Direct Problems

a). Quantum fluid dynamics formalism based on Hamilton-Jacoby equation are adapted for the numerical simulation and analysis of nanojet flow fields.

Reference, 6.

b) Quantum computational fluid dynamics numerical codes are developed for flow field calculation.

Reference, 6.

c) Two-slit jet flow field structures are calculated for a wide jet operating ranges of

quantum Reynolds number.

Reference, 6.

3). Quantum mechanical Equivalence:

Theory of quamlet, see nomenclature, is developed to examine the equivalence between the linear quantum wave field, described by Schrödinger's equation and the non-linear quantum flow field predicted by quantum fluid dynamics formalism.

Reference 3

II. Quantum Nanojet's Structures, Dynamics and Energetrics

The spatial distributions of density, velocity, quantum potentials of steady state nanojets are predicted in the broad range of quantum Reynolds number to examine the jets configurations, structural, dynamic and energetic behavior. Quantum *bubbling, branching* and *clustering,* see Glossary, are explained by wave propagation and axial tunneling. Interference and tunneling and their physical reasons are clarified.

1). Sensitivity Analysis

a) Sensitivity of two- and multi-slit nanojet structures on the quantum Reynolds number is assessed. Quantum wave interference is caused by multi-branch interaction, whereas the tunneling is due to the axial decay in the probability density when the kinetic energy associated with particle motion in transverse direction exceeds inlet particle energy.

References 2, 4, 5, 6, 7, 8

b) Quantum nanojets are classified into bubble jets, multi-branch jets and quasi-classical jets.

References 2, 4, 5, 6, 7

c).Key nanojet dynamic properties: jet kinetic energy and quantum potential and their dependence on quantum Reynolds number are examined. The exchange of the quantum potential energy and mean kinetic energy holds a key to the local jet acceleration and deceleration.

References: 2, 4, 5, 6, 7, 8.

2). Nanojet Scaling laws

Reference solutions are obtained for a set of reference jet velocity and particle density at the inlets. The solutions of the jets at other operating conditions are predicted from the scaling laws.

References 2, 4, 5, 6, 7

3). Comparative Study

Results of the jet structure sensitivity analysis of two-slit jets based on two formalisms are compared and found to be in good agreements.

Reference, 6.

III. Quantum Nanojet's Application.

Quantum nanojets exhibit number of interesting quantum structures and behaviors Involving bubbling, branching, clustering, interference and tunneling, which are uniquely suitable for various applications in nano-quantum transport of sub-atoms, atoms, molecules, interferometer, microscopes, nanoscopes, drug delivery, nanoelectronics and nano-micro scale optical tools in physical, chemical, biological and material research, and nanothrusters. Proper selection of injection conditions and slit geometry is essential for each application. Examples of applications are described below.

Reference 3

1). Low-quantum energetic nanojet systems*:* Strong quantum effects.

Applications*:* nano-sensors, nano-imaging, mass-spectrometer*, energy sensor interferometer, cryptography, nano-enrgetic, nanowires, nanoelectronics, nanooptoelectronics.

2).Intermediate quantum energetic nanojets; Moderate quantum effects

Applications: Nanofabricaltion, soft lithography, jet-assisted-nano assembling, spectrometer*, interferometer, nanoelectronics

3).High quantum energetic nanojets. Weak quantum effects

Applications; Nano & micro propulsion, see item a), below, Particle & molecular beams, hard-lithography quantum computation

In closing, we have successfully completed a comprehensive research project in a profoundly important area of nanoscience: Quantum Nanojets Technology. The one-year efforts led to the establishment of basic knowledge and fundamental data of nanojet physics and also provided remarkable insights for the potential future developments of nanoscientific devices: mass spectrometer, nanoimaging, lithography, nano-propulsions, nanowires, and nanotube technology. Among the most important findings are the critical roles played by the *quantum potential* and the *quantum potential forces*, which are induced by the quantum diffusion of the probability fluid. It is remarkable to point out that the quantum structures and dynamic behaviors of two-slit nanojet are strongly dependent on the quantum Reynolds number, which is defined as the ratio of the inertia force to the quantum potential force acting on the fluid. Nanojets exhibits two unique structural and dynamic behavior: 1) *quantum bubbling,* caused

by premature break-up of the jet at low Reynolds number, 2) *branching,* induced by multi branch-jets interaction which yields interference fringes, and 3) *quantum clustering*: formation of the high density cluster core along the jet axis, which yields the nanojets "signatures". The *clustering* is due to the intersection of right and left running waves from the slit surface which creates compression force, which facilitates the formation of the high density cluster core along the jet axis.

These unique dynamics and energetic behavior of nanojets offer broad areas of applications as nanodevices, sensors, imaging, and space thrusters.

The present writer and his associates wish to extend their appreciation for the unique opportunity in developing this remarkably interesting branch of new nanoscience under the sponsorship of the US Air Force Office of Scientific Research. We acknowledge that part of the works, in particular Ref. 1, 7 and 8, have been supported by National Science Council of Taiwan. Special thanks are due to Dr. F.L. Madarasz for his valuable contributions throughout the research works. Finally, I should like to warmly thank all my colleagues Professor S.Y. Lin, Professor K.R. Chen and our graduate students Mr C.T. Lin, Mr Y.S. Lin and Mr T.S Lin for their technical contributions toward successful completion of the research project. I should also like to thanks Dr.H.L. Tsai and Ms Evensa Su for their exceptional administrative assistance.

Nomenclature

Symbol:

b: half of slit separation in two-slit jet

E: particle energy at the exit of slit = $(1/2m)U^2$

m: mass of a particle

N: Quantum Reynolds number, N= $(2mE)^{1/2}$ $b/\pi\hbar$ *= Ub/D (Two-slit)

Ns: Quantum Reynolds number, N= $(2mE)^{1/2}$ $R/\pi\hbar$ *= UR/D (Single-slit)

R: half-width of a jet.

U: particle velocity at the slit.

Sub-script

cr: critical condition, i.e., transition from quantum to classical state

Glossary

- **Quantum Reynolds number:**

  Quantum Reynolds number represents the ratio of the inertia force to the quantum force acting on the fluid. (Chiu 2002)

- **Quantum nanojets**

  Quantum nanojet is defined as the streams or arrays of particles such as electrons,

atoms, molecules, neutrons, ions or photons, injected directly or through a injector of nanoscale, to a designated target space in the presence or absence of an external potential, and thereby exhibits quantum phenomena. (Chiu 2002)

- **Quantum potential**

  Quantum potential is defined as the sum of the kinetic energy and the dilatation energy associated with quantum diffusion velocity vector field of quantum fluid. (Chiu 2002, Reference 1)

- **Quantum potential force**

  The force derived from the gradient of the quantum potential.

- **Quamlets**

  Quantum flowlets associated with a single eigen-state or the linear superposition of two-degenerate states. (Reference 3)

- **Quantum nanojet phenomena**

  Three important quantum phenomena observed are *quantum bubbling, branching and clustering* in quantum nanojets at specific values of quantum Reynolds number.

Selected Highlights of nanojets

I. "Nanojet at a given quantum Reynolds number exhibits unique structural and dynamic behavior"

- Structural/dynamic complexities are the principal features of "Quantum Nanojet Energetic Hierarchical Systems"

a). Strong quantum jets:

i) Bubble jets, $N < 5$

ii) Multi-branch fan jets,

quantum force >> inertia force $N^{*} << N_{cr}^{*}$

iii) Diffusion dominated flow

b). Intermediate quantum jets:

i) Two-branch quantum jets

quantum force ~ Inertia force $N \sim N_{cr}$

ii) Mixed diffusion-convection flow

c). Two-primary quasi classical jets:

i) Two-primary classical jets

quantum force << Inertia force ~ $N >> N_{cr}$

ii) Convection dominated flow

- **Passive control of nanojets:**

  The structure and dynamic behaviors of nanojets can be controlled by the selection of appropriate quantum Reynolds number through the proper choice of any or all of the following parameters.

  i) Inlet particle energy

  ii) Slit width

  iii) Size of jet of each slit.

- **Active control of nanojets:**

  The structural and dynamic behaviors of nanojets can be controlled by the proper application of a tailored external potential, such as an electrostatic and/or a magnetic potential. The active control plays significantly important roles in the innovation and application of new nanodevices.

II Quantum bubbling,

"Formation of "bubbles" which are characterized by bubble-like structures appear when the quantum number is very low. The bubble-like structures occur when the jet momentum force is smaller than quantum potential force. The jet breaks up in discrete bubbles.

III. Quantum branching/confluencing:

"Phenomena displaying the formation of multi branches jets interaction, which yield interference fringe formation".

- Quantum wave harmonic generation, wave interactions and convective motion inter-coupling are the principal mechanisms of jet state transition and interference fringe formation

a). Phenomena:

(i). Jet-splitting results in the formation of multi branches at low to intermediate Reynolds number.

(ii). Center branch creates bright fringe on the central axis at low to intermediate Reynolds number.

(iii) Formation of jet-streamers on the nanojet surface at low to intermediate Reynolds number.

(iv). Interference fringes of various patterns: *single, double peaks, Mexican hat, M-hat and easter-hat fringe patterns.*

b). Mechanism:

(i). Harmonic wave generation and convective motion intercoupling.

(ii). Intersection of waves form the upper and lower slit jets on the plan of symmetry creates a center branch at low to intermediate Reynolds number.

(iii). Excitation of left and right running waves along the characteristic surfaces

c). Dynamic and structural impacts:

(i). Creation of rapidly varying quantum force in both transverse and axial direction in *Fresnel* region.

(ii). Complex fringe patterns caused by quantum potential under *branching* and *confluencing.*

IV. Quantum clustering:

"Formation of high density particle jet core, which serves as quantum nanojets "signatures""

- Signature of nanojet is formed by quantum clustering

(a). Phenomenon:

(i). High-density particle clusters: base and primary clusters appear in the jet cores. The size, location and shape of cluster are the structural signature of a nanojet.

(ii).Size and the location of cluster increases with respect to the quantum Reynolds number.

(b). Mechanism:

(i). Intersection of right and left running waves from the slit surface compresses the probability fluid and creates high density clusters on the nanojet axis.

(ii) Convective motion shifts the location and size of the clusters toward the downstream of nanojet flow.

(iii). Clusters decay in axial direction by quantum tunneling.

(c). Dynamic and structural impacts:

(i). Creation of rapidly varying quantum axial force due to quantum tunneling

(ii). Cluster spreads along axial direction and ultimately disperses in the full nanojet core at large value of N.

V. Invention of Nanojet based mass spectrometers and energy sensors"

"Based on the mechanisms of quantum branching, confluence and clustering, the following four types of nanojet-based devices can be developed for practical applications in nanoscience and quantum science".

(a). Mass spectrometer: Low Reynolds number device (Center-branch based design).

(b). Mass spectrometer: Intermediate Reynolds number device (Cluster based design).

(c). Energy sensors: Low Reynolds number device (Center-branch based design)

(d). Energy sensors: Intermediate Reynolds number device (Cluster based design)

1) Mass spectrometer and energy sensor:

"*Low Reynolds number devices"*

- **Center branch-based mass spectrometer.**

(a). Principle:

The center branch of a dual-slit jet starts at an axial location at distance, S, form the center of two slits. The S is dependent on N, i.e., S (N)-function, given by,

$$S(N) = S_0 + aN^{\alpha}$$

where S_0, a, and α are constants for a given two-slit geometry.

(b). Method:

When S is obtained from the experimental measurement, the mass of a particle, m, can be calculated from the above equation for given particle energy, E, at the slit, as follows:

$$m = (1/2E)\,(\pi\hbar/b)^2\,[(S-S_0)/a]^{2/\alpha}$$

- **Center-branch jet based energy sensor.**

(a). Principle:

By the same principle described above, we can predict the energy of the particle, E, at the slit, if S and m are known,

$$\mathbf{E} = (1/2m)(\pi\hbar/b)^2\,[(S-S)/a]^{2/\alpha}$$

(b). Method:

When S is measured, E can be calculated from the above equation for a given atomic weight

2) Mass spectrometer and energy sensor:

"*Intermediate Reynolds number devices"*

- **Cluster signature based mass spectrometer.**

(a). Principle:

The length of a cluster, L, of dual-slit jet is given as a function of N, i.e., L(N)-function, as follows,

$$L(N) = L_0 + bN^{\beta}$$

where, L_0, b and β are constants for a given two-slit jet and m is the atomic weight.

(b). Method:

When L is measured from the cluster signature, m can be calculated from the above equation for given particle energy, E, at the slit.

$$m = (1/2E)(\pi \hbar/b)^2 [(L-L_0)/b]^{2/\beta}$$

- **Cluster signature based energy sensor**

(a). Principle:

By the same principle described above, the energy of the particle at the slit exit is given by the following expression,

$$E = (1/2m)(\pi\hbar/b)^2 [(L-L_0)/b]^{2/\beta}$$

(b). Method:

When L is obtained experimentally, E can be calculated from the above equation for a given atomic weight m.

ACCOMPLISHMENTS

The research accomplishments are complied into two documents, identified by Part I, and Part II. Part 1 contains the major accomplishments which are accepted or submitted for publication in journals or conference papers, as listed below. Part II, includes PhD and MS dissertations of three graduate students who participated in the research projects.

PART I

A) Journal Publications:

1. *H.H. Chiu, "Quantum fluid dynamical and electronic structure of a hydrogen-like atom"*. Accepted for publication in the **Proceedings of the Royal Society of London 2005. AOARD-034039** and **NSC92-2212-E006-086**

2. *H.H. Chiu, C.T. Lin, S.Y. Lin, and F.L. Madarasz,,* **"***Quantum nanometer structures: quantum branching and clustering in two-slit electron jets" Submitted for publication.2005.* **AOARD-034039**

3. *H.H. Chiu, "Theory of quamlets of quantum systems" Submitted for publication 2005***. AOARD-034039**

B) Conference papers

4*. H.H. Chiu and C.T. Lin: "Structural and dynamic complexities of quantum fanjets" USAFOSR/Taiwan Nan science Initiative Workshop. Maui Hawaii, February 19-20 2004* **AOARD-034039**

5. *H.H. Chiu, C.T. Lin, S.Y. Lin, T.C, Hung, F.L. Madarasz*, "*Developments of quantum nanometer based Nan devices"* 11th International Conference on Composites/Niño Engineering August 8-14 2004, S.Carolina. **AOARD-034039**

PART II.

C) PhD dissertations

6. *C.T. Lin, "Structures, Dynamics and Energetic of Double-Slit Quantum Nanojet"* Submitted to the Institute of Aeronautics and Astronautics, National Cheng Kung University. July 2005 **AOARD-034039**

D) MS dissertations

7. *T.S. Lin, "Quantum Bubble Nanojet Structure"* Submitted to the Institute of Aeronautics and Astronautics, National Cheng Kung University. July 2005**. AOARD-034039** and **NSC92-2212-E006-086**

8. *Y.S. Lin, " Multi-Slit Quantum Nanojets "* Submitted to the Institute of Aeronautics and Astronautics, National Cheng Kung University. July 2005 **AOARD-034039** and **NSC92-2212-E006-086** (Prepared for the Second Cycle)

Quantum fluid mechanical and electronic structure of a hydrogen-like atom

By H. H. Chiu

Space Science and Technology Center and Institute of Aeronautics and Astronautics

National Cheng Kung University, Tainan, 70101, Taiwan

(hhchiu@htind1.iaa.ncku.edu.tw)

Quantum diffusive fluid dynamics formalism is adapted to examine the quantum mechanical significance of quantized energy and the mechanisms of detailed dynamic equilibria among the Coulomb field, vortex induced flow and the quantum potentials of elemental processes induced by the quantum diffusion of the probability fluid of the electron in a hydrogen-like atom. The quantized energy is found to be the negative of the kinetic energy of the asymptotic diffusion velocity of the probability fluid of the electron. The Coulomb force balances with the forces due to the total radial quantum potential induced by radial diffusion minus the centrifugal barrier force. With a finite magnetic quantum number, a line vortex is present in an atom structure. The kinetic energy of the vortex-induced flow is supplied by a part of the quantum dilatation energy associated with the diffusion in polar angular direction, whereas the remainder of the dilatation energy balances with the centrifugal barrier potential. An atom with a finite magnetic quantum number is structured with the vortex induced-flow dominated inner core with the line vortex extending beyond the Bohr radius along the polar axis, and the electrostatic potential dominates the exterior region of the core. In a state of zero magnetic quantum number the atom exhibits a pure electronic structure. The paper concludes with areas of future research on quantum energetic and dynamic equilibria in other quantum systems and the validity of the model.

Keywords: **quantum diffusive fluid dynamics; quantum energetic; hydrogen atom structure**

1. Introduction

Three profound issues, which remain un-addressed or imperfectly understood in a hydrogen atom, are: the quantum mechanical significance of the quantized energy, the mechanism of the dynamic balance of an electron under the Coulomb potential field, and the source of the kinetic energy of the vortex induced flow, in a stationary state, defined by a set of quantum numbers. An atom emits a photon when it is de-excited from a higher energy level to a lower state and absorbs quanta when

it is excited by radiative absorption or atomic collision.

The questions of exactly what the nature of the quantized energy is that accompanies the differential changes of energy in atomic and molecular absorption and emission, and why the energy of a stationary eigenstate takes on a particular constant value, however, have curiously remained unanswered despite the successful prediction of the quantized energy levels themselves by quantum theory. Additionally, the nature of dynamic equilibrium for maintaining the electron without falling upon nucleus under the Coulomb attractive force at the discrete quantized energy levels of an atom has been inadequately understood. Another dynamic phenomenon involving a line vortex induced flow in an atom under a finite magnetic quantum number provokes the question of how does the latter flow acquire the energy to sustain the motion. A review of literature reveals that the quantitative criteria for dynamic equilibria and detailed structure of a global atomic system in a stationary state are not known to a satisfactory level of detail. It is envisioned that the quantum phenomena related with the above three principal modes—quantized energy, Coulomb potential, and vortex motion—are interrelated issues, which need to be treated concomitantly by what may be described as global modal balance in an atomic system. The objectives of the present study are to develop a self-consistent atomic modal balance theory based on the frameworks of quantum diffusive fluid dynamics, and to examine the nature of energetic and dynamic equilibria of a hydrogen atom in a stationary state so as to establish a dynamic characterization of quantized energy and to gain a basic understanding of the electronic and fluid dynamic structures of an atom from the quantum fluid dynamics perspective.

In quantum theory the hydrogen atom is taken as a two-particle system, a proton and an orbital electron. However, in the fluid dynamics model presented here, the electron is viewed as a probability fluid whose density is the product of the wave function and its complex conjugate, which both satisfy the Schrödinger equation. The quantum probability fluid, whose stress tensor is constructed from the quantum potential induced by non-uniform spatial density distribution, obeys the laws of conservation of quantum fluid dynamics. There are two distinct developments in the formalism of quantum fluid dynamics or the quantum theory of motion: the Hamilton-Jacobi transformation applied to the Schrödinger equation; and alternatively, the formulation by stochastic mechanics of the classical theory of Brownian motion of particles. The development of two formalisms and historical highlights are described below.

Quantum fluid dynamics and the quantum theory of motion are usually viewed as

generalizations of Newton's classical mechanics in the Hamiltonian formalism. They have also been known for sometime via earlier theories: pilot wave of de Broglie (1928); the hidden-variable theory, Bohm (1952a, 1952 b); the causal interpretation and, later the ontological interpretation of quantum mechanics, Belinfante (1973), Bohm & Hiley (1993); and, most recently, the theory of quantum motion. An excellent book by Holland (1993) presents a comprehensive quantum theoretical account of the de-Broglie-Bohm's causal interpretation of quantum mechanics covering the broad exposition of the theory and critical review of specific issues: particle trajectory, quantum prediction, classical deterministic model, non-locality, mathematical features, quantum intuition, and a particle's reciprocal action on the associated wave. Of particular interest are historical dialogues and contingencies surrounding the Einstein-Podolosky-Rosen paradox (1935), Copenhagen interpretation by Bohr (1958), interconnectedness theorem of Bell (1966), and experiments on Bell's inequalities by Aspects (1982). While we do not elaborate on a detailed description of each issue cited above, we will focus our attention on the unique concept of a quantum potential, which arises through the Hamilton-Jacoby formalism, and its significance to the nature of the global atomic problems we intend to resolve. The rationale for this motivation is supported by the observation made by Holland (1993), who foresaw that "corresponding to the new theory of motion, i.e., generalized Hamilton-Jacoby theory, is a new conception of matter." In following this observation we first acknowledge that a salient feature of the new theory is that matter has an intrinsic field aspect: the mass points moving and interacting under the influence of the quantum potential, which is characterized as an organizational, self-referential form of potential energy that brings about inner stresses in the material system to which the mass points respond, Holland (1993). Secondly, we note that the quantum potential has a defining feature of being a holistic, context-dependent nonlocal potential that depends only on the "form" of the potential, and not its intensity or strength and the effects of such potential do not fall off with distance, Bohm and Hiley (1993). These two unique aspects of the quantum potential appear as a fundamental basis in formulating a concomitant global balance theory with the quantum potential giving rise to key dynamic and energetic factors that govern the structure of a hydrogen-like atom.

Other quantum fluid descriptions developed by Nelson (1966, 1985), Comisar (1965), and Kershaw (1964) are based on stochastic processes via the classical theory of Brownian motion. An extensive discussion of quantum fluctuations and a list of references can be found in excellent lecture notes published by Nelson (1985). The stochastic mechanical formulation, or Nelsonian

mechanics, does not share the physical basis of a causal theory but adapts a probability concept of classical theory, through which atomic processes are described by particle motion in space and time. However, despite of the profoundly different theoretical conceptual framework of classical stochastic mechanics and quantum mechanics, the theory shows that for observations, which may be reduced to position measurements, the two formalisms give the same quantum mechanical prediction, Nelson (1966). Two unique steps have been undertaken in the stochastic mechanical formalism. They are the introduction of quantum osmotic velocity, Nelson (1966), which is the negative of the diffusion velocity defined by Chiu (2002), and the formulation of the evolution equation of the osmotic velocity and the momentum equation. With the use of a Hamilton-Jacobi transformation, the equation governing the evolution of osmotic velocity can also be obtained from the continuity equation for the probability current density, as we shall show later. Thus the laws of conservation derived from the two formalisms are mathematically equivalent to each other.

While we will not elaborate on historical dialogues and contingencies between the Copenhagen vs. de-Broglie-Bohm interpretations of quantum mechanics, we will adopt a view that is based on an examination of the measurement process, which suggests that, within a limited framework, the two theories, quantum mechanics and quantum fluid dynamics, are equivalent, Nelson (1966). Thus the latter approach, i.e., the quantum fluid dynamics, is used as an alternative methodological framework for the proposed investigation of atomic modal balance. In §2 we recapitulate the quantum diffusive fluid mechanics formulation of the laws of conservation of probability density and energy. In §3 we elucidate the role of a quantum potential and how its presence gives rise to the dilatation and kinetic energies associated with diffusion field, which are in accord with the general framework of Nelson's stochastic formulation description. Principal modes and the elemental processes are introduced to facilitate modal balance analysis in §4. The nature of atomic modal energy balance and dynamic equilibria are investigated in §5. This analysis includes the examinations of physical significance of the quantized energy, the detailed balance among the Coulomb field, vortex induced flow, quantum potential, and the intercoupling modes of an atom. In §6 we present numerical results including the detailed electronic-hydrodynamic structures for an atom for selected quantum states and discuss the range of validity of the results. The paper concludes with the suggested areas of future research in quantum energetic of other atoms, molecules and many-particle systems.

2. Quantum Bernoulli's equation

The hydrogen atom, a proton and an electron, is a two-particle system with a central force acting on the line between the two particles. Canonically, the Schrödinger equation describing this system is separated into two independent different equations: one for the center-of- mass motion, and the other for the relative motion about the center-of-mass. The center-of-mass problem is treated as a single particle with a mass of $M = (m_e+m_P)$, where m_P and m_e are the masses of the proton and electron, respectively, translating through space. The relative motion problem is also treated as a single particle problem but with a reduced mass defined by $\mu = (m_P m_e)/M$. The ratio of the proton to electron mass is $m_P/m_e = 1837$. Since the proton is much more massive than the electron it is located very close to the center-of-mass, while the reduced mass is close to the electron's coordinates. Following Landau and Lifshitz (1985), we approximate the center of mass as the origin of the relative coordinate. Because of the above approximation, the solution is, in principle, invalid in a small spherical region of radius $(m_E/m_P)r_e$ centered at the origin of the coordinate, as in the similar treatment presented in standard texts. Thus for the hydrogen atom, the time dependent Schrödinger's equation for relative motion in Coulomb potential, V_e, is given by,

$$i\hbar\frac{\partial\psi}{\partial t} = -\frac{\hbar^2}{2m_e}\nabla^2\psi + V_e\psi \qquad (2.1)$$

where the reduced mass, μ, has been approximated by electron mass m_e and $\hbar$ is the Planck's constant divided by 2π.

In the present quantum fluid dynamics model, we assume that the electron consists of the Schrödinger's probability fluid, attracted by the Coulomb force induced by the positively charged nucleus. The probability fluid obeys the laws of conservation derived by the Hamilton-Jacobi method. Following Bohm (1952a) we first express the wave function in the polar form, $\psi = \rho^{1/2}\exp(im_e\phi/\hbar)$, where ρ is the probability density, ϕ, is a scalar potential. By inserting the latter expression of ψ, into Eq. (2.1), and separating into imaginary and real parts, we obtain the equations for the flow variables ρ and ϕ. The imaginary and real part gives the conservation equation of probability density and energy, respectively,

$$\frac{\partial \rho}{\partial t} + \nabla \bullet \mathbf{J} = 0, \tag{2.2}$$

$$\frac{\partial \phi}{\partial t} + \left(\frac{1}{2}\right)\mathbf{u} \bullet \mathbf{u} + \frac{\mathrm{V}_e}{m_e} - \prod_{\ln \rho} = \frac{\mathrm{E}}{m_e} \tag{2.3}$$

where ***J*** is the current density or Lagrangian density. The expressions for ρ and ***J*** are:

$$\rho = \psi \psi^*, \tag{2.4}$$

and

$$\mathbf{J} = \rho \mathbf{u} = \left(\frac{\hbar}{2\mathrm{i}m_e}\right)\left(\psi^* \nabla \psi - \psi \nabla \psi^*\right), \tag{2.5}$$

where, **u**, is the mean convective velocity, defined by the ratio of the probability current flux **J** with the density,

$$\mathbf{u} = \left(\frac{\hbar}{2\mathrm{im_e}}\right)\nabla\left(\ln \frac{\psi}{\psi^*}\right) = \nabla \phi. \tag{2.6}$$

The velocity field, Eq. (2.6), is irrotational, except at the nodal singularities where the wave function vanishes and vorticies are present. It has been shown by Carlen (1984) Nelson (1985), Bacciagaluppi (1998), and Berndl, et al (1995), that under certain regularity conditions on the initial wave function and the external potential, the particle has zero probability of entering the nodal surface from outside. Since the determination of the current density, **J** , Eq. (2.5) requires the simultaneous measurements of position and velocity of particle, which is not in compliance with the uncertainty principle, **J,** can not to be treated as the averaged measured particle flux at the point in space and time interpreted in classical fluid dynamics, except in the case when **J** varies slightly or not at all in a spatial coordinate so that an accurate velocity determination can be made without impairing the usefulness of the concept of flux.

The quantum potential, $\prod_{\ln \rho}$ appears in the fourth term on the left side of Eq. (2.3), has the functional form,

$$\Pi_{\ln\rho} = \left(\frac{\hbar^2}{4m_e^2}\right)\left[\nabla^2(\ln\rho) + \left(\frac{1}{2}\right)\nabla(\ln\rho)\bullet\nabla(\ln\rho)\right], \tag{2.7}$$

We will adapt the $\Pi_{\ln\rho}$ form of quantum potential and for notational convenience will denote it by just Π .

The momentum equation is obtained by taking the gradient of Eq. (2.3), as follows, see for example, Ghosh, & Deb. (1982),

$$\frac{\partial \mathbf{u}}{\partial t} + \mathbf{u}\bullet\nabla\mathbf{u} = -\frac{\nabla V_e}{m_e} + \nabla\Pi \tag{2.8}$$

This equation serves as guide for the examination of dynamic criteria of fluid equilibria.

3. The roles of quantum diffusion in modal dynamic balance

The Quantum potential, Π, plays a major role in quantum energetic involved in the large classes of quantum flow fields with non-uniform density distributions. In this section we will characterize it within the context of quantum diffusion processes. We introduce, in analogy with classical mass transport theory, the diffusion of the probability fluid characterized by the gradient induced diffusion velocity, $\mathbf{V}$, Chiu (2002), as follows,

$$\mathbf{V} = \frac{\mathfrak{J}}{\rho} = -\left(\frac{\hbar}{2m_e}\right)\nabla\ln\rho = -D\frac{\nabla\rho}{\rho} \ . \tag{3.1}$$

where $\mathfrak{J}$ is the diffusion current flux of the probability fluid, and the quantity $\hbar/2m_e$, which has the same physical dimension as the mass diffusivity, is termed as quantum diffusivity, designated by *D*. It is of special interest to note that Nelson (1966, 1985) defines the osmotic velocity as the mean value of the difference between the forward and backward velocities of Brownian particle motion with diffusion coefficient *D,* and no friction. According to Einstein's theory of Brownian motion, the osmotic velocity is the velocity acquired by a particle in equilibrium with respect to an external force, to balance with the osmotic force. By adapting the available data, for example, $D = 0.116\times10^{-3}$ m^2/sec and Bohr radius, *a*, of a hydrogen atom of 5.29×10^{-10} m, we estimate a

characteristic diffusion velocity to be approximately 2.3×10^{6} m/sec.

The physical significance of the first term of the quantum potential, $\left(\hbar^2/4m_e^{\,2}\right)\nabla^2\ln\rho$, can be obtained from the definition of the diffusion velocity, as follows. Taking the divergence of Eq. (3.1) yields,

$$\mathfrak{M}=\left(\frac{\hbar^2}{4m_e^2}\right)\nabla^2\left(\ln\rho\right)=\left(\frac{\hbar}{2m_e}\right)\left(\frac{\hbar}{2m_e}\right)\nabla\bullet\left(\frac{\nabla\rho}{\rho}\right)=-D\nabla\bullet\mathbf{V} \tag{3.2}$$

By comparison, it is seen that the first term in the quantum potential per unit mass, Eq. (2.7), represents the specific dilatation energy of diffusion field, $\mathfrak{M}=-D\nabla\bullet\mathbf{V}$, due to the divergence of the quantum diffusion velocity. The specific dilatation energy, Eq. (3.2), agrees with the negative of the dilatation of the osmotic velocity that appears in Nelson's stochastic mechanical formulation, Nelson (1966). The dilatation of the diffusion velocity field has a different physical significance from that of the mean convective velocity, discussed below.

The specific dilatation of a mean convective velocity is given by equation, (2.1) as,

$$-\nabla\bullet\mathbf{u}=\frac{\partial(\ln\rho)}{\partial\mathrm{t}}+\mathbf{u}\bullet\nabla\ln\rho=\frac{\partial(\ln\rho)}{\partial\mathrm{t}}-\frac{\mathbf{u}\bullet\mathrm{V}}{D}=\frac{\mathrm{d}(\ln\rho)}{\mathrm{dt}} \tag{3.3}$$

which is equal to substantive derivative, d/dt, describing the co-moving time rate of change of expansion or contraction of the fluid seen from the instantaneous rest frame of the actual fluid parcel. According to Eq. (3.3) we conclude that a steady state flow is a "convective dilatation free", when **u** and **V** are normal to each other throughout the flow field. We shall see later that the probability fluid flow field in a hydrogen atom at a stationary state described by a set of quantum numbers is convective dilatation free.

Similarly, the specific dilatation of the diffusion velocity is obtained by taking the divergence operator on (3.1) as follows,

$$-\nabla\bullet\mathbf{V}=\mathbf{V}\bullet\nabla\ln\rho+\left(\frac{\mathrm{D}}{\rho}\right)\nabla^2\rho \tag{3.4}$$

The second term appears in the right hand side of above equation, $\left(D/\rho\right)\nabla^2\rho$, originates from the

Fokker-Planck equation governing the diffusion of objects, Nelson (1966). By using an appropriate algebraic manipulation of Eq. (2.3) we find that $D\nabla^2\rho/\rho$ is equal to $D^{-1}[(1/2)(u^2+\mathrm{V}^2)+\mathrm{V}_e/m_e-E/m_e]$. Upon substituting the latter expression in (3.4), we have,

$$-\nabla\bullet\mathbf{V}=\mathbf{V}\bullet\nabla\ln\rho+D^{-1}[\frac{1}{2}(u^2+\mathrm{V}^2)+\frac{\mathrm{V}_e}{m_e}-\frac{E}{m_e}] \tag{3.5}$$

Thus, physically, the specific dilatation $-\nabla\bullet\mathrm{V}$ is equal to the rate of the change of expansion or contraction along the direction of the diffusion velocity plus the total kinetic energy, including the mean convective and diffusive fields, the specific external potential energy minus the specific total energy, E, divided by the diffusivity.

We define the diffusion field as a "diffusive dilatation free" when $-\nabla\bullet\mathbf{V}=0$. In contrast to the convective flow field, the dilatation of the diffusion velocity field in a hydrogen atom in a stationary state, as we show later, is not zero, even in atomic bound states. It is the dilatation energy of the latter "compressible diffusive field" and the kinetic energy of the corresponding diffusion process, both of which synergistically acting together to play a major role in preserving dynamic equilibria of probability fluid in an atom.

Typical dilatation energy of a diffusion field in a hydrogen atom, estimated by the approximate expression of m_eDV/a is 10 ev, is of the same order of magnitude of the ground state energy of a hydrogen atom.

Next, according to the definition of diffusion velocity, (3.1), the term defined by $\left(\hbar^2/4m_e^{\,2}\right)\left(1/2\right)\nabla\left(\ln\rho\right)\bullet\nabla\left(\ln\rho\right)$, represents the kinetic energy associated with the quantum diffusive velocity,

$$\Omega=\left(\frac{\hbar^2}{4m_e^{\,2}}\right)\left(\frac{1}{2}\right)\nabla\left(\ln\rho\right)\bullet\nabla\left(\ln\rho\right)=\left(\frac{1}{2}\right)\mathbf{V}\bullet\mathbf{V} \tag{3.6}$$

The characteristic specific kinetic energy of diffusion in a hydrogen atom is estimated to be 10 ev., which is also of the same order of magnitude of the ground state energy of hydrogen atom.

Thus, by introducing $\mathfrak{M}$ and Ω, we formally express the quantum potential $\prod$ as the sum of the specific dilatation energy and diffusion kinetic energy.

$$\prod = \mathfrak{M} + \Omega = \left[-D\nabla\bullet\mathbf{V} + \left(\frac{1}{2}\right)\mathbf{V}\bullet\mathbf{V} \right] \tag{3.7}$$

We conclude that the quantum potential, given by Eq. (3.7), is in agreement with the corresponding expression given by Nelson (1966).

It is to be noted that the equation governing the diffusion velocity and the momentum equation constitute the complete set of conservation equations given by Nelson (1966). However, the derivation of the Nelson's diffusion equation can be achieved through the use of the continuity equation (2.2) and diffusion velocity equation, (3.1), as follows. By taking a partial derivative with respect to time of the diffusion velocity Eq. (3.1) and using the continuity equation to replace $\partial\rho/\partial t$ by $-\nabla\bullet(\rho\mathbf{u})$, we arrive at,

$$\frac{\partial \mathrm{V}}{\partial t} = (\frac{\hbar}{2m_e})\nabla\nabla\bullet\mathbf{u} - \nabla(\mathbf{u}\bullet\mathbf{V}) \tag{3.8}$$

Thus, Nelson's equation governing the diffusion velocity is identical to the continuity equation of the probability density derived from the Hamilton-Jacobi formalism, together with the definition of the diffusion velocity given by (3.1).

4. Principal modes and elemental processes

By adopting the definitions of quantum diffusion and related energies, the Bernoulli's equation, Eq. (2.3), for the probability fluid of a hydrogen-like atom can be expressed as,

$$\frac{\partial\phi}{\partial t} + \frac{1}{2}(\mathbf{u}\bullet\mathbf{u} - \mathbf{V}\bullet\mathbf{V}) + \frac{\mathrm{V}_e}{m_e} + D\nabla\bullet\mathbf{V} = \frac{E}{m_e} \tag{4.1}$$

Bernoulli's equation is a statement of the balance of the mechanical energy among various modes represented by two types of flow variables. The first are those belonging to the principal modes:

quantized energy, Coulomb potential, the kinetic energy of the mean convective motion, and the energy associated with the temporal variation of the velocity potential. The next are those which belong to the quantum potential modes: dilatation, and kinetic energies of diffusion induced potentials. In the modal analysis method to be presented here, we decompose a quantum potential mode into a group of elemental processes each of which has either a part of the dilatation energy or kinetic energy or a combination of the both. The purpose of the modal analysis is to determine how each principal mode balances, energetically or dynamically, with an appropriate set of elemental processes. The successful determination of such sets of elemental processes provides the answer to three unsolved issues raised at the outset of this paper.

(a) Quantum modal balance theory

When the atom is in a stationary state Eq. (4.1) can be recast in spherical polar coordinates resulting in,

$$\frac{1}{2}u^2-\frac{Ze^2}{m_e r}-\frac{\hbar^2}{4m_e^{\,2}}\left\{\frac{1}{r^2}\frac{\partial}{\partial r}\left(r^2\frac{\partial}{\partial r}ln\rho\right)+\frac{1}{r^2\sin\theta}\frac{\partial}{\partial\theta}\left(\sin\theta\frac{\partial}{\partial\theta}ln\rho\right)\right.$$
$$\left.+\frac{1}{r^2\sin^2\theta}\frac{\partial^2}{\partial\varphi^2}ln\rho+\frac{1}{2}\left[\left(\frac{\partial ln\rho}{\partial r}\right)^2+\frac{1}{r^2}\left(\frac{\partial ln\rho}{\partial\theta}\right)^2+\frac{1}{r^2\sin^2\theta}\left(\frac{\partial ln\rho}{\partial\varphi}\right)^2\right]\right\}=\frac{E}{m_e} \tag{4.2}$$

where Z (=1) is the atomic number, e the charge on an electron. For algebraic convenience the terms of Eq. (4.2) can be regrouped and written as follows

$$\mathcal{K}(n,l,m)+\mathfrak{D}-\mathfrak{M}(n,l,m)-\Omega(n,l,m)=\mathfrak{E}(n). \tag{4.3}$$

Here, *n, l,* and *m* are the principle, orbital angular momentum and magnetic quantum numbers, respectively, for an atom in a stationary state. The terms of Eq. (4.3), which are all per unit mass, are sequentially: $\mathcal{K}(n,l,m)$ is the kinetic energy of mean flow induced by a line vortex; $\mathfrak{D}$ is the Coulomb mode, which is independent of the quantum state; $\mathfrak{M}(n,l,m)$ is the dilatation mode; $\Omega(n,l,m)$ is the diffusion kinetic energy mode; and $\mathfrak{E}(n)$ is the quantized state energy mode.

Formulation of the quantum modal analysis begins with the definition of elemental processes, described below. First, the dilatation and the kinetic energy associated with the diffusion of the probability fluid are decomposed into the radial, polar and azimuthal and components, as follows,

$$\mathfrak{M}_R = \frac{\hbar^2}{4m_e^{\,2}}\left[\frac{1}{r^2}\frac{\partial}{\partial r}\left(r^2\frac{\partial \ln\rho}{\partial r}\right)\right] \qquad \Omega_{\mathfrak{R}} = \frac{\hbar^2}{4m_e^{\,2}}\left[\frac{1}{2}\left(\frac{\partial \ln\rho}{\partial r}\right)^2\right] \tag{4.4}$$

$$\mathfrak{M}_\theta = \frac{\hbar^2}{4m_e^{\,2}}\left[\frac{1}{r^2\sin\theta}\frac{\partial}{\partial\theta}\left(\sin\theta\frac{\partial \ln\rho}{\partial\theta}\right)\right] \qquad \Omega_\theta = \frac{\hbar^2}{4m_e^{\,2}}\left[\frac{1}{2}\frac{1}{r^2}\left(\frac{\partial \ln\rho}{\partial\theta}\right)^2\right] \tag{4.5}$$

$$\mathfrak{M}_\varphi = \frac{\hbar^2}{4m_e^{\,2}}\left[\frac{1}{r^2\sin^2\theta}\frac{\partial^2(\ln\rho)}{\partial\varphi^2}\right] \qquad \Omega_\varphi = \frac{\hbar^2}{4m_e^{\,2}}\left[\frac{1}{2}\frac{1}{r^2\sin^2\theta}\left(\frac{\partial \ln\rho}{\partial\varphi}\right)^2\right] \tag{4.6}$$

where the subscripts R, θ, and φ designate the components in radial, polar, and azimuthal directions, respectively.

Secondly, each component of dilatation mode $\mathfrak{M}_{R,\theta,\phi}(n,l,m)$ and diffusion kinetic mode $\Omega_{R,\theta,\phi}(n,l,m)$ is further divided into a number of elemental processes $\mathfrak{M}_{\alpha_j}(n,l,m)$ and $\Omega_{\alpha_j}(n,l,m)$ as follows,

$$\mathfrak{M}_\alpha(n,l,m) = \sum_j \mathfrak{M}_{\alpha_j}(n,l,m), \tag{4.7}$$

$$\Omega_\alpha(n,l,m) = \sum_j \Omega_{\alpha_j}(n,l,m), \tag{4.8}$$

where the subscript α refers to the R, θ, or φ, and j represents the j th elemental process. These processes, $\mathfrak{M}_\alpha$ and Ω_{α_j}, are the unit processes, each of which contributes in such a manner that the sum of a set of selected elemental processes of $\mathfrak{M}$ or Ω modes, or combination of the two, balances with a specific principal mode: $\mathfrak{D}$, $\mathcal{K}(n,l,m)$ or $\mathfrak{E}(n)$. Additionally, there are cross-intercoupling elemental processes, which make no contribution in energy balance with a principal mode. They do serve, however, to maintain equilibrium among the remaining elemental processes, which are not participating in the principal modal balance.

(b) Quantum modal balance equations and scaling laws

Quantum modal balance analysis seeks to determine appropriate sets of elemental processes such that each set satisfies the conditions of modal balance, given below,

Coulomb mode:

$$\sum_j \mathfrak{M}^{\mathfrak{D}}_{\alpha_j}(n,l,m) + \sum_j \Omega^{\mathfrak{D}}_{\alpha_j}(n,l,m) = \mathfrak{D} = \frac{-Ze^2}{m_e r} \tag{4.9}$$

Vortex mode:

$$\sum_j \mathfrak{M}^{\mathfrak{K}}_{\alpha_j}(n,l,m) + \sum_j \Omega^{\mathfrak{K}}_{\alpha_j}(n,l,m) = \mathfrak{K}(n,l,m) = \frac{\hbar^2}{2m_e{}^2} \frac{m^2}{r^2 \sin^2\theta} \tag{4.10}$$

Quantized state energy mode:

$$\sum_j \mathfrak{M}^{\mathfrak{E}}_{\alpha_j}(n,l,m) + \sum_j \Omega^{\mathfrak{E}}_{\alpha_j}(n,l,m) = -\mathfrak{E}(n) = \frac{Z^2e^2}{2m_e a n^2} = \frac{Z^2e^4}{2\hbar^2 n^2} \tag{4.11}$$

Cross inter-coupling mode:

$$\sum_j \mathfrak{M}^{\Omega}_{\alpha_j}(n,l,m) + \sum_j \Omega^{\mathfrak{M}}_{\alpha_j}(n,l,m) = 0 \tag{4.12}$$

The kinetic energy, $\mathfrak{K}(n,l,m)$, of vortex induced flow appears in the right hand side of Eq. (4.11) is discussed in a later part of this sub-section.

In order to carry out the modal analysis it is convenient to first expand the probability density, ρ, in terms of hydrogen eigenfunctions expressed in spherical polar coordinates as follows, (Landau & Lifshitz 1985),

$$\rho_{nlm}(r,\theta,\phi) = \psi_{nlm}\psi^*_{nlm} = R^2_{nl}(r) Y_{lm}(\theta,\phi) Y^*_{lm}(\theta,\phi), \tag{4.13}$$

where $R_{nl}(r)$ is given by,

$$R_{nl}(r) = \beta\, \eta^l\, e^{-\eta/2}\, F_{nl}(\eta), \tag{4.14}$$

in which β = 2Z/na, a is the Bohr radius, $\mathrm{a} = \hbar/\mathrm{m_e e^2}$, and $\eta = \beta r$. The function F_{nl}, is proportional to the associated Laguerre polynomials, and is governed by the following differential equation:

$$\eta \frac{d^2F_{nl}}{d\eta} + (2l+2-\eta)\frac{dF_{nl}}{d\eta} + (n-l-1)F_{nl} = 0, \tag{4.15}$$

where, the allowed values of l are $l = 0, 1, 2, 3, \ldots n\text{-}1$.

The spherical harmonics, $Y_{lm}(\theta,\phi)$ can be separated into polar and azimuthal angular components,

$$Y_{lm}(\theta,\phi) = \Theta_{lm}\exp(im\phi), \tag{4.16}$$

where $\Theta_{lm}(\theta)$ are the solutions of the Legendre equation,

$$\frac{1}{\sin\theta}\frac{d}{d\theta}\left(\sin\theta\frac{d\Theta_{lm}}{d\theta}\right)+\left[l(l+1)-\frac{m^2}{\sin^2\theta}\right]\Theta_{lm} = 0, \tag{4.17}$$

and have the form,

$$\Theta_{lm}(\theta) = (-1)^m\sqrt{\frac{(2l+1)}{2}\frac{(l-|m|)!}{(l+|m|)!}}P_l^{|m|}(\cos\theta), \tag{4.18}$$

where m takes on the values of m = 0, ±1, ±2, … ±l, and $P_l^{|m|}$ are the associated Legendre polynomials. The Y_{lm} are normalized with respect to integration over the entire solid angle.

In order to calculate the kinetic energy, $\mathcal{K}(n,l,m)$, of vortex induced flow, Eq. (4.10), we first determine the velocity of the mean flow from Eq. (2.4),

$$\mathbf{u}_{nlm} = \left(\frac{\hbar}{2mi}\right)\nabla\ln\left(\frac{\psi_{nlm}}{\psi_{nlm}^*}\right) = \left(\frac{m\hbar}{m_e r\sin\theta}\right)\mathbf{e}_\phi. \tag{4.19}$$

The above velocity distribution corresponds to the flow induced by a line vortex extending in the direction of polar axis coinciding with the z-axis, which passes through the center of the mass of an atom. The kinetic energy, per unit mass, of the flow induced by the vortex mode is then,

$$\mathcal{K}(n,l,m) = \left(\frac{1}{2}\right)u_{nlm}^2 = \frac{\hbar^2}{2m_e^{\,2}}\frac{m^2}{r^2\sin^2\theta}. \tag{4.20}$$

By definition, the circulation strength of the vortex flow is given by,

$$\Gamma = \int\mathbf{u}\bullet d\mathbf{r} = \frac{m\hbar}{m_e}\int_0^{2\pi}\frac{r\sin\theta}{r\sin\theta}d\varphi = \frac{2\pi m\hbar}{m_e}, \tag{4.21}$$

where again m takes on the values of $0, \pm1, \pm2, \ldots \pm l$. Thus, the vortex in the atom is quantized with the magnetic quantum number, m.

We will now show that the Bernoulli's equation (4.3) can be cast in the form of a scaling law,

$$\mathfrak{C}_n \left\{ \tilde{\kappa}(n,l,m) + \tilde{\mathfrak{D}}(n) - \sum_{\alpha}\sum_{j} \tilde{\mathfrak{M}}_{\alpha_j}(n,l,m) - \sum_{\alpha}\sum_{j} \tilde{\Omega}_{\alpha_j}(n,l,m) - \varepsilon \right\} = 0 , \tag{4.22}$$

where $\mathfrak{C}_n$ is a quantum scaling parameter, and $\tilde{\kappa}$, $\tilde{\mathfrak{D}}$, $\tilde{\mathfrak{M}}$, $\tilde{\Omega}_{\alpha_j}$ and ε are the non-dimensional quantities corresponding to $\mathcal{K}$, $\mathfrak{D}$, $\mathfrak{M}$, Ω, and $\mathcal{E}$ of Eq. (4.3). The quantum scaling parameter $\mathfrak{C}_n$ is found to be equal to four times of the negative of quantized energy per unit mass,

$$\mathfrak{C}_n = \left(\frac{\hbar^2}{4m^2} \right) \left(2\beta_n^2 \right) = \frac{2Z^2 e^2}{m_e n^2 a} = -4E_n . \tag{4.23}$$

(c) Decomposition of quantum diffusion

The density distribution, Eq. (4.13), can be expressed as the product of four density functions,

$$\rho(n,\ell,m) = \left(\frac{2Z}{na}\right)^2 \rho_\ell \rho_A \rho_F \rho_\theta \tag{4.24}$$

where

$$\rho_l = \eta^{2l}, \qquad \rho_A = e^{-\eta}, \tag{4.25a,b}$$

$$\rho_F = F_{nl}^2(n), \qquad \rho_\theta = \Theta_{\ell m}^2(\theta) \tag{4.26a,b}$$

where, ρ_ℓ represents the power type distribution associated with the orbital angular momentum quantum state, ℓ, ρ_A, is an asymptotic distribution for large r, ρ_F, is the density distribution defined by Lagueere polynomials, and ρ_θ is the density distribution due to Legendre polynomial function. By using the definition Eq. (3.1), the diffusion velocity is expressed by the sum of four components,

$$\begin{aligned} \mathbf{V} &= -\mathrm{D}\nabla \ln \rho = \mathbf{V}_\mathrm{l} + \mathbf{V}_\mathrm{F} + \mathbf{V}_\mathrm{A} + \mathbf{V}_\theta \\ &= (\mathrm{V}_\mathrm{l} + \mathrm{V}_\mathrm{F} + \mathrm{V}_\mathrm{A})\mathbf{e}_\mathrm{r} + \mathrm{V}_\theta \mathbf{e}_\theta \end{aligned} \tag{4.27}$$

where, $\mathbf{e}_r$ and $\mathbf{e}_\theta$ are unit vectors and the four diffusion components, V_ℓ , V_F , V_A and V_θ are sequentially: power type, Lagueere, asymptotic, and polar diffusion velocity, respectively. These are given by

$$\mathbf{V}_l = -D\nabla \ln \rho_L = -D\nabla \ln \eta^{2l} = -(2\beta D \frac{l}{\eta})\ \mathbf{e}_r \tag{4.28}$$

$$\mathbf{V}_F = -D\nabla \ln \rho_F = -D\nabla \ln F_{nl}^2 = -2\beta D(\frac{1}{F_{nl}}\frac{dF_{nl}}{d\eta})\ \mathbf{e}_r \tag{4.29}$$

$$\mathbf{V}_A = -D\nabla \ln \rho_A = -D\nabla \ln e^{-\eta} = \beta D \mathbf{e}_r \tag{4.30}$$

$$\mathbf{V}_\theta = -D\nabla \ln \rho_\theta = -D\nabla \ln \Theta^2 = -2\beta D(\frac{1}{\eta\Theta}\frac{d\Theta}{d\eta})\mathbf{e}_\theta \tag{4.31}$$

where, $\beta D = Ze^2/n\hbar$.

The dilatation energy of diffusion field is also decomposed into the corresponding four parts,

$$\mathfrak{M} = -D\nabla\bullet\mathbf{V} = -D\nabla\bullet\mathbf{V}_l - D\nabla\bullet\mathbf{V}_F - D\nabla\bullet\mathbf{V}_A - D\nabla\bullet\mathbf{V}_\theta \tag{4.32}$$

where,

$$\mathfrak{M}_l = -D\nabla\bullet\mathbf{V}_l = -\frac{D}{r^2}\frac{\partial}{\partial r}(r^2\,\mathrm{V}_l) = 2\beta^2 D^2(\frac{l}{\eta^2}) \tag{4.33}$$

$$\mathfrak{M}_F = -D\nabla\bullet\mathbf{V}_F = -\frac{D}{r^2}\frac{\partial}{\partial r}(r^2\,\mathrm{V}_F) = 2\beta^2 D^2\left[\frac{1}{F_{nl}}\frac{d^2F_{nl}}{d\eta^2} - \left(\frac{1}{F_{nl}}\frac{dF_{nl}}{d\eta}\right)^2 + \frac{2}{\eta F_{nl}}(\frac{dF_{nl}}{d\eta})\right] \tag{4.34}$$

$$\mathfrak{M}_A = -D\nabla\bullet\mathbf{V}_A = -\frac{D}{r^2}\frac{\partial}{\partial r}(r^2\,\mathrm{V}_A) = 2\beta^2 D^2(\frac{1}{\eta}) \tag{4.35}$$

$$\begin{aligned}\mathfrak{M}_\theta = -D\nabla\bullet\mathbf{V}_\theta &= -\frac{D}{r\sin\theta}\frac{\partial}{\partial\theta}(\sin\theta\,\mathrm{V}_\theta) = \frac{2\beta^2D^2}{\eta^2}\left[\frac{1}{\Theta}\frac{d^2\Theta}{d\theta^2} - \left(\frac{1}{\Theta}\frac{d\Theta}{d\theta}\right)^2 + \frac{\cot\theta}{\Theta}\frac{d\Theta}{d\theta}\right] \\ &= -\frac{2\beta^2D^2}{\eta^2}\left[l(l+1) - \frac{m^2}{\sin^2\theta}\right]\end{aligned} \tag{4.36}$$

Next, the kinetic energy of diffusion Ω, is calculated from Eq. (4.27) as follows,

$$\Omega = \frac{1}{2}\mathrm{V}^2 = \frac{1}{2}(\mathbf{V}_l + \mathbf{V}_F + \mathbf{V}_A)\bullet(\mathbf{V}_l + \mathbf{V}_F + \mathbf{V}_A) + \frac{1}{2}(\mathbf{V}_\theta \bullet \mathbf{V}_\theta)$$
$$= \frac{1}{2}(\mathrm{V}_l^2 + \mathrm{V}_F^2 + \mathrm{V}_A^2) + \mathrm{V}_l\,\mathrm{V}_F + \mathrm{V}_F\,\mathrm{V}_A + \mathrm{V}_A\,\mathrm{V}_l + \frac{1}{2}\mathrm{V}_\theta^2 \tag{4.37}$$

where, V_ℓ ,, V_A , V_F are radial diffusion components and V_θ is the polar component given by Eqs. (4.28)-(4.31), respectively.

(d) Elemental processes of dilatation mode

The dilatation mode has three components, radial, azimuthal, and polar modes, each of which is calculated below. The radial component of the dilatation mode is decomposed into three elemental processes, $\widetilde{\mathfrak{M}}_{\alpha_j}\left(n,l,m\right)$, *j=1,2,3* , as follows,

$$\mathfrak{M}_R = \mathfrak{M}_{R_1} + \mathfrak{M}_{R_2} + \mathfrak{M}_{R_3} = -D\nabla\bullet\mathbf{V}_R = -D\nabla\bullet\mathbf{V}_l - D\nabla\bullet\mathbf{V}_F - D\nabla\bullet\mathbf{V}_A \tag{4.38}$$

where, $\mathfrak{M}_{R_1}$, $\mathfrak{M}_{R_2}$ and $\mathfrak{M}_{R_3}$ are,

$$\mathfrak{M}_{R_1} = \frac{\hbar^2}{4m_e^{\,2}}(2\beta^2)(\frac{1}{F_{nl}}\frac{d^2F_{nl}}{d\eta^2} + \frac{2}{F_{nl}}\frac{dF_{nl}}{d\eta} - \frac{1}{\eta}) = -D\nabla\bullet\mathbf{V}_F - D\nabla\bullet\mathbf{V}_A + \frac{1}{2}\mathrm{V}_F^2 \tag{4.39}$$

$$\mathfrak{M}_{R_2} = -\frac{\hbar^2}{4m_e^{\,2}}(2\beta^2)(\frac{1}{F_{nl}}\frac{dF_{nl}}{d\eta})^2 = -\frac{1}{2}\mathrm{V}_F^2 \tag{4.40}$$

$$\mathfrak{M}_{R_3} = \frac{\hbar^2}{4m_e^{\,2}}(2\beta^2)\left(\frac{l}{\eta^2}\right) = -D\nabla\bullet\mathbf{V}_1 \tag{4.41}$$

The dilatation mode in θ - direction, $\mathfrak{M}_\theta$, is decomposed into three elemental processes,

$$\mathfrak{M}_\theta = \mathfrak{M}_{\theta_1} + \mathfrak{M}_{\theta_2} + \mathfrak{M}_{\theta_3} = -D\nabla\bullet\mathbf{V}_\theta \tag{4.42}$$

where, $\mathfrak{M}_{\theta i}$ for *i = 1, 2* and *3* , is given by

$$\mathfrak{M}_{\theta_1} = \frac{\hbar^2}{4m_e^{\,2}}\left(2\beta^2\right)\left(\frac{m^2}{\eta^2\sin^2\theta}\right) = \Pi_\theta + \Pi_{R3}, \tag{4.43}$$

$$\mathfrak{M}_{\theta_2} = -\frac{\hbar^2}{4m_e^{\,2}}(2\beta^2)\left[\frac{1}{\eta^2}\left(\frac{1}{\Theta_{lm}}\frac{d\Theta_{lm}}{d\theta}\right)^2\right] = -\frac{1}{2}\mathrm{V}_\theta^2, \tag{4.44}$$

$$\mathfrak{M}_{\theta_3} = \frac{-\hbar^2}{4m_e^{\,2}}\left(2\beta^2\right)\frac{l\left(l+1\right)}{\eta^2} = D\nabla\bullet\mathbf{V}_\ell - \frac{1}{2}\mathrm{V}_l^2 . \qquad (4.45)$$

where, $\Pi_\alpha = \mathfrak{M}_\alpha + \Omega_\alpha$.

The component of the dilatation mode in ϕ- angular direction vanishes and makes no contribution in the energy balance,

$$\mathfrak{M}_\varphi = 0 . \qquad (4.46)$$

(e) Elemental processes of diffusion kinetic mode

The diffusion kinetic mode has the radial, azimuthal, and polar angular components. The radial component of diffusion kinetic mode, $\Omega_{R_j}\left(n,l,m\right)$, can be broken down into four elemental processes, Ω_{Ri} for *i = 1, 2, 3* and *4* respectively,

$$\Omega_R = \Omega_{R_1} + \Omega_{R_2} + \Omega_{R_3} + \Omega_{R_4} = \frac{1}{2}(\mathrm{V}_l + \mathrm{V}_F + \mathrm{V}_A)^2 \qquad (4.47)$$

$$\Omega_{R_1} = \frac{\hbar^2}{4m_e^{\,2}}(2\beta^2)\left[-\left(1-\frac{2l}{\eta}\right)\left(\frac{1}{F_{nl}}\frac{dF_{nl}}{d\eta}\right)-\frac{l}{\eta}\right] = (\mathrm{V}_l\,\mathrm{V}_F + \mathrm{V}_F\,\mathrm{V}_A + \mathrm{V}_A\,\mathrm{V}_l) \qquad (4.48)$$

$$\Omega_{R_2} = \Omega_F = \frac{\hbar^2}{4m_e^{\,2}}(2\beta^2)\left(\frac{1}{F_{nl}}\frac{dF_{nl}}{d\eta}\right)^2 = \frac{1}{2}\mathrm{V}_F^2 \qquad (4.49)$$

$$\Omega_{R_3} = \Omega_l = \frac{\hbar^2}{4m_e^{\,2}}(2\beta^2)\left(\frac{l^2}{\eta^2}\right) = \frac{1}{2}\mathrm{V}_l^2 \qquad (4.50)$$

$$\Omega_{R_4} = \Omega_A = \frac{\hbar^2}{4m_e^{\,2}}(2\beta^2)\frac{1}{4} = \frac{1}{2}\mathrm{V}_A^2 \qquad (4.51)$$

The diffusion kinetic mode in direction θ is represented by a single component, $\Omega_{\theta 2}$, given below,

$$\Omega_\theta = \Omega_{\theta_2} = \frac{\hbar^2}{4m_e^{\,2}}(2\beta^2)\frac{1}{\eta^2}\left(\frac{1}{\Theta_{lm}}\frac{d\Theta_{lm}}{d\theta}\right)^2 = \frac{1}{2}\mathrm{V}_\theta^2 . \qquad (4.52)$$

The azimuthal component vanishes and thus does not contribute in the modal balance,

$$\Omega_{\varphi} = 0 . \qquad (4.53)$$

(f) Kinematic and dynamic characteristics of probability fluid

The probability fluid flow in the hydrogen atom exhibits interesting flow characteristics, discussed below. The dilatation of the convective velocity is expressed in term of the inner product of **u** and **V**, defined by Eq. (3.4), and is given by

$$\nabla \bullet \mathbf{u} = \frac{(\mathbf{u} \bullet \mathrm{V})}{D} = \mathrm{u}\, \mathbf{e}_{\phi} \bullet [(\mathrm{V}_{l} + \mathrm{V}_{F} + \mathrm{V}_{A})\mathbf{e}_{r} + \mathrm{V}_{\theta}\, \mathbf{e}_{r}] = 0 \qquad (4.54)$$

Thus, the convective velocity fields of all the states defined by a set of n, l, and m of a hydrogen atom are convective dilatation free. Alternatively, we write the following identity,

$$\nabla \bullet \mathbf{u} = \frac{(\mathbf{u} \bullet \mathbf{V})}{D} = \frac{\hbar}{2im_{e}} [(\nabla \psi)^{2} - (\nabla \psi^{*})^{2}] \qquad (4.55)$$

If the state of an atom is described by of a superposition of eigenfunctions each of which has the different values of, *n*, and*, l,* but the same value of m, then we can show that the above equation vanishes. Accordingly the flow is convective dilatation free.

In a convective dilatation free flow, the velocity scalar potential satisfies Laplace equation, i.e.,

$$\nabla \bullet \mathbf{u} = \nabla \bullet \nabla \phi = \nabla^{2} \phi = 0 \qquad (4.56)$$

This is a uniquely interesting property, which permits the construction of the convective field by the potential flow theory of classical hydrodynamics, whereas the density is determined by Bernoulli's equation in conjunction with the convective velocity field.

5. Atomic modal balance

Modal analysis aims to determine the sets of elemental processes which satisfy the quantum modal balance equations, (4.9) to (4.12), and to ensure that the sum of all the sets of elemental processes is equal to the total quantum potential. The procedure, in general, involves the trial and error method to properly choose prospective elemental processes according to the nature of the radial decay, i.e., r^{-s}, for s = 0, 1 and 2, as described in the modal balance equations (4.9) to (4.12). However, the elemental processes, $\mathfrak{M}_{\alpha}$ and Ω_{α_j}, involve functions such as F_{nl}, $(F_{nl})^{-1}$

$(d^2F_{nl}/d\eta^2)$, $(F_{nl})^{-1}(dF_{nl}/d\eta)$, and $(F_{nl})^{-2}(dF_{nl}/d\eta)^2$. Since these latter terms reveal no explicit functional form of radial decay, i.e., r^{-s}, the selection of appropriate elemental processes requires knowledge of the functional characteristics of these special functions in order to facilitate the correct identification of the prospective elemental processes. While the trial and error method is in general carried out by inspection, the use of the momentum equation in conjunction it offers a physical guide to the selection of elemental processes.

Detailed energetic balance of each principal mode and cross inter-coupling modes are discussed in the following sub-sections. The results of the algebraic analysis of the modal balance are summarized in Table 1.

(a) Coulomb modal balance:M $_{R1}$, Ω_{R_1}

The Coulomb potential, V_e/m_e, which is a central force field, plays a major role in radial modal balance. We select the following two elemental processes $\mathfrak{M}_{R1}$ and Ω_{R_1} for the Coulomb modal balance,

$$\begin{aligned}
&\mathfrak{M}_R^{\,v} + R_R^{\,v} = \mathfrak{M}_{R_1} + \Omega_{R_1} = \frac{\hbar^2}{4m_e^{\,2}}\left(\frac{2\beta^2}{F_{nl}\eta}\right)\left\{\eta\frac{d^2F_{nl}}{d\eta^2} + (2l+2-\eta)\frac{dF_{n\ell}}{d\eta} - (l+1)F_{nl}\right\} \\
&= -D\nabla\bullet\mathbf{V}_F - D\nabla\bullet\mathbf{V}_A + (\mathrm{V}_\ell\,\mathrm{V}_F + \mathrm{V}_F\,\mathrm{V}_A + \mathrm{V}_A\,\mathrm{V}_\ell) + \frac{1}{2}\mathrm{V}_F^2 \qquad (5.1) \\
&= \Pi_R - \Pi_\ell - \frac{1}{2}\mathrm{V}_A^2
\end{aligned}$$

where, $V_A = \beta D = Ze^2/n\hbar$, and Π_ℓ is the centrifugal potential expressed by

$$\Pi_l = \Pi_{R3} = \mathfrak{M}_{R3} + \Omega_{R3} = \frac{\hbar^2}{2m^2}\frac{l(1+l)}{r^2} \qquad (5.2)$$

In order to verify that the sum of the above two terms, $\mathfrak{M}_{R_1}$ and Ω_{R_1}, is equal to the Coulomb potential, we multiply Eq. (4.15) by $(\hbar^2/4m_e^{\,2})(2\beta^2/F_{nl}\eta)$ and subtract the resulting equation from Eq. (5.1) to prove that the sum of $\mathfrak{M}_{R_1}$ and Ω_{R_1} indeed add up to Coulomb potential, as shown below,

$$\begin{aligned}\mathfrak{M}_{R_1}+\Omega_{R_1} &= \frac{\hbar^2}{4m_e{}^2}\left(\frac{2\beta^2}{F_{nl}\eta}\right)\left\{\eta\frac{d^2F_{nl}}{d\eta^2}+(2l+2-\eta)\frac{dF_{nl}}{d\eta}-(l+1)F_{nl}\right\}\\ &-\frac{\hbar^2}{4m_e{}^2}\left(\frac{2\beta^2}{F_{nl}\eta}\right)\left\{\eta\left(\frac{d^2F_{nl}}{d\eta^2}\right)+\left(2l+2-\eta\right)\left(\frac{dF_{nl}}{d\eta}\right)+\left(n-l-1\right)F_{nl}\right\} \qquad (5.3)\\ &=-\frac{\hbar^2}{m_e{}^2}\left(\frac{2\beta^2}{F_{nl}\eta}\right)\left(nF_{nl}\right)=\frac{-\hbar^2}{4m_e{}^2}\left(\frac{2\beta^2}{\eta}\right)n=-\frac{Ze^2}{m_e r}=\frac{\mathrm{V}_e}{\mathrm{m_e}}\end{aligned}$$

where $\eta=\beta r$, and $\beta = 2\mathrm{Z}/na$, were defined in Eq. (4.14). The above energy balance also gives the following picture of momentum equilibrium. Observing that $\mathrm{V}_A = Ze^2/n\hbar$ is constant, taking the partial derivative of Eq. (5.3), with respect to r gives the dynamic equilibrium of Coulomb with the quantum force,

$$\frac{\partial(\mathfrak{M}_{R_1}+\Omega_{R_1})}{\partial r}=\frac{\partial(\Pi_R-\Pi_l-\frac{1}{2}\mathrm{V}_A^2)}{\partial r}=\frac{\partial(\Pi_R-\Pi_l)}{\partial r}=(\frac{1}{m_e})(\frac{\partial \mathrm{V}_e}{\partial r}) \qquad (5.4)$$

The above equation states that the radial quantum potential force, $\partial\Pi_R/\partial r$ minus the centrifugal force, $\partial\Pi_l/\partial r$, balances with the Coulomb force for an atom in a stationary state. Significantly, it must be pointed out that contrary to previous claims, Bohm and Hiley, (1999), for example, which state that the total quantum force, $(\partial\Pi_R+\Pi_\theta)/\partial r$, is what balances the Coulomb force, $(1/m_e)(\partial \mathrm{V}_e/\partial r)$. The latter is inconsistent with the present criterion of radial dynamic equilibrium.

From the view point of dynamic balance, we are interested to know the relative importance of the dilatation, $\mathfrak{M}_{R_1}$ and the kinetic energy Ω_{R_1} of diffusion in the Coulomb modal balance. The fractions of the quantum potential contributing to the Coulomb modal balance may remain constant or exhibit spatial variations for the selected quantum numbers *n, l,* and *m* as shown in Table 2. The relative contribution of Ω_{R_1} and $\mathfrak{M}_{R_1}$ on the Coulomb modal balance as function of radial distance is given by,

$$\gamma=\frac{\Omega_{R_1}}{\mathfrak{M}_{R_1}}=\frac{-(1-\frac{2l}{\eta})(\frac{1}{F_{nl}}\frac{dF_{nl}}{d\eta})-\frac{l}{\eta}}{\frac{1}{F_{nl}}\frac{d^2F_{nl}}{d\eta^2}+\left(\frac{2}{\eta}\right)\left(\frac{1}{F_{nl}}\frac{dF_{nl}}{d\eta}\right)-\frac{1}{\eta}}. \qquad (5.5)$$

The asymptotic values of F_{nl} and its derivatives, which appear in (5.5) are,

$$\lim_{\eta\to\infty}\frac{1}{F_{nl}}\frac{dF_{nl}}{d\eta}=\frac{n-l-1}{\eta}+O\left(\frac{1}{\eta^2}\right) \tag{5.6}$$

$$\lim_{\eta\to\infty}\frac{1}{F_{nl}}\frac{d^2F_{nl}}{d\eta^2}=O\left(\frac{1}{\eta^2}\right) \tag{5.7}$$

Using these asymptotic forms in Eq. (5.5) γ becomes,

$$\lim_{\eta\to\infty}\gamma\to n-1\,. \tag{5.8}$$

Thus, the kinetic energy of diffusion dominates over the dilation energy at higher principal quantum number in the Coulomb modal balance. Numerical analysis, detailing the Coulomb modal balance and its dependence on the quantum numbers *n*, *l* and *m*, is presented in §6.

The ratio of the contribution by the dilatation energy $\mathfrak{M}_{R_1}$ in Coulomb modal balance to the total radial dilatation energy, $\mathfrak{M}_R$, at a non-dimensional radial distance is given by

$$\sigma_{\mathfrak{M}}=\frac{\mathfrak{M}_{R_1}}{\mathfrak{M}_{\Re}}=\frac{\left\{\frac{1}{F_{nl}}\frac{d^2F_{nl}}{d\eta^2}+\left(\frac{2}{\eta}\right)\left(\frac{1}{F_{nl}}\frac{dF_{nl}}{d\eta}\right)-\left(\frac{1}{\eta}\right)\right\}}{\left\{\frac{1}{F_{nl}}\frac{d^2F_{nl}}{d\eta^2}+\left(\frac{2}{\eta}\right)\left(\frac{1}{F_{nl}}\frac{dF_{nl}}{d\eta}\right)-\left(\frac{1}{F_{nl}}\frac{dF_{nl}}{d\eta}\right)^2-\frac{1}{\eta}+\frac{l}{\eta^2}\right\}}\,. \tag{5.9}$$

By substituting asymptotic forms given by Eqs. (5.6) and (5.7) in Eq. (5.9) we find the limiting value of $\sigma_{\mathfrak{M}}$ to be,

$$\lim_{\eta\to\infty}\sigma_{\mathfrak{M}}\to 1\,. \tag{5.10}$$

This result implies that the major fraction of dilatation energy contributes to the Coulomb potential balance at large radial distances.

Similarly, the fraction of diffusion kinetic energy contributing in modal balance is

$$\sigma_{\Omega}=\frac{\Omega_{R_1}}{\Omega_R}=\frac{\left[-(1-\frac{2l}{\eta})(\frac{1}{F_{nl}}\frac{dF_{nl}}{d\eta})-\frac{l}{\eta}\right]}{\left[\left(\frac{1}{F_{nl}}\frac{dF_{nl}}{d\eta}\right)^2-\left(\frac{1}{F_{nl}}\frac{dF_{nl}}{d\eta}\right)\left(1-\frac{2l}{\eta}\right)+\left(\frac{1}{4}\right)\left(1-\frac{2l}{\eta}\right)^2\right]}. \tag{5.11}$$

The asymptotic value of σ_{Ω} vanishes, i.e., $\lim_{\eta\to\infty}\sigma_{\Omega}\to 0$. Hence the fraction of the diffusion kinetic energy contributing in the Coulomb potential diminishes at large radial distances.

(b) Vortex modal balance: Π_{θ} and Π_{l}

The vortex induced flow, u_{ϕ}, in the azimuthal angular direction for a state with magnetic quantum number m, is driven by quantum potentials Π_{θ} and $\Pi_{l}(=\Pi_{R3})$, as follows,

$$\begin{aligned}\Pi_{\theta}+\Pi_{l}&=\mathfrak{M}_{\theta_1}+\Omega_{\theta}+\mathfrak{M}_{R3}+\Omega_{R3}=\Re(n,l,m)=\frac{1}{2}u_{nlm}^2=\frac{\hbar^2}{2m_e^{\,2}}\frac{m^2}{r^2\sin^2\theta}\\&=-D\nabla\bullet\mathbf{V}_{\theta}+\frac{1}{2}\mathrm{V}_{\theta}^2-D\nabla\bullet\mathbf{V}_{l}+\frac{1}{2}\mathrm{V}_{l}^2\end{aligned} \tag{5.12}$$

The appearance of the radial potentials $\Pi_{l}(=\Pi_{R3})$ in the kinetic energy of the azimuthal motion, $u_{\phi}=u_{nlm}$, in Eq. (5.12), suggests the presence of cross inter-coupling in the modal balance of $\Pi_{\theta}(\theta,r)+\Pi_{l}(r)$, and thus requires special attention. Since cross inter-coupling also occurs in radial direction, we shall discuss these aspects together in subsection *(d)*.

(c) State quantized energy modal balance: Ω_{R_4}

The elemental process that contributes to the quantized energy is equal to the negative of a part of radial diffusion kinetic energy, $\Omega_{R_4}=\frac{1}{2}\mathrm{V}_A^2$, as shown by the following equation,

$$\Omega_{R_4}=\frac{\hbar^2}{4m_e^{\,2}}\left(2\beta^2\right)\left(\frac{1}{4}\right)=\frac{\hbar^2}{8m_e^{\,2}}(\frac{2Z}{na})^2=\frac{z^2e^2}{2m_ean^2}=\frac{z^2e^4}{2\hbar^2n^2}=-\frac{E_n}{m_e} \tag{5.13}$$

The asymptotic diffusion velocity is a constant, $\mathrm{V}_A=Ze^2/n\hbar$, and thus the quantized energy has a constant value. We shall discuss the physical explanation of the term $\Omega_{R_4}=1/2\,\mathrm{V}_A^2$ as the quantized energy in subsection *(f)*.

Another element of the state quantized energy is the non-dimensional energy scaling parameter ε. Its value can be deduced from Eq.s (4.22) and (4.23) as follows,

$$\frac{E_n}{m_e} = \mathscr{C}_n \varepsilon = (\frac{\hbar^2}{4m_e^2})(2\beta_n^2)\varepsilon = (\frac{2Z^2e^2}{m_e n^2 a})\varepsilon = -\frac{4E_n\varepsilon}{m_e}. \tag{5.14}$$

The above relation yields $\varepsilon = -\frac{1}{4}$.

The fraction of diffusion kinetic energy contributing to the quantized energy is,

$$\varepsilon_{\Omega 4} = \frac{\Omega_{R4}}{\Omega_R} = \left(\frac{1}{4}\right)\left\{\left(\frac{1}{F_{nl}}\frac{dF_{nl}}{d\eta}\right)^2 - \left(\frac{1}{F_{nl}}\frac{dF_{nl}}{d\eta}\right)\left(1-\frac{2l}{\eta}\right) + \left(\frac{1}{4}\right)\left(1-\frac{2l}{\eta}\right)^2\right\}^{-1} \tag{5.15}$$

Using the asymptotic expressions given by Eqs. (5.6) and (5.7), the above equation reduces to,

$$\lim_{\eta\to\infty} \varepsilon_{\Omega 4} = 1. \tag{5.16}$$

Thus, the majority of diffusion kinetic energy at large radial distance contributes to the quantized energy. The spatial variation of the contribution by diffusion kinetic energy on quantized energy at quantum numbers, *n, l,* and *m* is presented in §6**.**

(d) Cross inter-coupling modal balance

Three cross inter-coupling modes occur among the components of quantum potentials in the hydrogen atom are identified below.

The expression for dilatation energy, given by Eq. (3.5), can be recast in the Bernoulli's equation,

$$\begin{aligned} -D\nabla\bullet\mathbf{V} + \frac{1}{2}\mathrm{V}^2 &= \Pi_R + \Pi_\theta + \Pi_\phi = (\mathfrak{M}_R + \Omega_R) + (\mathfrak{M}_\theta + \Omega_\theta) + (\mathfrak{M}_{\phi_1} + \Omega_\phi) \\ &= K + \frac{\mathrm{V}_e}{m_e} - \frac{E}{m_e} \end{aligned} \tag{5.17}$$

The above equation can be regrouped as the sum of the following six sets of potential/energy terms,

$$(\mathfrak{M}_{R1}+\Omega_{R1}-\frac{\mathrm{V}_e}{m_e})+(\mathfrak{M}_{\theta 1}-K)+(\Omega_{R4}+\frac{E}{m_e})+(\mathfrak{M}_{R2}+\Omega_{R2})+$$
$$(\mathfrak{M}_{\theta 2}+\Omega_{\theta 2})+(\mathfrak{M}_{\theta 3}+\mathfrak{M}_{R3}+\Omega_{R3})=0 \tag{5.18}$$

Since the first three sets describe principal modal balance, as shown by Eqs., (5.3) (5.12) and (5.13), hence each set vanishes. The remaining three sets do not contribute to the principal modal balance, hence they represent the cross inter-coupling modal balance, as detailed below.

(1) Cross inter-coupling modes in vortex mode

We identify two sets of cross inter-coupling modes in Eq. (5.18), as follows,

$$\mathfrak{M}_{\theta_2}+\Omega_{\theta_2}=-\frac{1}{2}\mathrm{V}_\theta^2+\frac{1}{2}\mathrm{V}_\theta^2=0\,, \tag{5.19}$$

$$\mathfrak{M}_{\theta_3}+\Pi_{R3}=\mathfrak{M}_{\theta_3}+\mathfrak{M}_{R3}+\Omega_{R3}=\mathfrak{M}_{\theta_3}-D\nabla\bullet\mathbf{V}_l+\frac{1}{2}\mathrm{V}_l^2$$
$$=\frac{\hbar^2}{4m_e{}^2}(2\beta^2)\frac{[-l(l+1)+l(l+1)]}{r^2}=0 \tag{5.20}$$

By substituting Eqs. (5.19) and (5.20) into (5.12), we find the kinetic energy consists of the first part of the dilatation in polar angular direction, $\mathfrak{M}_{\theta_1}$, as

$$\aleph(n,l,m)=\mathfrak{M}_{\theta_1}=\frac{\hbar^2}{4m_e{}^2}(2\beta^2)\frac{m^2}{\eta^2\sin^2\theta} \tag{5.21}$$

Observe that since $\mathfrak{M}_{\theta_2}=-\Omega_{\theta_2}$, the two modes balance each other in Eq. (5.19), hence they constitute cross inter-coupling modes. Equation (5.20) expresses the cross-intercoupling between the centrifugal potential, $\Pi_l=(\Pi_{R3})$, with dilatation energy, $\mathfrak{M}_{\theta_3}$, in the polar angular direction. It is interesting to observe that the ratio of the radial diffusion kinetic energy, Ω_l, to the radial dilatation $\mathfrak{M}_l$ in the centrifugal potential Π_l is equal to the orbital angular momentum quantum number, *l*, hence the effects of the kinetic energy of diffusion become more pronounced than those of the dilatation energy in their prospective contribution to the centrifugal potential at large value of l.

(2) Cross inter-coupling modal balance in radial mode

We note that the dilatational energy, $\mathfrak{M}_{R_2}$, Eq. (4.40) and the kinetic energy of diffusion, Ω_{R_2}, (4.49) are equal but have an opposite sign, hence both processes are cross inter-coupling modes,

$$\mathfrak{M}_{R_2} + \Omega_{R_2} = -\frac{1}{2}\mathrm{V}_F{}^2 + \frac{1}{2}\mathrm{V}_F{}^2 = 0 \tag{5.22}$$

(e) Global atomic modal balance

Global modal balance among all the principal modes and the quantum potentials can be validated by demonstrating that the sum of all the elemental processes contributing to the three principal modes, Eq. (5.3) (5.12) and (5.13), is equal to the total quantum potential. This is shown below.

$$\begin{aligned}\frac{\mathrm{V}_e}{m_e} + \mathfrak{K} - \frac{E_n}{m_e} &= (\Pi_R - \Pi_{R3} - \frac{1}{2}\mathrm{V}_A^2) + (\Pi_\theta + \Pi_{R3}) + \frac{1}{2}\mathrm{V}_A^2 \\ &= \Pi_R + \Pi_\theta + \Pi_\phi = \Pi_{total}\end{aligned} \tag{5.23}$$

Here we included, $\Pi_\phi = 0$, in the quantum potential for the completeness.

We summarize the global atomic modal balance of three major types of atomic states in Table 3.

Table 3. Global atomic modal balance in hydrogen atom

States	$\frac{\mathrm{V}_e}{m_e}$	$\mathfrak{K}$	$\frac{-E_n}{m_e}$	$\frac{\mathrm{V}_e}{m_e} + \mathfrak{K} - \frac{E_n}{m_e}$
$n \neq 0, l = 0, m = 0$	$\Pi_R - \frac{1}{2}\mathrm{V}_A^2$	0	$\frac{1}{2}\mathrm{V}_A^2$	Π_{total}
$n \neq 0, l \neq 0, m = 0$	$\Pi_R - \Pi_{R3} - \frac{1}{2}\mathrm{V}_A^2$	$\Pi_\theta + \Pi_{R3}(=0)$	$\frac{1}{2}\mathrm{V}_A^2$	Π_{total}
$n \neq 0, l \neq 0, m \neq 0$	$\Pi_R - \Pi_{R3} - \frac{1}{2}\mathrm{V}_A^2$	$\Pi_\theta + \Pi_{R3}(\neq 0)$	$\frac{1}{2}\mathrm{V}_A^2$	Π_{total}

Table 3 clarifies three issues, which are raised at the outset of this paper: (1) Quantized energy is

equal to the negative of the kinetic energy of the asymptotic diffusion field in an atom at a stationary state; (2) Coulomb potential force on electron probability density fluid is balanced by the total radial potential force minus the centrifugal force. (3) Kinetic energy of vortex induced flow is provided by the sum of the components of quantum potentials in the polar angular direction Π_{θ_1} and the centrifugal barrier potential Π_{l_1}.

(f) Physical significance of the quantized energy

A rather remarkable result is that the negative of kinetic energy of asymptotic diffusion, $\Omega_{R_4} = 1/2\,\mathrm{V}_A^2$, is equal to the quantized energy, as given by Eq. (5.13). Moreover, its value remains constant with respect to radial coordinate. These two facts merit further elucidation. First note that the asymptotic density distribution ρ_{A} has a log value of,

$$\ln \rho_A = -\eta = -\beta r \tag{5.24}$$

Since this is a linear function of the radial coordinate, r, multiplied by a constant coefficient β, hence the asymptotic diffusion velocity, V_A, is a constant equal to $D\beta = Z_e^2/n\hbar$. The physical significance of the asymptotic diffusion velocity is elucidated by the observation that the density distribution of probability fluid is governed by the Coulomb force, which attracts the fluid inward on one hand, and the quantum potential force that disperses the fluid outward on the other, see figure 1. Indeed, we show that the asymptotic density distribution depends on the relative preponderance of the absolute value of the characteristic Coulomb potential V_e^* and quantum potential, Π^*, both measured at the Bohr radius Π^*, as follows,

$$\rho_A = \exp(-\beta r) = \exp(-\frac{8}{n})(\frac{4\hbar^2}{m_e a^2})(\frac{r}{a}) = \exp(-\frac{8}{n})(\frac{\mathrm{V}_e^*}{m_e \Pi^*})(\frac{r}{a}) \tag{5.25}$$

where $\mathrm{V}_e^* = (ze^2/a)$ and $\Pi^* = 4\hbar^2/m_\theta^2 a^2$ respectively. The ratio of the two characteristic potentials $\mathrm{V}_e^*/m_e\Pi^*$ is equal to $z/4$. For a hydrogen atom $z=1$, thus the ratio of two characteristic potentials is 1 to 4.

It is noteworthy to mention that the linear dependence of the logarithm of the asymptotic density with respect to the radial coordinate, as shown above, gives a constant diffusion velocity, $\mathrm{V_A}$, which in turn yields a constant kinetic energy of diffusion, given by,

$$\left(\frac{1}{2}\right)\mathrm{V}_A{}^2=\left(\frac{\hbar^2}{4m_e{}^2}\right)\left(\frac{1}{2}\right)\left(\frac{\partial \ln e^{-\eta}}{\partial r}\right)^2=\left(\frac{\hbar^2}{4m_e{}^2}\right)\left(\frac{\beta^2}{2}\right)=\frac{z^2e^4}{2\hbar^2n^2} \tag{5.26}$$

We have thus established the following dynamic energetic relationship between the quantized energy with the kinetic energy of the asymptotic diffusion process:

$$\frac{E_n}{m_e}=-\Omega_{R_4}=-\frac{1}{2}\mathrm{V}_A{}^2 \tag{5.27}$$

The fact that the kinetic energy of gradient induced asymptotic diffusion velocity field is equal to the negative of the quantized energy bears some generality in quantum systems with a central force field with the asymptotic potential for large radial distances, which behaves like r^{-1}. For example, our recent studies show that in a diatomic molecule with a inter-atomic potential, *U,* described by the central field, $A/r^2 - B/r$, the negative of kinetic energy of the asymptotic diffusion is also equal to the quantized energy. On the other hand, however, we have found that the zero-point energy in a three dimensional harmonic oscillator, which has a potential kr^2 , is equal to the dilatation energy of the asymptotic diffusion velocity field.

6. Fluid mechanical and electronic structure of a hydrogen-like atom

In this section we present the results of numerical analysis of the quantum fluid mechanical characteristics of the modal balance, quantized energy and the structures of a hydrogen atom at selected states. The relative contribution of each elemental process on modal balance is also examined.

(a) Coulomb modal balance, fluid mechanical and electronic structures

The general energetic characteristics of Coulomb modal balance for selected quantum numbers are presented in figures 2~6. The Coulomb modal balance of Eq. (5.3) can be recast into the form, in which the Coulomb potential is normalized,

$$\frac{2Z}{n^2}(\widetilde{\mathfrak{M}}_{R_1}+\widetilde{\Omega}_{R_1})=-\frac{1}{\xi} \quad , \tag{6.1}$$

where $\xi = \frac{r}{a} = \frac{\eta}{(2Z/n)}$. The analytical expressions of the spatial distributions of $\widetilde{\mathfrak{M}}_{R_1}$ and $\widetilde{\Omega}_{R_1}$, and the relative contribution of two processes $\widetilde{\Omega}_{R_1}/\widetilde{\mathfrak{M}}_{R_1}$ for selected states are summarized in Table 2.

(1) Fractional and complementary modal balances.

Close examination of Table 2 and figures 2-6 suggests that there are, in general, two types of Coulomb modal balance: fractional and complementary balances. In the former case, each elemental process, i.e., $\widetilde{\mathfrak{M}}_{R_1}$ and $\widetilde{\Omega}_{R_1}$, assumes a fraction of the Coulomb potential. Remarkably, the latter fraction turns out to be $\tilde{\mathfrak{M}}_{R_1}/\tilde{\mathfrak{D}} = 1/n$, $\widetilde{\Omega}_{R_1}/\widetilde{\mathfrak{D}} = (n-1)/n$, and $\gamma = \widetilde{\Omega}_{R_1}/\tilde{\mathfrak{M}}_{R_1} = n-1$ throughout the space of range $0 < r < \infty$. The fractional balance occurs in those states wherein the orbital quantum number meets the following condition,

$$l = \text{n} - 1 \quad \text{for all values of n and m} \tag{6.2}$$

For example, the states, $|nlm\rangle = |100\rangle, |210\rangle, |21\pm1\rangle, |320\rangle, |32\pm1\rangle$, and $|32\pm2\rangle$, exhibit the fractional balance as shown in Table 2 and selected numerical examples are given in figures 2, 4 and 6.

From the expression, $\gamma = n-1$, we conclude that the dilatation plays a major role in the Coulomb modal balance for the ground state, whereas the diffusion kinetic energy becomes the dominating balancing mechanism for $n > 2$, see figure 7. The above results, $\gamma = \widetilde{\Omega}_{R_1}/\tilde{\mathfrak{M}}_{R_1} = n-1$, and the ratio, $\Omega_l / \mathfrak{M}_l = \widetilde{\Omega}_{R_3}/\widetilde{\mathfrak{M}}_{R_3} = l$, discussed in section 5*(d),* suggest that at higher quantum numbers n and l, the diffusion kinetic energy plays a greater role in dynamic and energetic atomic modal balance than dilatation mode.

In a complementary balance mode, the energy of each elemental process, i.e., $\widetilde{\mathfrak{M}}_{R_1}$ and $\widetilde{\Omega}_{R_1}$, is not a constant fraction of the Coulomb potential but varies in space as shown in Table 2 and figures 3, and 5. The spatial variation in γ also has singular behavior at the location where $\widetilde{\mathfrak{M}}_{R1}$ vanishes, as shown in figures 8. However, at a large radial distances where $r/a \to \infty$, $\widetilde{\mathfrak{M}}_{R_1}/\widetilde{\mathfrak{D}} \to 1/n$, and $\widetilde{\Omega}_{R_1}/\widetilde{\mathfrak{D}} \to (n\text{-}1)/n$. These ratios are the same as those of the fractional balance mode described

above. The complementary balance pattern occurs in the states where the condition of Eq. (6.2) is not met, for example, in the states $|200\rangle$, $|300\rangle$, and $|310\rangle$ and two examples are shown in figures 3 and 5.

(2) Singularities in complementary balance distributions.

The spatial distributions of the energies of an elemental process exhibit interesting behaviors at the nodal singularities where the dilatation and diffusion kinetic energies diverge. Since the Laguerre polynomial F_{nl} has the maximum of n-1 singularities, there are corresponding numbers of singularities where the divergence phenomena occur. For example, the state $|200\rangle$, n=2, has a singularity at $\xi = 2$ as shown in figure 3, whereas the state $|300\rangle$ has two singularities at $\xi \sim 2$, and $\xi \sim 7$, shown in figure 5. The quantities $\widetilde{\mathfrak{M}}_{R_1}$ and $\widetilde{\Omega}_{R_1}$ in the $|200\rangle$ state exhibit singularities at $\xi = 2$, which are shown in figure 3, and will be discussed. The probability fluid diffuses outward from the interior region, i.e., $\xi^- < 2$, where $R_{20} > 0$. The diffusion velocity, defined in Eq. (3.1), increases as the probability fluid approaches the singularity. The expanding flow is accompanied by a large value of negative dilatation energy. The density reduction continues toward the singular point where the diffusion velocity becomes infinite and the density reaches zero. The diffusion kinetic energy diverges to positive infinity, whereas the dilatation approaches negative infinity at $\xi = 2$. However, as ξ slightly exceeds 2, say ξ=2^+, the density of probability fluid increases in outward direction, and hence the fluid diffuses inward to the nodal point. At $\xi = 2^+$ the diffusion velocity approaches negative infinity, and thus the kinetic energy diverges. This abrupt change in the direction and magnitude of diffusion velocity from positive infinity to negative infinity is anticipated because of the vanishing inertia of the fluid. Likewise, a sudden change in the dilatation from negative infinity to a finite negative value is achieved at $\xi = 2^+$. A large deceleration, experienced at $\xi = 2^+$, yields a positive dilatation energy. Hence, upon crossing the ξ=2 singular point, the dilatation energy, $\widetilde{\mathfrak{M}}_{R_1}$, increases rapidly to a finite but negative value. The same divergence phenomena are observed at other singularity points for the states $|300\rangle$, shown in figure 5.

It is interesting to note that although the specific kinetic energy of diffusion and the dilatation energy per unit mass possess divergent singularities their corresponding energies per unit volume,

$\rho\mathfrak{M}_{R_1}$ and $\rho\Omega_{R_1}$, do not since the probability density vanishes more rapidly than the energies diverge at the singularity. That is,

$$(\rho\mathfrak{M}_{R_1})_{\text{sing}} \sim F_{nl}\frac{d^2F_{nl}}{d\eta^2}+\frac{2}{\eta}F_{nl}\frac{dF_{nl}}{d\eta}-\frac{1}{\eta}F_{nl}{}^2=0\ , \tag{6.3}$$

$$(\rho\Omega_{R_1})_{\text{sing}} \sim \left(1-\frac{2l}{\eta}\right)F_{nl}\frac{dF_{nl}}{d\eta}-\frac{1}{\eta^2}F_{nl}{}^2=0\ , \tag{6.4}$$

where the subscript "sing" implies an evaluation at the singularity point.

(3) Fractional contribution of the energy of elemental processes.

The fractions of the dilatation energy $\sigma_{\mathfrak{M}}=\widetilde{\mathfrak{M}}_{R_1}/\widetilde{\mathfrak{M}}_R$ and diffusion kinetic energy $\sigma_{\Omega}=\widetilde{\Omega}_{R_1}/\widetilde{\Omega}_R$, for selected states, $|100\rangle$, $|210\rangle$, and $|300\rangle$, are plotted in figures 2, 4, and 9, respectively. In general, the fractional contributions are spatially dependent, with the exception of the special case, $|200\rangle$, in which $\widetilde{\mathfrak{M}}_{R_1}/\widetilde{\mathfrak{M}}_R$ and $\widetilde{\Omega}_{R_1}/\widetilde{\Omega}_R$ remain constant throughout the space.

The distributions of $\varepsilon_{R_4}=\widetilde{\Omega}_{R_4}/\widetilde{\Omega}_R$ for the states $|100\rangle$, $|210\rangle$ and $|300\rangle$ are shown in figures 2, 4, and 10, respectively. Note that since the asymptotic value of $\varepsilon_{R_4}=\widetilde{\Omega}_{R_4}/\widetilde{\Omega}_R$ at a large radial distances is unity, see Eq. (5.16), all the dilatation energy contributes to the quantized energy.

(b) Vortex modal balance and core structure

When the magnetic quantum number *m* is associated with a bound state a line vortex is present in the core of the atom and extends from $-\infty$ to ∞ along the z-axis as shown in figures 11, 12 and 13. The flow field induced by a vortex, which is superimposed on the Coulomb field, makes the atomic core structure rather complex in the vicinity of the nucleus. A comparison of the relative magnitude of, $\mathfrak{K}$, and $\mathfrak{D}$, suggests that there are two different types of core structures depending on the magnetic quantum number. The first type is the Coulomb potential dominated electronic structure that occurs under any principal quantum number *n*, and orbital angular momentum quantum number *l*, but only when the magnetic quantum number is zero, $m=0$. The second type is the composite core structure, which consists of a region dominated by the vortex induced core flow and the Coulomb potential dominated outer region as shown in figures 11, 12, and 13. The

latter structure occurs at bound state values of *l, n*, and *m*. Two regions of the composite structure are separated by a critical radius, r_c, which is defined by the equality of $\mathfrak{K}$ with $\mathfrak{D}$. The critical radius, shown in figure 11, is given explicitly by

$$r_c(\theta) = \frac{m^2 a}{2Z} \frac{1}{\sin^2 \theta}. \tag{6.5}$$

The kinetic energy of the vortex-induced flow is greater than the Coulomb potential in the interior region r < r_c, whereas the opposite is true in the exterior region r > r_c. The critical radius r_c depends on the magnetic quantum number *m* and is independent of *n* and ℓ. We compare the critical radius with the expected value of the radial distance of the electron from the nucleus, given by ,

$$\langle r \rangle_{nl} = \iiint r^3 R_{nl}(r)^2 Y_{lm}^2(\theta,\varphi) \sin\theta d\theta d\varphi dr = \frac{a}{2z}\left[3n^2 - l(l+1)\right]. \tag{6.6}$$

In order to examine the effects of the vortex-induced flow on the value of $\langle r \rangle_{nl}$ we consider the limiting state, characterized by the largest magnetic quantum number, at a principal quantum number *n*. Let $l = l_{max} = n-1$, and $|m| = m_{max} = l_{max} = n-1$. The ratio of r_c to $\langle r \rangle_{nl}$ is ,

$$\frac{r_c}{\langle r \rangle_{nl}} = \frac{\frac{(n-1)^2}{\sin^2\theta}}{\left[3n^2 - n(n-1)\right]} = \frac{(n-1)^2}{(2n^2+n)\sin^2\theta}. \tag{6.7}$$

This ratio is plotted in figure 11 for the state $|433\rangle$. The region marked by a darker color is the vortex dominated inner core whereas the exterior region, in a lighter color, is Coulomb potential dominated. The size of the inner vortex core is *0.234* $\langle r \rangle_{43}$. The core size increases with an increase in the principal quantum number, which is seen in figure 12. It reaches a maximum value of $0.5\langle r \rangle_{n,n-1}$ when $n \to \infty$, at the state of ionization. Thus, the inner core of high magnetic quantum number is circulation flow dominated in contrast to a stagnant inner Coulomb core for the case of *m* = 0. However, it is noted that the structure described above is not valid within the spherical region of the radius of $(m_e/m_p)r_e$, centered at the origin, figure 13, because of the approximation made that the nucleus is located at the center-of-mass, which coincides with the origin of the coordinate, as discussed previously.

7. Conclusions

Based on the quantum diffusive fluid dynamics formalism, we examined the quantum mechanical significance of quantized energy, and dynamic equilibria of an electron among the Coulomb force field, the vortex induced flow and quantum potential in a hydrogen atom. In our model, a hydrogen atom in a stationary state is envisioned as an electron probability fluid attracted by the Coulomb potential field induced by the positively charged nucleus located at the origin coinciding with the center of the mass of two particles. Fundamental characteristics of quantum potential, the key internal potential for the energetic and dynamic equilibria in an atom, are examined through the dependence of the potential on the diffusion velocity field created by the non-uniform spatial distribution of the probability density in a stationary atomic state. The quantum potential field is classified on the basis of the four different types of density functions: ρ_A the asymptotic diffusion due to the asymptotic density distribution; ρ_F , the Laguerre diffusion induced by the Laguerre function type distribution; ρ_l , the power law diffusion due to the orbital angular distribution function ; and ρ_θ, the polar angular diffusion induced by density distribution in polar angular direction. Each diffusion field exhibits a non-uniform spatial distribution that creates the quantum potential. The latter potential consists of the dilatation and kinetic energies, whose spatial gradient yields a quantum force. The global energetic bearing diffusion process of the electron probability fluid is comprised of the sum of elemental processes. The quantum energetics of these elemental processes plays a major role in the modal balance between the quantum potential with each principal mode: quantized energy, Coulomb potential mode, and vortex induced flow mode.

Modal balance analysis predicted that the quantized energy is equal to the negative of the kinetic energy of asymptotic diffusion process of the probability fluid and is given by $E_n/m_e = -(1/2)\ V_A^2$. The analysis also gives a fundamental physical explanation of why the energy of eigenstate has a constant value, as summarized below. Since the logarithm of the asymptotic density $ln\rho_{An} = -\beta_n r$, is a linear function of the radial coordinate, the asymptotic diffusion velocity , $V_A = -Ddln\rho_{An}/dr = (ze^2/n\ \hbar)$, takes on a constant value for each quantum state n. Thus, based on the result of modal analysis, $E_n/m_e = -(1/2)\ V_A^2$, the quantized energy has a constant value, i.e., $E_n/m_e = -(1/2)\ (ze^2/n\ \hbar)^2$. It is noteworthy to point out that the classical law of equipartition of energy ceases to apply in an atomic energy balance. We found that not all the kinetic energies of

diffusion contribute equally into quantized energy. For example, the kinetic energy of diffusion in polar angular direction does not add up to the quantized energy because the former energy is balanced by an equal part of the dilatation energy. Furthermore, the kinetic energy of diffusion in azimuthal angular direction is zero, and thus yields no contribution to the quantized energy. Modal analysis reveals that the Coulomb attractive force, F_C, is balanced with an equal but opposite quantum force, $F_Q = F_R - F_1 = \partial(\Pi_R - \Pi_1)/\partial r$, to preserve radial equilibrium, and thus prevents the electron from falling on the nucleus. The latter result suggests that some of the previously held concepts, claiming the Coulomb force being balanced by the total quantum potential force $\partial\Pi_{\text{Total}}/\partial \text{r}$, or by the centrifugal force alone, are invalid.

It was also found that the diffusion kinetic energy dominates over the dilatation energy for relatively large principal and angular momentum numbers, except in the ground state. As a result, an atom in an excited state is portrayed as a diffusive probability fluid with high diffusion kinetic energy in comparison of the dilatation energy.

A uniquely interesting fluid dynamics feature of a hydrogen atom with a finite magnetic quantum number is the presence of a line vortex along the polar axis. The vortex-induced flow is found to be driven by the sum of the quantum potential due to the polar diffusion Π_θ and centrifugal potential, Π_l. However, only a part of polar dilatation, $\mathfrak{M}_{\theta_1}$, provides the kinetic energy of the vortex induced flow. The remaining energies are balanced with cross inter-coupling modes, and thus do not contribute in the principal modal balance. Specifically, the part of the polar dilatation, $\mathfrak{M}_{\theta_3}$ canceled with the centrifugal barrier potential Π_l.

By combining the electrostatic and fluid dynamic features, as described above, a hydrogen atom with a finite magnetic quantum number is envisioned as a fluid structure having a line vortex-flow with a dominant core that extends beyond the Bohr radius along the polar axis. The electrostatic potential becomes dominant in the region exterior of the vortex core, as shown in figure.13. For an atom with m = 0, the vortex structure is absent, and the atom has a Coulomb potential dominated core. Our model approximated the nucleus to be located at the center-of-mass between the proton and electron. The latter approximation, however, places a limit on the validity of model: the solution is invalid within the spherical region of the radius $\text{r} = (m_e/m_p)r_e$, where r_e is the electron coordinate measured from the center-of-mass, as shown in figure 13.

Modal balance analysis shows a number of unique features of quantum potential in a hydrogen atom. First of all, Bohm's description of non-locality of the quantum potential is indeed observed but in a rather discriminate manner. Of all the elemental processes of the quantum potential in a hydrogen atom, the kinetic energy due to the asymptotic diffusion, $\Omega_A = ½ V_A^2$, is constant throughout the full spatial domain and henceforth falls in the Bohm's characterization of non-local potential that does not fall-off with distance.

It is interesting to mention that in our recent studies, we also arrived at a conclusion that the Bohmian non-local dilatation energy, $\mathfrak{M}_A$, for a harmonic oscillator with a spring force potential, which is proportional to the square of a position coordinate, is equal to the specific zero-point energy, whereas the sum of both non-local kinetic energy and dilatation energy gives the n-th quantized energy. Secondly, there are elemental processes of quantum potential, which do not exhibit non-local behaviors. For example, all the dilatation energy and the kinetic energy of diffusion, with the exception of asymptotic diffusion, in a hydrogen atom do not exhibit non-local behavior, i.e., the effects of the quantum potential decay with distance. These latter parts of quantum potential contribute in the local dynamic equilibria associated with the Coulomb force, centrifugal force, and vortex induced flow.

It is relevant to mention that the results obtained from the present study preserve the same level of knowledge as rendered by standard quantum mechanics. This is so because the conservation equations of quantum fluid dynamics, which are used in the present modal balance equations, are formulated from the Schrödinger's equation through Hamilton-Jacobi transformation. Additionally, the solution of Schrödinger's equation for a hydrogen atom has been used to construct the solution of the present modal balance problem. The merit of the present approach and its results are, however, in the provision of the physical interpretation of quantum mechanical energetic and dynamic equilibria of an atom in the framework of the quantum theory of motion.

It is remarkable to conclude that within the framework of a quantum fluid description, results from a spectrum of interesting problems recently investigated, suggest that the quantum energetic balance, dynamic equilibria, and the organized structures of the atoms, molecules and many-particle systems, are manifestly governed by the quantum potentials of the sets of elemental processes associated with quantum diffusion provoked by non-uniform probability density distribution in quantum systems with an external force field and interaction potentials. The propositions, described above, are the potential areas of future research for their validation. The

conclusion, drawn above, appears to be in full accordance with Holland's profound view that "this new (quantum) theory of motion introduces a new conception of matter, which describing that the internal potential is an organizational or self-referential form of energy which brings about an inner tension in a the material system to which the mass points respond", Holland (1993).

The author acknowledges the supports by the National Science Council, Taiwan, under NSC 92 -2212-E006-086 and USAFOSR under AOARD-034039. I would like to thank for helpful discussions and comments with Professor S.H. Lin, Professor C.T. Chen, and Dr Steve Lottes. Special thank is due to Professor Frank L. Madarasz who brought the present work to the attention of U.S. Air Force Office of Scientific Research, and who read and critiqued the final manuscript rendering valuable comments.

References

Aspect, A., Dalibard, J., & Rodger, G. 1982 *Experimental test of Bell's inequalities using time-varying analyzer.* Phys. Rev. Lett., **49,** 1804-1807.

Bacciagaluppi, G. 1998 *Nelsonian mechanics revisited.* quant-ph/9811040 v1 1-19

Belinfante, F. J. 1973 *A survey of hidden-variables theories.* Oxford: Pergamon Press.

Bell, J. S. 1966 *On the problem of hidden variables in quantum mechanics.* Rev. of Modern Phys., 38, 447.

Berndl, K., Daumer, M., Durr, D., Goldstein, S., and Zanghi, N. 1995 *A survey of Bohmian mechanics.* Il Nuvo Cimento **110 B,** 737-750.

Bohm, D. 1952a *A suggested interpretation of quantum theory in terms of "hidden" variables. I* Phys. Rev. **85**, 166-179.

Bohm, D. 1952b *A suggested interpretation of quantum theory in terms of "hidden" variables. II* Phys. Rev. **85**, 180-189.

Bohm, D. & Hiley, B. J. 1999 *The Undivided Universe*. London: Routledge.

Broglie, L. de 1928 *La nouvelle dynamique des quanta' in Electrons et photons*. Rapports et discussions du cinquieme conseil de physique Solvay. Gauthier-Villars. 105-132.

Carlen, E. 1984 *Conservative diffusions*. Communications in Mathematical physics **94,** 293-315.

Chiu, H. H. 2002 *Quantum fluid dynamics and computational quantum fluid dynamics*. The 9th National Computational Fluid Dynamics Conference. Tainan, Taiwan. 30-48.

Comisar, G. G. 1965 *Brownian-Motion Model of Nonrelativistic Quantum Mechanics.*

Phys. Rev. **138**, B 1332

Ghosh, S.K. & Deb, B. M. 1982 *Densities, Density-functionals and electron fluids.* Physics Reports (Review Section of Physics Letter) **92,** 1, 1-44, North-Holland Publishing Company.

Holland, P. R. 1993 *The quantum theory of motion.* Cambridge University Press.

Kershaw, D. 1964 *Theory of Hidden Variables.* Phys. Rev. **136**, B 1850

Landau, L. D. & Lifshitz, E. M. 1985. *Quantum mechanics*. Oxford: Pergamon Press.

Nelson, E. 1966 *Derivation of the Schrödinger equation from Newtonian mechanics.* Phys. Rev. **150**, 1079-1085

Nelson, E. 1985 *Quantum fluctuation.* Princeton University Press.

Table 1. Dilatation, $\mathfrak{M}$, and diffusion kinetic energy, Ω, of quantum elemental processes in hydrogen atom

$\Pi(n\ell m)$	$\mathfrak{M}(n\ell m)=\frac{\hbar^2}{4m_e^{\,2}}\left\{\frac{1}{r^2}\frac{\partial}{\partial r}(r^2\frac{\partial}{\partial r}\ell n\rho_{n\ell m})+\frac{1}{r^2\sin\theta}\frac{\partial}{\partial\theta}(\sin\theta\frac{\partial}{\partial\theta}\ell n\rho_{n\ell m})+\frac{1}{r^2\sin^2\theta}\frac{\partial^2}{\partial\varphi^2}(\ell n\rho_{n\ell m})\right\}$ $\Omega(n\ell m)=\frac{\hbar^2}{4m_e^{\,2}}\frac{1}{2}\left[(\frac{\partial\ell n\rho_{n\ell m}}{\partial r})^2+\frac{1}{r^2}(\frac{\partial\ell n\rho}{\partial\theta})^2+\frac{1}{r^2\sin^2\theta}(\frac{\partial\ell n\rho_{n\ell m}}{\partial\varphi})^2\right]\Big\}$			
j	1	2	3	4
$\mathfrak{M}_{R_j}(n\ell m)$	$\frac{\hbar^2}{4m_e^{\,2}}(2\beta_n^{\,2})(\frac{1}{F_{n\ell}}\frac{d^2F_{n\ell}}{d\eta^2}+\frac{2}{\eta F_{n\ell}}\frac{dF_{n\ell}}{d\eta}-\frac{1}{\eta})$ Coulomb mode	$-\frac{\hbar^2}{4m_e^{\,2}}(2\beta_n^{\,2})(\frac{1}{F_{n\ell}}\frac{dF_{n\ell}}{d\eta})^2$ Intercoupling mode	$\frac{\hbar^2}{4m_e^{\,2}}(2\beta_n^{\,2})\left(\frac{\ell}{\eta^2}\right)$ Intercoupling mode	0
$\Omega_{R_j}(n\ell m)$	$\frac{\hbar^2}{4m_e^{\,2}}(2\beta_n^{\,2})\left[-(1-\frac{2\ell}{\eta})(\frac{1}{F_{n\ell}}\frac{dF_{n\ell}}{d\eta})-\frac{\ell}{\eta}\right]$ Coulomb mode	$\frac{\hbar^2}{4m_e^{\,2}}(2\beta_n^{\,2})(\frac{1}{F_{n\ell}}\frac{dF_{n\ell}}{d\eta})^2$ Intercoupling mode	$\frac{\hbar^2}{4m_e^{\,2}}(2\beta_n^{\,2})\left(\frac{\ell^2}{\eta^2}\right)$ Intercoupling mode	$\frac{\hbar^2}{4m_e^{\,2}}(2\beta_n^{\,2})\frac{1}{4}$ State energy mode
$\mathfrak{M}_{\theta_j}(n\ell m)$	$\frac{\hbar^2}{4m_e^{\,2}}(2\beta_n^{\,2})(\frac{m^2}{\eta^2\sin^2\theta})$ Vortex mode	$-\frac{\hbar^2}{4m_e^{\,2}}(2\beta_n^{\,2})\left[\frac{1}{\eta^2}\left(\frac{1}{\Theta_{\ell m}}\frac{d\Theta_{\ell m}}{d\theta}\right)^2\right]$ Intercoupling mode	$\frac{-\hbar^2}{4m_e^{\,2}}(2\beta_n^{\,2})\frac{\ell(\ell+1)}{\eta^2}$ Intercoupling mode	0
$\Omega_{\theta_j}(n\ell m)$	0	$\frac{\hbar^2}{4m_e^{\,2}}(2\beta_n^{\,2})\left[\frac{1}{\eta^2}\left(\frac{1}{\Theta_{\ell m}}\frac{d\Theta_{\ell m}}{d\theta}\right)^2\right]$ Intercoupling mode	0	0
$\mathfrak{M}_{\phi_j},\Omega_{\varphi_j}$	0	0	0	0

$\beta_n=\frac{2Z}{na}$, a=Bohr radius$=\frac{\hbar^2}{m_e e^2}$, n=principal quantum number, ℓ=orbital angular momentum quantum number, m=magnetic quantum number

Table 2. Modal energy balance of hydrogen atom at selected states

	Coulomb mode $\mathfrak{M}_{R_1}+\Omega_{R_1}=\mathfrak{D}$			Vortex mode $\mathfrak{M}_{\theta_1}=\mathfrak{K}$	State energy mode $\Omega_{R_4}=-E_n/m_e$
	Elemental process energy		Energy ratio	Elemental process energy	Elemental process energy
State	$\mathfrak{M}_{R_1}^{\mathfrak{D}}/\mathfrak{D}$	$\Omega_{R_1}^{\mathfrak{D}}/\mathfrak{D}$	$\Omega_{R_1}^{\mathfrak{D}}/\mathfrak{M}_{R_1}^{v}$	$\mathfrak{M}_{\theta_1}=\mathfrak{K}$	$\Omega_{R_4}=-E_n/m_e$
$\lvert 100\rangle$	-1	0	0	0	$\frac{\hbar^2}{4m_e^2}(2\beta_1^2)\frac{1}{4}$
$\lvert 200\rangle$	$-\frac{1}{2}\frac{\eta-4}{\eta-2}$	$-\frac{\eta}{2(\eta-2)}$	$\frac{\eta}{\eta-4}$	0	$\frac{\hbar^2}{4m_e^2}(2\beta_2^2)\frac{1}{4}$
$\lvert 210\rangle$	$-\frac{1}{2}$	$-\frac{1}{2}$	1	0	$\frac{\hbar^2}{4m_e^2}(2\beta_2^2)\frac{1}{4}$
$\lvert 21\pm1\rangle$	$-\frac{1}{2}$	$-\frac{1}{2}$	1	$\frac{\hbar^2}{4m_e^2}(2\beta_2^2)\frac{1}{\eta^2\sin^2\theta}$	$\frac{\hbar^2}{4m_e^2}(2\beta_2^2)\frac{1}{4}$
$\lvert 300\rangle$	$-\frac{1}{3}(\frac{\eta^2-10\eta+18}{\eta^2-6\eta+6})$	$-\frac{2}{3}(\frac{\eta^2-4\eta}{\eta^2-6\eta+6})$	$-\frac{2(\eta^2-4\eta)}{\eta^2-10\eta+18}$	0	$\frac{\hbar^2}{4m_e^2}(2\beta_3^2)\frac{1}{4}$
$\lvert 310\rangle$	$-\frac{1}{3}(\frac{\eta-6}{\eta-4})$	$-\frac{2}{3}(\frac{\eta-3}{\eta-4})$	$\frac{2(\eta-3)}{\eta-6}$	0	$\frac{\hbar^2}{4m_e^2}(2\beta_3^2)\frac{1}{4}$
$\lvert 31\pm1\rangle$	$-\frac{1}{3}(\frac{\eta-6}{\eta-4})$	$-\frac{2}{3}(\frac{\eta-3}{\eta-4})$	$\frac{2(\eta-3)}{\eta-6}$	$\frac{\hbar^2}{4m_e^2}(2\beta_3^2)\frac{1}{\eta^2\sin^2\theta}$	$\frac{\hbar^2}{4m_e^2}(2\beta_3^2)\frac{1}{4}$
$\lvert 320\rangle$	$-\frac{1}{3}$	$-\frac{2}{3}$	2	0	$\frac{\hbar^2}{4m_e^2}(2\beta_3^2)\frac{1}{4}$
$\lvert 32\pm1\rangle$	$-\frac{1}{3}$	$-\frac{2}{3}$	2	$\frac{\hbar^2}{4m_e^2}(2\beta_3^2)\frac{1}{\eta^2\sin^2\theta}$	$\frac{\hbar^2}{4m_e^2}(2\beta_3^2)\frac{1}{4}$
$\lvert 32\pm2\rangle$	$-\frac{1}{3}$	$-\frac{2}{3}$	2	$\frac{\hbar^2}{4m_e^2}(2\beta_3^2)\frac{4}{\eta^2\sin^2\theta}$	$\frac{\hbar^2}{4m_e^2}(2\beta_3^2)\frac{1}{4}$

$\beta_n=\frac{2Z}{na}$ and $\eta=\beta_n r$

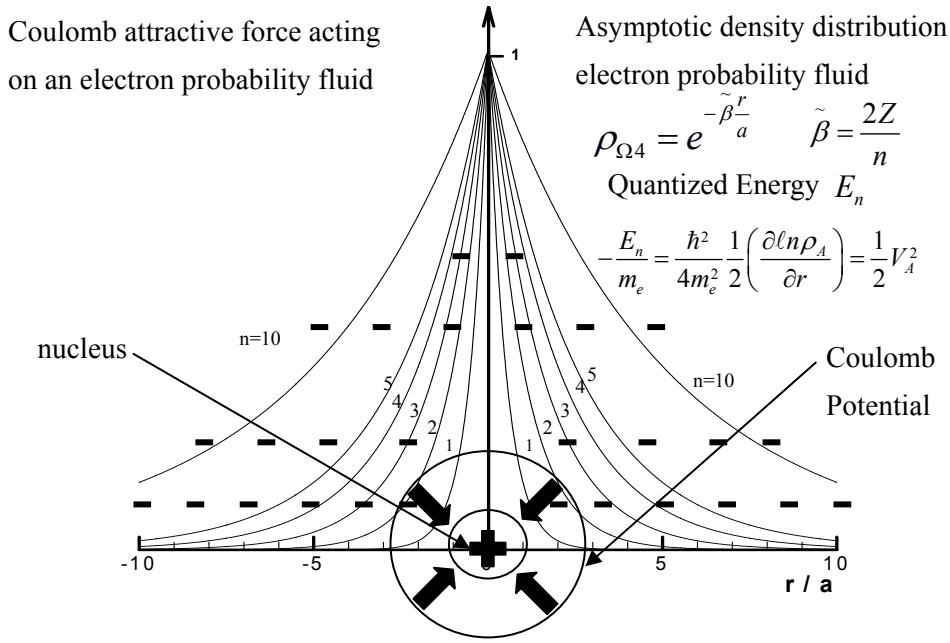

Figure 1. Quantized energy is the diffusion kinetic energy of a negatively charged probability fluid under the asymptotic density distribution formed by the Coulomb attractive force

H.H.Chiu

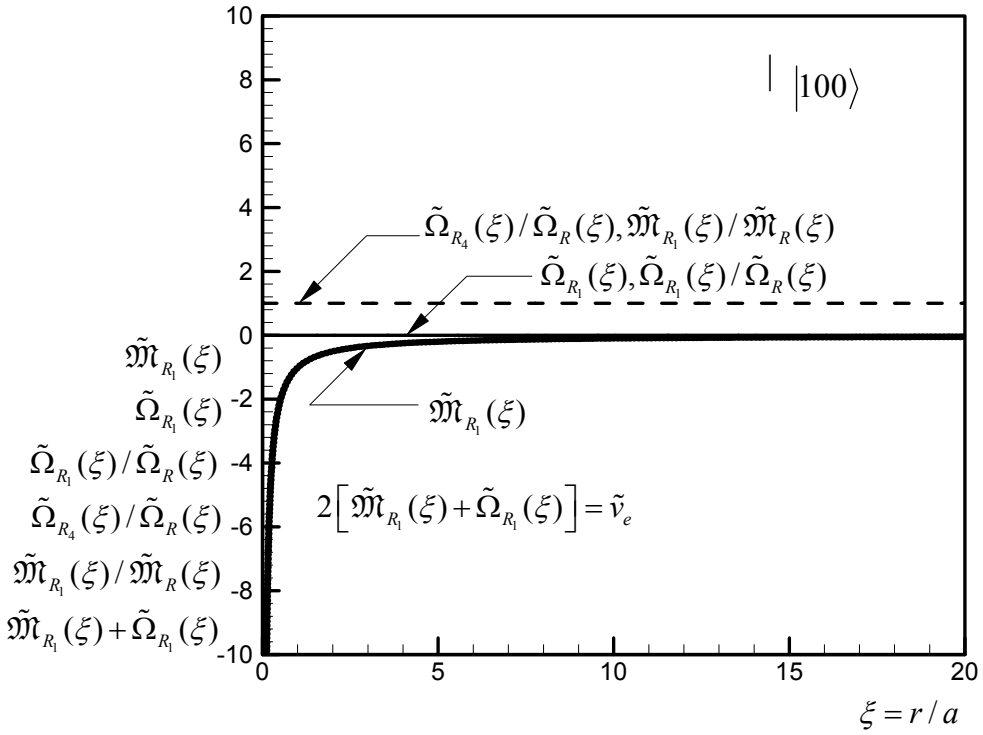

Figure 2. Fractional balance of Coulomb and quantum potentials at ground state $|100\rangle$

$\tilde{\Omega}_{R_1} = \tilde{\Omega}_{R_2} = \tilde{\Omega}_{R_3} = 0, \tilde{\Omega}_{R_4} = \tilde{\Omega} = -\varepsilon$ and $\tilde{v}_e = -1/\xi$.

H.H. Chiu

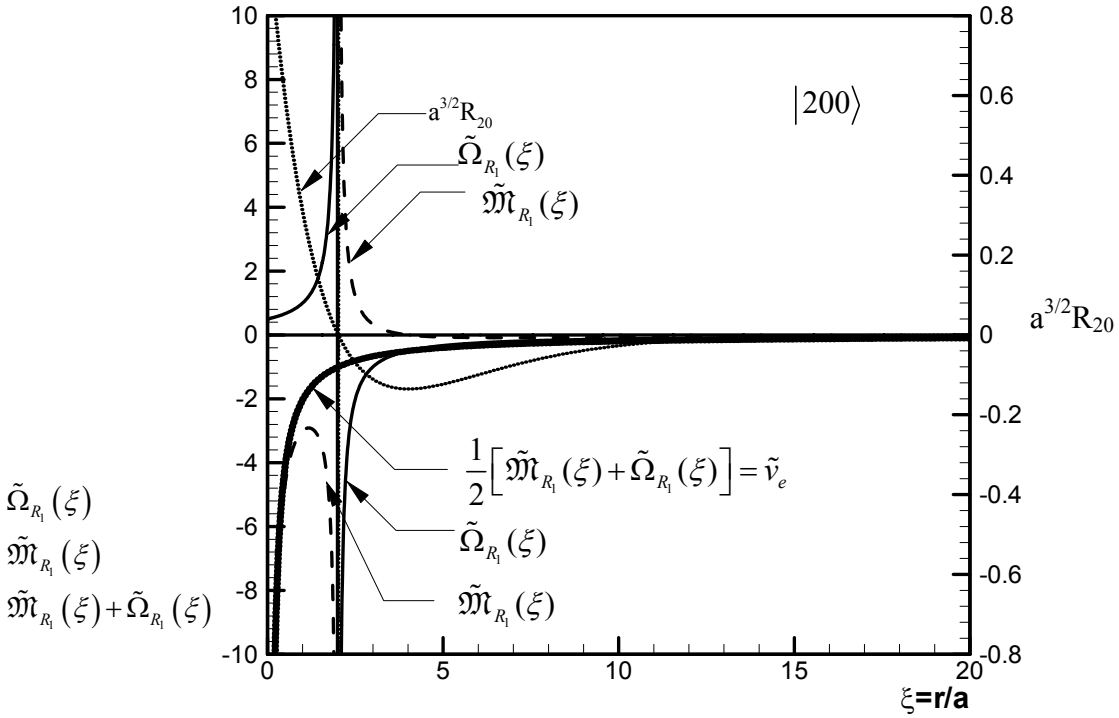

Figure 3. Complementary modal balance of Coulomb and quantum potential at state $|200\rangle$, $\tilde{v}_e=-1/\xi$

H.H.Chiu

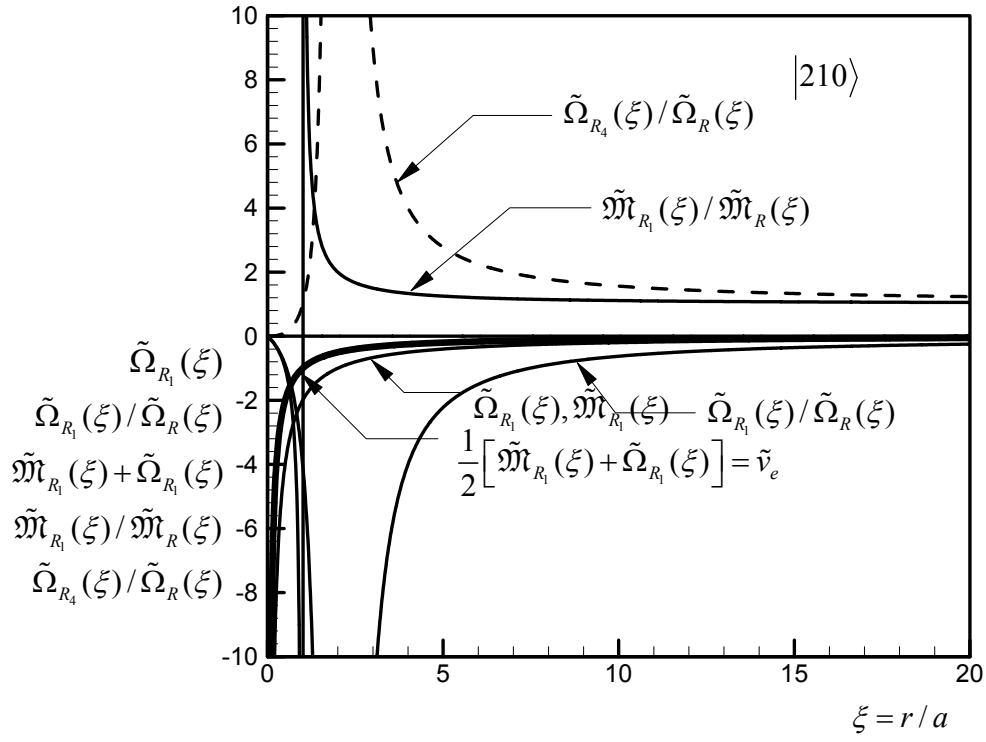

Figure 4. Fractional modal balance of Coulomb and quantum potentials at state $|210\rangle$ $\tilde{\Omega}_{R_1}=0,\tilde{\Omega}_{R_4}=\tilde{\Omega}=-\varepsilon$ and $\tilde{v}_e=-1/\xi$.

H.H. Chiu

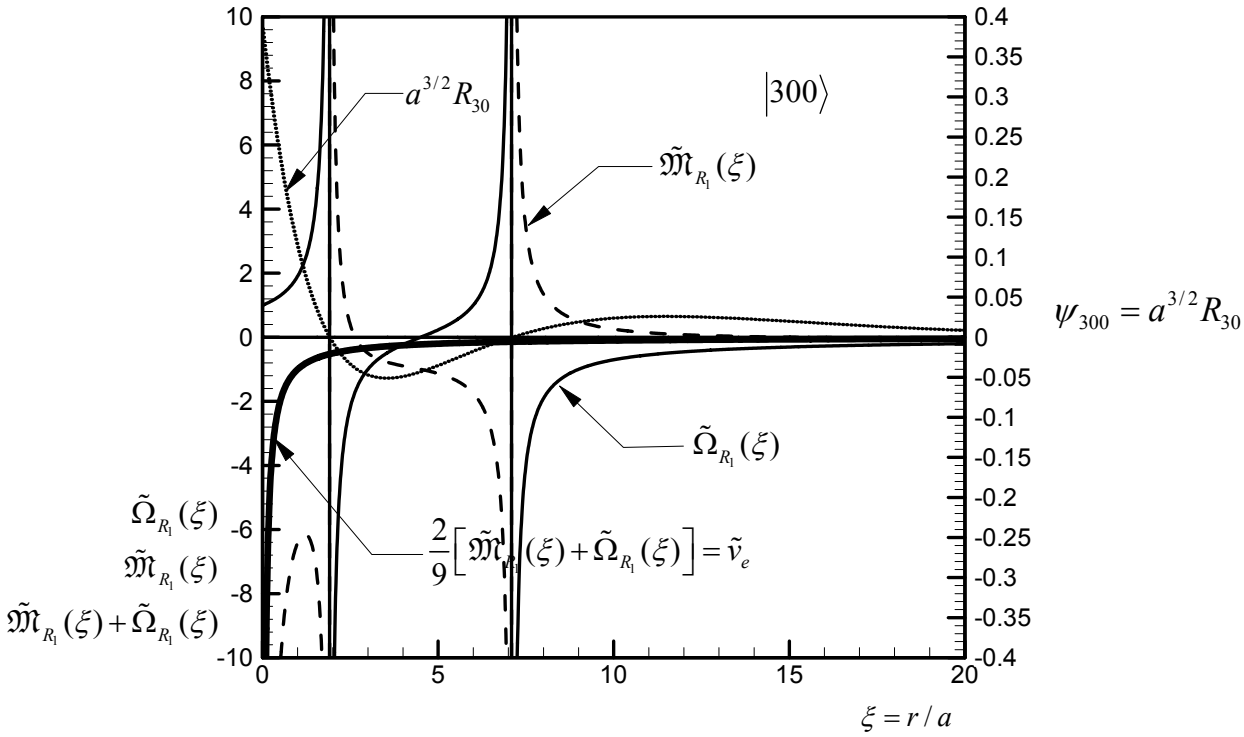

Figure 5. Complementary balance of Coulomb and quantum potentials at state $|300\rangle$ $\tilde{v}_e=-1/\xi$.

H.H. Chiu

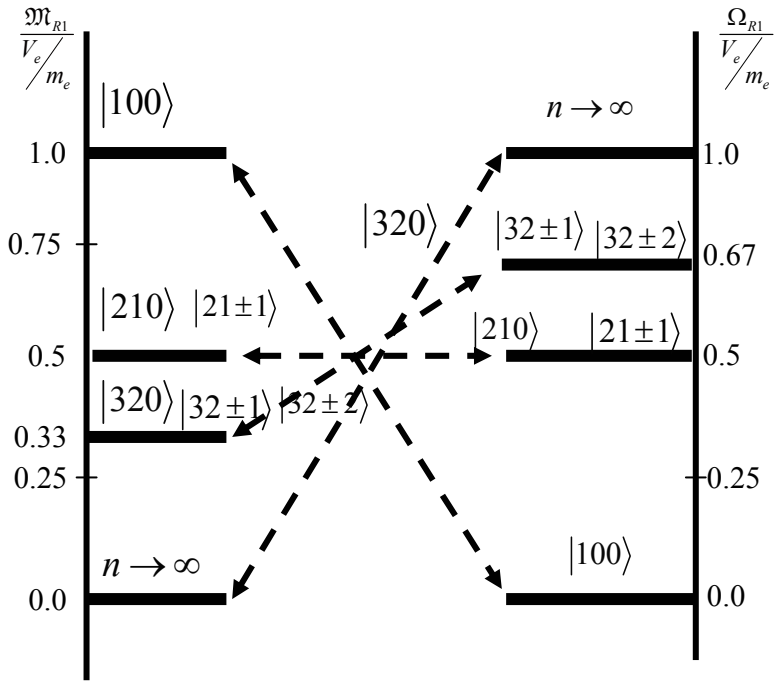

Figure 6. Fractional modal balance of the Coulomb potential with dilatation and diffusion kinetic energy for the selected stated : $|100\rangle, |210\rangle, |21+1\rangle, |320\rangle, |32+2\rangle$,and $n\to\infty$ with $l=n-1$

H.H.Chiu

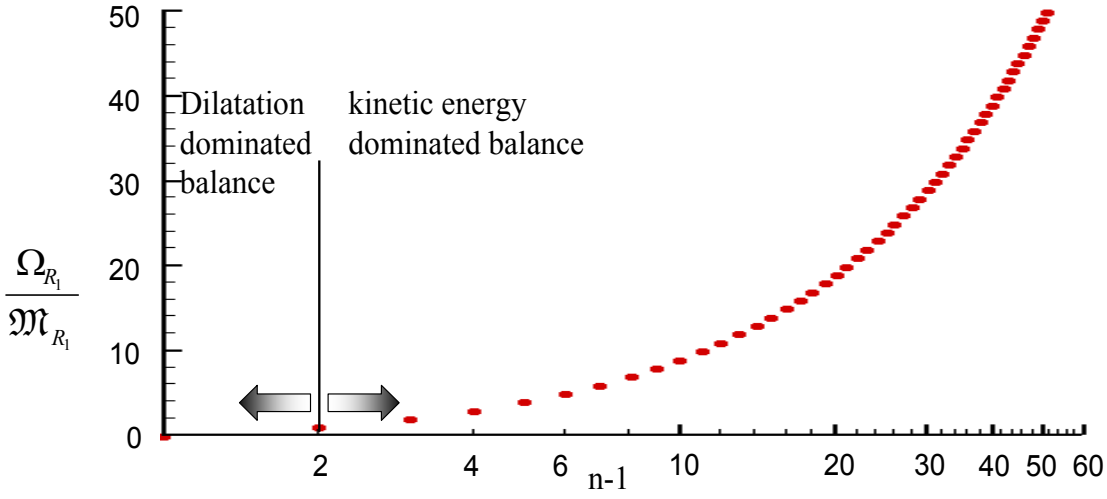

Figure 7.Variation in the relative importance of diffusion kinetic energy and dilation energy in Coulomb fractional balance mode. In complemental mode $\Omega_{R_1}/\mathfrak{M}_{R_1}$ represents of the figure also, the asymptotic value of the relative magnitude of Ω_{R_1} and $\mathfrak{M}_{R_1}$ at large radial distance. $\frac{\Omega_{R_1}}{\mathfrak{M}_{R_1}}$

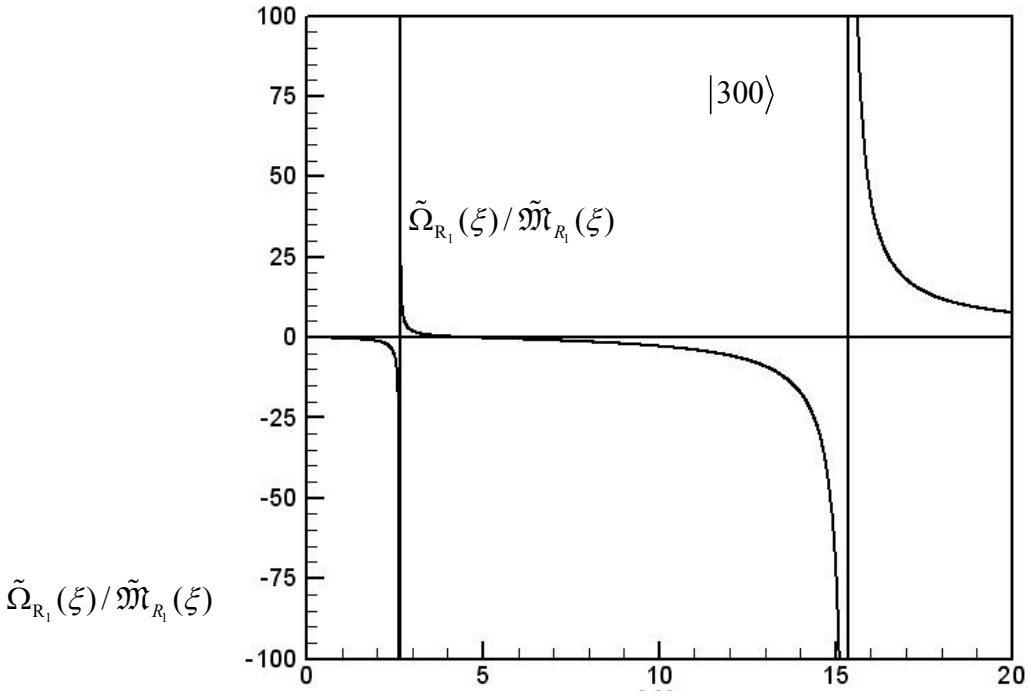

Figure 8. The ratio of $\tilde{\Omega}_{R_1}(\xi)$ and $\tilde{\mathfrak{M}}_{R_1}(\xi)$ for Coulomb mode balance at state $|300\rangle$ The asymptotic value of the ratio approaches to n-1=2 at $\xi \to \infty$.

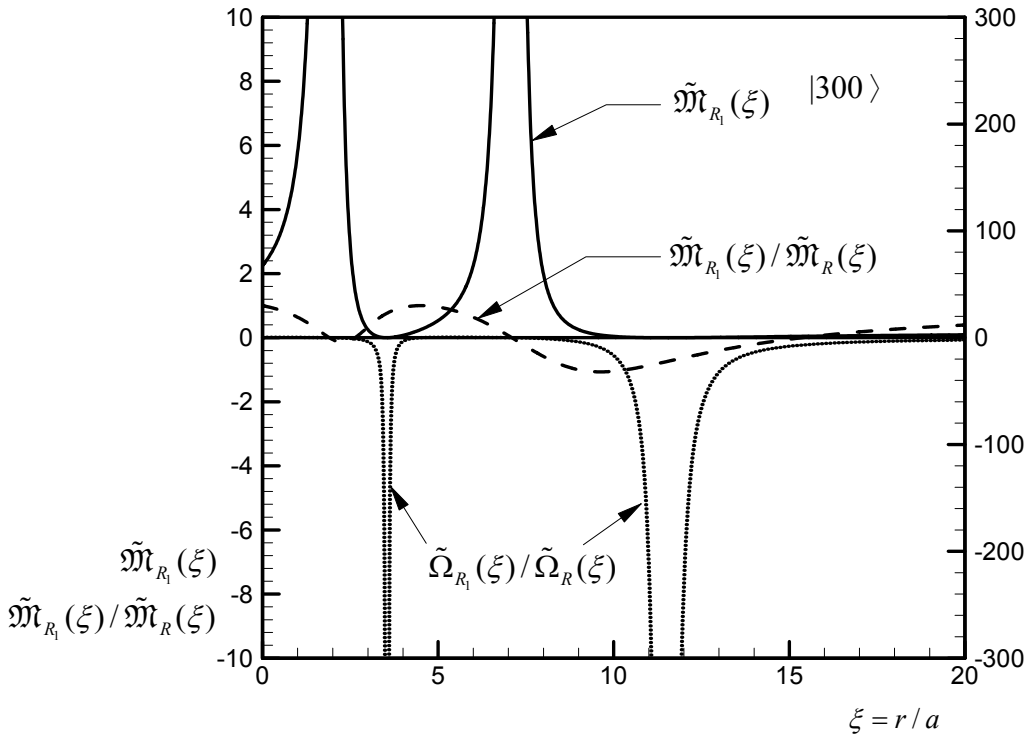

Figure 9. Fraction of dilatation energy and diffusion kinetic energy contributing in Coulomb mode balance at state $|300\rangle$ .The asymptotic values of $\tilde{\mathfrak{M}}_{R_1}/\tilde{\mathfrak{M}}_R$ and $\tilde{\Omega}_{R_1}/\tilde{\Omega}_R$ approach to 1 and 0 respectively.

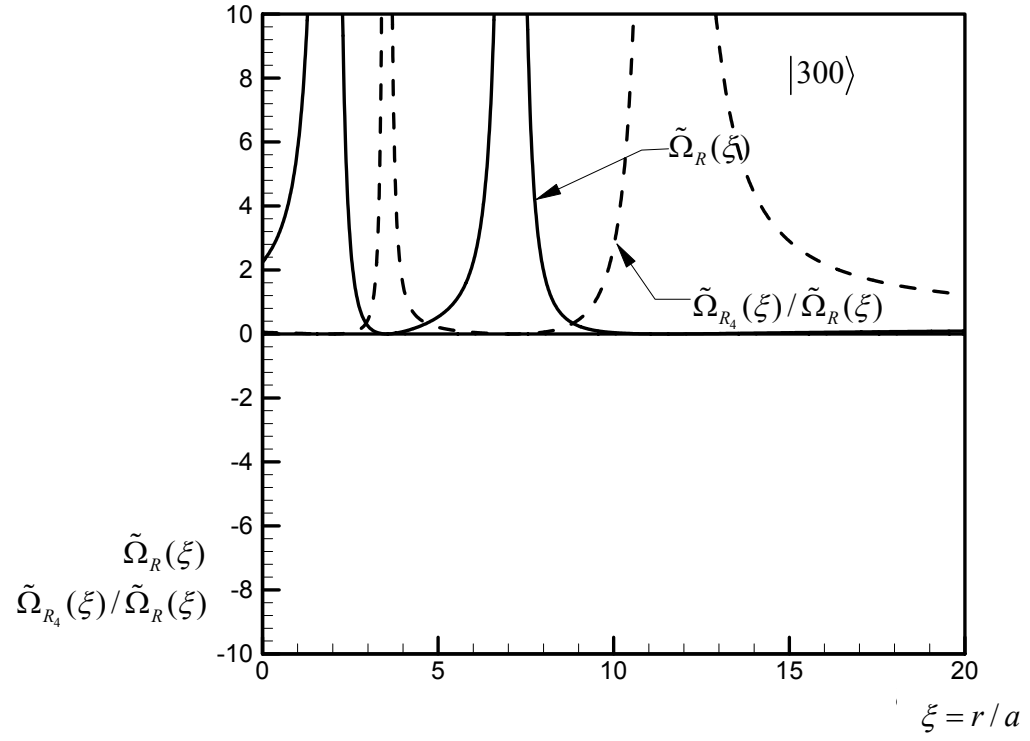

Figure 10. Distributions of diffusion kinetic energy and the ratio of $\tilde{\Omega}_{R_4}$ and $\tilde{\Omega}_R$ at $|300\rangle$ The asymptotic value of $\tilde{\Omega}_{R_4}/\tilde{\Omega}_R$ approaches to 1 at $\xi \to \infty$.

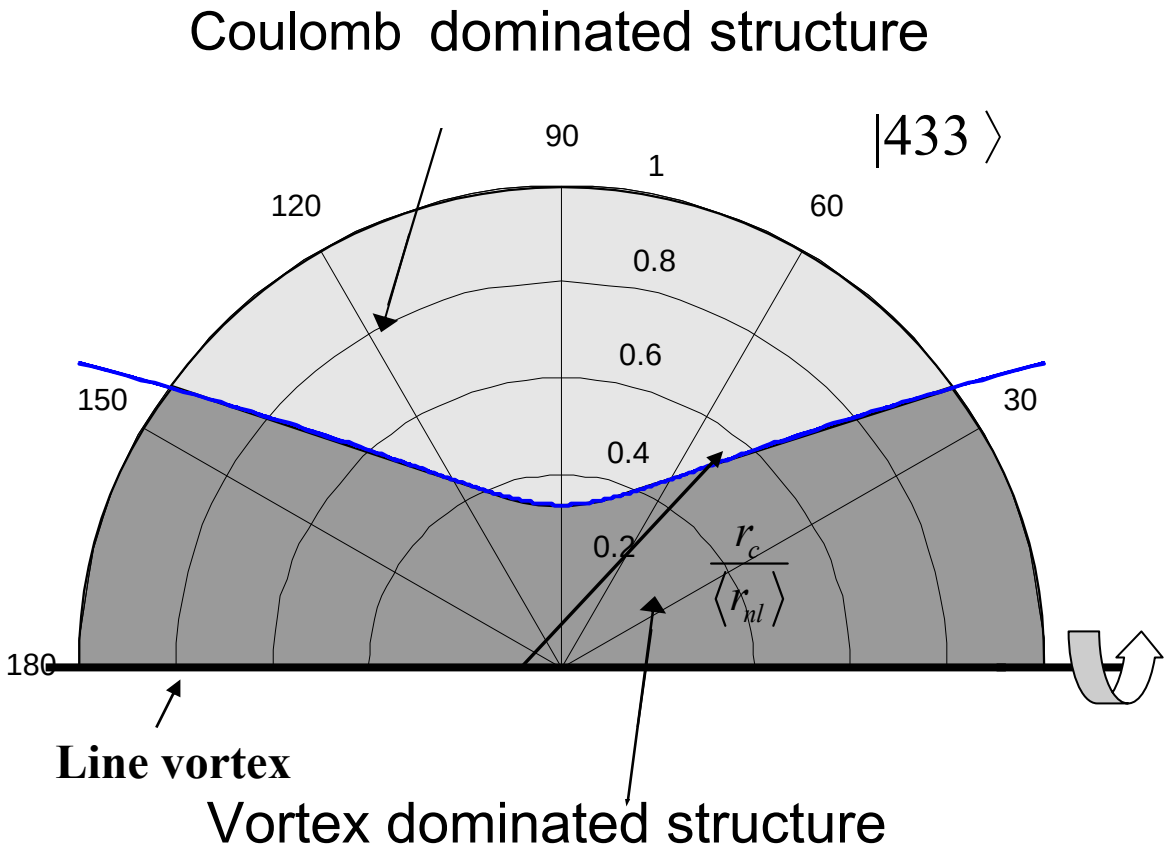

Figure 11. Electronic and hydrodynamic structure featured by vortex dominated inner core and Coulomb potential dominated exterior region for |433〉.

H.H. Chiu

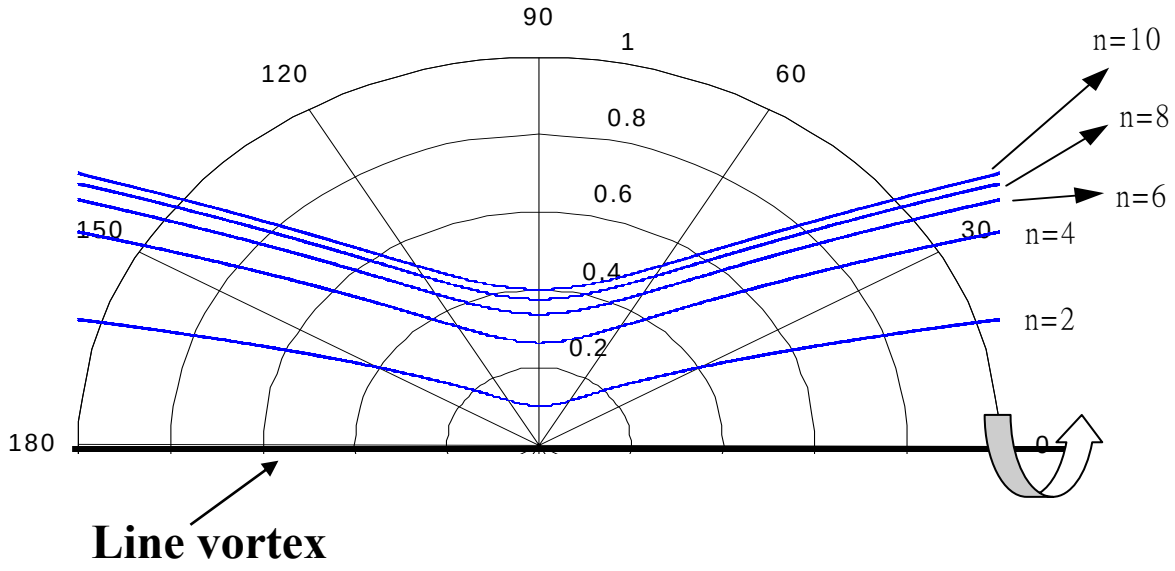

Figure 12. Dependence of the vortex dominated core size on the principal quantum, orbital angular momentum quantum number and magnetic quantum number for |n,n-1,n-1〉 state.

H.H. Chiu

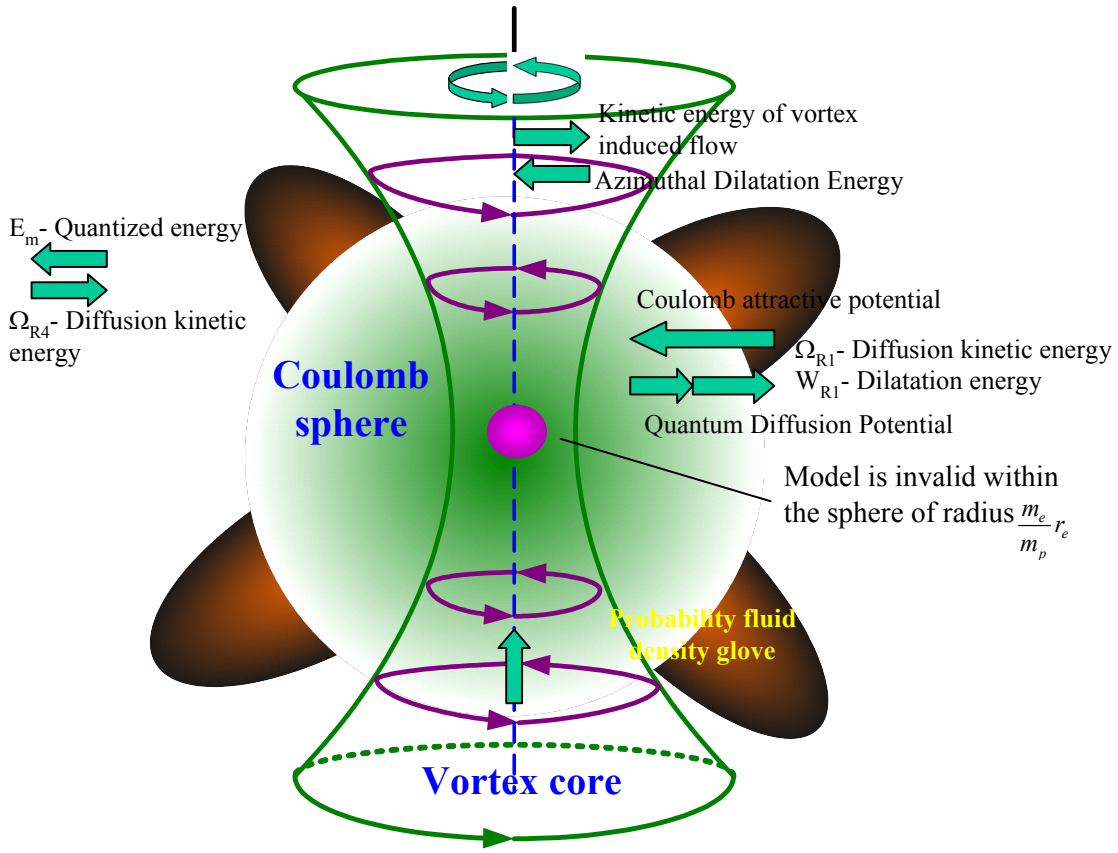

Figure 13. Schematic of electronic and fluid dynamic structure of hydrogen atom at the state |32±2〉, exhibiting the modal balance between the principal modes , quantum dilatation and diffusion kinetic energy modes.

H.H. Chiu

Quantum nanojet structures: quantum branching and clustering in two-slit electron jets

H.H. Chiu*, [a], C.T. Lin[b], and S.Y. Lin[c]
Space Science and Technology Center, and
Institute of Aeronautics and Astronautics
National Cheng Kung University
Tainan, Taiwan 70101

[a] Phone: 886) 06 – 2757575 – 63695
[a] FAX: (886) 06 – 2389940
[a] Email: hhchiu@htind1.iaa.ncku.edu.tw

[b] Phone: (886) 06 –2757575 – 63695
[b] FAX: (886) 06 – 2389940
[b] Email: oldk@sprax.iaa.ncku.edu.tw

[c] Phone: (886) 06 – 2757575 – 63691
[c] FAX: (886) 06 – 2389940
[c] Email: sylin@mail.ncku.edu.tw

and

F. L. Madarasz
Center for Applied Optics
University of Alabama in Huntsville
Huntsville, Alabama 35899 USA
Phone: (256) 895 – 9865
FAX: (256) 895 – 9865
Email: madarasz@knology.net
(Currently at East West Enterprises, Inc., Huntsville, Alabama.)

Abstract

A theory of dual electron beam nanojets is developed from the perspective of quantum fluid dynamics. The structural and dynamic behavior of the dual beams are investigated over a large range of quantum Reynolds numbers, N. For low to intermediate $N < 100$, the dual beams exhibit a strong wave-like character. This wave-like character manifests itself as a merging of the two separate jet streams into a multiple branched beam with each branch fanning out at different angular displacements relative to the jet axis, overlapping a creating and interference pattern. As N increases the merging and branching occur further away from the jet nozzles. At higher $N \geq 400$, branching occurs at a considerable distance from the jet nozzles; the fanning collapses into a forward propagating beam with little angular spread. Eventually, at very high $N \geq 800$ the beam splits into two distinct forward propagating beams very much like that produced by classical jets. Quantum clustering is another feature that arises when $N \geq 20$. This is the formation of regions in the jet with abnormally high probability density and is the combined result of self-interference and tunneling within each branch. The clusters shift down stream with higher N. The size and density of the cluster also increases with an increase in N. The complexities of these properties are studied in detail. The unique properties of a dual beam quantum nanojet are applicable to a variety of nano-scale applications, including: mass spectroscopy, imaging, sensors, and lithography.

Key Words: quantum nanojets, quantum Reynolds number, branching, clustering

I. INTRODUCTION

Electron double-slit experiments, resulting in the interference fringes of their associated matter waves, have long been at the heart of quantum theory. These dual beam experiments have provoked a historical controversy as to the interpretation of their exact nature, e.g., Copenhagen interpretation, pilot-wave theory, hidden variable theory, and causal effects which more recently have been folded into the quantum theory of motion[1]. There have been extensive and impressive experimental studies focused on the interference phenomenon and its possible applications (See, for example, Refs. 2, 3, and 4). Nevertheless, little in the way of analytical studies, aimed at a detailed explanation or clarification of the dual beam interference characteristics over a broad range of operating conditions, has been reported. Phillipidis, Bohm, and Kayes[5] were among the first to examine analytically a two-slit jet operating at high particle energy. Their work suggests that the quantum theory of motion, based on the causal theory of de-Broglie-Bohm, explains how a "quantum potential" plays a dominant role on the electron behavior in the dual beam interference phenomenon. According to the causal theory, the quantum potential is an organizational or self-referential form of energy, which brings about an inner tension in the material system to which the mass points respond (See Ref. 1). The present work builds upon our previous efforts[6,7] that used the theory of de-Broglie-Bohm as a starting point.

The present work contrasts well with the seminal work of Moseler and Landman[8] (ML), and that of Eggers.[9] ML studied the formation, stability, and break up of a liquid jet a few nanometers in diameter through the use of a molecular dynamics simulation. They compared these results with those obtained from a classical continuum hydrodynamics model. The atomistic description was related to the hydrodynamics model through their derivation of a

stochastic lubrication equation, which allow for the description of free surface flow problems. Eggars extended that work by employing a path integral formulation, which describes the most probable configuration for jet break up.

In both the ML and Eggars's calculations classical Newtonian laws of motion govern the particle motion and no quantum effects are present. The present work, however, approaches the problem from the viewpoint of quantum fluid dynamics. This allows us to study the wave-like features of the jet particles with low to intermediate quantum Reynolds numbers. At higher quantum Reynolds numbers, viz., higher energies, our theory automatically approaches the classical regime of the particle motion. That is, since we have limited our theory to low particle densities, the theory at high particle energies produces results that would be obtained from the use of the conservation equations of classical fluid dynamics.

In summary, the work of ML and Eggars focuses on the classical regime of the jet particle motion whereas the present work focuses on the quantum regime; the two approaches complement each other.

In section II we use the independent single particle model to introduce definitions and concepts necessary for the transition to a quantum fluids model. Based on a quantum mechanical formalism, specific elements of the mathematical analysis, which relate to quantum branching and clustering are detailed in section III. In section IV we discuss the structural and dynamical aspects of the results of our dual nanojet beam calculation. Lastly, in section V, we summarize the salient features of our results, discuss modifications of the theory for our next publication, and review possible nanojet technologies for practical use.

II. DEFINITIONS AND CONCEPTS

From elementary quantum theory the total wave function of a dual slit is given as $\psi = \psi_{Slit1} + \psi_{Slit2}$. Each of the slit wave functions satisfies the Schrödinger equation for an independent, single particle. Boundary conditions are built into each of the slit wave functions. Squaring the above expression results in a dual jet beam probability density, which includes the necessary interaction terms. With this, a parametric study can now easily be carried out by varying the slit width, the slit separation distance, and the energy of the emerging particle plotted as a function of the axial distance from the slit screen. This is a very direct approach. However, the approach we take in the present paper is to view the system as a quantum fluid. In this model we do not separate out the wave functions for each individual slit but construct a single wave function, representing the dual slit system, directly from the slit boundary conditions. While slightly more complicated this approach results in a physical interpretation of quantum interference and tunneling which leads to the processes of quantum branching and quantum clustering. A schematic of the dual slit system we will treat in this paper is shown in Fig. 1.

We start by reviewing the properties of an independent, single particle solution to the Schrödinger equation, from which the solutions of a multiple particle dual jet stream are constructed. Since the electrons are taken as free particles of energy E, we assume their wave functions are stationary state plane waves and are of the form $\Psi(x,y,t) = \psi(x,y)\exp(-iEt/\hbar)$. The time-dependent Schrödinger equation of motion governing the electrons is,

$$i\hbar\frac{\partial\Psi}{\partial t} = -\frac{\hbar^2}{2m_e}\nabla^2\Psi\,, \tag{1}$$

where $\hbar$ is the Planck's constant divided by 2π, and m_e is the rest mass of an electron. The probability density, ρ, of the electron is then,

$$\rho = \psi\psi^*, \tag{2.a}$$

where ψ^* is the complex conjugate of the wave function ψ. A probability current density, **J**, is defined as,

$$\mathbf{J} = \left(\frac{\mathrm{h}}{2\mathrm{i}m_e}\right)\left(\psi^*\nabla\psi - \psi\nabla\psi^*\right), \tag{2.b}$$

$$= \rho\mathbf{u}, \tag{2.c}$$

where the particle velocity **u** is defined as the ratio of the probability current flux **J** with the density. These two quantities are related through a continuity equation, which is analogous to what one finds in classical fluid dynamics. The transition from a wave mechanical interpretation to a fluid mechanical one begins with a focus on these two quantities.

A time independent equation is obtained by the substitution of the stationary state $\Psi(\mathrm{x},\mathrm{y},\mathrm{t})$ into Equation (1). Casting the time independent Schrödinger equation into a non-dimensional form allows us to define a quantum Reynolds number, N: the first step toward our fluids model. Thus, with the appropriate algebraic manipulation and redefining of independent variables such that $\mathrm{x} \rightarrow \pi\mathrm{x}/\mathrm{b}$ and $\mathrm{y} \rightarrow \pi\mathrm{y}/\mathrm{b}$, where 2b is the slit separation in the dual slit problem shown in Fig. 1, the time independent non-dimensional Schrödinger equation becomes,

$$\nabla^2\psi(\mathrm{x},\mathrm{y}) + \mathrm{N}^2\psi(\mathrm{x},\mathrm{y}) = 0, \tag{3}$$

where

$$\mathrm{N}^2 = \frac{2\mathrm{m_e E}}{\mathrm{h}^2}\frac{\mathrm{b}^2}{\pi^2}, \tag{4.a}$$

which may also be written in terms of the deBroglie wavelength, $\lambda_{dB}^2 = \hbar^2 / 2m_e E$,

$$N^2 = \left(\frac{\lambda_b}{\lambda_{dB}} \right)^2 \tag{4.b}$$

where $\lambda_b = b / \pi$.

Alternatively, N can be viewed as a quantum Reynolds number that is defined by the ratio of typical inertial force to quantum viscous force. Thus $N = u_o b / (h\pi / m_e) = u_o b / \nu_Q$, where m_e is the rest mass of electron, u_o the initial velocity of a particle corresponding to its energy E, and $\nu_Q = h\pi / m_e$ is the quantum viscosity.

The dual slit wave function in the fluids model is written as the sum of several Fourier transform integrals. Similar to classical optics, in which there are near and far regions of diffraction, these integrals represent physical distinct regions as well. The definition of these regions can be obtained by taking the Fourier transform of the Schrödinger equation given in Equation (3). The resulting equation is,

$$\frac{d^2\phi}{dx^2} + (N^2 - \eta^2)\phi = 0, \tag{5}$$

where wave function ϕ is given by the Fourier transform,

$$\phi(x, \eta) = \frac{1}{\sqrt{2\pi}} \int_{-\infty}^{\infty} \psi(x, y)\, e^{i\eta y}\, dy. \tag{6}$$

In transforming Equation (3), the boundary conditions for $\psi(x, y)$ and its spatial derivative with respect to y are,

$$\psi(x, y)\big|_{y \to \text{large}} \to 0 \qquad \left[\partial\psi(x, y)/\partial y \right]_{y \to \text{large}} \to 0, \tag{7.a, b}$$

for all values of x. In Appendix A we derive a detailed expression for the total wave function in terms of a sum of Fourier integrals. In Appendices A and B we apply boundary conditions to the initial particle velocity, u_o, and initial number of particles, n_o, emanating from the slit, as well as to the wave function and its spatial derivatives, which results in an expression for the wave function of a multiple particle dual jet beam. This wave function is succinctly written as: $\psi(x,y) = \psi_F^<(x,y) + \psi_G^<(x,y) + \psi_F^>(x,y)$. This component notation will be used in the following sections in which the sub and superscript notation are defined.

Equation (5) possesses two regions of validity for its solution. The first is in the region where $|\eta| < N$. We call this region the sub-critical region. In this region the general solution is made up of two propagating waves of the form $\exp(\pm i\alpha x)$, where $\alpha = +\sqrt{N^2 - \eta^2}$. Similarly the second region is where $|\eta| > N$, is call the super-critical region. The general solution in this region has the form $\exp(-\beta x)$, where $\beta = +\sqrt{\eta^2 - N^2}$. This has some elements of analogy to particles incident on a step potential in one dimension. The two propagating waves in the sub-critical region give rise to interference, whereas the solution in the super-critical region decays exponentially is viewed as tunneling. This analogy will be exploited later sections of the paper.

For computational purposes to be used later in the paper, we define the transformed functions $F(\eta)$ and $G(\eta)$:

$$F(\eta) = \phi(0,\eta) = \frac{1}{\sqrt{2\pi}} \int_{-\infty}^{\infty} \psi(0,y)\, e^{i\eta y}\, dy, \tag{8.a}$$

$$G(\eta) = \frac{d\phi(0,\eta)}{dx} = \frac{1}{\sqrt{2\pi}} \int_{-\infty}^{\infty} \frac{\partial\psi(0,y)}{\partial x}\, e^{i\eta y}\, dy. \tag{8.b}$$

Equation (8) corresponds to the boundary conditions on $\psi(x,y)$ and its derivative with respect to x denoted by $\psi(x,y)|_{x=0,\,y=\text{slit}} = \psi(0,y)$ and $\left[\partial\psi(x,y)/\partial x\right]_{x=0,\,y=\text{slit}} = \partial\psi(0,y)/\partial x$. That is, they are evaluated at x = 0 and over width of the slit.

We have now laid the groundwork for the dual slit problem viewed as non-interacting multi-particle system, which will be developed in the next section. The physical parameters of that system are as follows. We consider dilute jets of non-interacting electrons emitted from a dual-slit/nozzle injector in the x-direction with an energy E into a vacuum of two-dimensional space, in the absence of an external potential. The slits are separated by a distance of 2b, and their widths are taken to be 0.4b. Again, a schematic diagram of this dual-slit configuration is shown in Fig. 1.

III. WAVE PROPAGATION, INTERFERENCE AND TUNNELING

A. Sub-critical wave field: $|\eta| < N$

Since $|\eta| < N$ it is advantageous to write $\eta = N - \zeta$ so that the sub-critical wave field can be expressed as the sum of four integrals with respect to ζ as shown in Equation (9). The separation of the wave function as such is explained in Appendix A. The subscript notation of *F* and *G* on the wave functions, ψ and Ψ, is related to the Fourier transforms of the boundary conditions given in Equation (8). The superscript, <, is just a reminder that these functions are associated with the sub-critical region $|\eta| < N$. Thus,

$$\Psi_F^<(x,y,t,N)+\Psi_G^<(x,y,t,N)=\left[\psi_F^<(x,y)+\psi_G^<(x,y)\right]e^{-i(E/\hbar)t}$$

$$=\int_0^N\left(A_\zeta+B_\zeta\right)\exp\left[i\left(\kappa_{x\zeta}x+\kappa_{y\zeta}y-\frac{Et}{\hbar}\right)\right]d\zeta+\int_0^N\left(A_\zeta+B_\zeta\right)\exp\left[i\left(\kappa_{x\zeta}x-\kappa_{y\zeta}y-\frac{Et}{\hbar}\right)\right]d\zeta \quad (9)$$

$$+\int_0^N\left(A_\zeta-B_\zeta\right)\exp\left[-i\left(\kappa_{x\zeta}x-\kappa_{y\zeta}y+\frac{Et}{\hbar}\right)\right]d\zeta+\int_0^N\left(A_\zeta-B_\zeta\right)\exp\left[-i\left(\kappa_{x\zeta}x+\kappa_{y\zeta}y+\frac{Et}{\hbar}\right)\right]d\zeta$$

The coefficients, A_ζ and B_ζ, and the κ's in the exponentials are given by,

$$A_\zeta=\frac{F_0}{4\pi}(1+i)\left\{\frac{\sin(N-\zeta)-\sin\left[0.6(N-\zeta)\right]}{(N-\zeta)}\right\}, \quad (10.a)$$

$$B_\zeta=\frac{G_0}{4\pi}(-1-i)\left\{\frac{\sin(N-\zeta)-\sin\left[0.6(N-\zeta)\right]}{\sqrt{2N\zeta-\zeta^2}(N-\zeta)}\right\}, \quad (10.b)$$

$$\kappa_{x\zeta}=\sqrt{2N\zeta-\zeta^2}\,, \quad (10.c)$$

$$\kappa_{y\zeta}\equiv\eta=N-\zeta\,, \quad (10.d)$$

$$\kappa_\zeta=N^2\,, \quad (10.e)$$

Corresponding expressions related to the coefficients A_ζ and B_ζ are derived in Appendix A. The coefficients F_0 and G_0 are scaling factors[7], which are derived in Appendix B. Their functional forms are:

$$F_0=\left[2n_o\right]^{1/2}, \quad (11.a)$$

$$G_0=\frac{m_e u_0 b}{\hbar\pi}F_0\,. \quad (11.b)$$

Equation (9) may be rewritten in a more succinct form in terms of what we have designated as ζ waves, each of which has a wave characteristic function defined in the exponential terms in Equation (9),

$$\Psi_F^<(x,y,t,N)+\Psi_G^<(x,y,t,N)=\zeta_f^+ +\zeta_f^- +\zeta_b^+ +\zeta_b^- . \tag{12}$$

Each term corresponds respectively with those in Equation (9). Here again, wave propagation is in both the "forward" and "backward" directions, which coincide with the directions normal to the corresponding wave characteristic surfaces, thus the subscripts f and b on the ζ waves. Moreover, these waves propagate at a radial angle, θ, with respect to the x-axis. In fact, they propagate in a symmetric fashion above and below the x-axis, thus the superscripts plus (+) and minus (-), respectively.

The angle of propagation is given by,

$$\theta=\pm\tan^{-1}\frac{\kappa_{y\zeta}}{\kappa_{x\zeta}}=\pm\tan^{-1}\frac{\left(2N\zeta-\zeta^2\right)^{1/2}}{\left(N-\zeta\right)} \tag{13}$$

where the plus (+) sign applies to the ζ_f^+ and ζ_b^+ waves, and minus (–)sign to ζ_f^- and ζ_b^- waves, respectively. A review of Equation (13) reveals the following.

For small values of N, and fixed ζ, θ is large. On the other hand, when N takes on larger values θ decreases as

$$\lim_{N\to\infty}\theta:\ \pm\left(\frac{2\zeta}{N}\right)^{1/2}\to 0, \tag{14}$$

Essentially, the beam splits into two distinct forward propagating beams parallel to the x-axis with a structure very much like that produced by classical jets. This suggests that at some point,

a transition occurs between quantum behavior and that of a classical sand/grain like jet. Our study shows that this transition occurs at a critical value for the Reynolds number of $N_C = N \sim 100$. As we will see below, low Reynolds numbers are associated with a predominately wave-like behavior consistent with quantum behavior and high Reynolds numbers give rise to a purely particle picture consistent with a classical behavior.

Another feature of note is that for a fixed value of N the Fourier components with a larger values of ζ (equivalently smaller values of η) has a large radial angle. This basic rule helps us to understand the nature of wave structure of the nanojets as we shall see in the section 4.

B. Super-critical wave field: $|\eta| > N$

As with the sub-critical region the super-critical wave field can be expressed as a Fourier transform with respect to ζ, which is also shown in Appendix A.

$$\begin{aligned}\Psi_F^{>}(x,y,t,N) &= \psi_F^{>}(x,y)e^{-i(E/\hbar)t} \\ &= \int_0^{\infty} C_\zeta \exp(-\beta x)\cos\left(N+\zeta\right)y\exp(-iEt/\hbar)\,d\zeta\end{aligned} \tag{15}$$

The subscript *F* on the psi functions is again related to the Fourier transforms of the boundary conditions given in Equation (8). The superscript, >, is just a reminder that these functions are associated with the super-critical region $|\eta| > N$. The parameter $\beta = (2N\zeta + \zeta^2)^{1/2}$. As with A_ζ and B_ζ, the coefficient C_ζ has a related expression derived in Appendix A. Then, C_ζ is identified as,

$$C_\zeta = \frac{F_0}{\pi}(1+i)\left\{\frac{\sin(N+\zeta) - \sin\left[0.6(N+\zeta)\right]}{(N+\zeta)}\right\}. \tag{16}$$

So in this super-critical region we have a standing wave, which decays exponentially in an axial direction as indicated by the $\exp(-\beta x)\cos(N+\zeta)y\exp(-iEt/\hbar)$ factors. The axial decay is caused by quantum tunneling. We note that when $x<(2N\zeta+\zeta^2)^{-1/2}$ i.e., there is negligible amplitude decay resulting in a high probability density. However, when $x>(2N\zeta+\zeta^2)^{-1/2}$ the wave decreases rapidly. Later in the paper we will show that the formation of a cluster down stream is in part due to a region in which $x<(2N\zeta+\zeta^2)^{-1/2}$ is followed by a rapid exponential decay.

As with the sub-critical region it is advantageous for further discussion in later sections to divide this region into its own set of ζ waves as follows.

$$\Psi_F^{>}(x,y,t,N)=\int_0^{\infty}C_\zeta\exp(-\beta x)\exp(+i\lambda_{y\zeta}y)\exp(-iEt/\hbar)d\zeta$$

$$+\int_0^{\infty}C_\zeta\exp(-\beta x)\exp(-i\lambda_{y\zeta}y)\exp(-iEt/\hbar)\,d\zeta \qquad (17)$$

$$=\zeta_S^{+}+\zeta_S^{-}$$

where we have defined $\lambda_{y\zeta}=N+\zeta$. Here again, we have identified two terms as ζwaves, ζ_S^{+} and ζ_S^{-}, with plus (+) and minus (-) superscripts referring to their propagation in the direction of increasing and decreasing values of the y-coordinate, respectively, and a subscript S that indicates these waves are standing waves.

IV. STRUCTURAL AND DYNAMIC COMPLEXITIES OF ELECTRON DUAL-SLIT NANOJETS

In the present work our numerical studies focus on the variations in the structure and

dynamics of a two-slit electron jet having quantum Reynolds numbers ranging from 10 to 1000. This corresponds to the initial velocities (kinetic energies) ranging from 3.6×10^6 cm/s to 3.6×10^8 cm/s (0.004 eV to 37 eV), respectively. The geometric parameters used in the calculations were: slit separation of 2b = 200 nm, and a slit width of 0.4b = 40 nm. The initial probability density at the slit inlet was normalized, $n_o = 1$. Finally, given the conditions above, the current density per unit width of slit in y-direction ranges from 9.0×10^{11} particle sec^{-1} to 9.0×10^{13} particle sec^{-1}, respectively.

The analysis of our numerical results is broken up into to primary regions of quantum Reynolds numbers: $10 \leq N < 100$, and $100 < N \leq 1000$. When N is approximately 100 the systems exhibits a transition from a quasi-quantum regime, just below N = 100, to a quasi-classical region, just above N = 100. This critical value of N is designated as $N_C = 100$.

We further divide the analysis into two ranges of the coordinate x. The range of $0 < x < 5$ is a near field region, or, in analogy with classical optics, the Fresnel region. The range of $5 < x < 30$ is the far field region, or the Franuhofer region. The Fresnel and Fraunhofer regions are illustrated by our results depicted in Figs. 2a – 2f, and Figs. 3a – 3f, respectively.

A. Quantum branching and structural transition: quantum to classical

In general, quantum jets corresponding to lower Reynolds numbers, $10 \leq N < 100$, exhibit "multi-branching" effects. Branching is clearly observed in both the Fresnel and Fraunhofer regions depicted in Figs. 2a – 2c, and Figs. 3a – 3c. In these figures the magnitude of the electron probability density parallels the visible spectrum with the lower densities on the blue end of the spectrum and the higher densities toward the red end. Note that each branch has associated with it a width and branching angle θ given by Equation (13). The quantum

branches are formed by two distinct mechanisms.

The first mechanism is the generation of high harmonic ζ waves downstream from the slit where the electron jet splits into two branches, clearly observed in Figs. 2a, 2b, 3a, and 3b. The second mechanism contributing to the jet branching is the intersection of in phase ζ^+ and ζ^- waves on the x-axis. Figures. 2a and 2b illustrate the formation of a central branch parallel to the x-axis, by the intersection of a ζ^- wave emanating from the upper slit with a ζ^+ wave emanating from the lower slit. Moreover, there is a reflection of ζ^- and ζ^+ waves back into the regions from which they were generated, where upon interference with the primary jets, which emanate from the upper and lower slits, takes place. The strength of the interference is a function of the phase between the reflected wave and the primary one. The effect of interference can clearly be observed in Figs. 2a – 2c for the lower Reynolds numbers where the branching angles are the largest.

Figures 2a – 2d and 3a – 3d correspond to Reynolds numbers in the range of $10 \leq N \leq 100$. Following the evolution of the jet structure from N = 10 to N = 100 in these figures clearly shows: 1. a reduction in the branching angles resulting in a forward propagation of the jets from each emanating from each slit, 2. a reduction in the widths of the branches, and, 3. the formation of the central branch taking place further downstream from the jet slits. At approximately N = 100, the two jets are for the most part disengaged and function independently of each other. For this reason we have designated N = 100 as N_C the critical Reynolds number. For $N < N_C$ the figures demonstrate basic quantum behavior including: spatial density fall-off, complex interference fringes and tunneling.

For values of $N > N_C$ the system continues to evolve with increasing N into a more classical-like structure. Clearly, in the Fresnel region when $N \approx N_C$, Fig. 2d, the branching angles have

pretty much collapsed so that the respective branches are coincident resulting in two primary, forward propagating, sand/grain-like jets emanating from the upper and lower jet slits. However, this is not the case in the Fraunhofer region as can be seen in Fig. 3d; multiple branching continues to be present for values of $x > 10$. As N is increased beyond N_C the formation of multiple branching occurs further and further downstream from the jet slits extending the range of the primary but separate jet streams trailing the branching point (See Figs. 3e – 3f). When $N \approx 400$ the complete range of $0 < x < 30$ covering both Fresnel and Fraunhofer regions is devoid of any significant branching and branch interactions. Essentially what are left are the two primary forward propagating jets of electrons. Fig. 2e, N = 500, clearly demonstrates this effect over the range of $0 < x < 50$ for N = 500.

Finally, when $N >> N_C$, Figs. 2e, 2f, and 3e, 3f, the two primary jets become quite focused into pencil sharp beams of particles over the entire range of x propagating in the forward direction with no interaction between them, which is characteristic of classical particle beams. Clearly the evolution of the dual slit jet structure with increasing Reynolds numbers exhibits the classic wave-particle duality. At the lower Reynolds numbers there is a clear indication of wave like properties with branching and interference. At the higher Reynolds numbers we have observed a significant reduction in branching resulting in little of no interference and two forward propagating beams of classical particles propelled through their respective slits.

In the following two sections, B and C, we take a closer look at the phenomena of quantum clustering and interference.

B. Quantum clustering and axial structure

In Fig. 4 we have plotted the electron probability density as a function of axial distance for various values of quantum Reynolds numbers over the entire range of $10 \leq N \leq 1000$. The

apparent broadband outlining of these plots is in fact due to the rapid oscillations of density within a short distance of the wave propagation. Most noticeable is the growth of a large maximum whose initial presence can be seen in Fig. 4a, where N = 10, in the very near field regime, $x \approx 0.1$. For values of N > 20, this peak quickly grows to a value of 1.8, which is 1.8 times greater than the initial density at the slit surface show in Fig. 4a. The formation of an abnormally high-density region suggests a "quantum clustering" of the probability density, initially introduced and described in section 3. As the Reynolds number increases the cluster shifts downstream away from the origin at the slit; in addition, it broadens out covering a larger range of the propagation distance. This progression can be clearly tracked by sequential viewing figures 4a – 4e. Quantum clustering can be attributed to self-intersection of the $\zeta_f^{\pm}$ and $\zeta_b^{\pm}$ waves in each jet stream (see Equations (12) and (17)). Since the wave angle θ of the $\zeta_f^{\pm}$ and $\zeta_b^{\pm}$ waves becomes smaller at large value of N, the clustering occurs at larger x for higher value of N. The interference of these two waves can clearly be seen in the density plots, Fig. 3c, 3d, and 3f, where they intersect each other on the axis of each jet stream. The standing waves due to $\zeta_S^{\pm}$ also contribute to the higher density in the region of smaller x, and reduced density at larger x due to axial tunneling.

Finally, in Fig. 5 we plot a series of probability density curves for different values of N. By placing different but increasing N value density curves next to each other we are able to display the evolutional progression of cluster growth in one figure. In this figure L_a, L_b, and L_c are the displacement values, on the jet axis of propagation, where the cluster initially starts to grow, for the cluster maximum, and for the effective end of the cluster, respectively. In passing we note that it is this correlation between the peak, or maximum, values of each N valued cluster that

forms the foundation for using nanojets as a mass spectrometer.[7]

C. Quantum interference fringes

Figure 6 is a parametric study of the effects of different slit separation width of 2b on the probability density and its corresponding interference patent, where b takes on the values of b = 80nm, 100nm, 150nm, 200nm, 250nm, and 300nm, corresponding respectively to the figure panels (a – f). It shows the cross sectional contours probability densities and their corresponding interference patents of the advancing jet streams at the axial displacement of x = 10 for different values of slit separations, and for a value of N = 10. Calculations have been carried out for several values of x spanning the near (Fresnel) and far (Franuhofer) regions. We have chosen to report the results at x = 10, which is an overlap of the two regions and typifies the comparison of the probability density and its corresponding interference pattern in areas of meaningful interest.

The effects of a change in the Reynolds number on interference fringes are displayed in Fig. 7 as a function of axial displacement. We note that for the lower values of N, approximately N < 100, the familiar multiple fringe patterns due to interference are present. For values of N > 500, the interference fringes increasingly fade with increasing N until there are only two vertical lines indicating the almost complete eradication of quantum interference with two distinct streams of classical particles emanating from the slits. Note that the central branch is present for all values of x when $N \leq 50$. It does, however, disappear when N = 100 at x = 5, but reappears at x = 15 and 30. This is consistent with the discussion given in Section IV A of Figs. 2 and 3 in which the formation of the central branch progressively shifts down stream away the slits with increasing value of N. Eventually, as illustrated in Fig. 3i, when N > 500, the formation of the central branch has essentially shifted to infinity and thus only two branches, one

for each slit, are displayed.

V. CONCLUSION

The theory of dual-slit dilute electron nanojets was formulated in terms of a quantum Reynolds number, N. A critical Reynolds number, $N_C = 100$, was identified. For values of $N < N_C$ the dual-slit system exhibited the quantum features of branching and clustering. And for values of $N > N_C$ the system tended toward a more classical picture in which two, apparently independent, beams of electrons propagate in straight line trajectories from each slit.

The dual-slit wave function was constructed from the solutions of the non-interacting, multi-particle Schrödinger equation and the appropriate boundary conditions on the jet slits. The field of propagation was resolved into two regions: the sub-critical region of propagating waves and the super-critical region in which the waves decay exponentially. A Fourier decomposition of the wave function in these regions showed that the wave function could be written in terms of six basis functions: $\zeta_f^+ + \zeta_f^- + \zeta_b^+ + \zeta_b^-$ in the sub-critical region, and $\zeta_S^+ + \zeta_S^-$ in the super-critical region.

Quantum branching, the appearance of multiple branches radiating at different angles in a fan shaped design, is induced by the interaction of the two families of ζ^+ and ζ^- waves emanation from both slits. Quantum clustering, spatial regions of high probability densities, on the other hand, arise though the interaction of the ζ^+ and ζ^- waves emanating from the same slit. Moreover, quantum and classical behavior are manifest in the ζ wave angle, θ. When the wave angle is large the jets exhibit strong quantum structure, whereas a small angle leads to sand/grain like jet structure indicative of a classical jet stream of particles. Thus the ζ waves are key to the interpretation of wave-particle phenomena.

In contrast to Copenhagen interpretation, the causal interpretation by de-Broglie and Bohm also gives the nanojet structure based on the quantum fluid dynamics model. The two rival interpretations, however, give the same results.[6]

As a follow on to this paper we are in the process of recasting the present work and interpreting its results in terms of a full quantum "diffusive" fluid dynamics theory[8]. Recasting the theory in these terms will allow us to identify a quantum potential. With this potential a more fundamental understanding of the driving mechanisms of the problem can be had. The present calculation is limited to relatively dilute densities of non-interacting particles within the jet stream. Recasting the problem in terms of a quantum diffusive fluid dynamical theory will set the background needed to address moderate to high densities of jet particles and their mutual interactions. Quantum diffusive fluid dynamics has been successfully used by one of the authors, H.H. Chiu, to identify the dynamic origin of quantized energy and the mechanisms of detailed dynamic equilibrium within a hydrogen atom induced by the diffusion of the probability fluid of the electron.[10] The new aspect of the theory is the consideration of quantum diffusion hereto not formally addressed to any extent in the literature.

Once the full theory, addressing a broad range of particle densities in the jet(s), is completed it is our intention to extend the problem to multi-beam components, such as different ions. At this stage we will have a theoretical tool that may be used for parametric studies of design parameters to guide and optimize the experimental development of specific device applications.

Finally, nanojets have a myriad of important, modern day applications for which our model can be used: nano- circuitry and electronics; nano- propulsion / thruster systems; fuel injectors for microscopic engines; atomic optics and interferometry; etching and lithography; drug delivery systems; injecting genes into cells; mass spectrometer; and quantum sensors. Our goal

with the present publication and research in progress is to provide a theoretical foundation to: 1. understand the fundamental physics which governs nanojet operation under various circumstances; and 2. act as tool in guiding the design and optimizing the operational functions for the various applications.

ACKNOWLEDGEMENTS

The authors extend their appreciation for the research support awarded by USAFOSR AOARD03-4039.

APPENDIX A: DUAL BEAM WAVE FUNCTION AND BOUNDARY CONDITIONS

The time independent wave function of two-slit jet, $\psi(x,y) = \psi_F^<(x,y) + \psi_G^<(x,y) + \psi_F^>(x,y)$, given in integrands of Equations (9) and (15) of the text, is obtained by the method of Fourier transform as follows. The superscripts "<" and ">" refer to the sub and super critical regions.

When the single particle Schrödinger equation, Equation (3), is Fourier transformed the resulting equation, Equation (7), is

$$\frac{d^2\phi}{dx^2} + (N^2 - \eta^2)\phi = 0 \tag{A.1}$$

As discussed at the end of Sec. II of the text, the solution of Equation (A.1) possesses two regions of validity. The first is in the region where $|\eta| < N$: the sub critical region. In this region the general solution is made up of two propagating waves of the form $\exp(\pm i\alpha x)$, where $\alpha = +\sqrt{N^2 - \eta^2}$, or

$$\phi^<(x,\eta) = C_1 e^{+i\alpha x} + C_2 e^{-i\alpha x} \tag{A.5}$$

The second region is where $|\eta| > N$: the super critical region. The general solution in this region has the form $\exp(-\beta x)$, where $\beta = +\sqrt{\eta^2 - N^2}$, or

$$\phi^{>}(x,\eta) = C_3 e^{-\beta x} \tag{A.6}$$

We note that $\phi^{\lessgtr}(0,\eta) = F^{\lessgtr}(\eta)$ and $d\phi^{\lessgtr}(0,\eta)/dx = G^{\lessgtr}(\eta)$, where $F^{\lessgtr}(\eta)$ and $G^{\lessgtr}(\eta)$ are the Fourier transforms of $\psi^{\lessgtr}(0,y)$ and $d\psi^{\lessgtr}(0,y)/dx$ given in Equations (8.a) and (8.b), respectively. With this we can determine the coefficients $C_1, C_2,$ and C_3 in terms of $F^{\lessgtr}(\eta)$ and $G^{\lessgtr}(\eta)$. Then $\phi^{\lessgtr}(x,\eta)$ may be written in the following general form:

$$\phi^{\lessgtr}(x,\eta) = H^{\lessgtr}(x,\eta)F^{\lessgtr}(\eta) + K^{\lessgtr}(x,\eta)G^{\lessgtr}(\eta) \quad \text{for } |\eta| \lessgtr N, \tag{A.7}$$

where

$$H^{<}(x,\eta) = \frac{1}{2}\left[e^{+i\alpha x} + e^{-i\alpha x}\right] = \cos(\alpha x), \tag{A.8}$$

$$K^{<}(x,\eta) = \frac{1}{2i\alpha}\left[e^{+i\alpha x} - e^{-i\alpha x}\right] = \frac{\sin(\alpha x)}{\alpha}, \tag{A.9}$$

$$H^{>}(x,\eta) = e^{-\beta x}, \tag{A.10}$$

$$K^{>}(x,\eta) = 0. \tag{A.11}$$

The real space solution $\psi^{\lessgtr}(x,y)$ of the Schrödinger equation, Equation (3), is obtained by taking the appropriate inverse Fourier transforms:

$$\psi^{\lessgtr}(x,y) = \frac{1}{\sqrt{2\pi}}\int_{-\infty}^{\infty} H^{\lessgtr}(x,\eta)F^{\lessgtr}(\eta)e^{i\eta y}\,dy + \frac{1}{\sqrt{2\pi}}\int_{-\infty}^{\infty} K^{\lessgtr}(x,\eta)G^{\lessgtr}(\eta)e^{-i\eta y}\,dy \tag{A.12}$$

In addition, because this is a two-dimensional problem and we assume reflection symmetry in the vertical plane about the line of propagation of the particle beam Equation (A.12) may be rewritten as,

$$\psi^{\lessgtr}(x,y) = \frac{2}{\sqrt{2\pi}} \int_0^{\infty} \left[H^{\lessgtr}(x,\eta) F^{\lessgtr}(\eta) + K^{\lessgtr}(x,\eta) G^{\lessgtr}(\eta)) \right] \cos(\eta y)\ d\eta \qquad (A.13)$$

The total real space wave function is a linear combination of the wave functions of the sub and super critical regions. Using Equations (A.8) – (A.13) in the appropriate regions results in the total wave function:

$$\psi(x,y) = \psi_F^{<}(x,y) + \psi_G^{<}(x,y) + \psi_F^{>}(x,y) =$$

$$\frac{2}{\sqrt{2\pi}} \int_0^{N} \left\{ F^{<}(N-\zeta) \cos\left[\sqrt{2N\zeta - \zeta^2}\, x \right] + \frac{G^{<}(N-\zeta)}{\sqrt{2N\zeta - \zeta^2}} \sin\left[\sqrt{2N\zeta - \zeta^2}\, x \right] \right\} \cos\left[(N-\zeta) y \right] d\zeta \qquad (A.14)$$

$$+ \frac{2}{\sqrt{2\pi}} \int_0^{N} F^{>}(N+\zeta) e^{-\sqrt{2N\zeta+\zeta^2}\, x} \cos\left[(N+\zeta) y \right] d\zeta$$

where $\eta = N - \zeta$ when $|\eta| < N$, and $\eta = N + \zeta$ when $|\eta| > N$.

Equation (A.14) can be recast into a form consistent with the boundary conditions over the dual slits, which are defined in Equations (B2) – (B5). The final result of this dual slit wave function is:

$$\begin{aligned} \psi(x,y) &= \psi_F^{<}(x,y) + \psi_G^{<}(x,y) + \psi_F^{>}(x,y) \\ &= \xi F_0 \Omega^{<}(x,y) + \delta G_0 \Theta^{<}(x,y) + \xi F_0 \Omega^{>}(x,y) \end{aligned} , \qquad (A.15)$$

where $\xi = 1 + i$, $\delta = -1 + i$,

$$\Omega^{<}(x,y) = \frac{2}{\sqrt{2\pi}} \int_0^{N} Y^{<}(N-\zeta) \cos\left[+\sqrt{2N\zeta - \zeta^2}\, x \right] \cos\left[(N-\zeta) y \right] d\zeta , \qquad (A.16.a)$$

$$\Omega^{>}(x,y) = \frac{2}{\sqrt{2\pi}} \int_0^{\infty} Y^{>}(N+\zeta)\ \exp\left[-\sqrt{2N\zeta+\zeta^2}\, x \right] \cos\left[(N+\zeta) y \right] d\zeta , \qquad (A.16.b)$$

$$Y^{\lessgtr}(N\, m\zeta) = \sqrt{\frac{1}{2\pi}} \left\{ \frac{\sin(N\, m\zeta) - \sin\left[0.6 (N\, m\zeta) \right]}{N\, m\zeta} \right\} , \qquad (A.17.a, b)$$

$$\Theta^{<}(x,y)=\frac{2}{\sqrt{2\pi}}\int_0^N Z^{<}(N-\zeta)\sin\left[\sqrt{2N\zeta-\zeta^2}\,x\right]\cos\left[(N-\zeta)y\right]d\zeta, \qquad (A.18)$$

$$Z^{<}(N-\zeta)=\sqrt{\frac{1}{2\pi}}\left\{\frac{\sin(N-\zeta)-\sin\left[0.6(N-\zeta)\right]}{\sqrt{2N\zeta-\zeta^2}\,(N-\zeta)}\right\}, \qquad (A.19)$$

and F_0 and G_0 are coefficients, determined by a scaling method described in Appendix B, that depend on the density and velocity of the particles on the slit surfaces.

The three functions $Y^{<}, Y^{>}$, and $Z^{<}$ are determined consistent with the boundary conditions on the probability density, **J**, and the particle velocity, **u**, of the jet beam given by Equations (B.2), (B.3), and (B.4) in Appendix B. The probability density and the particle velocity of the jet are calculated by a substitution of the dual slit wave function, Equation (A.15), into Equation (2). The methods for the determination of $Y^{<}$ and $Y^{>}$ involve Fourier transforms, whereas $Z^{<}(N-\zeta)$ involves the solution of Fredholm type integral equation. In the determination of the solution of $Z^{<}(N-\zeta)$, we used an approximation method. In all cases the fractional difference—the difference between the calculated mean value of the particle velocity and its initial boundary value velocity divided by the initial boundary value velocity—was on the order of or less than 10^{-3}. For very large N, the error decreases to smaller values. For example, the latter ratio is 3.8 x 10^{-3} for N = 10, and 2.6 x 10^{-4} at N = 100, and is 1.5 x 10^{-4} for N = 1000. The integral expressions given in Equation (9) and (15) for the time dependent solutions, $\Psi_F^{<}(x,y,t,N)+\Psi_G^{<}(x,y,t,N)$ and $\Psi_F^{>}(x,y,t,N)$, respectively, along with their respective coefficients, A_ζ, B_ζ, and C_ζ, are obtained with the use of Equations (A.15) – (A.19) and some tedious but straight-forward algebra and trigonometric identities.

APPENDIX B. SCALING LAWS

Here we follow Phillippidis et al.[5] who assumed that the number of particles impinging on the entrance of the two slits is one at any given instant. Thus, with no external influence the probability of finding the particle emanating from either slit is 0.5. When the number of particles impinging on the slits is more than one, i.e., n_o as defined below, Equation (A.15) represent the un-normalize solution for both slits,

$$\psi = \xi F_0 \Omega + \delta G_0 \Theta . \tag{B.1}$$

We no proceed to show that this wave function can be written as the product of a normalized wave function, χ, times a scaling factor, F_0, to establish a scaling law for the wave function.

The boundary conditions at the surface of the jet slits for initial particle velocity, u_o, which is in the axial x-direction, and initial number of particles, n_o, are as follows:

$$\rho(0,y) = 0, \quad u(0,y) = 0 \quad , \quad 0 < y < 0.6 \quad \text{and} \quad 0 > y > -0.6 \tag{B.2}$$

$$\rho(0,y) = \rho_o, \quad u(0,y) = u_o, \quad 0.6 < y < 1.0 \quad \text{and} \quad -0.6 > y > -1.0 \tag{B.3}$$

$$\rho(0,y) = 0, \quad u(0,y) = 0 , \quad y > 1 \quad \text{and} \quad y < -1.0 \tag{B.4}$$

Since the Heisenberg Uncertainty Principle limits the precision with which one can simultaneously determine the position and velocity of a particle the velocity $u_o = u(0,y)$ must be interpreted as an average velocity equal to $J_x(0,y)/\rho(0,y) = (2E/m_e)^{1/2}$.

In order to determine F_0 we follow Phillippidis et al.[5] The expectation value of the number of particles per unit length present in each slit is given by,

$$n_o = \int_0^\infty \rho(0,y)\, dy = \int_0^\infty \psi(0,y)\psi^*(0,y)\, dy = \xi\xi^* F_0^2 \int_0^\infty \Omega^2\, dy = \xi\xi^* F_0^2 . \tag{B.5}$$

Here the boundary conditions on $\Omega(x,y)$, given in Appendix A, have been used to obtain the final result. In this expression the scaling factor F_0 as been defined; it is

$$F_0 = \left[2n_o\right]^{1/2}. \tag{B.6}$$

It is of interest to note that when $n_0 = 1/2$, or $F_0 = 1$, the corresponding wave function is essentially the normalized wave function of Phillippidis et al.[5]

An expression for the scaling factor G_0 is obtained directly from probability current density,

$$\mathbf{J} = \rho\mathbf{u} = \left(\frac{h}{2im_e}\right)\left(\psi^*\nabla\psi - \psi\nabla\psi^*\right). \tag{B.7}$$

Since the particles are assumed to emanate from the slits parallel to the x-axis (B.7), the mean particle velocity in axial direction is given by

$$u = \frac{J_x}{\rho} = \frac{h}{m_e}\frac{G_0}{F_0}\frac{\pi}{b}\left[\frac{-\Theta\,\Omega_x + \Omega\,\Theta_x}{\Omega^2 + \left(G_0/F_0\right)^2\Theta^2}\right], \tag{B.8}$$

where the subscript x indicates the partial derivative with respect to x as introduced in Appendix A. By using the boundary conditions for the initial mean particle velocity, u_o, we can determine the scaling factor G_0 in terms of F_0 and u_o. Substituting the dual slit wave function, Equation (A.15), and its component parts, Equations (A.16) - (A.19), into (B8) we find,

$$u(0, y) = 0, \quad 0 < y < 0.6 \quad \text{and} \quad 0 > y > -0.6, \tag{B.9.a}$$

$$u(0,y) = u_o = \frac{h}{m_e}\frac{G_0}{F_0}\frac{\pi}{b}(1+\Delta), \quad 0.6 < y < 1.0 \quad \text{and} \quad -0.6 > y > -1.0, \tag{B.9.b}$$

$$u(0, y) = \quad 0, \quad y > 1 \quad \text{and} \quad y < -1.0, \tag{B.9.c}$$

In Equation (B.9.b), the symbol Δ is the error associated with the approximation occurring in the evaluation of the Fredholm integral related to $Z^{<}(N-\zeta)$ given in Appendix A for selected values of N used in the calculation.

Within this approximation, we write

$$\frac{G_0}{F_0} = \frac{m_e u_o b}{h\pi}. \tag{B.10}$$

However, the definition of the Reynolds number given in the text is $N = u_o b/(h\pi/m_e)$. Thus it should be now obvious that we can recast N as ratio of the scaling factors,

$$N = \frac{G_0}{F_0} = \frac{m_e u_0 b}{h\pi}, \tag{B.11}$$

or alternatively by Equation (4.a), is equal to the ratio $\lambda_b = b/\pi$ with the deBroglie wavelength λ_{dB}, $G_0/F_0 = \lambda_b/\lambda_{dB}$.

Using Equation (B.11) along with Eq, (B.6) in Equation (B.1) yields a dual slit wave function as a function of the Reynolds number,

$$\psi(x, y, N) = \xi F_0 \Omega + \delta G_0 \Theta = \left[2n_o\right]^{1/2}\left(\xi \Omega + \delta N \Theta\right) \tag{B.12}$$

Equation (B.12) is normalized when n_0=1/2. That is, the normalized wave function is

$$\chi(x, y, N) = \left(\xi \Omega + \delta N \Theta\right). \tag{B.13}$$

Substituting (B.13) back into (B.12) results in the scaling law for the wave function consistent with Fitts,[11]

$$\psi(x, y, N) = \left[2n_o\right]^{1/2} \chi(x, y, N). \tag{B.14}$$

REFERENCES

1. P.R. Holland, The Quantum Theory of Motion, (Cambridge, New York, 1993).
2. H. Licht, Phil Trans R. Soc. London, **A360**, 897 (2002)**.**
3. M P. Silverman, Waves and Grains, (Princeton University Press, Princeton, N.J., 1998) pp. 77 – 95.
4. A. Howie and J.E. Fowcs Williams, Phil Trans Royal Soc of London, **360**, 803 (2002).
5. C. Philippidis, D. Bohm, and R.D. Kayes, Nuovo Cimento, **71**B, 75 (1982).
6. H.H. Chiu, C.T., Lin, S.Y. Lin, T.C. Hung, and F.L. Mardarasz, *Developments of Quantum Nanojet based Nanodevices*, ICEE11, Hilton Head (2004).
7. H.H. Chiu and C.T. Lin, *Structural and dynamic complexities of nanojets,* Air Force Office of Scientific Research / Taiwan Nanoscience Initiative Workshop, Maui (2004).
8. M. Moseler and U. Landman, Science, **289**, 1165 (2000).
9. Jens Egers, Phys. Rev. Lett., **89**, 084502 (2002).
10. H.H. Chiu, Proceedings of the Royal Society (London), accepted, publication pending (2005).
11. Donald, D Fitts. Principles of Quantum Mechanics As Applied to Chemistry and Chemical Physics (Cambridge University, New York, N.Y., 1999) pp. 38 –40.

FIGURE CAPTIONS

Figure 1. Dual jet slit schematic diagram.

Figure 2. Probability density of near field (Fresnel) jet streams density versus axial distance as a function of quantum Reynolds number. The magnitude of the probability density is color coded in the key next to each figure.

Figure 3. Probability density of near field (Fresnel) and far field (Fraunhofer) jet streams density versus axial distance as a function of quantum Reynolds number. The magnitude of the probability density is color coded in the key next to each figure.

Figure 4. Probability density versus axial distance as a function of quantum Reynolds number**.**

Figure 5. Probability density versus axial distance and quantum Reynolds number. L_a, L_b, and L_c are the displacement values, on the jet axis of propagation, where the cluster initially starts to grow, for the cluster maximum, and for the effective end of the cluster, respectively

Figure 6. Parametric study of the effects of different slit separation width of 2b on the cross-sectional contours, at x = 10, of probability density and its corresponding interference pattern. b takes on the values of b = 0.8nm, 1.0nm, 1.5nm, 2.0nm, 2.5nm, and 3.0nm, corresponding respectively to the figure panels (a – f). The value of quantum Reynolds number is N = 10.

Figure 7. Effects of a change of quantum Reynolds number, N, on interference fringes as a function of axial displacement, x.

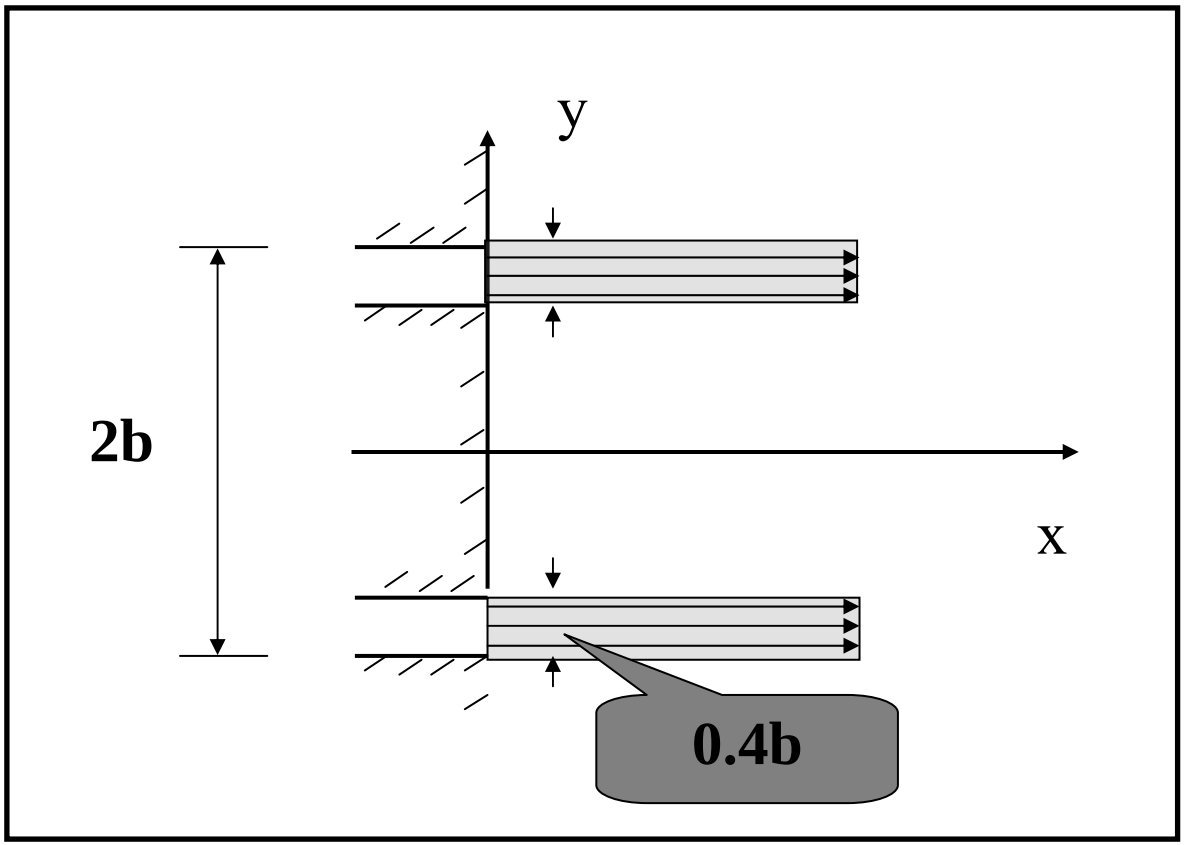

Fig. 1 Chiu et al.

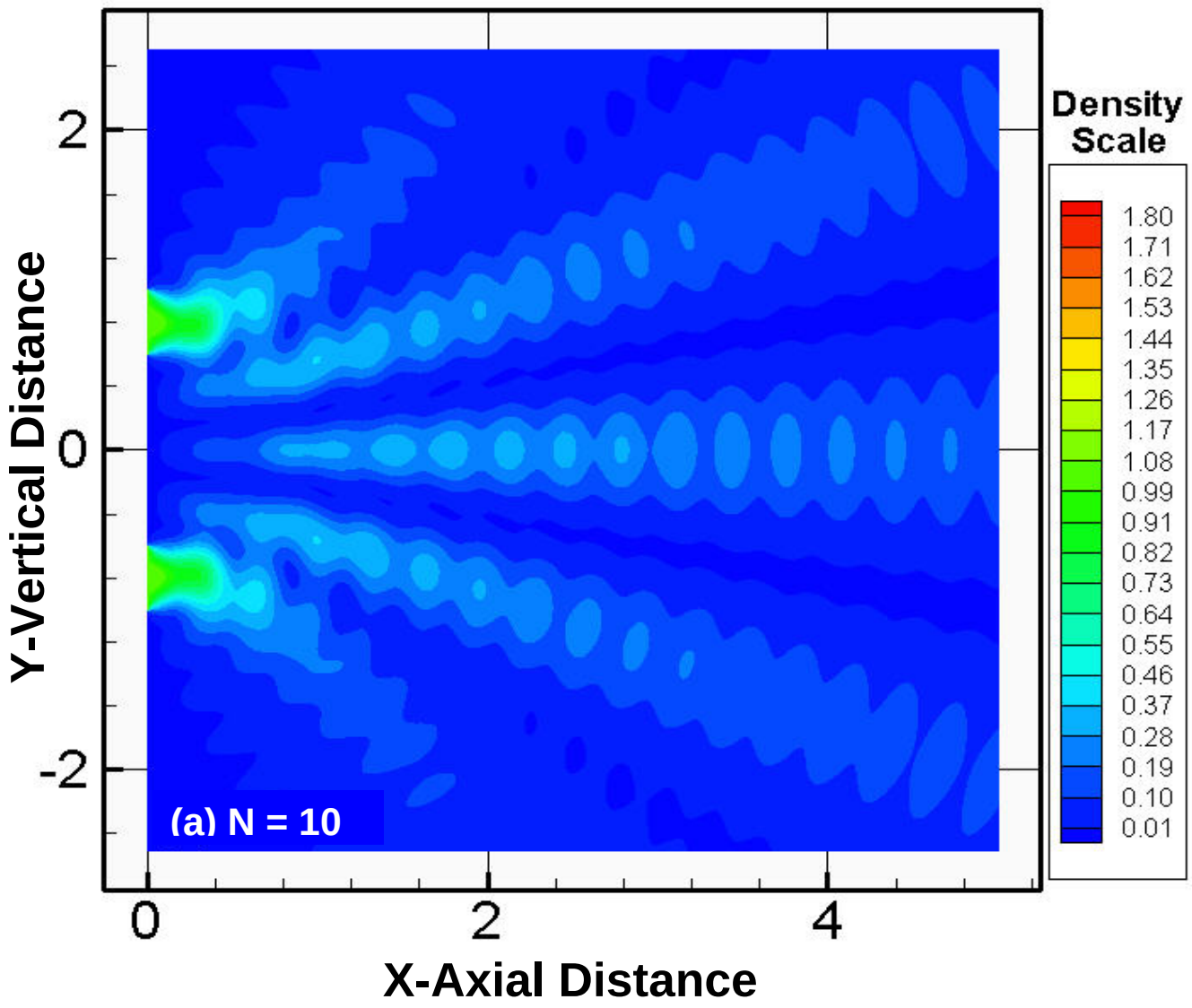

Fig. 2a Chiu et al.

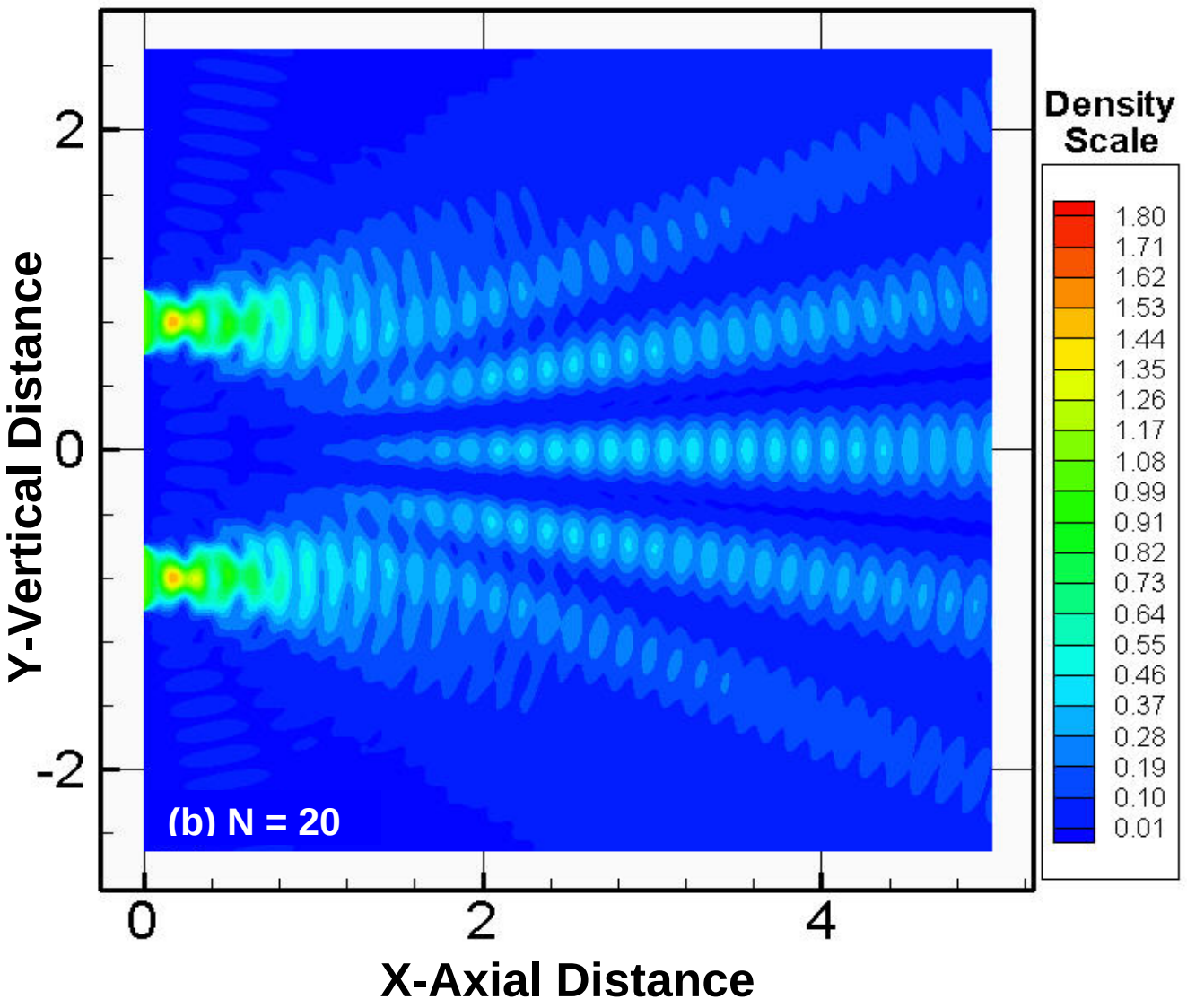

Fig. 2b Chiu et al.

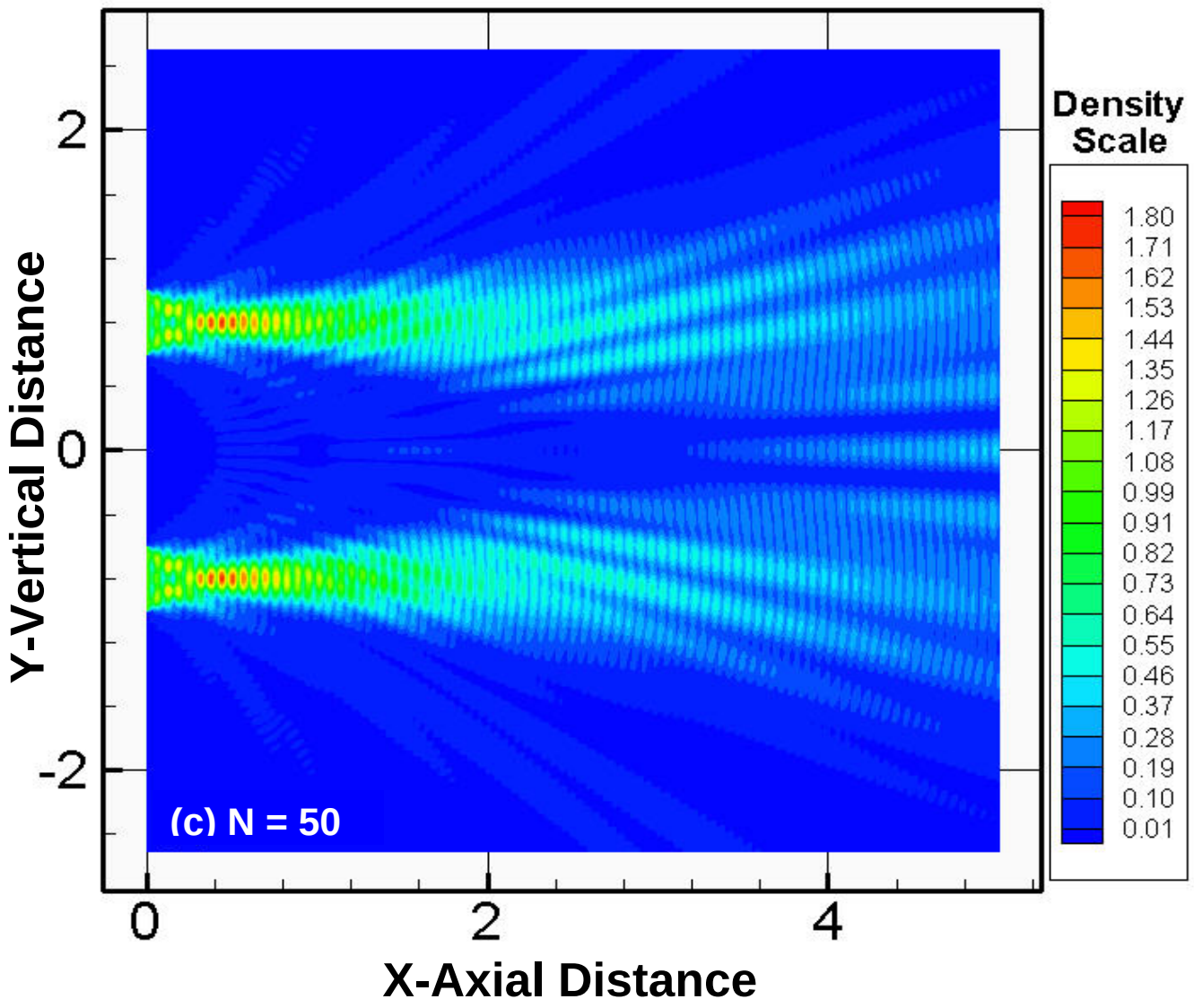

Fig. 2c Chiu et al.

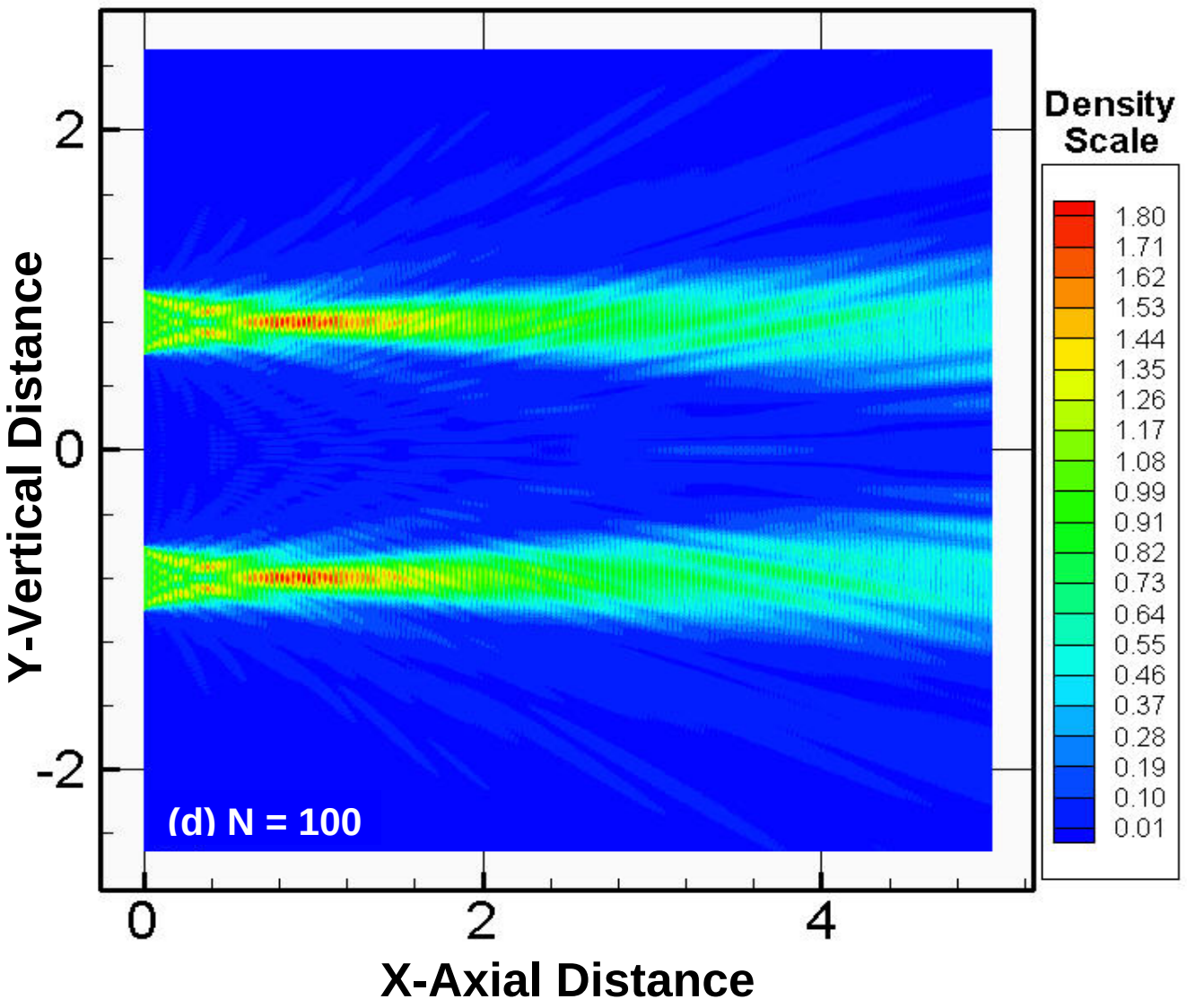

Fig. 2d Chiu et al.

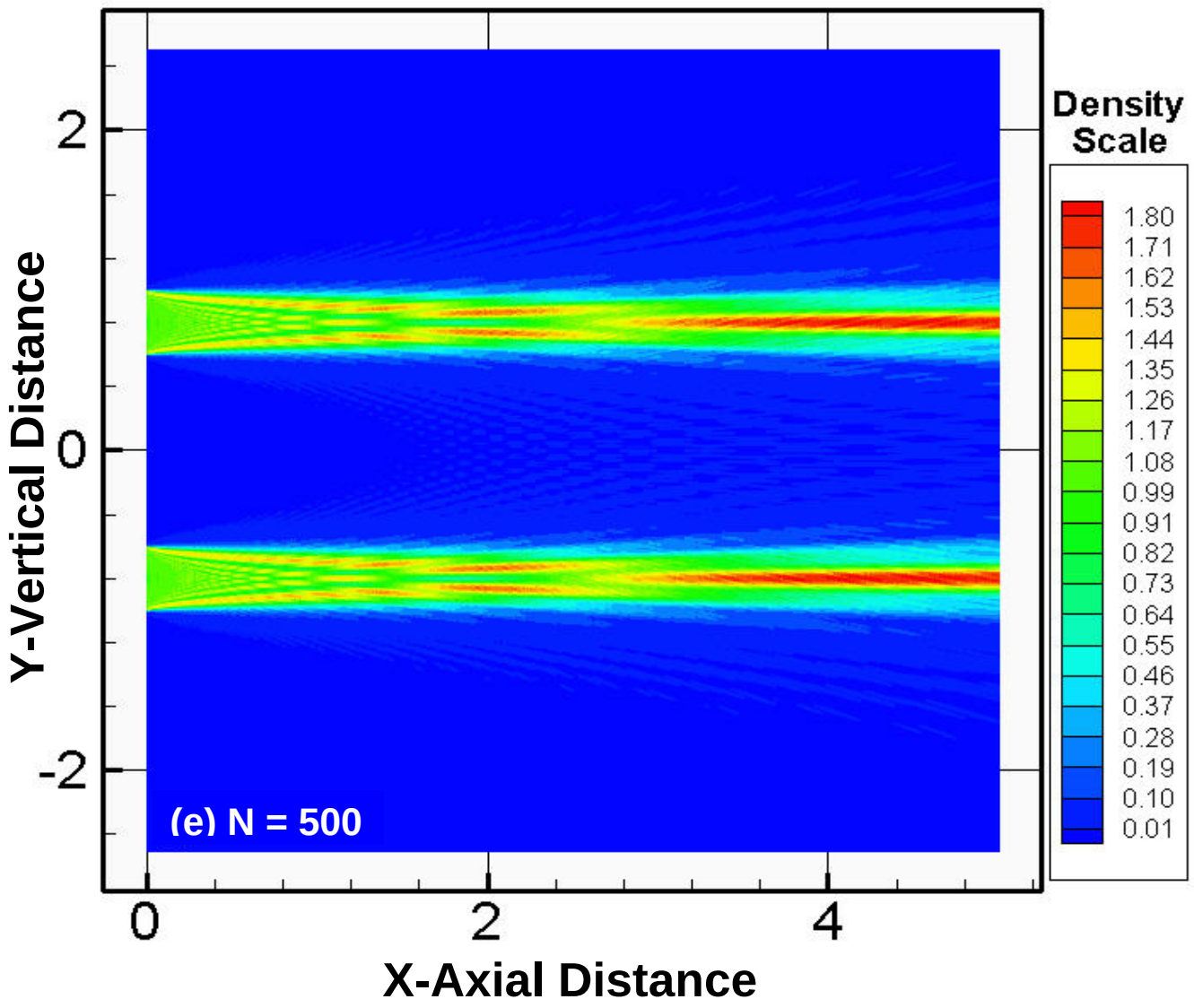

Fig. 2e Chiu et al.

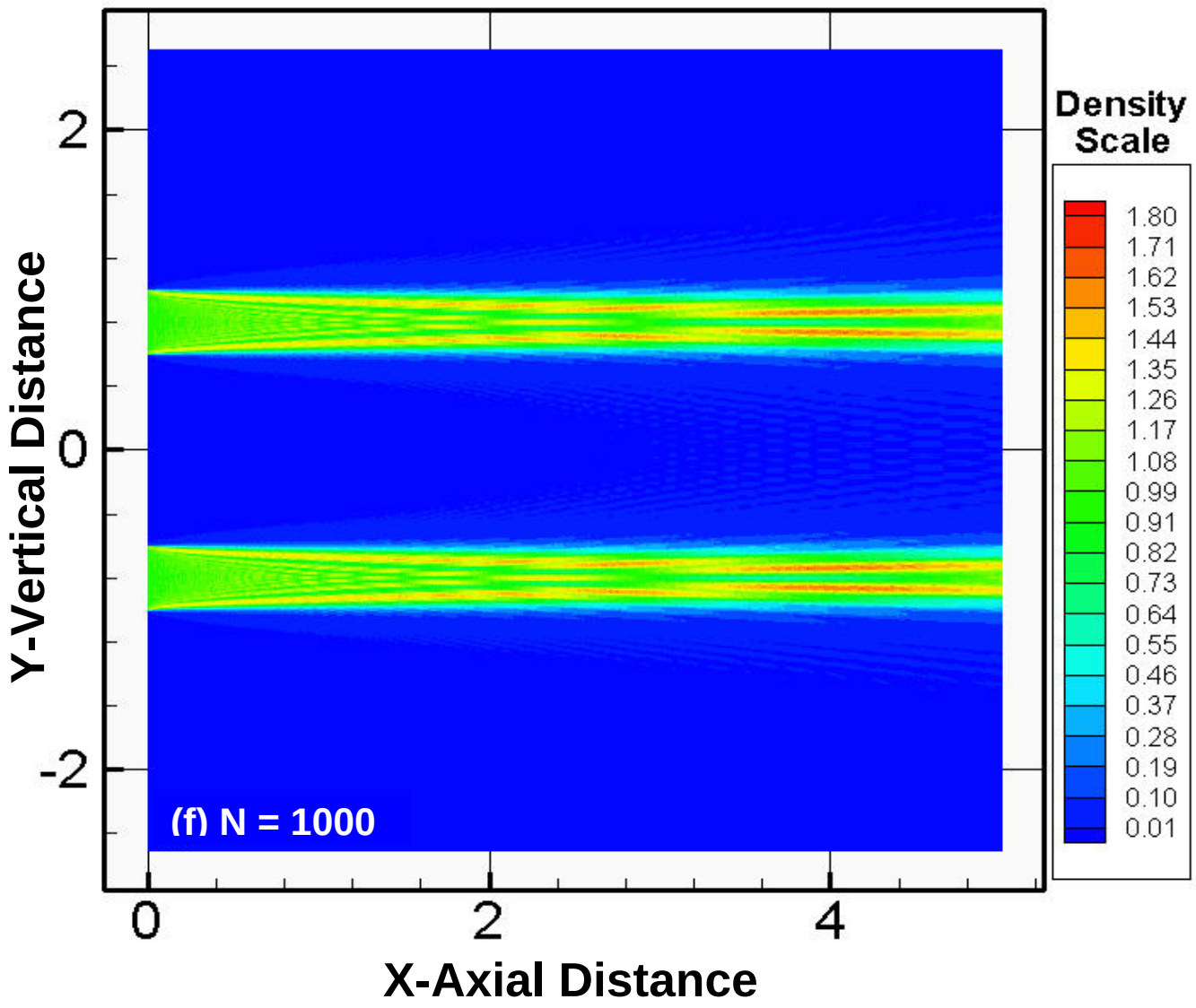

Fig. 2f Chiu et al.

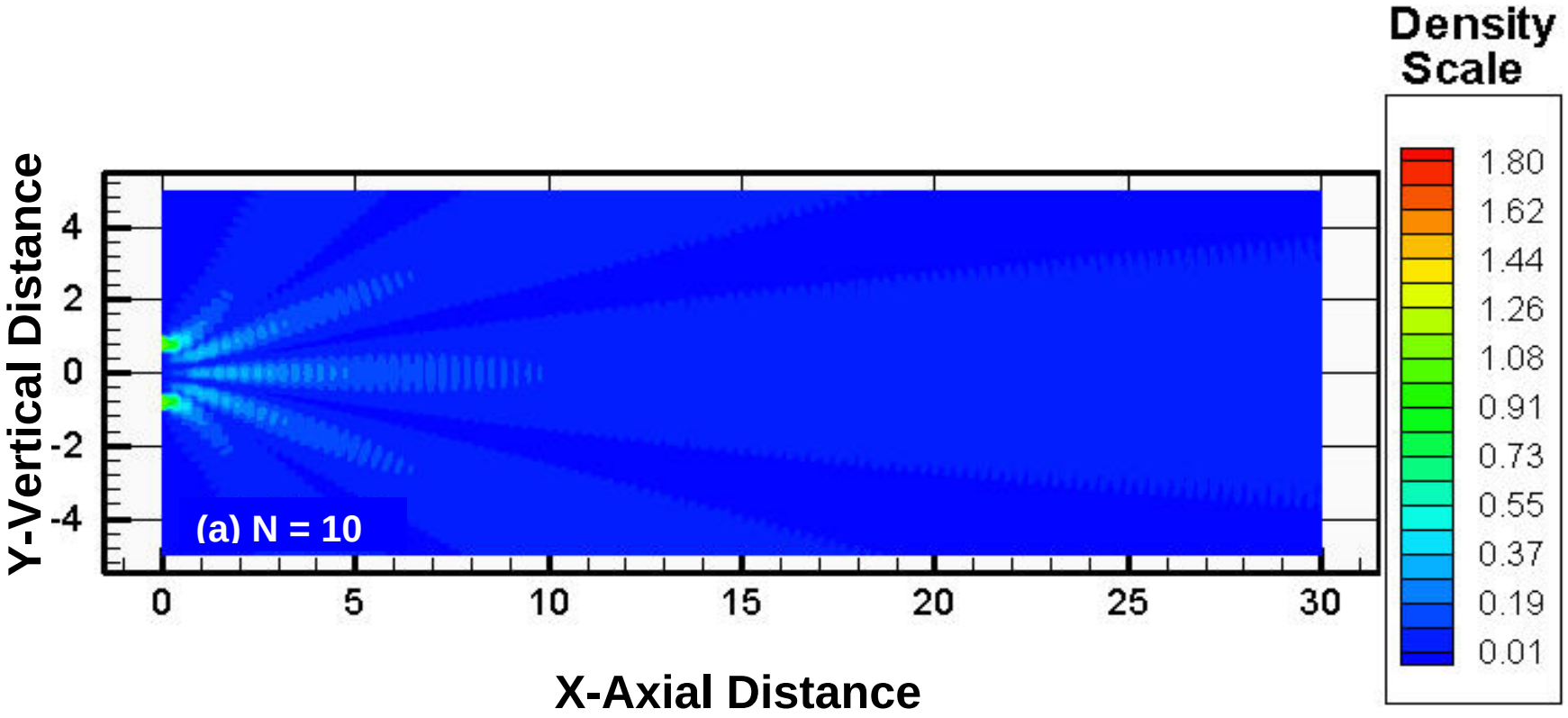

Fig. 3a Chiu et al.

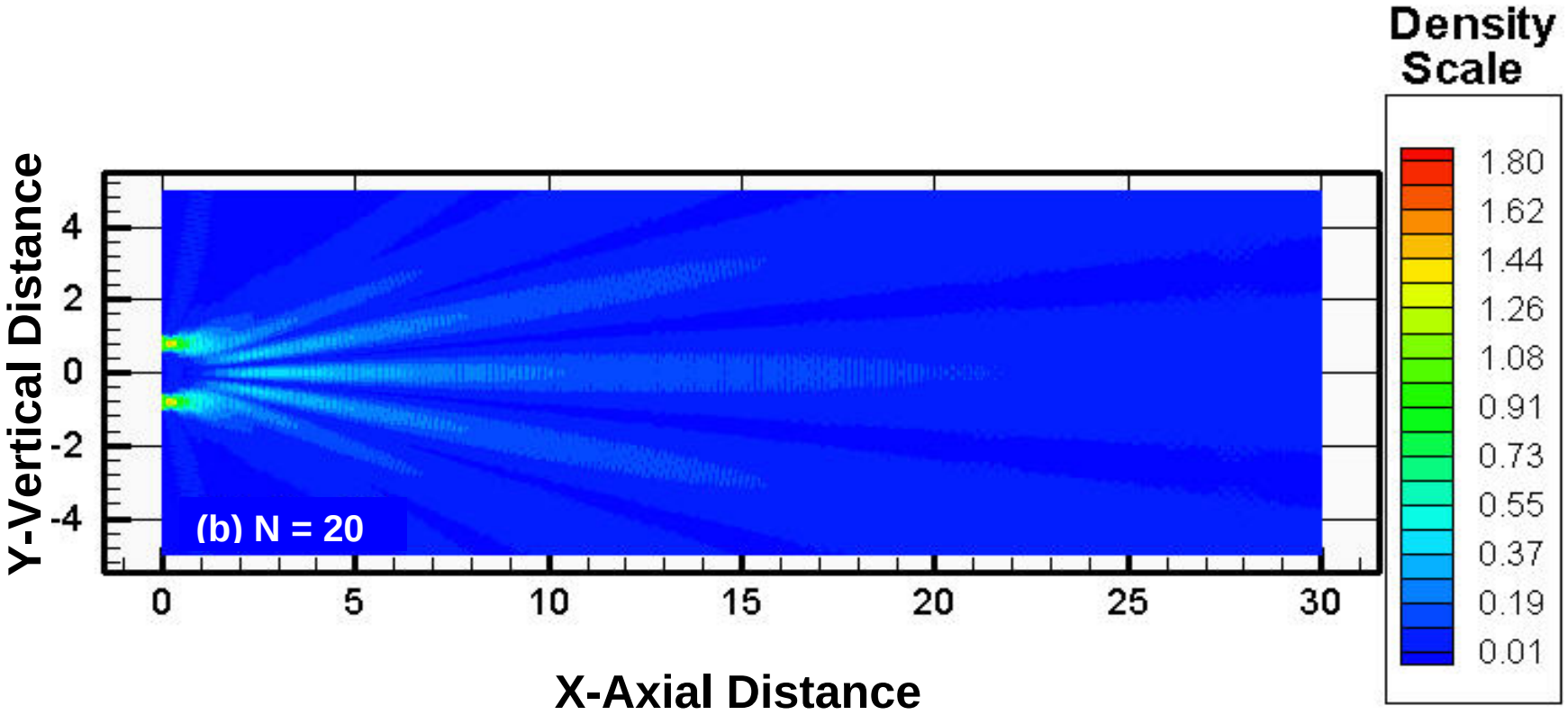

Fig. 3b Chiu et al.

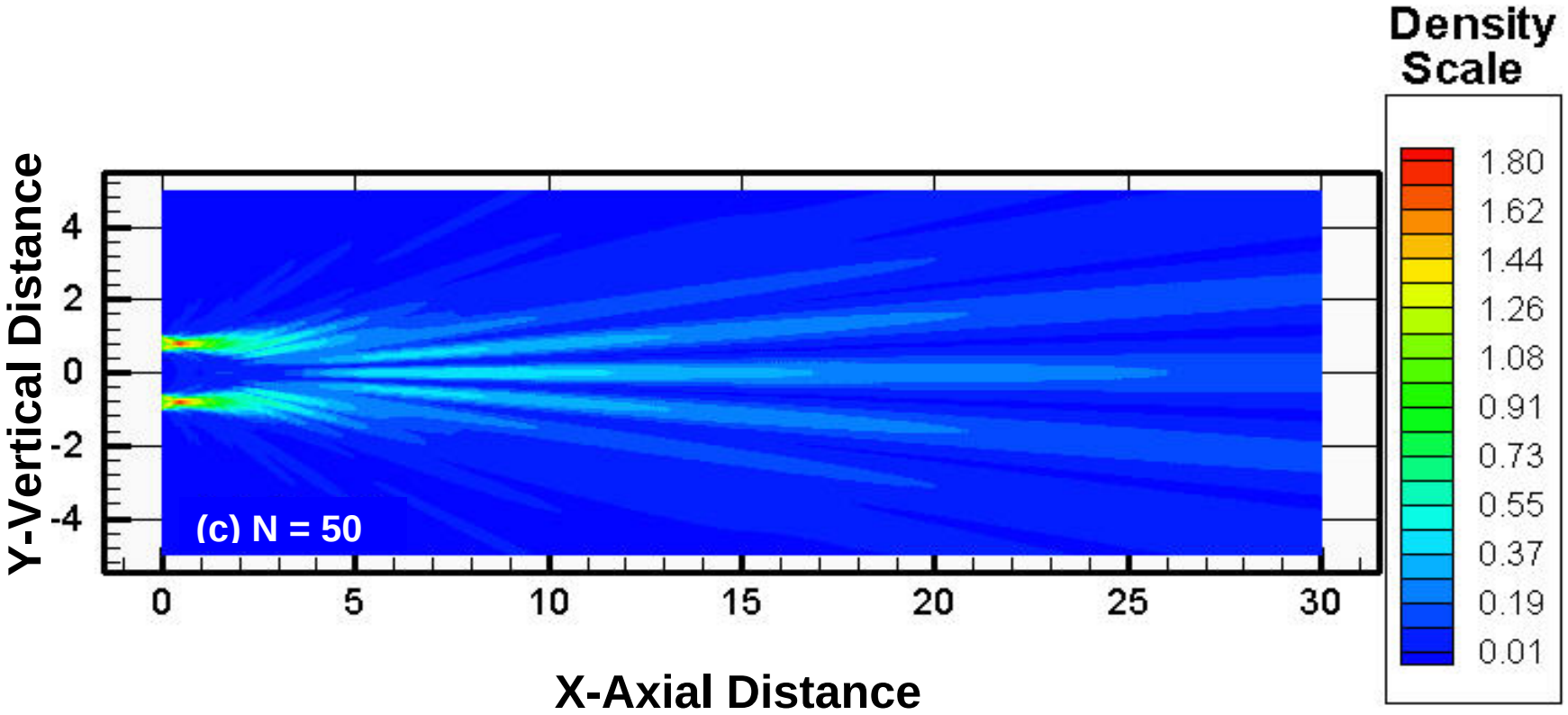

Fig. 3c Chiu et al.

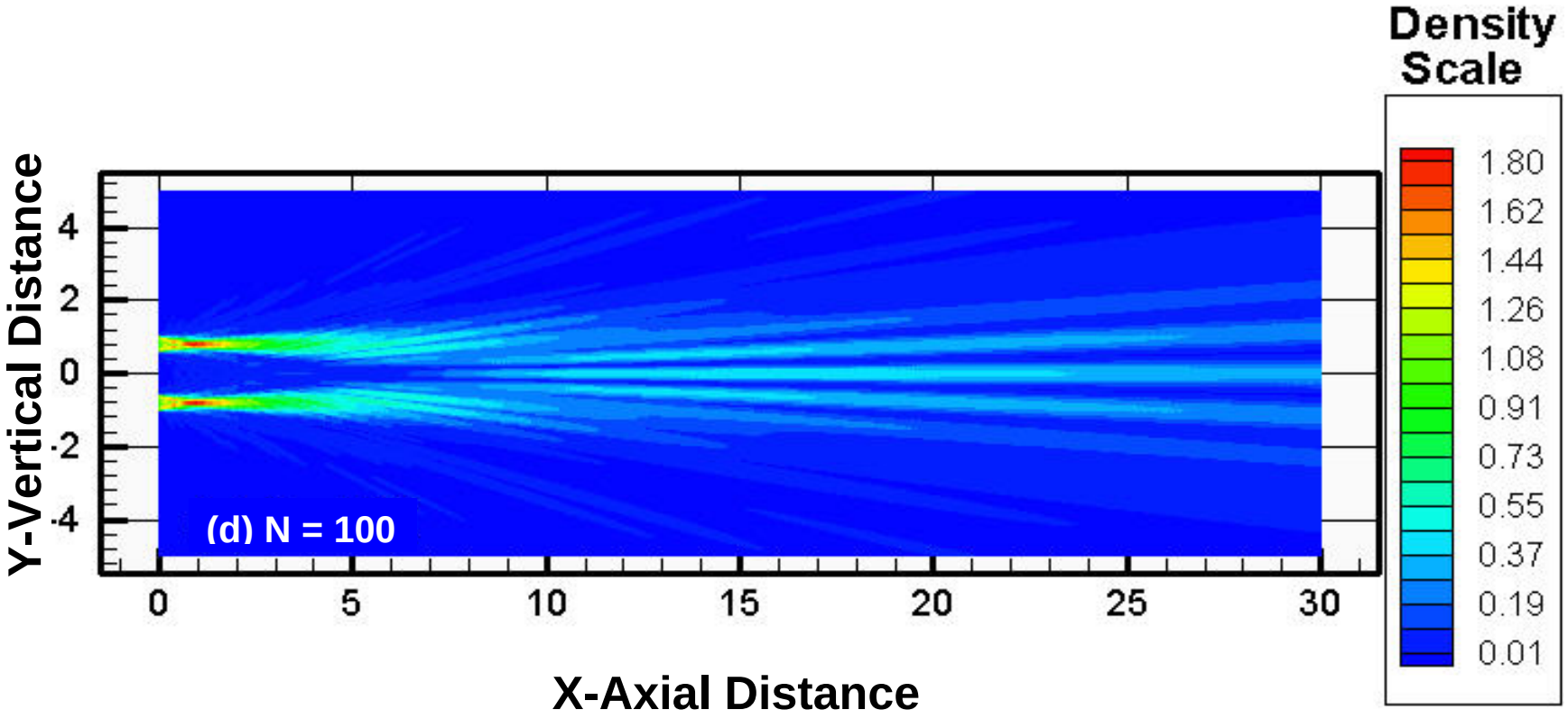

Fig. 3d Chiu et al.

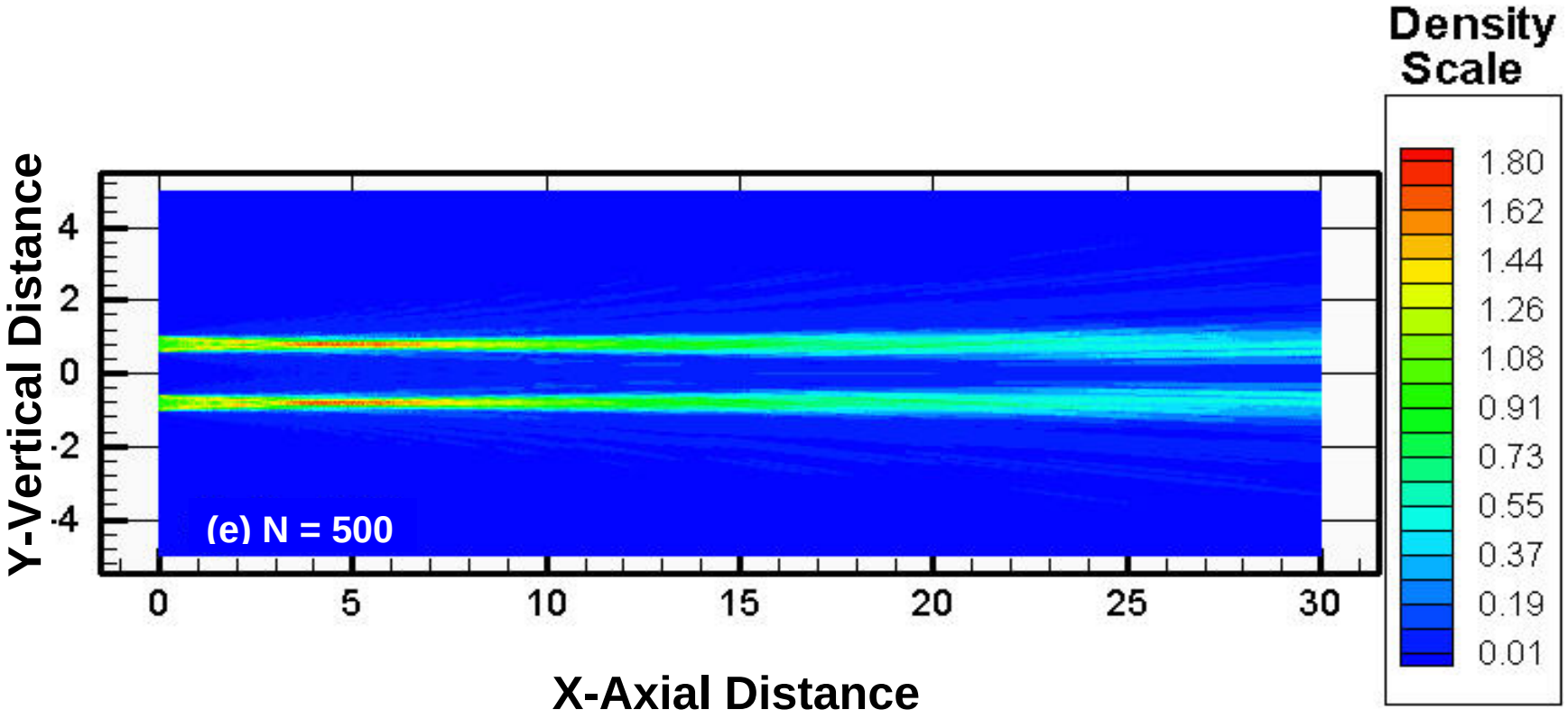

Fig. 3e Chiu et al.

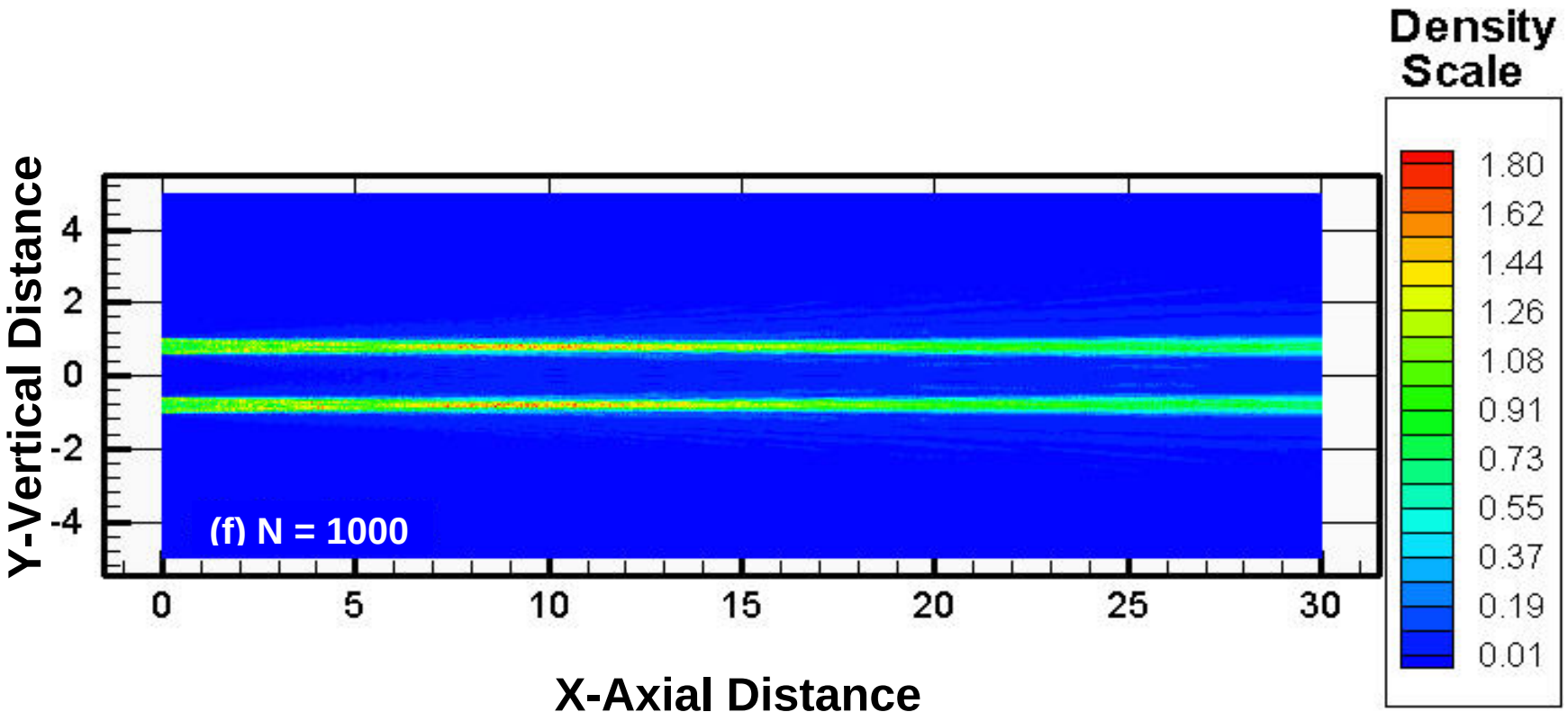

Fig. 3f Chiu et al.

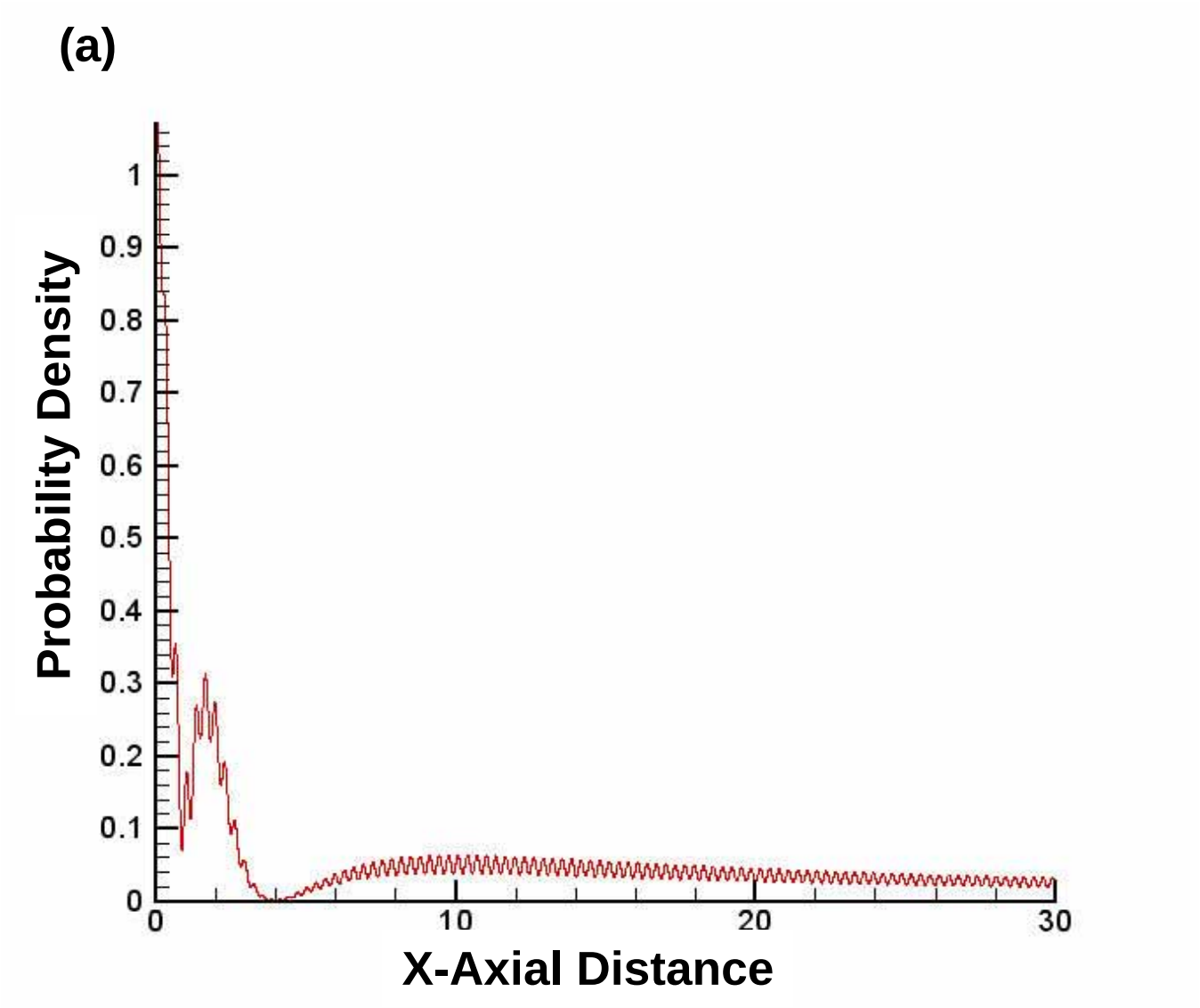

Fig. 4a Chiu et al.

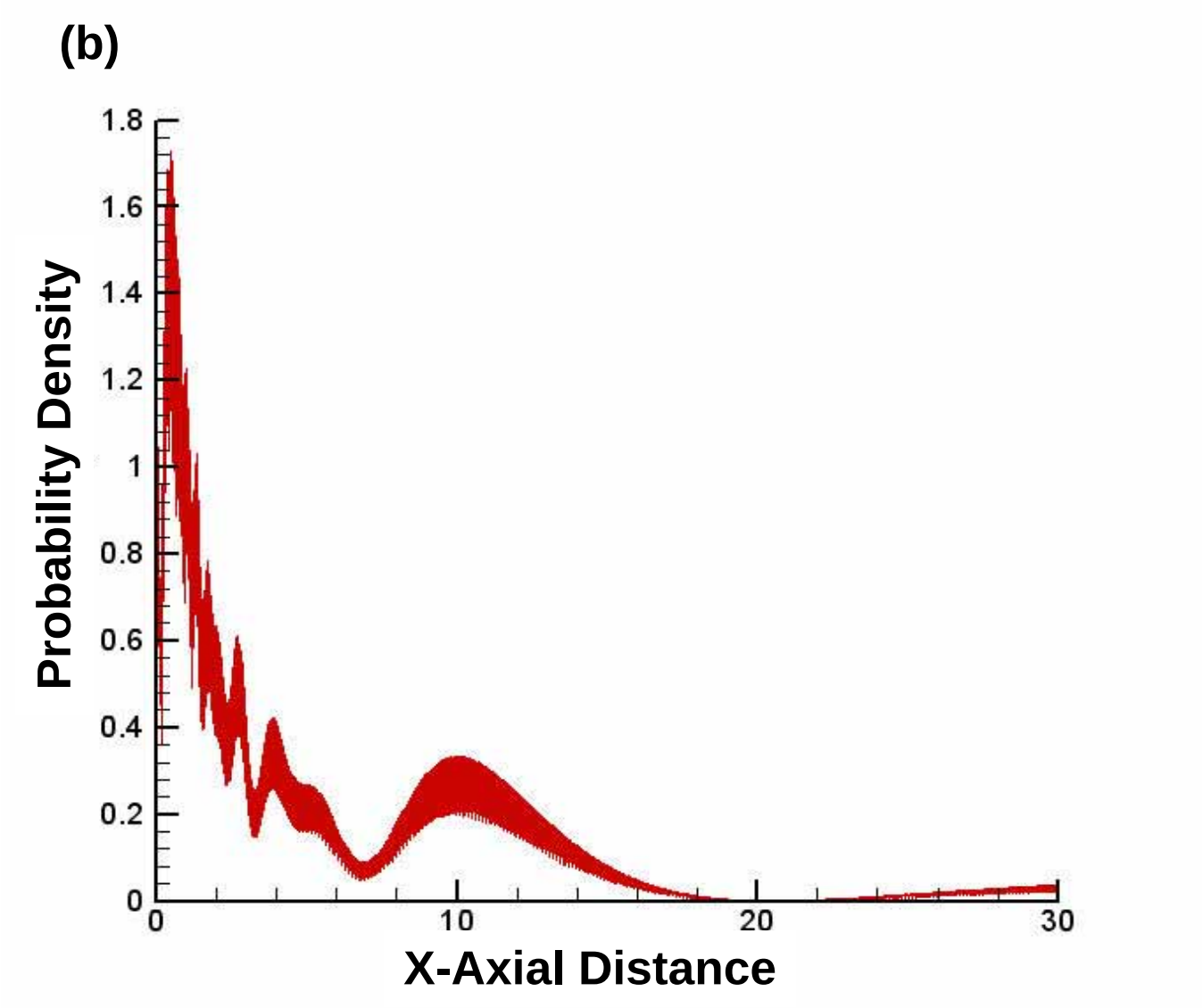

Fig. 4b Chiu et al.

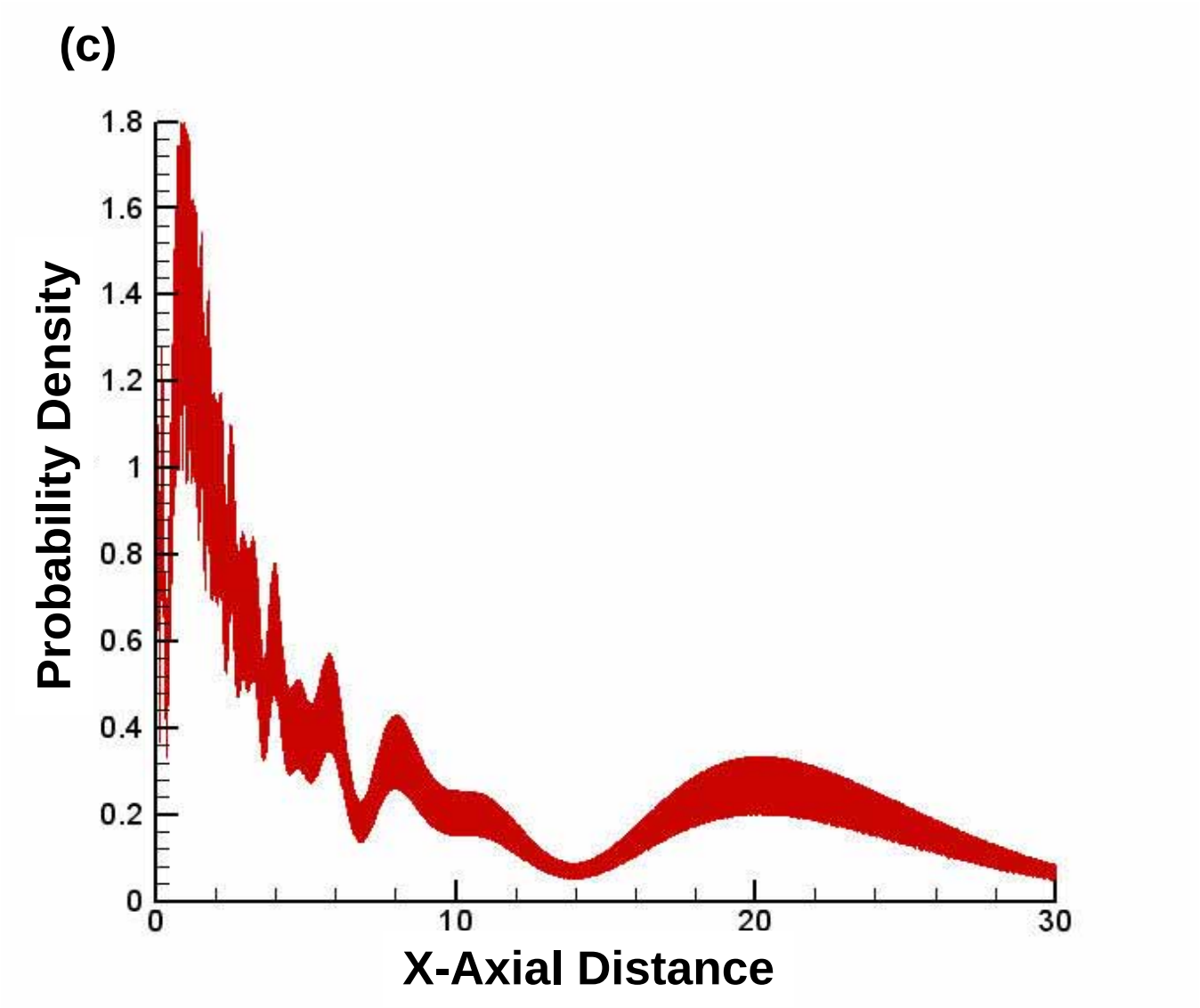

Fig. 4c Chiu et al.

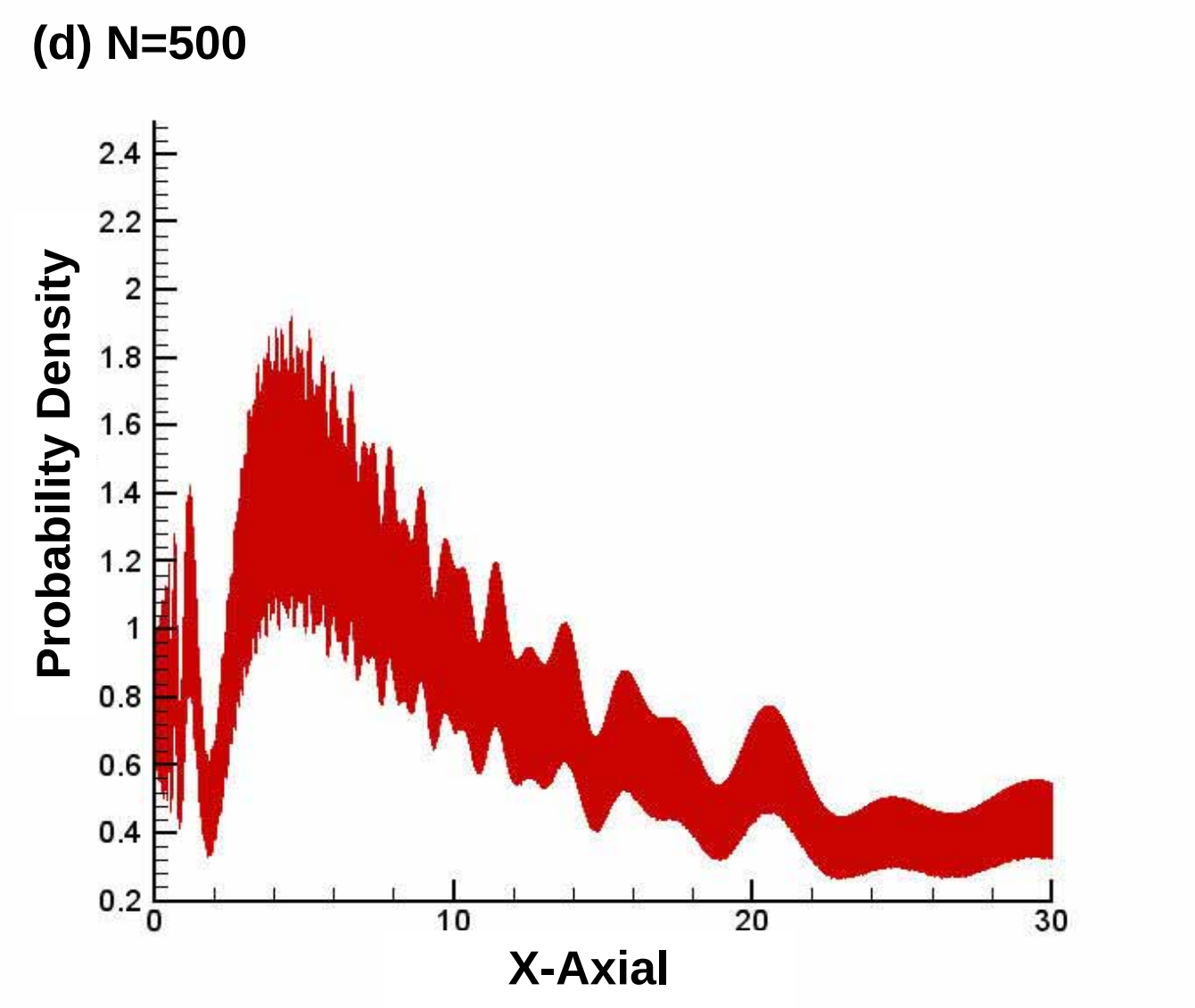

Fig. 4d Chiu et al.

(e) N=1000

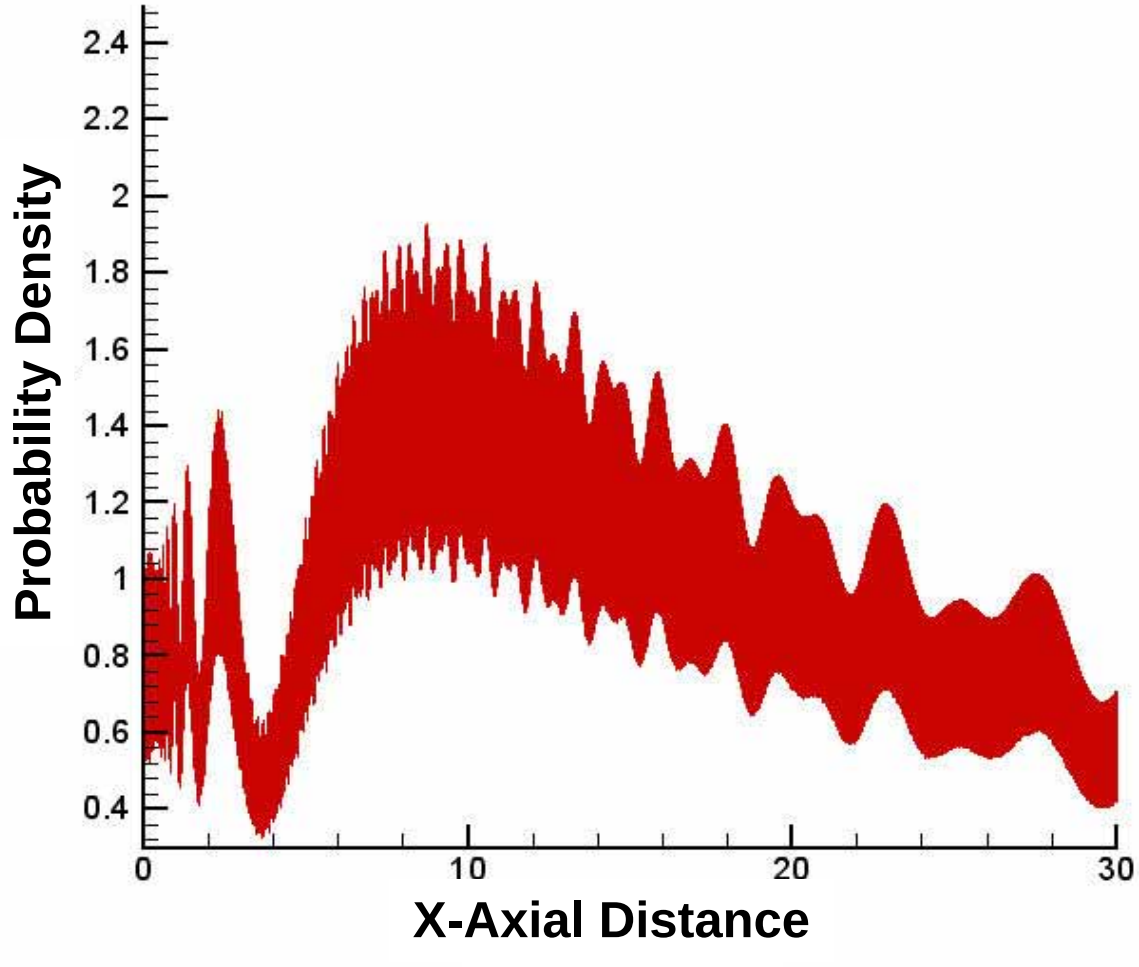

Fig. 4e Chiu et al.

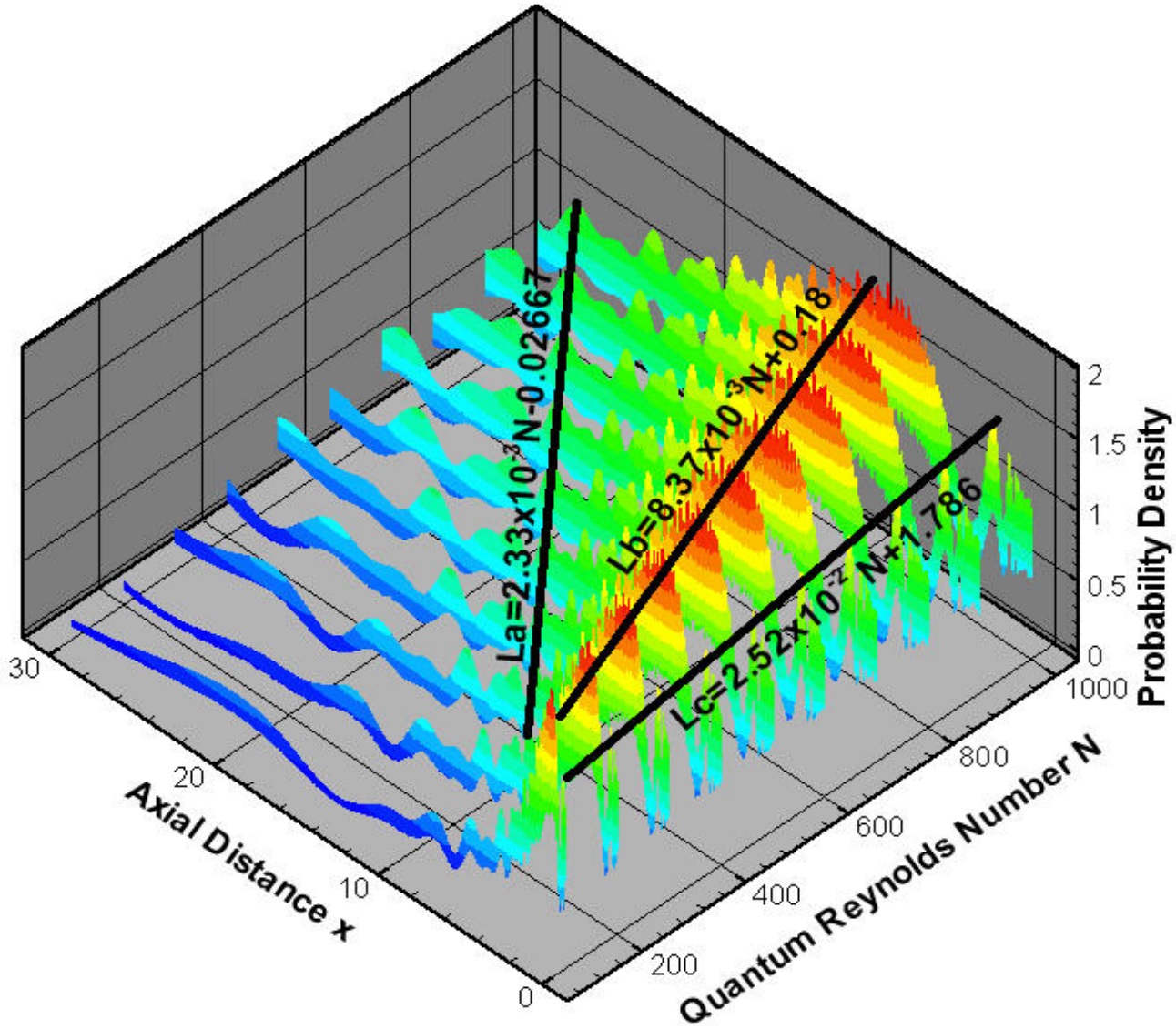

Fig. 5 Chiu et al.

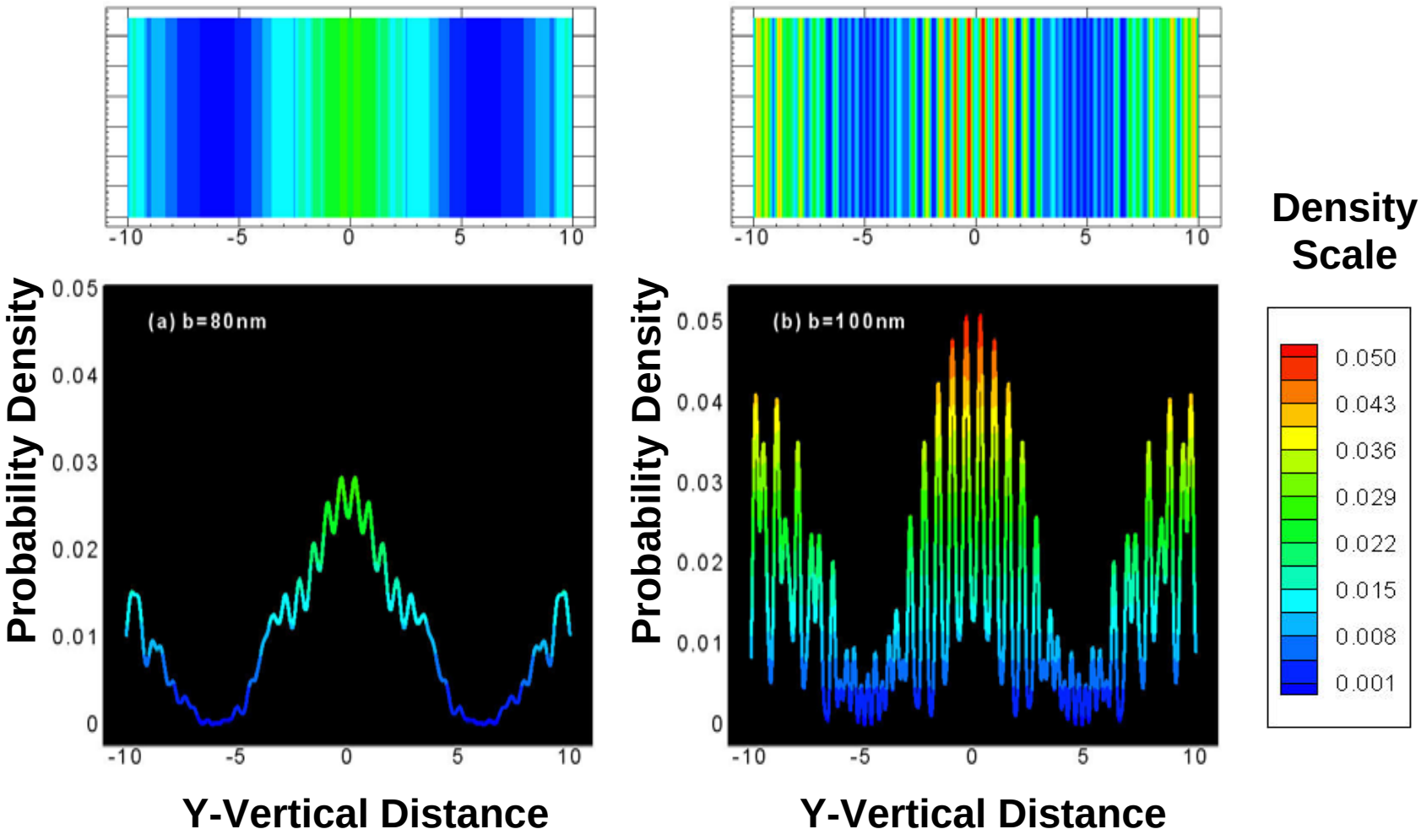

Fig. 6a Chiu et al.

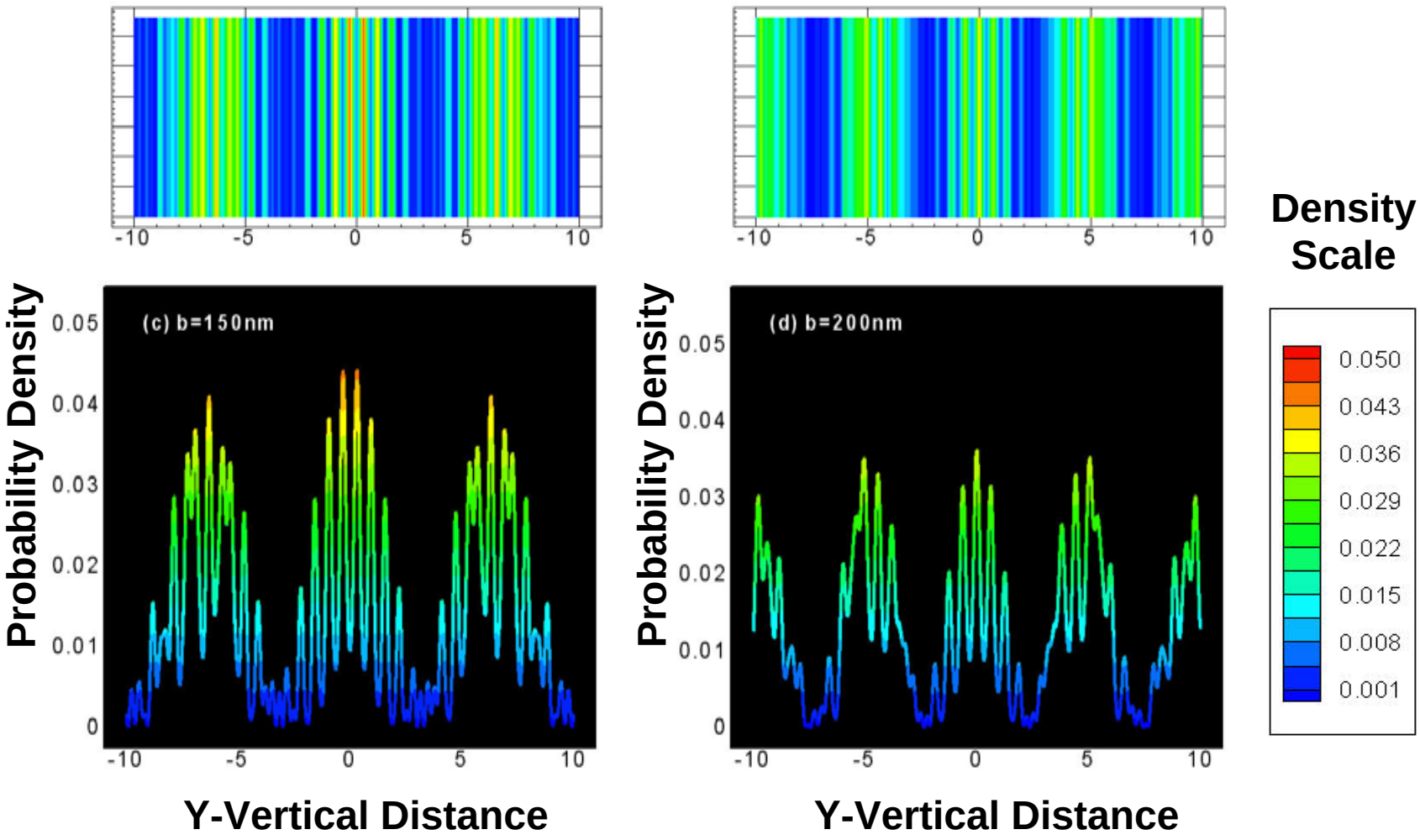

Fig. 6b Chiu et al.

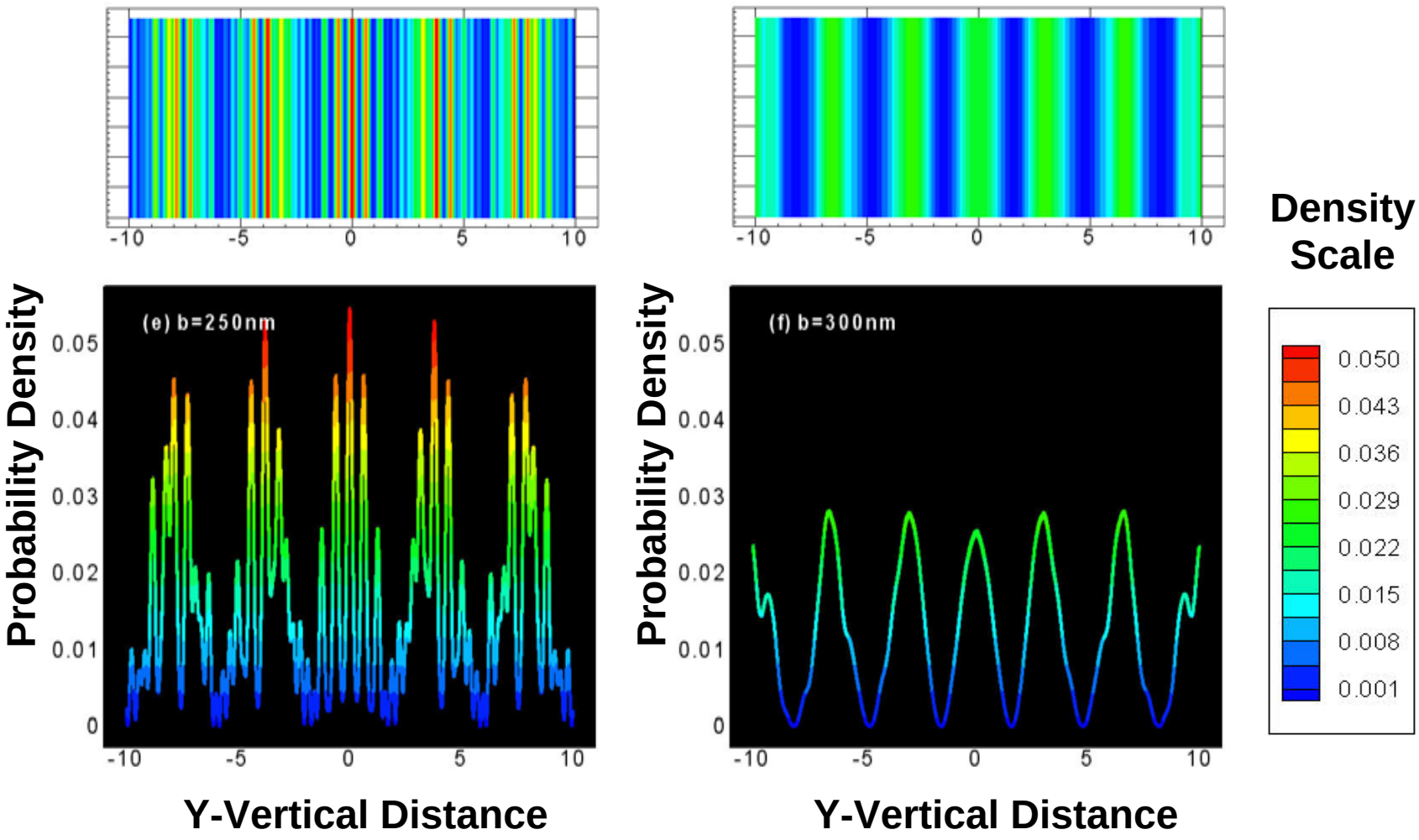

Fig. 6c Chiu et al.

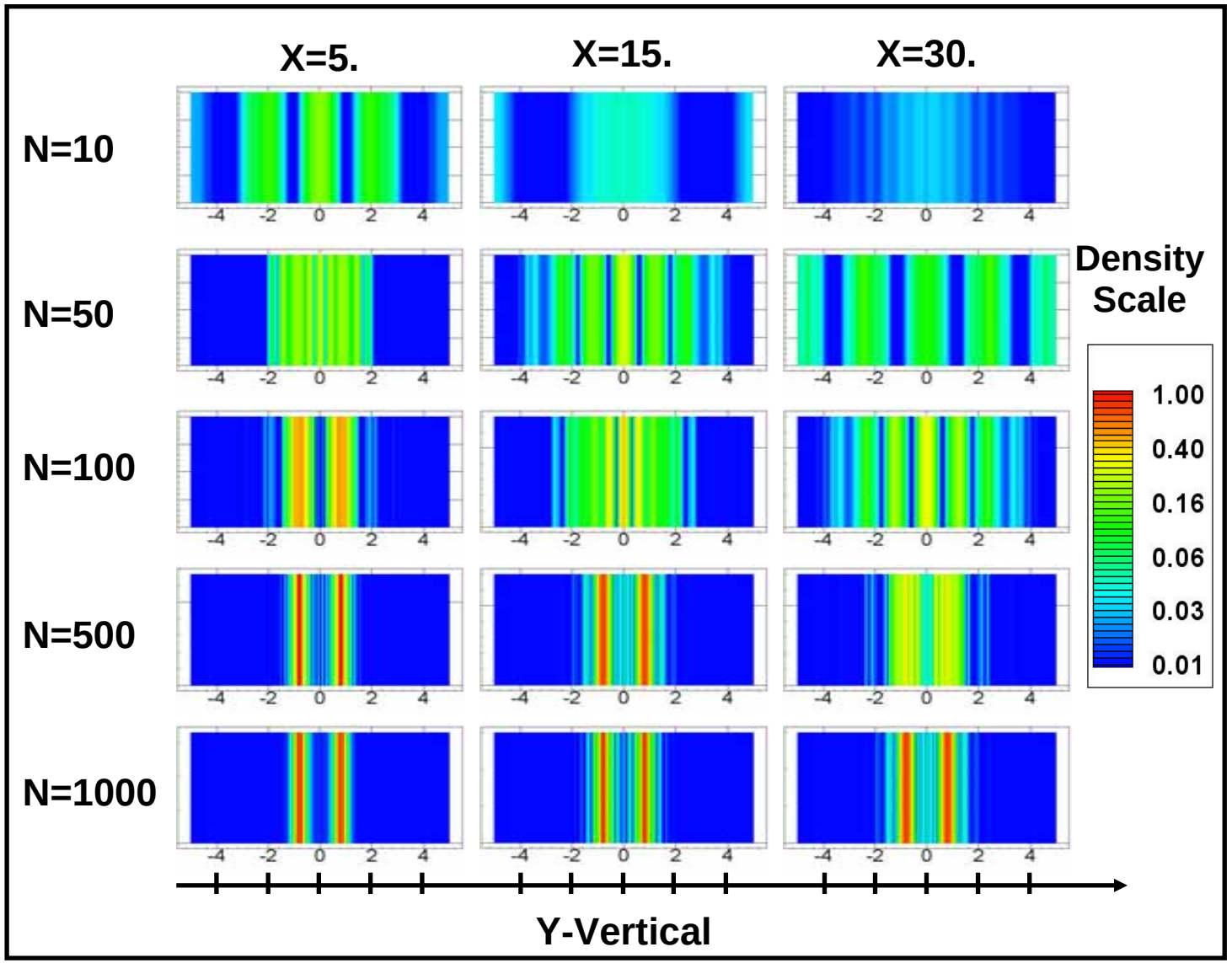

Fig. 7 Chiu et al.

Theory of quamlets of quantum systems

H.H. Chiu
Space science and Technology Center
National Cheng Kung University
Tainan, 70101 Taiwan

Two leading quantum mechanical formalisms: Schrödinger's wave mechanics and the quantum fluid dynamics, which is based on Hamilton-Jacoby equation, are compared to assess their quantum mechanical equivalence between the linear and non-linear fields. A quantum system in a stationary state, described by the linear superposition of eigenfunctions corresponding to the same degeneracy energy level is found to be equivalent to the mixture of the "elemental and interactive quantum flowlets", termed "quamlets", each of which is constructed by the bilinear product of eigenfunctions and their complex conjugates.. We show that the equivalence between two formalisms is met if each quamlet obeys the non-linear equations of conservation of the probability density and energy when the global quantum flow field, which consists of the quamlet mixture, satisfies the non-linear equations of the conservation as well as the quantization condition, as in the quantum theory. An example of the quamlets in two-dimensional flow is given to illustrate the properties and the compliance of the conservations of the elemental and interactive quamlets. The equivalence principle also provides the guides and criteria required for the analytical and numerical simulation of complex quantum systems by fluid dynamic approaches, and quantum computational fluid dynamics.

I. INTRODUCTION

Quantum mechanics has been successfully applied in various areas of quantum physics: atoms, molecules, nuclear physics, superconductivity, and chemistry, nevertheless there have been number of attempts proposed to offer alternative interpretations based on the fluid mechanical description, notably by Madelung [1], de Broglie[2] since the early developmental stage of quantum theory and later, followed by Bohm's hidden variables [4,5,6], and the theory of stochastic mechanical approach by Nelson and others[6-16]. Various aspects of fluid dynamics including basic formulation, Takabayashi [17-18], Kan and Griffin [19], vortex motion, Bialynicki-Birula and Sliwa [20], quantization condition, [17,18], Wallstrom[21,22]. The motivations and the physical significance underlying the reformulation of quantum mechanics to fluid dynamic, which will be referred to as QM-QFD reformulation, are presented by Holland [23]. One of the basic motivations for the QM-QFD reformulation is prompted by the criticism on the lack of the ontological interpretation by quantum mechanical theory, which renders limited physical insight for the mechanisms of quantum phenomena. Unique advantage of the reformulation is the conversion of abstract wave physics to the familiar physics of the fluid flow of the equivalent quantum fluid, characterized by the density and velocity of the probability fluid whereby the quantum phenomena are explained by the principles of the conservation of probability fluid density, mechanical energies, including external potential, mean flow kinetic energy and quantum potential energy. For example, in the recent analysis based on QFD formalism, Chiu [24], identified that the quantized energy

of hydrogen atom is equal to the kinetic energy of the asymptotic diffusion velocity of the electron probability fluid, and that the radial dynamic equilibrium of the electron is maintained by the balance between the quantum potential forces, induced by the gradient of dilatation and diffusion kinetic energy, with the central Coulomb force. The kinetic energy of the vortex induced flow is provided by the quantum dilatation energy associated with the diffusion in polar angular direction. It is also reported that the zero-point energy in a simple harmonic oscillator is found to be the dilatation energy associated with the asymptotic diffusion of the quantum probability fluid at the zero-point state. The advantages of QFD are not limited to the provision of ontological interpretation of the quantum phenomena, as described by few examples illustrated above, but also the access to well-established fluid mechanical theorems and principles, together with the direct simulation of complex quantum systems by computational fluid dynamics. Needless to say that the quantum fluid dynamics characterization must be in compliance with established quantum uncertainty principles associated with measurements and the inherent limitation set-forth by quantum theory.

The basic issue of the QM-QFD reformulation is the quantum mechanical equivalence between the "linear" wave field description by QM and the "non-linear" fluid flow fields described by QFD. In these regards we ask: How the equivalence between linear wave field, QM, and the non-linear field, QFD, is ensured? Specifically, what are the necessary and sufficient conditions for the preservation of quantum mechanical equivalence? These are the basic motivations of the present study. Some fundamental aspects concerning the equivalence of two formalisms are described below.

Quantum fluid dynamic formulation is built on the basis of the Hamilton-Jacobi, *H-J*, transformation, which relates the Schrödinger's wave function with the density and a velocity potential of the quantum flow field. The flow variables obey the H-J equations of the continuity of probability density and Bernoulli's equations. The quantum mechanical equivalence between the quantum mechanics and fluid dynamical descriptions, are preserved if (1) the flow variables obey the H-J equations of the continuity of probability density and Bernoulli's equations and, (2) The quantum flow field satisfy the quantization conditions, as in quantum theory.[17, 18, 21,22].

The objectives of this study are to examine the necessary and sufficient conditions for the QM-QFD equivalence by adopting the view that a quantum system, characterized by a linear superposition of eigenfunctions, is equivalent to the mixture of quantum flowlets, termed, for simplicity, "quamlets". The quamlets are the basic flowlets constructed by the bilinear products of the wave function and its complex conjugate. In this approach, the question of the QM-QFD equivalence is reduced to seek the necessary and sufficient conditions that the sum of the quamlets jointly creates the non-linear field that is equivalent to the linear wave field.

Section 2 presents the description of quantum diffusive fluid dynamics, (QDFD), to introduce basic theoretical and physical terms, which will lead to the physical concepts behind the quamlets: Section 3 introduces the flow variables of quamlets and their mixture, together with the relevant algebraic rules relating to the laws of superposition of elemental and interactive quamlets. Section 4 describes the laws of the conservation of

quamlets, general properties and structure of quamlets. Finally, section 5 presents the necessary and sufficient conditions for the conditions of the QM-QFD equivalence. An example is given to illustrate the application of quamlets in the analysis of quantum flows in the selected simple systems.

II. QUANTUM DIFFUSIVE FLUID DYNAMICS OF QUANTUM SYSTEMS

A wave function of a quantum system in the presence of external potential is governed by the Schrodinger's equation, given by

$$i\hbar\frac{\partial\psi}{\partial t} = -\frac{\hbar^2}{2im_e}\nabla^2\psi + \mathbf{V}_e\psi \tag{2.1}$$

where ψ is the wave function, m_e is the mass of the particle, $\hbar$ is the Planck's constant divided by 2π and V_e is the potential. The QFD conservation equations of the probability density and the mechanical energy are formulated by the Hamilton-Jacobi transformation. Following Bohm [3] we first express the wave function in polar form, $\psi = \rho^{1/2}\exp(im_e\Phi/\mathrm{h})$ where ρ is the probability density, and Φ is a scalar potential. By inserting the latter expression for ψ into Eq. (2.1) and separating the result into imaginary and real parts we obtain the equations for the flow variables ρ and Φ. The imaginary and real part gives the conservation equation of probability density and energy, respectively. The continuity equation probability density is given by,

$$\frac{\partial\rho}{\partial t} + \nabla\bullet\mathbf{J} = 0 \tag{2.2}$$

where the probability density ρ and current density ***J*** or Lagrangian density are,

$$\rho = \psi\psi^* \tag{2.3}$$

$$\mathbf{J} = \rho\mathbf{u} = \left(\frac{\hbar}{2im_e}\right)\left(\psi^*\nabla\psi - \psi\nabla\psi^*\right) \tag{2.4}$$

The energy equation or alternatively, the quantum Bernoulli's equation, is given by

$$\frac{\partial\phi}{\partial t} + \left(\frac{1}{2}\right)\mathbf{u}\bullet\mathbf{u} + \frac{V_e}{m_e} - \Pi_{\mathrm{lnp}} = \frac{E}{m_e} \tag{2.5}$$

where V_e is the external potential, E is the Bernoulli's constant, and the fourth term is the quantum potential energy $\Pi_{\ln\rho}$

The velocity **u** is defined by the ratio of the probability current flux **J** with the density ρ as

$$\mathbf{u} = \left(\frac{\hbar}{2\mathrm{im_e}}\right)\nabla\left(\ln\frac{\psi}{\psi^*}\right) \tag{2.6}$$

The velocity field is irrotational except at the nodal singularities where the wave function vanishes and the vortices are present. Under certain regularity conditions on the initial wave function and the external potential, the particle has zero probability of entering the nodal surface from outside region, Carlen [25], Nelson [7], and Berndl, et al. [26]. It is added here that since the determination of the current density, **J**, requires the simultaneous measurements of position and velocity of particle, which is not in compliance with the Heisenberg uncertainty principle, hence **J** cannot be treated as the averaged measured particle flux at the point in space and time as interpreted in classical fluid dynamics.

The quantum potential $\Pi_{\ln\rho}$, which appears in the right hand side of Eq. (2.5) is expressed by,

$$\Pi_{\ln\rho} = \left(\frac{\hbar^2}{4m_e^2}\right)\left[\nabla^2(\ln\rho) + \left(\frac{1}{2}\right)\nabla(\ln\rho)\bullet\nabla(\ln\rho).\right] \tag{2.7}$$

It can be shown that the following two alternative forms of quantum potentials, Π_ρ and $\Pi_{\rho^{1/2}}$, are equivalent to $\Pi_{\ln\rho}$. They are given by,

$$\Pi_\rho = \frac{\hbar^2}{4m_e^2}\left[\frac{\nabla^2\rho}{\rho} + \frac{1}{2}\frac{\nabla\rho\bullet\nabla\rho}{\rho^2}\right], \tag{2.8}$$

$$\Pi_{\rho^{1/2}} = \frac{\hbar^2}{4m_e^2}\left[\frac{\nabla\rho^{1/2}}{\rho^{1/2}}\right]. \tag{2.9}$$

The last form $\Pi_{\rho^{1/2}}$ appears most frequently in the traditional Madelung formulation Grosh & Deb [27]. However, the quantum potential expressed in the form $\Pi_{\ln\rho}$ appears ontologically and methodologically superior to other forms in treating the quamlet analysis, which will be performed in section 5. We will adopt the $\Pi_{\ln\rho}$ form of the quantum potential and for notational convenience will denoted it by just Π.

The physical significance of the quantum potential $\Pi_{\ln\rho.}$ has been illustrated by decomposing the quantum potential into the sum of the dilatation and the kinetic energy due to the diffusion of the probability fluid as described below. The gradient induced diffusion velocity **V** is defined by Chiu [24]

$$\mathbf{V} = \frac{\mathbf{J}}{\rho} = -\left(\frac{\hbar}{2m_e}\right)\nabla\ln\rho = -D\frac{\nabla\rho}{\rho} \tag{2.10}$$

where ϑ is the diffusion flux of the probability fluid and the quantity $\hbar/2m_e$, which has the same physical dimension as the mass diffusivity, is the quantum diffusivity, *D,* in analogy with conventional terminology. The diffusion velocity is the negative of the osmotic velocity, Neson [7], which is the mean of the difference between the forward and backward velocities of Brownian motion without friction.

In addition to the flow velocity, **u** , Eq. (2.6) and diffusion velocity V, Eq. (2.11), we define a complex velocity ***w*** as follows,

$$\mathbf{w} = \frac{1}{2}(\mathbf{V} - i\mathbf{u}) = -D\nabla \ln \psi \tag{2.11}$$

$$\mathbf{w}^* = \frac{1}{2}(\mathbf{V} + i\mathbf{u}) = -D\nabla \ln \psi \tag{2.12}$$

The physical significance of the first term of the quantum potential, $(\hbar^2/4m_e)\nabla^2(\ln\rho)$, in Eq. (2.8) is obtained from definition of the diffusion velocity **V**. By taking the divergence of Eq. (2.11) we have,

$$\mathsf{M} = \left(\frac{\hbar^2}{4m_e^2}\right)\nabla^2\left(\ln\rho\right) = \left(\frac{\hbar}{2m_e}\right)\left(\frac{\hbar}{2m_e}\right)\nabla\bullet\left(\frac{\nabla\rho}{\rho}\right) = -D\nabla\bullet V \tag{2.13}$$

Hence, the first term in the quantum potential per unit mass represents the specific dilatation energy of diffusion field, $\mathsf{M} = -D\nabla\bullet V$ due to the divergence of the quantum diffusion velocity.

Next, based on the Eq. (2.11) we show that the term $(\hbar^2/4m_e)(1/2)\nabla(\ln\rho)\bullet\nabla(\ln\rho)$, in Eq. (2.8) is the kinetic energy associated with the quantum diffusive velocity,

$$\Omega = \left(\frac{\hbar^2}{4m_e^{\,2}}\right)\left(\frac{1}{2}\right)\nabla\left(\ln\rho\right)\bullet\nabla\left(\ln\rho\right) = \frac{1}{2}V\bullet V \tag{2.14}$$

Thus, quantum potential is the sum of the dilatation energy M and diffusion kinetic energy, Ω

$$\prod_{\ln\rho} = \mathsf{M} + \Omega = \left[-D\nabla\bullet\mathbf{V} + \left(\frac{1}{2}\right)\mathbf{V}\bullet\mathbf{V}.\right] \tag{2.15}$$

At steady state, the Bernoulli's equation is expressed by

$$\left(\frac{1}{2}\right)\left(\mathbf{u}^2 + \mathbf{V}^2\right) + D\nabla\cdot\mathbf{V} = \left[\left(\frac{E}{m_e}\right) - \left(\frac{V_e}{m_e}\right)\right] \tag{2.16}$$

The above Bernoulli's equation, as we shall show later, can be rewritten as follows,

$$\left(\frac{1}{2}\right)\left(\mathbf{w}.\mathbf{w}^{*}\right)+\left(\frac{\mathrm{D}}{\rho}\right)\nabla\cdot\left(\rho\mathbf{V}\right)=\left(\frac{E}{m_e}-\frac{V_e}{m_e}\right) \tag{2.17}$$

Thus a wave function at a specific quantum state can be represented by the quanum flow field, whose flow variables: density and velocities are obtained from the transformation relations and obeys the continuity equation (2.2) and the Bernoulli's equation (2.5).

III. QUAMLETS AND ALGEBRAIC RULES OF QUAMLET MIXTURE

A quantum system in a stationary state is, in general, described by a linear superposition of eigenfunctions $\psi_\alpha(E, \mathbf{x})$, corresponding to the same degenerate energy level,

$$\Psi\left(\mathrm{E},\mathrm{x},\mathrm{t}\right)=\sum^{\mathrm{N}}\psi_{\alpha}\left(\mathrm{E},\mathrm{x}\right)\mathrm{e}^{-\mathrm{iEt}/\mathrm{h}} \qquad \alpha=1,2,3....\mathrm{N} \tag{3.1}$$

The wave function function is expressed by $\psi_\alpha = A_\alpha \phi_\alpha$, where A_α is a constant and ϕ_α is α–th eigenfunction of a degenerate energy level.

A. Elemental and interactive quamlet

We first investigate the flow field corresponding to a stationary state described by a single wave function, ψ_α. The product of single wave function, ψ_α, with its complex conjugate is defined as an "elemental flowlet", which is termed, in short, a $\alpha\alpha^*$-th "quamlet". The elemental flow field is characterized by a set of quantum flow variables: the density, $\rho_{\alpha\alpha^*}$ and velocity $\boldsymbol{u}_{aa^*}$ of $\alpha\alpha^{*}$ elemental quamlet flow field, given by,

$$\rho_{\alpha\alpha^*}=\psi_{\alpha}\psi^{*}_{\alpha^*} \qquad\qquad \mathbf{u}_{\alpha\alpha^*}=\frac{\hbar}{2\mathrm{im}_{\mathrm{e}}}\nabla\ln\left(\frac{\psi_{\alpha}}{\psi_{\alpha^*}}\right) \tag{3.2}$$

$$\mathbf{V}_{\alpha\alpha^*}=\frac{-\hbar}{2\mathrm{m}_{\mathrm{e}}}\nabla\left(\ln\psi_{\alpha}+\ln\psi_{\alpha}^{\ *}\right) \tag{3.3}$$

$$\mathbf{w}_{\alpha}=\left(1/2\right)\left(\mathbf{V}_{\alpha\alpha^*}-\mathbf{u}_{\alpha\alpha^*}\right)=\frac{\hbar}{2\mathrm{m}_{\mathrm{e}}}\nabla\left(\ln\psi_{\alpha}\right) \tag{3.4}$$

$$\mathbf{w}_{\alpha^*}=\left(1/2\right)\left(\mathbf{V}_{\alpha\alpha^*}-\mathrm{i}\mathbf{u}_{\alpha\alpha^*}\right)=\frac{\hbar}{2\mathrm{m}_{\mathrm{e}}}\nabla\left(\ln\psi_{\alpha^*}\right) \tag{3.5}$$

Note that the complex velocity $\boldsymbol{w}_a$ does not depend on $ln\psi_{\alpha^*}$, hence the second index α^* does not appear in the complex velocity. Being a physical entity describing a fluid flow field, each elemental quamlet satisfies the continuity and Bernoulli's equations, i.e.,

$$\frac{\partial\rho_{\alpha\alpha^*}}{\partial\mathrm{t}}+\nabla\cdot\left(\rho_{\alpha\alpha^*}\mathbf{u}_{\alpha}\right)=0 \tag{3.6}$$

$$\left(\frac{1}{2}\right)\left(\mathbf{u}_{\alpha\alpha*}^2 - \mathbf{V}_{\alpha\alpha*}^2\right) + D\nabla\cdot\mathbf{V}_\alpha = [(\frac{E}{m_e}) - (\frac{V_e}{m_e})] \tag{3.7}$$

Now we turn our attention to the quamlets representation of the complete flow field, corresponding to the wave field consists of the linear superposition of the degenerate wave functions. Like quantum wave formalism wherein a superposition of the degenerate eigenfunction gives a complete field, one is led to conjecture that a complex quantum system can be represented by the superposition of "quamlets" : elemental quamlets, , and the interactive quamlets, which are created by the bi-linear interaction between a pair of eignefunctions: $\alpha\beta*$ and $\alpha*\beta$, where the latter quamlet is the complex conjugate of the former. Detailed mathematical characterization of the flow filed by quamlets is discussed in following.

B. Quamlets flow variables

$$\rho = \Sigma_\alpha\left[\psi_\alpha(\Sigma_{\beta*}\psi_{\beta*})\right] = \Sigma_\alpha\Sigma_{\alpha*}\left(\psi_\alpha\psi_{\alpha*}\right) + \Sigma_\alpha\sum_{\substack{\beta* \\ \alpha*\neq\beta*}}\psi_\alpha\psi_{\beta*} + \Sigma_{\alpha*}\sum_{\substack{\beta \\ \alpha\neq\beta}}\psi_{\alpha*}\psi_\beta \tag{3.8}$$

In the above expression the double summation, $\Sigma_\alpha\,(\Sigma_{\beta*})$ is carried out first with respect to the second index, β^*, followed by the first index, α, and $\Sigma_{(\beta\neq\alpha)}$ represents the sum of β for the entire set of degenerate states, except α-th eigenstate. There are two types of densities: real valued density, $\rho_{\alpha\alpha*}$ and complex densities, $\rho_{\alpha\beta*}$ and $\rho_{\alpha\beta*}$ as follows,

$$\rho = \Sigma_\alpha\Sigma_{\alpha*}\rho_{\alpha\alpha*} + \Sigma_\alpha\sum_{\substack{\beta* \\ \alpha*\neq\beta*}}\rho_{\alpha\beta*} + \Sigma_{\alpha*}\sum_{\substack{\beta \\ \alpha\neq\beta}}\rho_{\alpha*\beta} \tag{3.9}$$

where, the quantity $\rho_{\alpha\alpha*} = \rho_{\alpha*\alpha} = \psi_\alpha\psi_{\alpha*}$, is the density of the elemental quamlets and $\rho_{\alpha*\beta}$ is the complex density of an interactive quamlet field, created by the product of two different eigenfunctions $\rho_{\alpha*\beta} = \psi_{\alpha*}\psi_\beta$, and $(\rho_{\alpha*\beta}) = \psi_{\alpha*}\psi_\beta = (\rho_{\alpha\beta*})*$. The elemental quamlets obey the linear superposition, whereas, the interactive quamlets comply with special algebraic rules involving the summation of binomial products. The addition rule involving the linear superposition of elemental quamlets and summation of binomial products, for in interactive quamlets is the consequence of the non-linearity of fluid dynamics.

C. Algebraic rules of quamlet mixture

Following the definition of the density of quamlet mixture, we define the quamlets concentration of $\alpha\beta*$, by $z_{\alpha\beta}$, expressed by,

$$z_{\alpha\beta*} = \frac{\rho_{\alpha\beta*}}{\rho} \tag{3.10}$$

By virtue of (3.9), the sum of the concentrations of all the quamlets, is unity,

$$\sum_{\alpha}\left(\sum_{\beta*}\frac{\rho_{\alpha\beta*}}{\rho}\right)=\sum_{\alpha}\left(\sum_{\beta*}z_{\alpha\beta*}\right)=1 \tag{3.11}$$

Alternatively, we write

$$\sum_{\alpha}(\sum_{\beta*}\mathrm{z}_{\alpha\beta*})=\sum_{\alpha}\sum_{\alpha*}\left(\mathrm{z}_{\alpha\alpha*}\right)+\sum_{\substack{\alpha}}\sum_{\substack{\beta*\neq\alpha*}}\mathrm{z}_{\alpha\beta*}+\sum_{\substack{\alpha*}}\sum_{\substack{\beta\neq\alpha}}\mathrm{z}_{\alpha*\beta}=1 \tag{3.12}$$

Next, by using the definition of the quamlet concentration, we show the following rules of the multiplication of the concentrations $z_{\alpha\beta*}$ and $z_{\alpha*\gamma}$,

$$z_{\alpha\beta*}z_{\alpha*\gamma}=(\psi_{\alpha}\psi_{\beta*})(\psi_{\alpha*}\psi_{\gamma})/\rho^{2}=\rho_{\alpha\alpha*}\rho_{\beta*\gamma}/\rho^{2}=z_{\alpha\alpha*}z_{\beta*\gamma} \tag{3.13}$$

$$\mathrm{z}_{\alpha*\beta}\mathrm{z}_{\alpha\gamma*}=(\psi_{\alpha*}\psi_{\beta})(\psi_{\alpha}\psi_{\gamma*})/\rho^{2}=\rho_{\alpha\alpha*}\rho_{\beta\gamma*}/\rho^{2}=\mathrm{z}_{\alpha\alpha*}\mathrm{z}_{\beta\gamma*} \tag{3.14}$$

Next, by (3.13) and (3.14), we obtain the rules of the sum of the product of the concentrations, with respect to β and $\gamma*$, as follows,

$$\sum_{\beta*}(\sum_{\gamma}\mathrm{z}_{\alpha\beta*}\mathrm{z}_{\alpha*\gamma})=\mathrm{z}_{\alpha\alpha*}\sum_{\beta*}(\sum_{\gamma}\mathrm{z}_{\beta*\gamma})=\mathrm{z}_{\alpha\alpha*} \tag{3.15}$$

$$\sum_{\beta}(\sum_{\gamma*}\mathrm{z}_{\alpha*\beta}\mathrm{z}_{\alpha\gamma*})=\mathrm{z}_{\alpha*\alpha}\sum_{\beta}(\sum_{\gamma*}\mathrm{z}_{\beta\gamma*})=\mathrm{z}_{\alpha*\alpha} \tag{3.16}$$

These multiplication rules of quamlets concentration, (3.13) and (3.14) are used in the analysis, which involves the algebraic operations, addition and multiplication of the quamlet concentrations, as described in the latter part of the analysis.

D. Quamlet fluxes and velocities

The flux of probability fluid, $\boldsymbol{J}=\rho\boldsymbol{u}$, of the global flow field is expressed by the sum of the flux of elemental, $J_{\alpha\alpha*}$, and that of interactive quamlets, $J_{\alpha\beta*}$, as follows,

$$\mathbf{J}=\sum_{\alpha*}\mathbf{J}_{\alpha\alpha*}+\sum_{\alpha}\sum_{\substack{\beta*\\ \beta*\neq\alpha*}}\mathbf{J}_{\alpha\beta*}+\sum_{\alpha*}\sum_{\substack{\beta\\ \beta\neq\alpha}}\mathbf{J}_{\alpha*\beta} \tag{3.17}$$

where, fluxes of elemental and interactive quamlets are given by

$$\mathbf{J}_{\alpha\alpha*}=\rho_{\alpha\alpha*}\mathbf{u}_{\alpha}=i\rho z_{\alpha\alpha}\left(\mathbf{w}_{\alpha}-\mathbf{w}_{\alpha*}\right) \tag{3.18}$$

$$\mathbf{J}_{\alpha\beta*}=\mathrm{i}\rho\mathrm{z}_{\alpha\beta*}\left(1/2\right)\left[(\mathbf{V}_{\alpha\alpha*}-\mathbf{V}_{\beta\beta*})-\mathrm{i}(\mathbf{u}_{\alpha\alpha*}+\mathbf{u}_{\beta\beta*})\right]=\mathrm{i}\rho\mathrm{z}_{\alpha\beta*}(\mathbf{w}_{\alpha}-\mathbf{w}_{\beta*}) \tag{3.19}$$

$$\mathbf{J}_{\alpha*\beta}=-\mathrm{i}\rho\mathrm{z}_{\alpha*\beta}\left(1/2\right)\left[(\mathbf{V}_{\alpha\alpha*}-\mathbf{V}_{\beta\beta*})+\mathrm{i}(\mathbf{u}_{\alpha\alpha*}+\mathbf{u}_{\beta\beta*})\right]=-\mathrm{i}\rho\mathrm{z}_{\alpha*\beta}(\mathbf{w}_{\alpha*}-\mathbf{w}_{\beta}) \tag{3.20}$$

$$\begin{aligned}\mathbf{J}=&\,\mathrm{i}\rho\sum_{\alpha}\sum_{\alpha*}\mathrm{z}_{\alpha\alpha*}\left(\mathbf{w}_{\alpha}-\mathbf{w}_{\alpha*}\right)\\&+\mathrm{i}\rho\left[\sum_{\alpha}\sum_{\substack{\beta*\\ \beta*\neq\alpha*}}\mathrm{z}_{\alpha\beta*}\left(\mathbf{w}_{\alpha}-\mathbf{w}_{\beta*}\right)-\sum_{\alpha*}\sum_{\substack{\beta\\ \beta\neq\alpha}}\mathrm{z}_{\alpha*\beta}\left(\mathbf{w}_{\alpha*}-\mathbf{w}_{\beta}\right)\right]\end{aligned} \tag{3.21}$$

By dividing the ***J***-flux by the fluid density, we obtain the velocity of the complete flow in terms of the quamlet concentration and complex velocity as follows

$$\begin{aligned}\mathbf{u} = \mathbf{J}/\rho = \mathrm{i}\sum_{\alpha}\sum_{\alpha^*} z_{\alpha\alpha^*}\left(\mathbf{w}_{\alpha} - \mathbf{w}_{\alpha^*}\right) \\ + \mathrm{i}\left[\sum_{\alpha}\sum_{\beta^*} z_{\alpha\beta^*}\left(\mathbf{w}_{\alpha} - \mathbf{w}_{\beta^*}\right) - \sum_{\alpha^*}\sum_{\beta} z_{\alpha^*\beta}\left(\mathbf{w}_{\alpha^*} - \mathbf{w}_{\beta}\right)\right]\end{aligned} \tag{3.22}$$

We define the mean velocities of quamlets as follows,

$$\mathbf{u}_{\alpha\alpha^*} = \mathrm{i}z_{\alpha\alpha^*}(\mathbf{w}_{\alpha} - \mathbf{w}_{\alpha^*}) \qquad \mathbf{u}_{\alpha\beta^*} = \mathrm{i}z_{\alpha\beta^*}(\mathbf{w}_{\alpha} - \mathbf{w}_{\beta^*}) \quad \mathbf{u}_{\alpha^*\beta} = \mathrm{i}z_{\alpha^*\beta}(\mathbf{w}_{\alpha^*} - \mathbf{w}_{\beta}) \tag{3.23}$$

One important aspect of the equivalence between the quantum flow description and quantum mechanics is the quantization condition must be met in the former flow field, i.e.,

$$\oint_C \mathbf{u}\bullet\mathrm{d}\mathbf{r} = 2\pi m \tag{3.24}$$

which is rewritten by

$$i\oint_C \left[\sum_{\alpha}\sum_{\alpha^*} z_{\alpha\alpha^*}\left(\mathbf{w}_{\alpha} - \mathbf{w}_{\alpha^*}\right) + \sum_{\alpha}\sum_{\beta^*} z_{\alpha\beta^*}\left(\mathbf{w}_{\alpha} - \mathbf{w}_{\beta^*}\right) - \sum_{\alpha^*}\sum_{\beta} z_{\alpha^*\beta}\left(\mathbf{w}_{\alpha^*} - \mathbf{w}_{\beta}\right)\right]\bullet\mathrm{d}\mathbf{r} = 2\pi m \tag{3.25}$$

where, m is an integer and the subscript c is any closed counter.

The flux of diffusion of probability fluid $\Im = \rho V$, is given by

$$\mathfrak{J} = \sum_{\alpha}\sum_{\alpha^*}\mathfrak{J}_{\alpha\alpha^*} + \sum_{\substack{\alpha \\ \alpha^*\neq\beta^*}}\sum_{\beta^*}\mathfrak{J}_{\alpha\beta^*} + \sum_{\substack{\alpha^* \\ \alpha\neq\beta}}\sum_{\beta}\mathfrak{J}_{\alpha^*\beta} \tag{3.26}$$

where, fluxes of elemental and interactive quamlet are given by

$$\mathfrak{J}_{\alpha\alpha^*} = \rho_{\alpha\alpha^*}\mathbf{V}_{\alpha} = \rho z_{\alpha\alpha^*}(\mathbf{w}_{\alpha} + \mathbf{w}_{\alpha^*}) \tag{3.27}$$

$$\mathfrak{J}_{\alpha\beta^*} = \rho z_{\alpha\beta^*}(\frac{1}{2})[(\mathbf{V}_{\alpha\alpha^*} + \mathbf{V}_{\beta\beta^*}) - \mathrm{i}(\mathbf{u}_{\alpha\alpha} + \mathbf{u}_{\beta\beta^*})] = \rho z_{\alpha\beta^*}(\mathbf{w}_{\alpha} + \mathbf{w}_{\beta^*}) \tag{3.28}$$

$$\mathfrak{J}_{\alpha^*\beta} = \rho z_{\alpha^*\beta}(\frac{1}{2})[(\mathbf{V}_{\alpha\alpha^*} + \mathbf{V}_{\beta\beta^*}) - \mathrm{i}(\mathbf{u}_{\alpha\alpha^*} + \mathbf{u}_{\beta\beta^*})] = \rho z_{\alpha^*\beta}(\mathbf{w}_{\alpha^*} + \mathbf{w}_{\beta}) \tag{3.29}$$

$$\begin{aligned}\mathfrak{J} = \rho\sum z_{\alpha\alpha^*}(\mathbf{w}_{\alpha} + \mathbf{w}_{\alpha^*}) + \rho[\sum_{\substack{\alpha \\ \alpha^*\neq\beta^*}}\sum_{\beta^*} z_{\alpha\beta^*}(\mathbf{w}_{\alpha} + \mathbf{w}_{\beta^*}) \\ + \sum_{\alpha^*}\sum_{\substack{\beta \\ \alpha\neq\beta}} z_{\alpha^*\beta}(\mathbf{w}_{\alpha^*} + \mathbf{w}_{\beta})]\end{aligned} \tag{3.30}$$

The diffusion velocity of the complete flow field is given by

$$\mathbf{V} = \frac{\mathfrak{I}}{\rho} = \sum_{\alpha} \sum_{\alpha^*} z_{\alpha\alpha^*}(\mathbf{w}_{\alpha} + \mathbf{w}_{\alpha^*}) + [\sum_{\substack{\alpha \\ \alpha^* \neq \beta^*}} \sum_{\beta^*} z_{\alpha\beta^*}(\mathbf{w}_{\alpha} + \mathbf{w}_{\beta^*}) + \sum_{\alpha^*} \sum_{\substack{\beta \\ \alpha \neq \beta}} z_{\alpha^*\beta}(\mathbf{w}_{\alpha^*} + \mathbf{w}_{\beta})] \tag{3.31}$$

We define the diffusion velocities of quamlets as follows,

$$\mathbf{V}_{\alpha\alpha^*} = z_{\alpha\alpha^*}(\mathbf{w}_{\alpha} + \mathbf{w}_{\alpha^*}),\ \mathbf{V}_{\alpha\beta^*} = z_{\alpha\beta^*}(\mathbf{w}_{\alpha} + \mathbf{w}_{\beta^*}),\ \mathbf{V}_{\alpha^*\beta} = z_{\alpha^*\beta}(\mathbf{w}_{\alpha^*} + \mathbf{w}_{\beta}) \tag{3.32}$$

Similarly, the probability flux based on the complex velocity, ***w,*** is expressed by

$$\chi = \left(\tfrac{1}{2}\right)(\mathfrak{I} - i\mathbf{J}) \tag{3.33}$$

$$\chi_{\alpha\alpha^*} = \rho_{\alpha\alpha^*}\mathbf{w}_{\alpha} = \rho z_{\alpha\alpha^*}\mathbf{w}_{\alpha} \tag{3.34}$$

$$\chi_{\alpha\beta^*} = \rho z_{\alpha\beta^*}\mathbf{w}_{\alpha} \quad \chi_{\alpha^*\beta} = \rho z_{\alpha^*\beta}\mathbf{w}_{\alpha^*} \tag{3.35}$$

$$\chi = \rho \sum_{\alpha} \sum_{\alpha^*} z_{\alpha\alpha^*}\mathbf{w}_{\alpha} + \rho[\sum_{\alpha} \sum_{\substack{\beta^* \\ \alpha^* \neq \beta^*}} z_{\alpha\beta^*}\mathbf{w}_{\alpha} + \sum_{\alpha^*} \sum_{\substack{\beta \\ \alpha \neq \beta}} z_{\alpha^*\beta}\mathbf{w}_{\alpha^*}] \tag{3.36}$$

The complex velocity $\mathbf{w}$ of the complete field is,

$$\mathbf{w} = \left(\frac{1}{2}\right)(\mathbf{V} - i\mathbf{u}) = \sum_{\alpha} \sum_{\alpha^*} z_{\alpha\alpha^*}\mathbf{w}_{\alpha} + \rho[\sum_{\alpha} \sum_{\substack{\beta^* \\ \alpha^* \neq \beta^*}} z_{\alpha\beta^*}\mathbf{w}_{\alpha} + \sum_{\alpha^*} \sum_{\substack{\beta \\ \alpha \neq \beta}} z_{\alpha^*\beta}\mathbf{w}_{\alpha^*}] \tag{3.37}$$

The complex velocities of quamlets are given by,

$$\mathbf{w}_{\alpha\alpha^*} = z_{\alpha\alpha^*}\mathbf{w}_{\alpha} \qquad \mathbf{w}_{\alpha\beta^*} = z_{\alpha\beta^*}\mathbf{w}_{\alpha} \qquad \mathbf{w}_{\alpha^*\beta} = z_{\alpha^*\beta}\mathbf{w}_{\alpha^*} \tag{3.38}$$

IV. PRINCIPLE OF EQUIVALENCE

The equivalence between the quantum flow field, described by (3.9), (3.22) and the quantum mechanical characterization by wave function (3.1) requires that the overall flow field, represented by the sum of all the qaumlets, must obeys the conservation equations (2.2) and (2.5), and moreover the global flow meet the quantization condition as described by Eq. (3.24)

A. Continuity equation

We shall first examine the necessary condition under which ensures the quamlet mixture obeys the law of continuity of probability density.

The application of a divergence operator on the mass flux, Eq. (3.17), gives

$$\nabla \bullet \rho \mathbf{u} = \sum_{\alpha} \sum_{\alpha^*} \nabla \bullet \rho_{\alpha\alpha^*} (\mathbf{w}_{\alpha} - \mathbf{w}_{\alpha^*}) +$$

$$\mathrm{i}\left[\sum_{\substack{\alpha \\ \alpha^* \neq \beta^*}} \sum_{\beta^*} \nabla \bullet \rho_{\alpha\beta^*} (\mathbf{w}_{\alpha} - \mathbf{w}_{\beta^*}) - \sum_{\substack{\alpha^* \\ \alpha \neq \beta}} \sum_{\beta} \nabla \bullet \rho_{\alpha^*\beta} (\mathbf{w}_{\alpha^*} + \mathbf{w}_{\beta}) \right] \tag{4.1}$$

At stationary state, the continuity requires that the above expression must vanishes, i.e., $\nabla \cdot \rho \mathbf{u} = 0$.

To prove that the above expression (4.1) is zero, we first examine the divergence of the flux of an elemental quamlet of $\rho_{\alpha\alpha^*}$,

$$\nabla \bullet \rho_{\alpha\alpha^*} \mathbf{u}_{\alpha\alpha^*} = \mathrm{i} \sum \nabla \bullet \rho_{\alpha\alpha^*} (\mathbf{w}_{\alpha} - \mathbf{w}_{\alpha^*}) = -\mathrm{iD} \sum \nabla (\psi_{\alpha} \psi_{\alpha^*}) (\ln \psi_{\alpha} - \ln \psi_{\alpha^*})$$

$$= \mathrm{D}\{(\psi_{\alpha} \nabla^2 \psi_{\alpha^*} - \nabla \psi_{\alpha^*} \nabla \psi_{\alpha}) - (\psi_{\alpha^*} \nabla^2 \psi_{\alpha} - \nabla \psi_{\alpha^*} \nabla \psi_{\alpha}) = \mathrm{D}(\psi_{\alpha} \nabla^2 \psi_{\alpha^*} - \psi_{\alpha^*} \nabla^2 \psi_{\alpha^*}) \tag{4.2}$$

The last expression, in the above equation, can be further deduced as follows. First, we multiply the Schrodinger's equation (2.1) of the degenerate eigenfunction ψ_{γ^*} by ψ_{γ}. By carrying out the same step as above except that we interchange the role of ψ_{γ} by ψ_{γ^*}. Next, by subtracting the two resulting equations from each other, we have

$$\frac{\hbar^2}{2\,\mathrm{m}_e} \left(\psi_{\alpha} \nabla^2 \psi_{\alpha^*} - \psi_{\alpha^*} \nabla^2 \psi_{\alpha} \right) = (E - V_e)(\psi_{\alpha} \psi_{\alpha^*} - \psi_{\alpha} \psi_{\alpha^*}) = 0 \tag{4.3}$$

Thus, the elemental quamlet $\alpha\alpha^*$ satisfies the law of continuity, as expected, i.e.,

$$\nabla \bullet \left[\rho_{\alpha\alpha^*} (\mathbf{w}_{\alpha} - \mathbf{w}_{\alpha^*}) \right] = 0 \tag{4.4}$$

Next, we calculate the divergence of the interactive quamlet, $\alpha\beta^*$, represented by the second term of Eq. (4.1),

$$\mathrm{i} \nabla \bullet \rho_{\alpha\beta^*} (\mathbf{w}_{\alpha} - \mathbf{w}_{\beta^*}) = \mathrm{iD} \nabla \bullet (\psi_{\alpha} \psi_{\beta^*}) (\nabla \ln \psi_{\beta^*} - \nabla \ln \psi_{\alpha})$$

$$= \mathrm{iD}\{(\psi_{\alpha} \nabla^2 \psi_{\beta^*} - \nabla \psi_{\beta^*} \nabla \psi_{\alpha}) - (\psi_{\beta^*} \nabla^2 \psi_{\alpha} - \nabla \psi_{\beta^*} \nabla \psi_{\alpha}) = \mathrm{iD}(\psi_{\alpha} \nabla^2 \psi_{\beta^*} - \psi_{\beta^*} \nabla^2 \psi_{\alpha}) \tag{4.5}$$

By the similar procedure used in the above analysis, we can show that the last term of the above equation vanishes, i.e.,

$$\frac{\hbar^2}{2m_e} \left(\psi_{\alpha} \nabla^2 \psi_{\beta^*} - \psi_{\beta^*} \nabla^2 \psi_{\alpha} \right) = (E - V_e)(\psi_{\alpha} \psi_{\beta^*} - \psi_{\beta^*} \psi_{\alpha}) = 0 \tag{4.6}$$

Thus, the quamlet, $\alpha\beta^*$, satifies the continuity of the probability fluid as follows,

$$i\nabla \bullet \rho_{\alpha\beta^*}(\mathbf{w}_\alpha - \mathbf{w}_{\beta^*}) = 0 \tag{4.7}$$

By decomposing the above equation into real and imaginary parts, we get,

$$\left(\frac{1}{2}\right) i\nabla \bullet [\rho\zeta_{\alpha\beta^*}(\mathbf{V}_{\alpha\alpha^*} - \mathbf{V}_{\beta\beta^*})] - \left(\frac{1}{2}\right)\nabla \bullet [\rho\eta_{\alpha\beta^*}(\mathbf{u}_{\alpha\alpha^*} - \mathbf{u}_{\beta\beta^*})] = 0 \tag{4.8}$$

where, $\zeta_{\alpha\beta}$ and $\eta_{\alpha\beta}$ are the real and imaginary part of $\rho_{\alpha\,\beta^*}$ given by,

$$\rho\zeta_{\alpha\beta} = (\phi_\alpha\phi_\beta + \omega_\alpha\omega_\beta) \tag{4.9}$$

$$\rho\eta_{\alpha\beta} = (\phi_\beta\omega_\alpha - \phi_\alpha\omega_\beta) \tag{4.10}$$

in which ϕ_λ and ω_λ are the real and imaginary parts of ψ_λ respectively.

Similarly the continuity of $\alpha^*\beta$ is given by,

$$i\nabla \bullet \rho_{\alpha^*\beta}(\mathbf{w}_{\alpha^*} - \mathbf{w}_\beta) = 0 \tag{4.11}$$

$$-(1/2)i\nabla\bullet\left[\rho\zeta_{\alpha\beta}(\mathbf{v}_{\alpha\alpha^*} - \mathbf{v}_{\beta\beta^*})\right] - (1/2)\nabla\bullet\left[\rho\eta_{\alpha\beta}(\mathbf{u}_{\alpha\alpha^*} + \mathbf{u}_{\beta\beta^*})\right] = 0 \tag{4.12}$$

Thus by comparing two sets of continuity equations for $\alpha\beta^*$ (4.8) and $\alpha^*\beta$, (4.12) we find that the probability of the two quamlets are satisfied provided,

$$\nabla\bullet\left[\rho\eta_{\alpha\beta}(\mathbf{u}_{\alpha\alpha^*} + \mathbf{u}_{\beta\beta^*})\right] = 0 \tag{4.13}$$

$$\nabla\bullet\left[\rho\zeta_{\alpha\beta}(\mathbf{v}_{\alpha\alpha^*} - \mathbf{v}_{\beta\beta^*})\right] = 0 \tag{4.14}$$

We conclude that the necessary condition for the global flow to obey the continuity is that each quamlet satisfies independently the continuity equation of each quamlet flow.

C. Bernoulli's equation of quamlets

We next investigate the necessary condition required for the quamlet mixture flow to obey the Bernoulli's equation.

The dilatation term, $D\ \nabla \bullet \boldsymbol{v}$, represented by the second term on the right hand side of the above equation, can be reformulated in the following form,

$$D\nabla\bullet V = D\nabla\bullet\left(\frac{\mathfrak{I}}{\rho}\right) = \left(\frac{D}{\rho}\right)\nabla\bullet\mathfrak{I} + D\mathfrak{I}\nabla\left(\frac{1}{\rho}\right) = \left(\frac{D}{\rho}\right)\nabla\bullet\mathfrak{I} + V^2 \tag{4.15}$$

Substitution of (4.15) into (2.16), gives,

$$\left(\frac{1}{2}\right)\left(u^2+\mathbf{V}^2\right)+\frac{D}{\rho}\nabla\bullet\Im=[(\frac{E}{m_e})-(\frac{V_e}{m_e})] \tag{4.16}$$

By using Eqs.(3.4) (4-15) we re-express the above equation in the following form,

$$\begin{aligned}&2\left(\mathbf{w}\bullet\mathbf{w}^*\right)+\left(\frac{D}{\rho}\right)\nabla\bullet\left[\sum_\alpha\sum_{\alpha^*}\Im_{\alpha\alpha^*}+\sum_{\beta^*\neq\alpha^*}\alpha\sum_{\beta^*\neq\alpha^*}\beta^*\Im_{\alpha\beta^*}+\sum_{\beta\neq\alpha}\alpha^*\sum_{\beta\neq\alpha}\beta\sum\Im_{\alpha^*\beta}\right]\\&\quad=[(\frac{E}{m_e})-(\frac{V_e}{m_e})]\end{aligned} \tag{4.18}$$

The right hand side of the above expression can be recast in the form representing the net energy (E-V)/m_e contributed by the sum of all the quamlets. This is made by the following two steps. First, we multiply the latter sum of energies on the right hand side of the equation.by the following expression, Eq. (3.12).

$$\sum_\alpha\sum_{\alpha^*}\left(z_{\alpha\alpha^*}\right)+\sum_\alpha\sum_{\beta^*}(z_{\alpha\beta^*})+\sum_{\alpha^*}\sum_\beta(z_{\alpha^*\beta})=1 \tag{4.19}$$

Next by substituting (3.37) and (3.26) into Eq. (4.18) and by expanding each term appears in the above expression through the use of (3.13) to (3.16), we have

$$\begin{aligned}&2\sum_\alpha\sum_{\alpha^*}\left[\sum_{\beta^*}(z_{\alpha\beta^*})\sum_\gamma\left(z_{\alpha^*\gamma}\right)\right]\mathbf{w}_\alpha\bullet\mathbf{w}_{\alpha^*}+2\sum_\alpha\sum_{\beta^*}\left[\sum_{\lambda^*}\left(z_{\alpha\lambda^*}\right)\sum_\gamma\left(z_{\beta^*\gamma}\right)\right]\mathbf{w}_\alpha\bullet\mathbf{w}_{\beta^*}\\&2\left\{\sum_{\alpha^*}\sum_\beta\left[\sum_\lambda\left(z_{\alpha^*\lambda}\right)\sum_{\gamma^*}\left(z_{\beta\gamma^*}\right)\right]\mathbf{w}_{\alpha^*}\bullet\mathbf{w}_\beta\right\}+\left(\frac{D}{\rho}\right)\left\{\sum_\alpha\sum_{\alpha^*}\nabla\bullet\left[\rho_{\alpha\alpha^*}\left(\mathbf{w}_\alpha+\mathbf{w}_{\alpha^*}\right)\right]\right\}\\&+\sum_\alpha\sum_{\beta^*}\nabla\bullet\left[\rho_{\alpha\beta^*}(\mathbf{w}_\alpha+\mathbf{w}_{\beta^*})\right]+\sum_{\alpha^*}\sum_\beta\nabla\bullet\left[\rho_{\alpha^*\beta}(\mathbf{w}_{\alpha^*}+\mathbf{w}_\beta)\right]\\&=[(\frac{E}{m_e})-(\frac{V_e}{m_e})]\left\{\sum_\alpha\sum_{\alpha^*}\mathrm{z}_{\alpha\alpha^*}+\sum_\alpha\sum_{\beta^*}\mathrm{z}_{\alpha\beta^*}+\sum_{\alpha^*}\sum_\beta\mathrm{z}_{\alpha^*\beta}\right\}\end{aligned} \tag{4.20}$$

The objective of the remaining part of the analysis is to prove the equality of the left hand side of Eq.(4.20) with that of the right handside. The detail analysis of this assertion is given below.

Following the quamlet analysis for the continuity equation, we examine the conservation of the energy for three types of quamlets: $\alpha\alpha^*$, $\alpha\beta^*$,and $\alpha^*\beta$.

First, by the application of quamlet multiplication rules (3.13) and (3.14), we have

$$(z_{\alpha\beta^*})(z_{\alpha^*\gamma})=(z_{\alpha\alpha^*})(z_{\beta^*\gamma})\quad(z_{\alpha\lambda^*})(z_{\beta^*\gamma})=(z_{\alpha\beta^*})(z_{\lambda^*\gamma})\quad(z_{\alpha^*\lambda})(z_{\beta\gamma^*})=(z_{\alpha^*\beta})(z_{\lambda\gamma^*}) \tag{4.21}$$

By substituting the above expressions in the kinetic energy of mean motion appear in Eq. (4.20) we have,

$$2\left[\sum_{\alpha}\sum_{\alpha^*}(z_{\alpha\alpha^*})\right]\left[\sum_{\beta^*}\sum_{\gamma}(z_{\beta^*\gamma})\right](\mathbf{w}_{\alpha}\bullet\mathbf{w}_{\alpha^*})+2\left[\sum_{\alpha}\sum_{\beta^*}(z_{\alpha\beta^*})\right]\left[\sum_{\lambda^*}\sum_{\gamma}(z_{\lambda^*\gamma})\right]$$
$$(\mathbf{w}_{\alpha}\bullet\mathbf{w}_{\beta^*})+2\left\{\sum_{\alpha^*}\sum_{\beta}z_{\alpha^*\beta}\left[\sum_{\lambda}\sum_{\gamma^*}(z_{\lambda\gamma^*})\right](\mathbf{w}_{\alpha^*}\bullet\mathbf{w}_{\beta})\right\} \tag{4.22}$$

Secondly, we write the following summation rules based on (3.11) ,

$$\sum_{\beta^*}\sum_{\gamma}(z_{\beta^*\gamma})=1 \quad , \quad \sum_{\lambda^*}\sum_{\gamma}(z_{\lambda^*\gamma})=1 \quad , \quad \sum_{\lambda}\sum_{\gamma^*}(z_{\lambda\gamma^*})=1 \tag{4.23}$$

Thus, the total kinetic energy is reduced to the sum of the energy of elemental quamlets and interactive quamlets as follows,

$$2\sum_{\alpha}\sum_{\alpha^*}(z_{\alpha\alpha^*})(\mathbf{w}_{\alpha}\bullet\mathbf{w}_{\alpha^*})+2\sum_{\alpha}\sum_{\beta^*}(z_{\alpha\beta^*})(\mathbf{w}_{\alpha}\bullet\mathbf{w}_{\beta^*})+2\sum_{\alpha^*}\sum(z_{\beta})(\mathbf{w}_{\alpha^*}\bullet\mathbf{w}_{\beta}) \tag{4.24}$$

By substituting above expression into (4.22) and collecting the terms associated with each quamlet group as follows we have the following global Bernoulli's equation,

$$2\sum_{\alpha}\sum_{\alpha^*}\left(z_{\alpha\alpha^*}\right)\left(\mathbf{w}_{\alpha}\bullet\mathbf{w}_{\alpha^*}\right)+\left(\frac{D}{\rho}\right)\left\{\sum_{\alpha}\sum_{\alpha^*}\nabla\bullet\left[\rho_{\alpha\alpha^*}\left(\mathbf{w}_{\alpha}+\mathbf{w}_{\alpha^*}\right)\right]\right\}$$
$$+2\sum_{\alpha}\sum_{\beta^*}\left(z_{\alpha\beta^*}\right)\left(\mathbf{w}_{\alpha}\bullet\mathbf{w}_{\beta^*}\right)+\left(\frac{D}{\rho}\right)\left\{\sum_{\alpha}\sum_{\beta^*}\nabla\bullet\left[\rho_{\alpha\beta^*}\left(\mathbf{w}_{\alpha}+\mathbf{w}_{\beta^*}\right)\right]\right\}$$
$$+2\sum_{\alpha^*}\sum_{\beta^*}\left(z_{\beta}\right)\left(\mathbf{w}_{\alpha^*}\bullet\mathbf{w}_{\beta}\right)+\left(\frac{D}{\rho}\right)\left\{\sum_{\alpha^*}\sum_{\beta}\nabla\bullet\left[\rho_{\alpha^*\beta}\left(\mathbf{w}_{\alpha^*}+\mathbf{w}_{\beta}\right)\right]\right\}$$
$$=[(\frac{E}{m_e})-(\frac{V_g}{m_e})]\left\{\sum_{\alpha}\sum_{\alpha^*}z_{\alpha\alpha^*}+\sum_{\alpha}\sum_{\beta^*}z_{\alpha\beta^*}+\sum_{\alpha^*}\sum_{\beta}z_{\alpha^*\beta}\right\} \tag{4.25}$$

We shall examine the energy balance of the quamlet mixture as follows.

First of all, by collecting all the terms associated with $\alpha\alpha^*$ terms on the left hand side of (4.25),

$$2\sum_{\alpha}\sum_{\alpha^*}\left(z_{\alpha\alpha^*}\right)\left(\mathbf{w}_{\alpha}\bullet\mathbf{w}_{\alpha^*}\right)+\left(\frac{D}{\rho}\right)\left\{\sum_{\alpha}\sum_{\alpha^*}\nabla\bullet\left[\rho_{\alpha\alpha^*}\left(\mathbf{w}_{\alpha}+\mathbf{w}_{\alpha^*}\right)\right]\right\} \tag{4.26}$$

By using (3.4) and (3.5), we re-express the dilatation energy given by the second term in the above equation, as follows,

$$\left(\frac{D}{\rho}\right)\sum_{\alpha}\sum_{\alpha^*}\nabla\bullet\rho_{\alpha\alpha^*}\left(\mathbf{w}_{\alpha}+\mathbf{w}_{\alpha^*}\right)=-(\frac{D^2}{\rho})\sum_{\alpha}\sum_{\alpha^*}\nabla\bullet\left\{\rho_{\alpha\alpha^*}\left[\nabla\left(\ln\psi_{\alpha}+\ln\psi_{\alpha^*}\right)\right]\right\} \tag{4.27}$$

By expanding the gradients of logarithmic terms in (4.27) and by the applications of divergence operator, we have,

$$\frac{-\mathrm{D}^2}{\rho}\left\{\Sigma_\alpha \Sigma_{\alpha^*}\left[\left(\psi_{\alpha^*}\nabla^2\psi_\alpha\right)+\left(\psi_\alpha\nabla^2\psi_{\alpha^*}\right)\right]\right\}-2\left\{\Sigma_\alpha \Sigma_{\alpha^*}\rho_{\alpha\alpha^*}\left(\mathbf{w}_\alpha\bullet\mathbf{w}_{\alpha^*}\right)\right\} \tag{4.28}$$

The terms in the first curly bracket can be further reduced, as follows. Multiply the Schrödinger equation, governing ψ_{α^*} by ψ_α and by repeating the same procedure, except by interchanging the role of ψ_α with ψ_{α^*}. Next, by adding the resulting equations we obtain,

$$-\frac{\hbar^2}{4\mathrm{m_e}^2}\left(\psi_\alpha\nabla^2\psi_{\alpha^*}+\psi_{\alpha^*}\nabla^2\psi_\alpha\right)=-\left(\frac{1}{2\,\mathrm{m_e}\,\rho}\right)\left\{\psi_\alpha\left(\frac{\hbar^2}{2\,\mathrm{m_e}}\right)\left(\nabla^2\psi_{\alpha^*}\right)+\psi_{\alpha^*}\left(\frac{\hbar^2}{2\,\mathrm{m_e}}\right)\nabla^2\psi_\alpha\right\}$$

$$=\left(\frac{\psi_\alpha\psi_{\alpha^*}}{\rho}\right)\left(\frac{E}{m_\mathrm{e}}-\frac{V_e}{m_e}\right)=\left(\mathrm{z}_{\alpha\alpha^*}\right)\left(\frac{E}{m_e}-\frac{V_e}{m_e}\right) \tag{4.29}$$

Thus, the dilatation energy of all the elemental quamlets, $\alpha\alpha^*$, is

$$\left(\frac{\mathrm{D}}{\rho}\right)\Sigma_\alpha \Sigma_{\alpha^*}\nabla\bullet\rho_{\alpha\alpha^*}\left(\mathbf{w}_\alpha+\mathbf{w}_{\alpha^*}\right)=\Sigma_\alpha \Sigma_{\alpha^*}\left(\mathrm{z}_{\alpha\alpha^*}\right)[(\frac{E}{m_e})-(\frac{V_e}{m_e})]-2\Sigma_\alpha \Sigma_{\alpha^*}\mathrm{z}_{\alpha\alpha^*}\left(\mathbf{w}_\alpha\bullet\mathbf{w}_{\alpha^*}\right) \tag{4.30}$$

The sum of the kinetic energy and dilatational energy of elemental quamlets is obtained by substituting (4.30) into (4.26) as follows,

$$2\Sigma_\alpha \Sigma_{\alpha^*}\left(\mathrm{z}_{\alpha\alpha^*}\right)\left(\mathbf{w}_\alpha\bullet\mathbf{w}_{\alpha^*}\right)+\left(\frac{\mathrm{D}}{\rho}\right)\left\{\Sigma_\alpha \Sigma_{\alpha^*}\nabla\bullet\left[\rho_{\alpha\alpha^*}\left(\mathbf{w}_\alpha+\mathbf{w}_{\alpha^*}\right)\right]\right\}$$

$$=2\Sigma_\alpha \Sigma_{\alpha^*}\left(\mathrm{z}_{\alpha\alpha^*}\right)\left(\mathbf{w}_\alpha\bullet\mathbf{w}_{\alpha^*}\right)+\Sigma_\alpha \Sigma_{\alpha^*}[(\frac{E}{m_e})-(\frac{V_e}{m_e})]\mathrm{z}_{\alpha\alpha^*}-2\Sigma_\alpha \Sigma_{\alpha^*}\left(\mathrm{z}_{\alpha\alpha^*}\right)\left(\mathbf{w}_\alpha\bullet\mathbf{w}_{\alpha^*}\right)$$

$$=\Sigma_\alpha \Sigma_{\alpha^*}[(\frac{E}{m_e})-(\frac{V_e}{m_e})]\mathrm{z}_{\alpha\alpha^*} \tag{4.31}$$

Following the similar algebraic procedure, we reduce the dilatation energy of the interactive quamlets $\alpha\beta^*$ and $\alpha^*\beta$ appear in (4.25) as follows,

$$\left(\frac{\mathrm{D}}{\rho}\right)\Sigma_\alpha \Sigma_{\beta^*}\nabla\bullet\left[\rho_{\alpha\beta^*}\left(\mathbf{w}_\alpha+\mathbf{w}_{\beta^*}\right)\right]=\Sigma_\alpha \Sigma_{\beta^*}[(\frac{E}{m_e})-(\frac{V_e}{m_e})]\mathrm{z}_{\alpha\beta^*}-2\Sigma_\alpha \Sigma_{\beta^*}\mathrm{z}_{\alpha\beta^*}\left(\mathbf{w}_\alpha\bullet\mathbf{w}_{\beta^*}\right) \tag{4.32}$$

$$\left(\frac{\mathrm{D}}{\rho}\right)\Sigma_{\alpha^*} \Sigma_\beta\nabla\bullet\left[\rho_{\alpha^*\beta}\left(\mathbf{w}_{\alpha^*}+\mathbf{w}_\beta\right)\right]=\Sigma_{\alpha^*} \Sigma_\beta[(\frac{E}{m_e})-(\frac{V_e}{m_e})]\mathrm{z}_{\alpha^*\beta}-2\Sigma_{\alpha^*} \Sigma_\beta\mathrm{z}_{\alpha^*\beta}\left(\mathbf{w}_{\alpha^*}\bullet\mathbf{w}_\beta\right) \tag{4.33}$$

The dilatation of interactive quamlets consists of two parts: the quantized energy of the quamlets, represented by the first term appears on the right hand side of the above expressions, and the negative of the kinetic energy of the quamlets, expressed by the second term.

Thus by adding (4.30) (4.32) and (4.33) we obtain the dilatation energy as follows,

$$\left(\frac{D}{\rho}\right)\left\{\sum_{\alpha}\sum_{\alpha^*}\nabla\bullet\left[\rho_{\alpha\alpha^*}\left(\mathbf{w}_{\alpha}+\mathbf{w}_{\alpha^*}\right)\right]\right\}+\left(\frac{D}{\rho}\right)\left\{\sum_{\alpha}\sum_{\beta^*}\nabla\bullet\left[\rho_{\alpha\beta^*}\left(\mathbf{w}_{\alpha}+\mathbf{w}_{\beta^*}\right)\right]\right\}$$

$$+\left(\frac{D}{\rho}\right)\left\{\sum_{\alpha^*}\sum_{\beta}\nabla\bullet\left[\rho_{\alpha^*\beta}\left(\mathbf{w}_{\alpha^*}+\mathbf{w}_{\beta}\right)\right]\right\}$$

$$=[(\frac{E}{m_e})-(\frac{V_e}{m_e})]\left\{\sum_{\alpha}\sum_{\alpha^*}\mathrm{z}_{\alpha\alpha^*}+\sum_{\alpha}\sum_{\beta^*}\mathrm{z}_{\alpha\beta^*}+\sum_{\alpha^*}\sum_{\beta}\mathrm{z}_{\alpha^*\beta}\right\}$$

$$-2\sum_{\alpha}\sum_{\alpha^*}\mathrm{z}_{\alpha\alpha^*}\left(\mathbf{w}_{\alpha}\bullet\mathbf{w}_{\alpha^*}\right)-2\sum_{\alpha}\sum_{\beta^*}\left(\mathbf{w}_{\alpha}\bullet\mathbf{w}_{\beta^*}\right)-2\sum_{\alpha^*}\sum_{\beta}\left(\mathbf{w}_{\alpha^*}\bullet\mathbf{w}_{\beta}\right) \tag{4.34}$$

Finally by substituting all the dilation energy obtained in (4.36) into the left side of the global Bernoulli's equation (4.25), we show that the left hand side of the equation is indeed equal to the right hand side, i.e. $[(E/m_e) - (V_e/m_e)]$

$$2\sum_{\alpha}\sum_{\alpha^*}\left(\mathrm{z}_{\alpha\alpha^*}\right)\left(\mathbf{w}_{\alpha}\bullet\mathbf{w}_{\alpha^*}\right)+2\sum_{\alpha}\sum_{\beta^*}\left(\mathrm{z}_{\alpha\beta^*}\right)\left(\mathbf{w}_{\alpha}\bullet\mathbf{w}_{\beta^*}\right)+2\sum_{\alpha^*}\sum_{\beta}\left(\mathrm{z}_{\alpha^*\beta}\right)\left(\mathbf{w}_{\alpha^*}\bullet\mathbf{w}_{\beta}\right)$$

$$\left\{\sum_{\alpha}\sum_{\alpha^*}\left(\mathrm{z}_{\alpha\alpha^*}\right)+\sum_{\alpha}\sum_{\beta^*}\left(\mathrm{z}_{\alpha\beta^*}\right)+\sum_{\alpha^*}\sum_{\beta}\left(\mathrm{z}_{\alpha^*\beta}\right)\right\}[(\frac{E}{m_e})-(\frac{V_e}{m_e})]$$

$$-2\sum_{\alpha}\sum_{\alpha^*}\left(\mathrm{z}_{\alpha\alpha^*}\right)\left(\mathbf{w}_{\alpha}\bullet\mathbf{w}_{\alpha^*}\right)-2\sum_{\alpha}\sum_{\beta^*}\left(\mathrm{z}_{\alpha\beta^*}\right)\left(\mathbf{w}_{\alpha}\bullet\mathbf{w}_{\beta^*}\right)$$

$$-2\sum_{\alpha^*}\sum_{\beta}\left(\mathrm{z}_{\alpha^*\beta}\right)\left(\mathbf{w}_{\alpha^*}\bullet\mathbf{w}_{\beta}\right)$$

$$=\left\{\sum_{\alpha}\sum_{\alpha^*}\left(\mathrm{z}_{\alpha\alpha^*}\right)+\sum_{\alpha}\sum_{\beta^*}\left(\mathrm{z}_{\alpha\beta^*}\right)+\sum_{\alpha^*}\sum_{\beta}\left(\mathrm{z}_{\alpha^*\beta}\right)\right\}[(\frac{E}{m_e})-(\frac{V_e}{m_e})] \tag{4.35}$$

$$=[(\frac{E}{m_e})-(\frac{V_e}{m_e})]$$

We have proved that the quamlet mixture satisfies the global Bernoulli's equation. This is one of the basic criteria for the QM-QFD equivalence. We shall show that the necessary condition to meet the criterion is that each quamlet must be the solution of the Bernoulli's equation of individual quamlet, as described in the following subsections.

Energy balance of elemental quamlets: $\alpha\alpha^*$

By collecting the terms associated with $\alpha\alpha^*$ terms in the left hand side of Eq. (4.35), we have,

$$2\sum_{\alpha}\sum_{\alpha^*}\left(z_{\alpha\alpha^*}\right)\left(\mathbf{w}_{\alpha}\bullet\mathbf{w}_{\alpha^*}\right)+\left(\frac{D}{\rho}\right)\left\{\sum_{\alpha}\sum_{\alpha^*}\nabla\bullet\left[\rho_{\alpha\alpha^*}\left(\mathbf{w}_{\alpha}+\mathbf{w}_{\alpha^*}\right)\right]\right\}$$

$$=2\sum_{\alpha}\sum_{\alpha^*}\left(\mathrm{z}_{\alpha\alpha^*}\right)\left(\mathbf{w}_{\alpha}\bullet\mathbf{w}_{\alpha^*}\right)+\sum_{\alpha}\sum_{\alpha^*}\left(\mathrm{z}_{\alpha\alpha^*}\right)[(\frac{E}{m_e})-(\frac{V_e}{m_e})]$$

$$-2\sum_{\alpha}\sum_{\alpha^*}\left(\mathrm{z}_{\alpha\alpha^*}\right)\left(\mathbf{w}_{\alpha}\bullet\mathbf{w}_{\alpha^*}\right)=\sum_{\alpha}\sum_{\alpha^*}\left(\mathrm{z}_{\alpha\alpha^*}\right)[(\frac{E}{m_e})-(\frac{V_e}{m_e})] \tag{4.36}$$

The degenerate wave functions are linearly independent solution of the Schrödinger's equation, hence if the wave functions are continuous up to the first derivatives, then the necessary condition for the validity of the Eq. (4.36) is that each elemental quamlet, $\alpha\alpha*$ satisfies the following the "elemental quamlet Bernoullis equation" .

$$2\sum_{\alpha}\sum_{\alpha^*}\left(\mathrm{z}_{\alpha\alpha^*}\right)\left(\mathbf{w}_{\alpha}\bullet\mathbf{w}_{\alpha^*}\right)+\left(\frac{\mathrm{D}}{\rho}\right)\nabla\bullet\left[\rho_{\alpha\alpha^*}\left(\mathbf{w}_{\alpha}+\mathbf{w}_{\alpha^*}\right)\right]=[(\frac{E}{m_e})-(\frac{V_e}{m_e})]\mathrm{z}_{\alpha\alpha^*} \tag{4.37}$$

Balance of interactive quamlets: $\alpha\beta*$ and $\alpha*\beta$

Following the same mathematical steps, we find that the sum of interactive quamlets $\alpha\beta*$ obeys the following equation,

$$+2\sum_{\alpha}\sum_{\beta^*}\left(z_{\alpha\beta^*}\right)\left(\mathbf{w}_{\alpha}\bullet\mathbf{w}_{\beta^*}\right)+\left(\frac{D}{\rho}\right)\left\{\sum_{\alpha}\sum_{\beta^*}\nabla\bullet\left[\rho_{\alpha\beta^*}\left(\mathbf{w}_{\alpha}+\mathbf{w}_{\beta^*}\right)\right]\right\}$$

$$=2\sum_{\alpha}\sum_{\beta^*}\left(\mathrm{z}_{\alpha\beta^*}\right)\left(\mathbf{w}_{\alpha}\bullet\mathbf{w}_{\beta^*}\right)+\sum_{\alpha}\sum_{\beta^*}\left(\mathrm{z}_{\alpha\beta^*}\right)[(\frac{E}{m_e})-(\frac{V_e}{m_e})]-2\sum_{\alpha}\sum_{\beta^*}\left(\mathrm{z}_{\alpha\beta^*}\right)\left(\mathbf{w}_{\alpha}\bullet\mathbf{w}_{\beta^*}\right)$$

$$=\sum_{\alpha}\sum_{\beta^*}\left(\mathrm{z}_{\alpha\beta^*}\right)[(\frac{E}{m_e})-(\frac{V_e}{m_e})] \tag{4.38}$$

If the degenerate wave functions for α and $\beta*$, which are linearly independent solutions of the wave equation of degenerate energy level, are continuous up to the first order derivative, then the above equality hold when each interactive quamlet, $\alpha\beta*$ satisfies the interactive quamlet Bernoulli's equation.

$$2\left(\mathrm{z}_{\alpha\beta^*}\right)\left(\mathbf{w}_{\alpha}\bullet\mathbf{w}_{\beta^*}\right)+\left(\frac{\mathrm{D}}{\rho}\right)\nabla\bullet\left[\rho_{\alpha\beta^*}\left(\mathbf{w}_{\alpha}+\mathbf{w}_{\beta^*}\right)\right]$$

$$=2\left(\mathrm{z}_{\alpha\beta^*}\right)\left(\mathbf{w}_{\alpha}\bullet\mathbf{w}_{\beta^*}\right)+\left(\mathrm{z}_{\alpha\beta^*}\right)[(\frac{E}{m_e})-(\frac{V_e}{m_e})]-2\left(\mathrm{z}_{\alpha\beta^*}\right)\left(\mathbf{w}_{\alpha}\bullet\mathbf{w}_{\beta^*}\right)$$

$$=\left(\mathrm{z}_{\alpha\beta^*}\right)[(\frac{E}{m_e})-(\frac{V_e}{m_e})] \tag{4.39}$$

Thus, we conclude that the quamlet, $\alpha\beta*$, satisfies the Bernoulli's equation of $\alpha*\beta$.

$$2\left(\mathrm{z}_{\alpha\beta*}\right)\left(\mathbf{w}_{\alpha}\bullet\mathbf{w}_{\beta*}\right)+\left(\frac{\mathrm{D}}{\rho}\right)\nabla\bullet\left[\rho_{\alpha\beta*}\left(\mathbf{w}_{\alpha}+\mathbf{w}_{\beta*}\right)\right]=\left(\mathrm{z}_{\alpha\beta*}\right)[(\frac{E}{m_e})-(\frac{V_e}{m_e})] \tag{4.40}$$

By the similar method described above, we show that satisfy the following equation.

$\alpha*\beta$ quamlets

$$2\left(\mathrm{z}_{\alpha*\beta}\right)\left(\mathbf{w}_{\alpha*}\bullet\mathbf{w}_{\beta}\right)+\left(\frac{\mathrm{D}}{\rho}\right)\nabla\bullet\left[\rho_{\alpha*\beta}\left(\mathbf{w}_{\alpha*}+\mathbf{w}_{\beta}\right)\right]=\left(\mathrm{z}_{\alpha*\beta}\right)[(\frac{E}{m_e})-(\frac{V_e}{m_e})] \tag{4.41}$$

By expressing the above equations in terms of the mean velocity, and the diffusion velocity, i.e., real valued velocities we arrive at the following Bernoulli's equations for three types of quamlets

Bernoulli's equation of $\alpha\alpha*$ elemental quamlets

$$\left(\frac{1}{2}\right)\mathrm{z}_{\alpha\alpha*}\left(\mathbf{u}_{\alpha\alpha*}\bullet\mathbf{u}_{\alpha\alpha*}+\mathbf{v}_{\alpha\alpha*}\bullet\mathbf{v}_{\alpha\alpha*}\right)+\left(\frac{\mathrm{D}}{\rho}\right)\nabla\bullet\left(\rho_{\alpha\alpha*}\mathbf{v}_{\alpha\alpha*}\right)=\mathrm{z}_{\alpha\alpha*}[(\frac{E}{m_e})-(\frac{V_e}{m_e})] \tag{4.42}$$

The real part of the Bernoulli's equation $\alpha\beta*$ is given by,

$$\left(\frac{1}{2}\right)\left[\left(\rho\zeta_{\alpha\beta}\right)\left(\mathbf{v}_{\alpha\alpha*}\mathbf{v}_{\beta\beta*}+\mathbf{u}_{\alpha\alpha*}\mathbf{u}_{\beta\beta*}\right)+\rho\eta_{\alpha\beta}\left(\mathbf{u}_{\alpha\alpha*}\mathbf{v}_{\beta\beta*}+\mathbf{u}_{\alpha\alpha*}\mathbf{v}_{\beta\beta*}\right)\right]$$

$$+\left(\frac{\mathrm{D}}{\rho}\right)\nabla\bullet\left\{\rho\zeta_{\alpha\beta*}\left(\mathbf{v}_{\alpha\alpha*}+\mathbf{v}_{\beta\beta*}\right)+\rho\eta_{\alpha\beta}\left(\mathbf{u}_{\alpha\alpha*}-\mathbf{v}_{\beta\beta*}\right)\right\}$$

$$=\left(\rho\zeta_{\alpha\beta*}\right)[(\frac{E}{m_e})-(\frac{V_e}{m_e})] \tag{4.43}$$

The imaginary parts is

$$\left(\frac{1}{2}\right)\left[\left(\rho\zeta_{\alpha\beta}\right)\left(\mathbf{v}_{\alpha\alpha*}\mathbf{v}_{\beta\beta*}+\mathbf{u}_{\alpha\alpha*}\mathbf{u}_{\beta\beta*}\right)-\rho\eta_{\alpha\beta}\left(\mathbf{u}_{\alpha\alpha*}\mathbf{v}_{\beta\beta*}-\mathbf{u}_{\alpha\alpha*}\mathbf{v}_{\beta\beta*}\right)\right]$$

$$+\left(\frac{\mathrm{D}}{\rho}\right)\Sigma_{\alpha}\Sigma_{\beta*}\nabla\bullet\left\{\rho\eta_{\alpha\beta*}\left(\mathbf{v}_{\alpha\alpha*}+\mathbf{v}_{\beta\beta*}\right)-\rho\zeta_{\alpha\beta}\left(\mathbf{u}_{\alpha\alpha*}-\mathbf{u}_{\beta\beta*}\right)\right\}$$

$$=\Sigma_{\alpha}\Sigma_{\beta*}\left(\rho\zeta_{\alpha\beta*}\right)[(\frac{E}{m_e})-(\frac{V_e}{m_e})] \tag{4.44}$$

It is concluded that the necessary and sufficient conditions for the equivalence between the quantum flow field with the wave field are that each component of quamlet satisfies the equations of continuity of probability, Eqs.(4.4) (4.7), (4.11), the Bernoulli's equations (4.40) (4.43) and (4.44) and the global flow field satisfies the quantization condition, (3.24).

E. Quamlet energy balance

We consider electrons moving with energy E in two-dimensional space bounded by parallel plates with the separation between two plates being equal to b. The plates extend from x = 0 to infinity.

Since the electrons are taken as free particles of energy E, we assume their wave functions are stationary state plane waves and are of the form $\Psi = \psi(x, y)\ \exp(iEt/\hbar)$. The time-dependent Schrödinger equation of motion governing the electrons is,

$$i\hbar \frac{\partial \Psi}{\partial t} = -\frac{\hbar^2}{2m_e} \nabla^2 \Psi \,, \tag{4.45}$$

where $\hbar$ is the Planck's constant divided by 2π, and m_e is the rest mass of an electron. The probability density, ρ. of the electron is then,

$$\rho = \psi \psi^* , \tag{4.46}$$

where ψ^* is the complex conjugate of the wave function ψ

Time independent equation, governing the stationary wave function, ψ, is obtained by substituting $\Psi = \psi(x, y)\ \exp(iEt/\hbar)$ into Eq. (4.45), as follows,

$$\nabla^2 \psi(x, y) + N^2 \psi(x, y) = 0 \,, \tag{4.47}$$

where, $\nabla^2 = \partial^2/\partial x^2 + \partial^2/\partial y^2$, $x = \pi \underline{x}/b$, $y = \pi \underline{y}/b$ and $N^2 = (2m_e/\hbar^2)(b/\pi)^2 E$, in which b is the plate separation, and N is given by,

$$N^2 = \frac{2m_e E}{\hbar^2} \frac{b^2}{\pi^2} , \tag{4.48}$$

which may also be written in terms of the deBroglie wavelength, $\lambda_{dB}^2 = \hbar^2 / 2m_e E$,

$$N^2 = \left(\frac{\lambda_b}{\lambda_{dB}} \right)^2 \tag{4.49}$$

where $\lambda_b = b/\pi$. Alternatively, N can be view as a quantum Reynolds number that is defined by the ratio of typical inertial force to quantum viscous force. Thus $N = u_o b/(\hbar\pi/m_e) = u_o b/\nu_Q$, where m_e The solution of the particle field is constructed by the linear superposition of the wave functions, which satisfies Eq. (4.47), as follows,

$$\psi(E,x) = \sum A_\alpha \psi_\alpha(E,x) \qquad \alpha = 1,2,3,.... \tag{4.50}$$

The wave function of α-th degenerate state is given by,

$$\psi_\alpha = A_\alpha \exp[-i\alpha y - i(N^2 - \alpha^2)^{1/2} x] \tag{4.51}$$

$$\psi_\beta = B_\alpha \exp[-i\beta y - i(N^2 - \beta^2)^{1/2} x] \tag{4.52}$$

The above wave function for α-th state creates an elemental quamlet α–α^* whose density and velocities are given by,

$$\rho_{\alpha\alpha^*} = \psi_\alpha \psi_{\alpha^*} = A_a{}^2 \exp[-i\alpha y - i(N^2 - \alpha^2)^{1/2} x] \exp[i\alpha y + i(N^2 - \alpha^2)^{1/2} x] = A_a{}^2 \tag{4.53}$$

$$\rho_{\alpha\beta^*} = \psi_\alpha \psi_{\beta^*} = A_a A_{\beta^*} \exp\{-i(\alpha - \beta) y - i(N^2 - \alpha^2)^{1/2} - (N^2 - \beta^2)^{1/2} x]\} \tag{4.54}$$

$$\mathbf{w}_\alpha = -(h\pi / 2m_e b)\nabla([-i\alpha y - i(N^2 - \alpha^2)^{1/2} x] = -(h\pi / 2m_e b)[-i(\alpha \mathbf{e}_y + (N^2 - \alpha^2)^{1/2} \mathbf{e}_x] \tag{4.55}$$

$$\mathbf{w}_{\beta^*} = -(h\pi / 2m_e b)\nabla([i\beta y + i(N^2 - \beta^2)^{1/2} x] = -(h\pi / 2m_e b)[i(\beta \mathbf{e}_y + (N^2 - \beta^2)^{1/2} \mathbf{e}_x] \tag{4.56}$$

$$\mathbf{w}_\alpha - \mathbf{w}_{\beta^*} = -(h\pi / 2m_e b)([-i(\alpha + \beta)\mathbf{e}_y - i[(N^2 - \alpha^2)^{1/2} + (N^2 - \beta^2)^{1/2} \mathbf{e}_x] \tag{4.57}$$

$$\begin{aligned} \mathbf{u}_{aa^*} &= (h / 2im_e b)\nabla \ln(\psi_\alpha / \psi_\alpha{}^*) = (h / m_e b)\nabla[-\alpha y - (N^2 - \alpha^2)^{1/2} x] \\ &= (h / m_e b)[\alpha \mathbf{e}_y + (N^2 - \alpha^2)^{1/2} \mathbf{e}_x] \end{aligned} \tag{4.58}$$

$$\mathbf{v}_{aa^*} = -h / 2m_e \nabla(\ln \psi_\alpha + \ln \psi_\alpha{}^*) = 0 \tag{4.59}$$

We shall prove that each quamlet satisfies the conservation equation,

The elemental quamlets, satisfies the continuity equation, (4.4), as follows,

$$\begin{aligned} &\nabla \bullet (\rho_{\alpha\alpha^*} \mathbf{u}_\alpha) = A_a{}^2 (h / m_e b)\nabla \bullet \{\exp[-i\alpha y - i(N^2 - \alpha^2)^{1/2} x][\alpha \mathbf{e}_y + (N^2 - \alpha^2)^{1/2} \mathbf{e}_x]\} \\ &= A_a{}^2 (h / m_e b)\{\alpha(-i)(N^2 - \alpha^2)^{1/2}] + (N^2 - \alpha^2)^{1/2}(-ia)\} \exp[-i\alpha y - i(N^2 - \alpha^2)^{1/2} x] = 0 \end{aligned} \tag{4.60}$$

This proves the compliance of the continuity law of $\alpha\alpha*$-th elemental quamlets, $\alpha\alpha*$ and $\beta\beta*$. Next, the interactive quamlet, $\alpha\beta*$, satisfies continuity (4.7), as shown below,

$$\begin{aligned} &i\nabla \bullet \rho_{\alpha\beta^*}(\mathbf{w}_\alpha - \mathbf{w}_{\beta^*}) = 0 \\ &= -(h\pi / 2m_e b) A_a A_{\beta^*} i\nabla \bullet \{\exp[-i(\alpha - \beta) y - i(N^2 - \alpha^2)^{1/2} - (N^2 - \beta^2)^{1/2} x] \\ &x\{-i(\alpha + \beta)\mathbf{e}_y - i[(N^2 - \alpha^2)^{1/2} + (N^2 - \beta^2)^{1/2} \mathbf{e}_x\} \end{aligned} \tag{4.61}$$

After some algebraic manupilation we have,

$$i\nabla \bullet \rho_{\alpha\beta^*}(\mathbf{w}_\alpha - \mathbf{w}_{\beta^*}) = -(h\pi/2m_e b)A_a A_{\beta^*} i\{[-i(\alpha^2-\beta^2)-(N^2-\alpha^2)+(N^2-\beta^2)]$$
$$\exp\{-i(\alpha+\beta)y - i[(N^2-\alpha^2)^{1/2}+(N^2-\beta^2)^{1/2}x]\} = 0 \tag{4.62}$$

Thus, the $\alpha\beta*$, satisfies continuity law. By the similar algebraic procedure, we can prove that $\alpha*\beta$ satisfies the continuity equation (4.11) .

Next we illustrate that each type of quamlet satisfies the Bernoulli's equation as follows.

Based on (4.37), the elemental quamlet $\alpha\beta*$ obeys Benoulli's equation ,

$$2(z_{\alpha\beta^*})(\mathbf{w}_\alpha \mathbf{w}_{\beta^*}) + (D/\rho)\nabla \bullet [\rho_{\alpha\beta^*}(\mathbf{w}_\alpha + \mathbf{w}_{\beta^*})] = (\frac{E}{m_e})z_{\alpha\beta^*} \tag{4.63}$$

Following the procedure used above, we substitute all the terms appear on the left hand side of the above equation to establishe the equality, as follows.

$$2D^2\rho_{\alpha\beta^*}\nabla\ln(\psi_\alpha)\bullet\nabla\ln(\psi_\alpha) - D^2\nabla\bullet[\rho_{\alpha\beta^*}\left(\ln\psi_\alpha + \ln\psi_{\beta^*}\right)] = (\frac{E}{m_e})(\rho_{\alpha\beta^*}) \tag{4.64}$$

By substituting the density and velocities given by (4.54) in the above equation and expanding the left hand side of above equation we have,

$$\begin{aligned}
&D^2 A_a A_{\beta^*}\exp\{-i(\alpha-\beta)y - i[(N^2-\alpha^2)^{1/2}-(N^2-\beta^2)^{1/2}]\}\\
&x\{2\alpha\beta + 2(N^2-\alpha^2)^{1/2}(N^2-\beta^2)^{1/2} + [(N^2-\alpha^2) - 2(N^2-\beta^2)^{1/2}(N^2-\alpha^2)^{1/2} + (N^2-\beta^2)^{1/2}]\} =\\
&D^2 A_a A_{\beta^*}\exp\{-i(\alpha-\beta)y - i[(N^2-\alpha^2)^{1/2}-(N^2-\beta^2)^{1/2}]\}\\
&x\{2\alpha\beta + 2(N^2-\alpha^2)^{1/2}(N^2-\beta^2)^{1/2} + (\alpha-\beta)^2 + [(N^2-\alpha^2) - 2(N^2-\beta^2)^{1/2}(N^2-\alpha^2)^{1/2} + (N^2-\beta^2)]\} =\\
&D^2 A_a A_{\beta^*}\exp\{-i(\alpha-\beta)y - i[(N^2-\alpha^2)^{1/2}-(N^2-\beta^2)^{1/2}]\}(2N^2)\\
&= D^2\rho_{\alpha\beta^*}(2N^2) = (\hbar/4m_e^2)(\pi/b)^2\rho_{\alpha\beta^*} = \rho_{\alpha\beta^*}(E/m_e)
\end{aligned} \tag{4.65}$$

We have shown that the sum of the left hand side of the above equation agrees with the right hand side of Eq. (4.64), i.e.,

$$2D^2\rho_{\alpha\beta^*}\nabla\ln(\psi_\alpha)\bullet\nabla\ln(\psi_\alpha) - D^2\nabla\bullet\left[\rho_{\alpha\beta^*}\left(\ln\psi_\alpha + \ln\psi_{\beta^*}\right)\right] = (\frac{E}{m_e})(\rho_{\alpha\beta^*}) \tag{4.66}$$

Thus, we prove that the quamlet $\alpha\beta*$ satisfies the Bernoulli's equation of $\alpha\beta*$

The proof of the compliance of $\alpha\alpha*$ can be made by replacing $\beta*$ by $\alpha*$ in the above analysis, whereas that of $\alpha*\beta$ can be demonstrated by exchange the role of α and β form that of the quamlet $\alpha\beta*$.

CONCLUSIONS

The quantum fluid dynamics (QFD) formalism based on the Hamilton-Jacobi transformation, incorporated with the quantum diffusion, is adapted to examine the equivalence between QFD non-linear field with quantum mechanical description based on Schrödinger's equation of linear wave field. The latter systems, which are characterized by a linear superposition of the wave functions of same degeneracy energy level, envisioned as the mixture of both elemental and interactive quantum flowlets, termed quamlets. Each elemental quamlet has the probability density equal to the product of a degenerate eigenfunction and its complex conjugate, whereas the density of an interactive quamlet is the product of a degenerate wave function and the complex conjugate of other degenerate wave function. The necessary and sufficient conditions for the equivalence between QM and QFD are that each quamlet obeys the laws of conservation: the continuity of probability, and mechanical energy of each quamlet, and that the global QFD field satisfies the quantization condition. The quamlets formalism provides the theoretical guides and criteria required for the analytical and numerical simulation of complex quantum systems by fluid dynamic methods, in particular, the quantum computational fluid dynamics, (QCFD). The validity of the later approach is ensured through the implementation of the quamlet formalism, which provides a physical and mathematical equivalence between the quantum fluid dynamic and Schrodinger's wave field descriptions. Specifically, the formalism ensures the compliance of the quantization, uncertainty principles, and exclusion principles, which are embodied in the wave formalism.

Acknowledgement

The author acknowledges the supports by the USAFOSR under AOARD-034039. I

---

[1] E. Madelung, Z.Phys.40,322 (1926)

[2] Broglie, L. de *La nouvelle dynamique des quanta' in Electrons et photons*, (Rapports et discussions du cinquieme conseil de physique Solvay.) (Gauthier-Villars. 105-132 ,1928)

[3] D. Bohm, Phys. Rev. **85**, 166 (1952)

[4] D. Bohm, Phys. Rev. **85**, 180, (1952)

[5] D. Bohm and B.J. Hiley, B. J., *The Undivided Universe*, (London: Routledge. 1999)

[6] H.E. Wilhelm, Phys, D1, 2278 (1970)

[7] E. Nelson, Phys. Rev. **150**, 1079 (1966)

[8] E. Nelson, *Quantum fluctuations,* (Princeton University Press. 1985)

[9] P. Garbaczewsky and J.P. Vigier, Phys.Rev A 46,4634 (1992)

[10] P. Garbaczewsky Phys. Lett. A 162, 129 (1992)

[11] F Guerra and L.M. Morato, Phys.Rev.D 27, 1774 (1983)

[12] D. Kershaw, Phys. Rev. **136**, B 1850 , (1964)

[13] R. Marra, Phys.Rev. D 36, 1724 (1987)

[14] L.M. Morato, D 32, 1982 (1985)

[15] M.S. Wang, Phys. Lett A 137 (1989)

[16] M. Daidson, Lett Math. Phys.3, 271 (1979)

[17] T. Takabayashi, Prog. Theor. Phys, 8 143 (1952)

[18] T. Takabayashi, Prog. Theor. Phys, 9 187 (1953)

[19] K.K. Kan and Griffin, Phys. Rev.C 15, 1126 (1927)

[20] I. Bialynicki-Birula, Z. Bialynica-Biura, and C. Sliwa, Phys.Rev A 61 032110 (2000)

[21] T.C. Wallstrom, Found. Phys. Lett, A 141, 9 (1989)

[22] T.C. Wallstrom, Phys.Rev. A 49, 1613 (1994)

[23] P.R. Holland, *The quantum theory of motion,*(Cambridge University Press.1993)

[24] H. H. Chiu, Proceedings A Royal Society of London, Accepted for publication, (2005)

[25] E. Carlen, *Conservative diffusions*, Communications in Mathematical physics **94,** 293-315. (1984)

[26] K. Berndl, M. Daumer, D. Durr, S. Goldstein, and N. Zanghi Nuvo Cimento **110 B,** 737 (1995),

[27] S.K. Ghosh, B.M. Deb, Phys. Rep. **92,** 1, (1982)

Structural and dynamic complexities of quantum nanojets

H.H. Chiu and C.T. Lin

Space Science and Technology Center
Institute of Aeronautics and Astronautics
National Cheng Kung University
Tainan, Taiwan 70101

Presented at
US Air Force/Taiwan Nanoscience Initiative Workshop
Maui Hawaii February 19-20 2004

Acknowledgements

- The authors extend their appreciations for the financial support awarded by the *US Airforce Office of Scientific Research*, 2003-USAF/Taiwan Nanoscience Initiative under the grant AOARD-03-4039, #7AFOS31760401.
- The privilege for an extensive use of computational facilities offered by *National High Speed Computation Center,* NARL, Taiwan, is appreciated.
- Special efforts rendered by all the members of *SPRAX* Laboratory at IAA, NCKU in this research are appreciated.

Objectives

- Nanojet , *sine qua non* tool of quantum nanoprocessing
- Quantum nanojet theory of dual-slit electron interferometer
- Structural and dynamic complexities
  - *Quantum transition: quantum-classical transition*
  - *Quantum branching: multi-branch configurations*
  - *Quantum clustering: dynamic clustering*
  - *Interference fringe complexities*
- Conclusions

Quantum nanojets 1

- **Definition:**

  Quantum nanojet refers to the streams or arrays of particles of atoms, sub-atoms, molecules, neutrons, ions or photons, injected or emitted from a particle source, directly or through a injector of *nanoscale*, to a designated target space in the presence or absence of an external potential, whereby exhibiting structural and dynamic quantum phenomena.

- **Quantum wave modes*:***

  Quantum waves in a jet exhibit *propagation, tunneling, interference, reflection* and *refraction*, and create hierarchical jet structures.

- **Nanojet: *sine qua non* tool of functional quantum processes**
  - **Transport of particles and creation of dynamic field**
  - **Formation of particle density and flux distribution patterns,**
  - **Excitations of particle-particle interaction,**
  - **Photon-particle interaction,**
  - **Transition of particle states**
  - **State transition and formation of interference fringes**

Quantum jet complexities and their relevance in nanodevice applications

Nanodevice applications	Jet configuration	Jet structure	Non-cluster particle jet	Clustered particle jet	Interference fringe	Transport of Particle & energy
Nanofabrication (lithography, nanoparticle,assembling)	shape, size, beam focusing	beam uniformity	fine lithography	particle/cluster assembling		beam energy distribution
nanoelectronics (single electron transistor, QDT	single, multi-particle array	inter-particle spacing	uniform current			·excited state transport, ·current/voltage
nanowires	wire geometry	current uniformity	conductance, inductance	particle/wire interaction		
nanoimaging (STM, SEM)		Image uniformity	fine resolution	Coarse resolution		current/voltage image/fabrication
nanointerferometer (two/slit particle beam)	number of fringes	fringe uniformity	Conventional fringes	Cluster signature	single, two,& multiple fringe	Particle path depends on quantum poential
nanooptoelectronic	stream, array	Light-particle interaction				
nanosensors	Single, multi-branch	Non-Uniform				Complexities of sensor

Molecular jet mass spectrometer

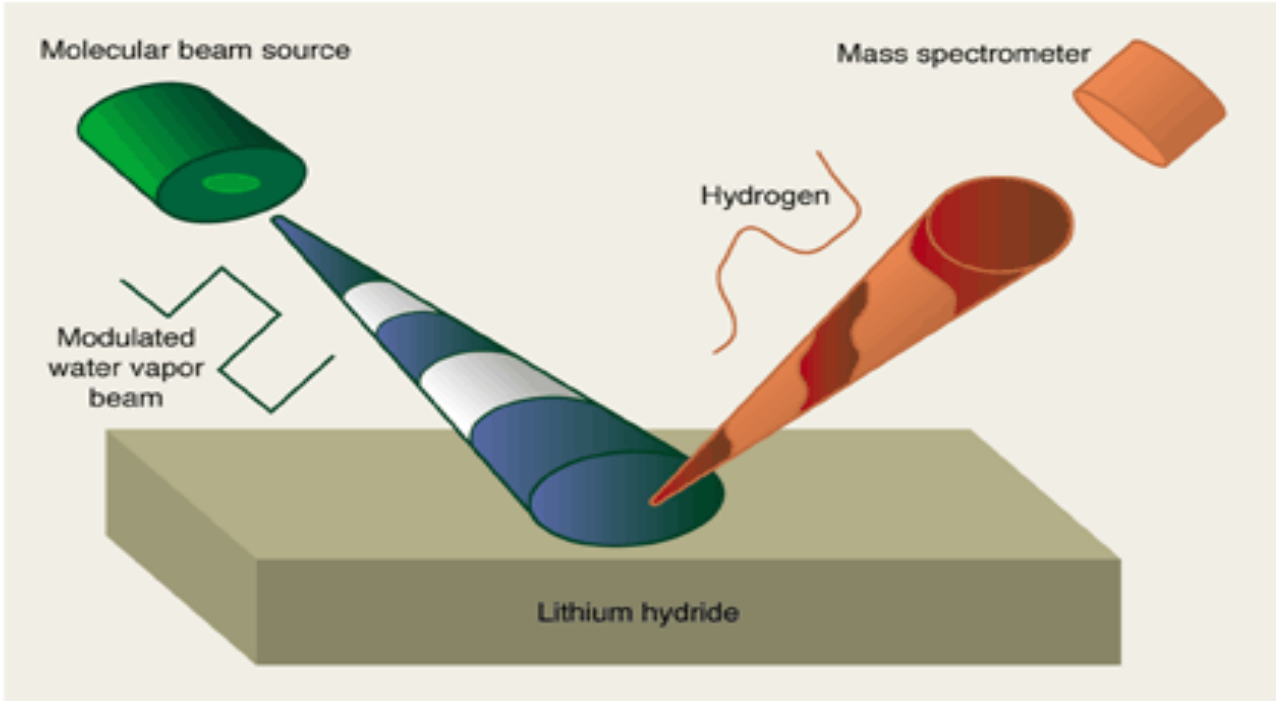

Figure 6. This schematic shows a modulated molecular-beam mass spectrometer being used to study the effects of water vapor on lithium hydride. The beam of water vapor directed at the lithium hydride is turned on and off at brief, regular intervals, as shown in the square pattern of the incoming beam. The outgoing beam of molecular hydrogen has a different shape, indicating a brief residence time in the lithium hydride.

Scanning Tunnel Microscope

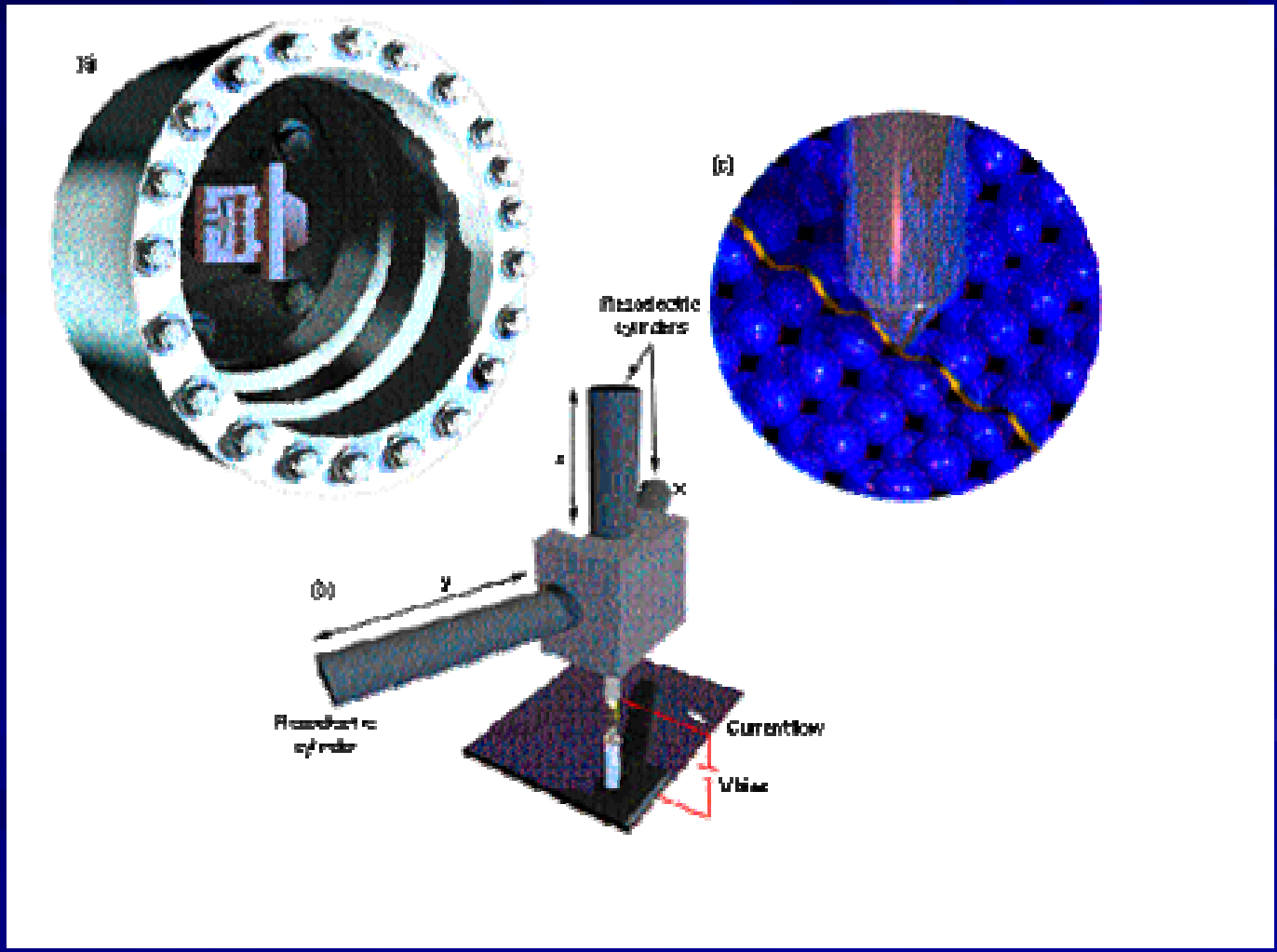

Quantum nanojets 2

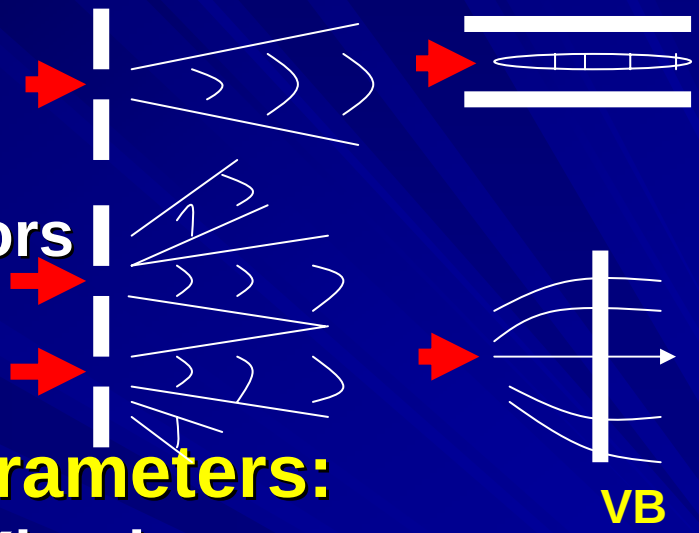

- **Nanojet Type**
  - Single injector
  - Double-slit, or Multi-slit injectors
  - Free jet, confined jet
  - External potential
- **Quantum nanojet control parameters:**
  - Injection conditions: particle Kinetic energy, injector geometry.
  - Quantum Reynolds Number N
- **Physical significance**
  - Inertial force/quantum force
  - Injector width/de-Bloglie wave length

Double-slit quantum nanojet

Double-slit electron interferometer: Young's Experiment

Electron energy E

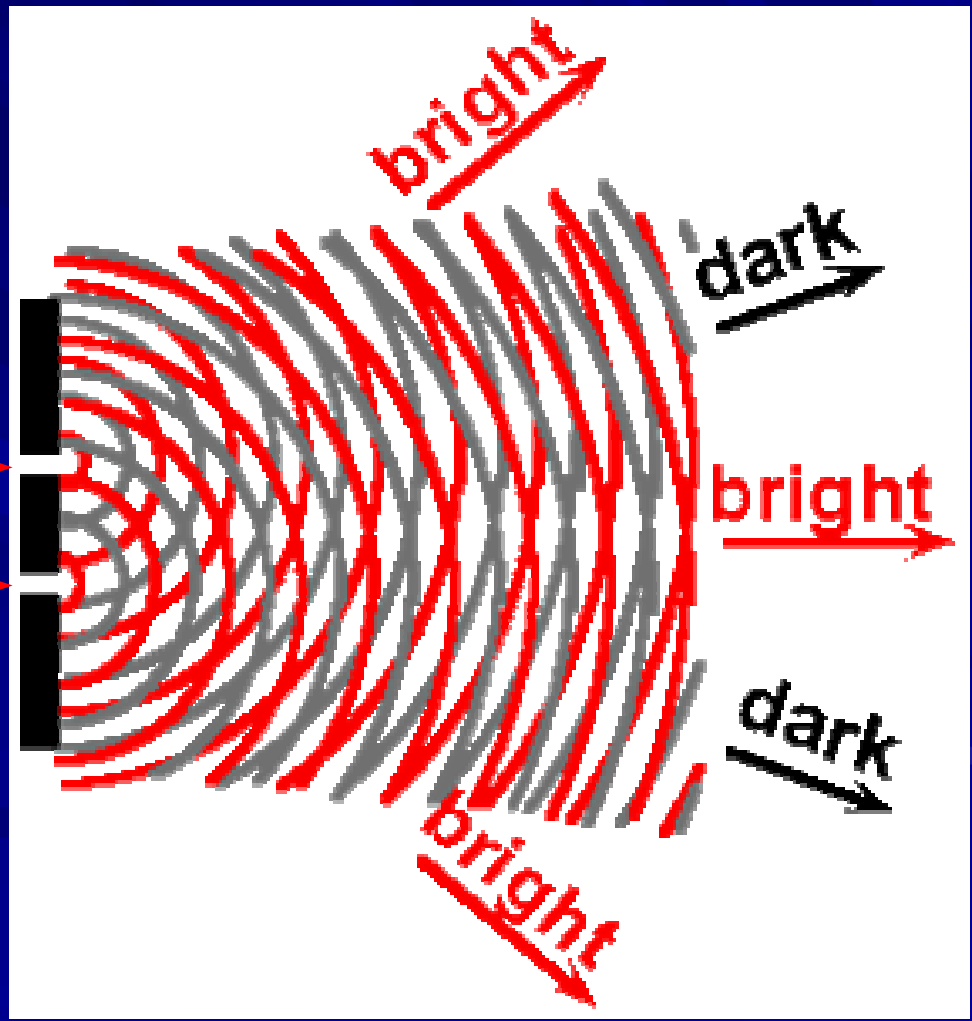

Double-slit quantum jet - Electron interfeometer

- **Quantum mechanical analysis of two-slit quantum jet**

Schrodinger's equation of Double-slit jet

$$i\hbar\frac{\partial\Psi}{\partial t}=-\frac{\hbar^2}{2m}\left(\frac{\partial^2\Psi}{\partial\bar{x}^2}+\frac{\partial^2\Psi}{\partial\bar{y}^2}\right)$$

$$\Psi(t,X)=e^{\frac{-iEt}{\hbar}}\psi(\bar{x},\bar{y})$$

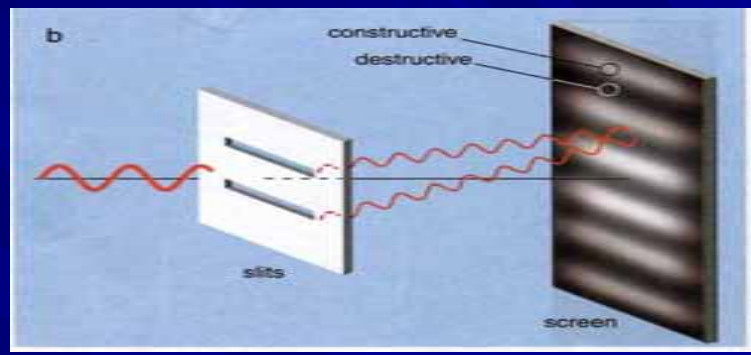

In non-dimensional form, $\psi(x,y)$ is governed by

$$\frac{\partial^2\psi}{\partial x^2}+\frac{\partial^2\psi}{\partial y^2}+N^2\psi=0 \qquad N^2=\frac{2mE}{\hbar^2}\frac{b^2}{\pi^2}=\left(\frac{\lambda_b}{\lambda_{dB}}\right)^2 \qquad \mathrm{x}=\frac{\pi\bar{x}}{b} \qquad \mathrm{y}=\frac{\pi\bar{y}}{b}$$

Wave function Fourier transform

$$\phi(x,\eta)=\frac{1}{\sqrt{2\pi}}\int_{-\infty}^{\infty}\psi(x,y)e^{i\eta y}dy \qquad \psi(x,y)=\frac{1}{\sqrt{2\pi}}\int_{-\infty}^{\infty}\phi(x,\eta)e^{-i\eta y}d\eta$$

Wave function of Double-slit electron nanojet

$$\psi = \psi_F^- + \psi_F^+ + \psi_G^-$$

$$\psi_F^- = \frac{2}{\sqrt{2\pi}} \int_0^N F^-(N-\varsigma)\cos\left(\sqrt{2N\varsigma-\varsigma^2}\,x\right)\cos\left((N-\varsigma)y\right)d\varsigma$$

$$\psi_F^+ = \frac{2}{\sqrt{2\pi}} \int_0^\infty F^+(N+\varsigma)\exp\left(-\sqrt{2N\varsigma+\varsigma^2}\,x\right)\cos\left((N+\varsigma)y\right)d\varsigma$$

$$\psi_G^- = \frac{2}{\sqrt{2\pi}} \int_0^N \frac{G^-(N-\varsigma)}{\sqrt{2N\varsigma-\varsigma^2}}\sin\left(\sqrt{2N\varsigma-\varsigma^2}\,x\right)\cos\left((N-\varsigma)y\right)d\varsigma$$

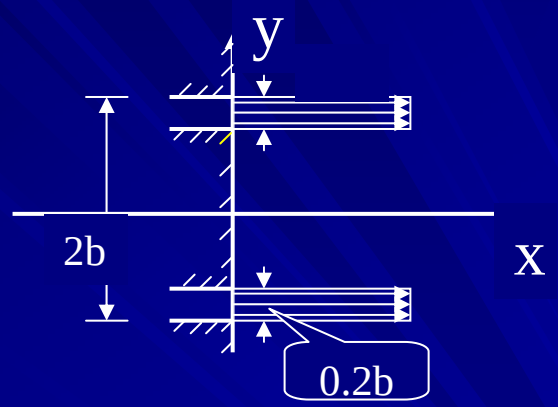

$$F^-(N-\varsigma) = f_0\sqrt{\frac{2}{\pi}}\left\{\cos\left[(N-\varsigma)*0.8\right] + i\cos\left[(N-\varsigma)*0.8\right]\right\}\frac{\sin\left[(N-\varsigma)*0.2\right]}{N-\varsigma}$$

$$F^+(N+\varsigma) = f_0\sqrt{\frac{2}{\pi}}\left\{\cos\left[(N+\varsigma)*0.8\right] + i\cos\left[(N+\varsigma)*0.8\right]\right\}\frac{\sin\left[(N+\varsigma)*0.2\right]}{N+\varsigma}$$

$$G^-(N-\varsigma) = f_0\sqrt{\frac{2}{\pi}}\left\{-\cos\left[(N-\varsigma)*0.8\right] + i\cos\left[(N-\varsigma)*0.8\right]\right\}\frac{\sin\left[(N-\varsigma)*0.2\right]}{N-\varsigma}$$

$$\bar{u} = \frac{\hbar}{2mi}\left[\psi^*\nabla\psi - \psi\nabla\psi^*\right]$$

$$u_x = \frac{\hbar}{2mi}\left[\psi^*\frac{\partial\psi}{\partial x} - \psi\frac{\partial\psi^*}{\partial x}\right] = \frac{\hbar}{m}\left[\psi_R\frac{\partial\psi_I}{\partial x} - \psi_I\frac{\partial\psi_R}{\partial x}\right]$$

$$u_y = \frac{\hbar}{2mi}\left[\psi^*\frac{\partial\psi}{\partial y} - \psi\frac{\partial\psi^*}{\partial y}\right] = \frac{\hbar}{m}\left[\psi_R\frac{\partial\psi_I}{\partial y} - \psi_I\frac{\partial\psi_R}{\partial y}\right]$$

Quantum nanojet Fraunhofer structural complexities

- Quantum-classical transition-

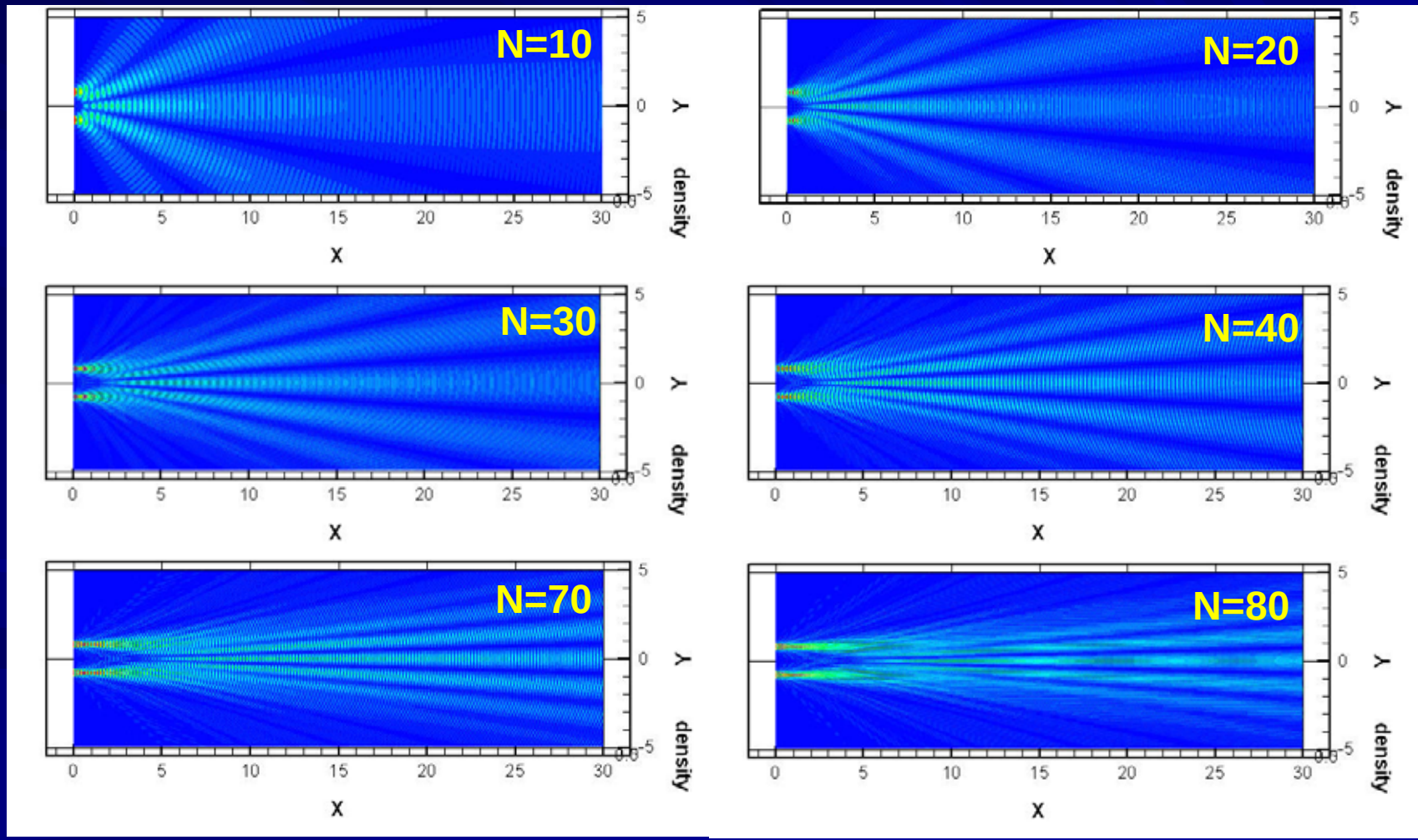

Quantum nanojet Fraunhofer structural Complexities

- Quantum-classical transition-

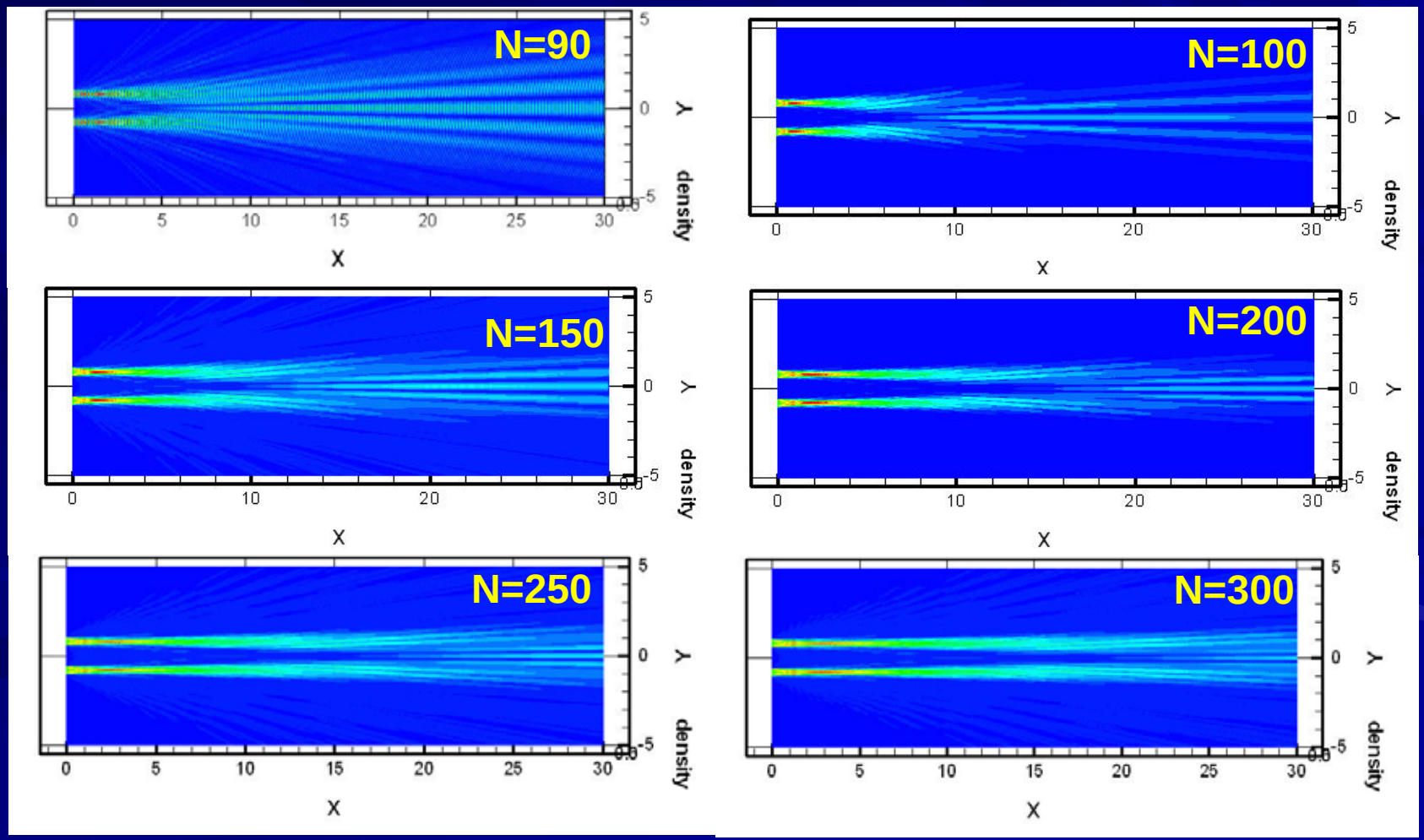

Quantum nanojet Fraunhofer structural Complexities

- Quantum-classical transition-

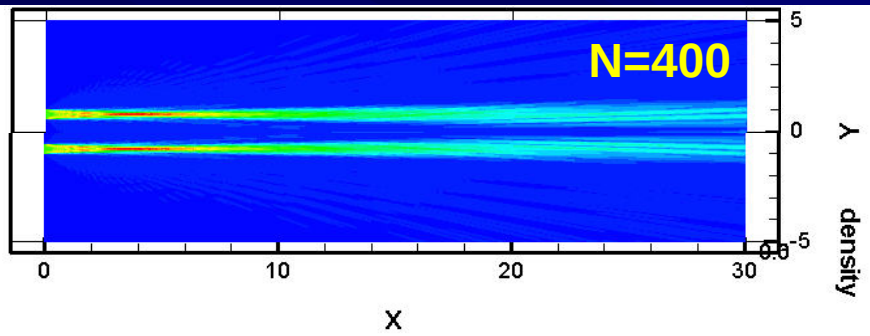

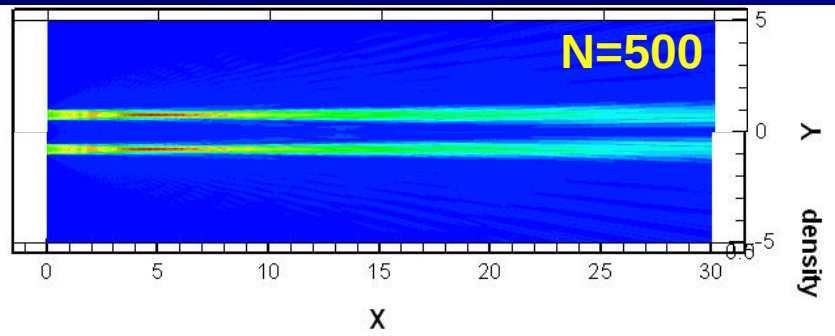

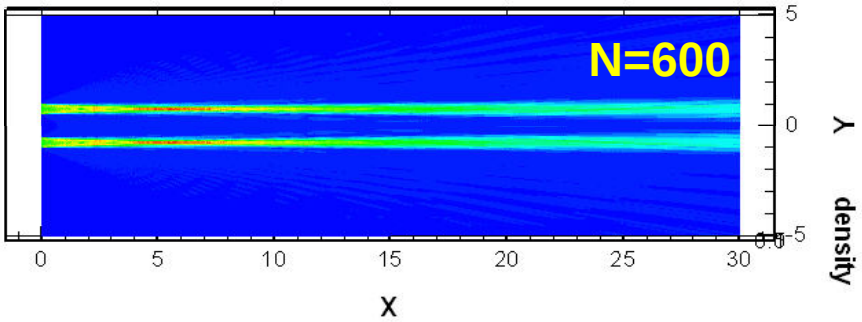

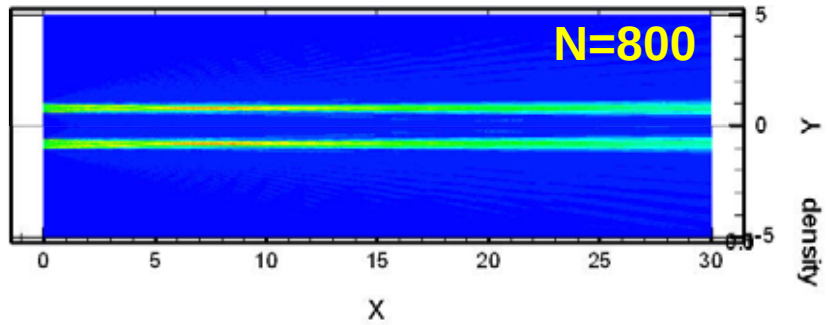

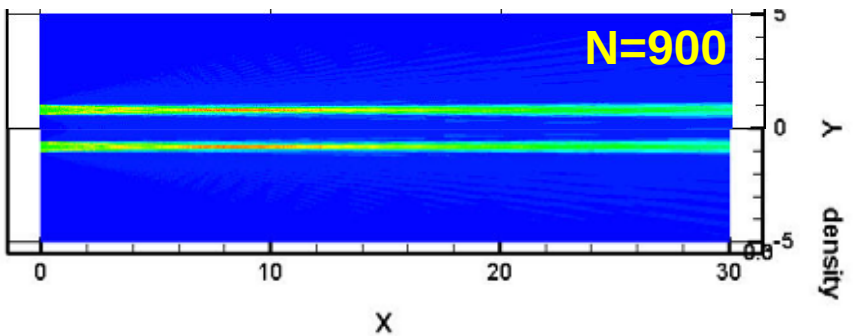

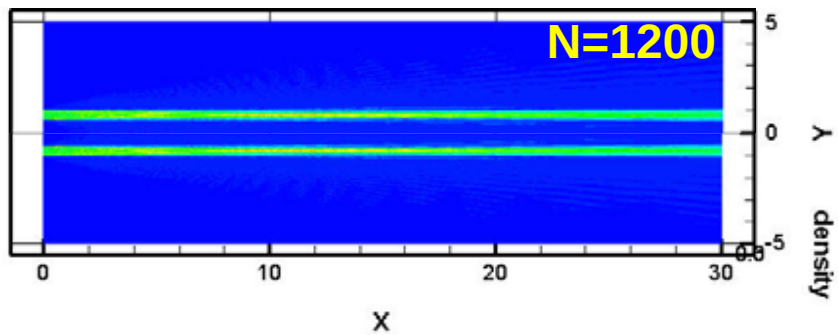

Quantum nanojet Fresnel structural complexities

-Quantum branching and clustering-

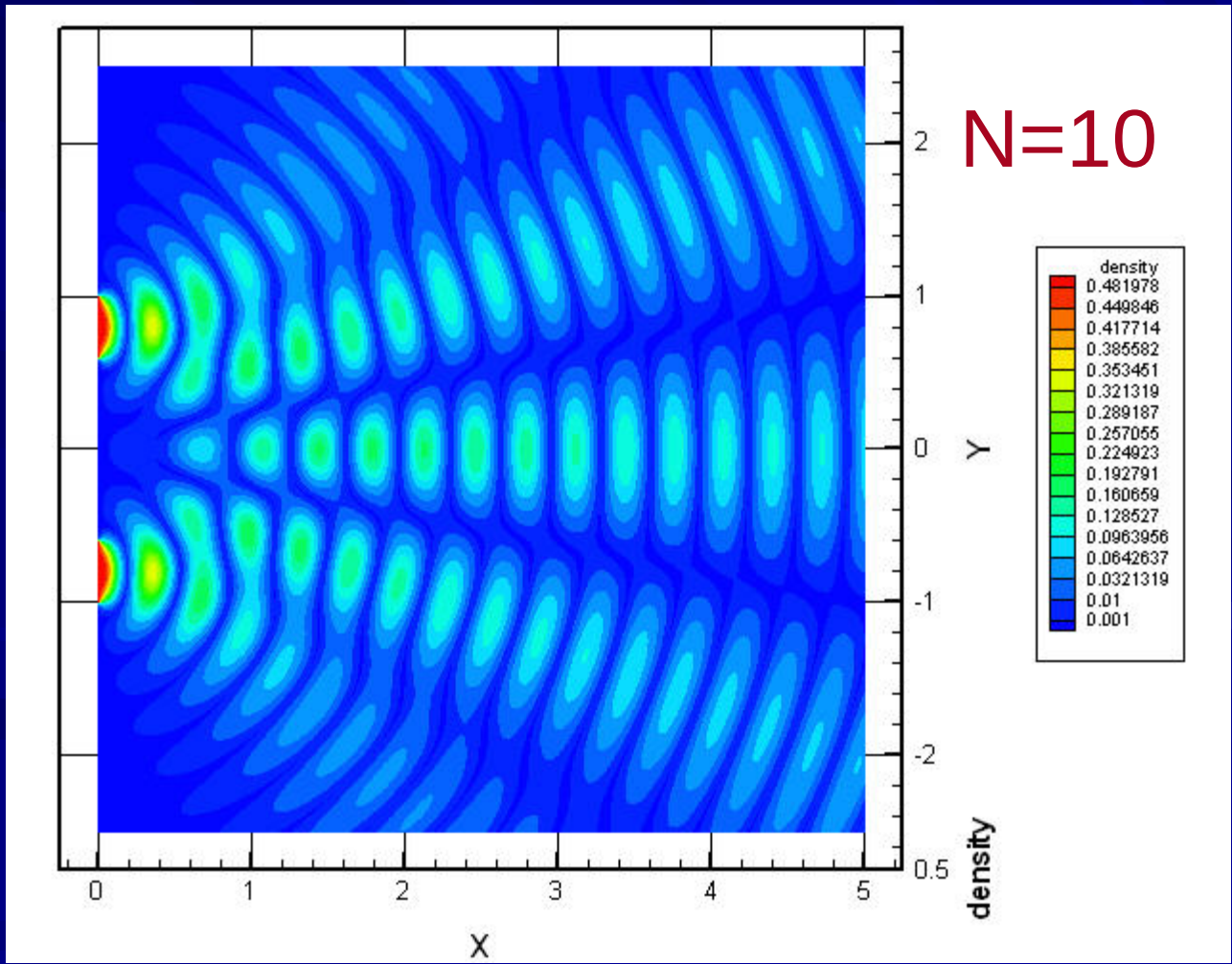

Quantum nanojet Fresnel structural complexities

-Quantum branching and clustering-

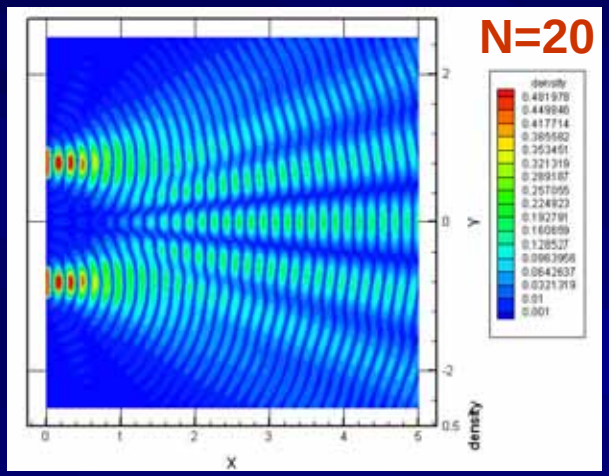

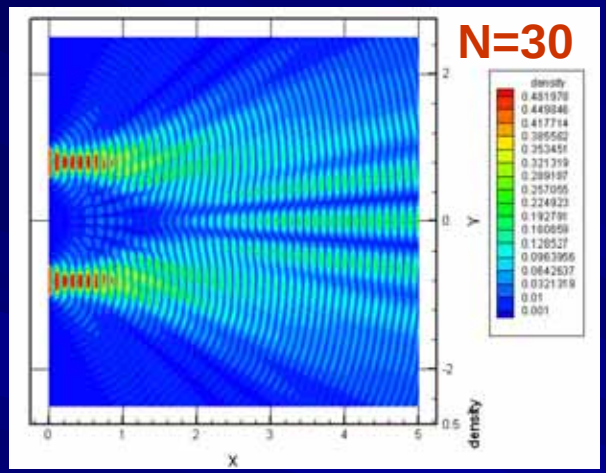

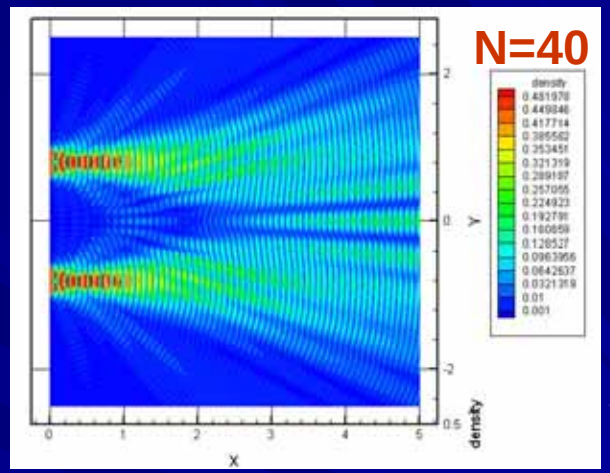

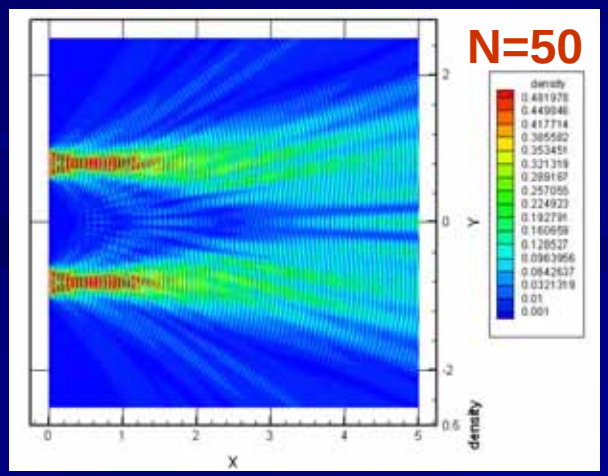

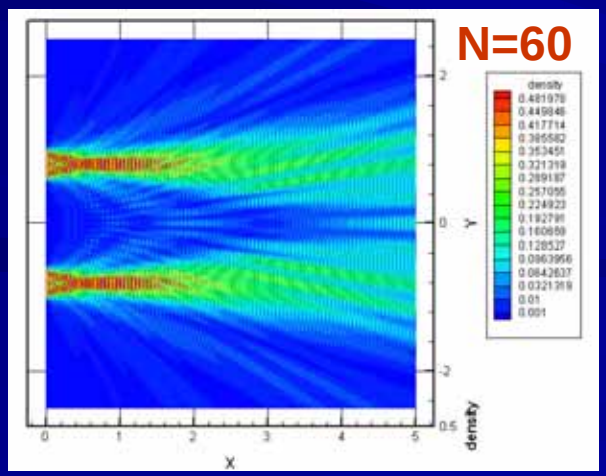

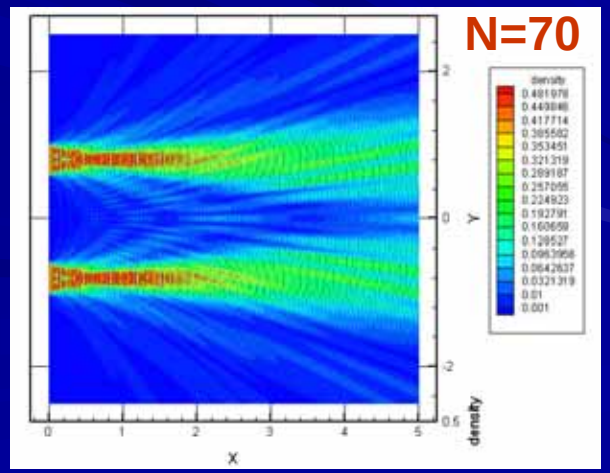

Quantum nanojet Fresnel structural complexities

-Quantum branching and clustering-

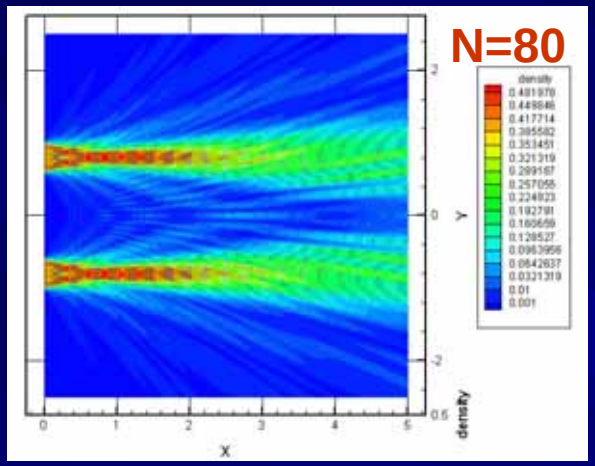

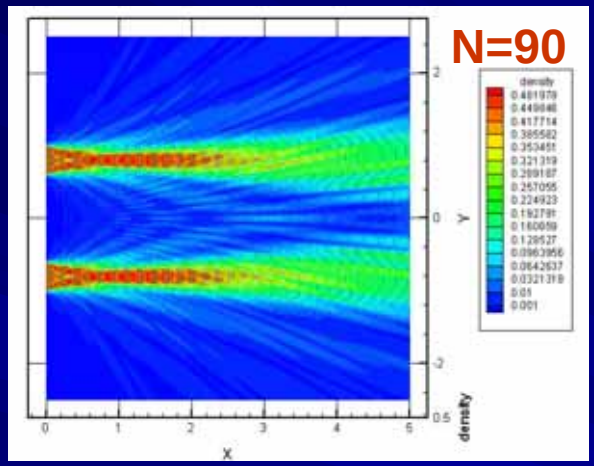

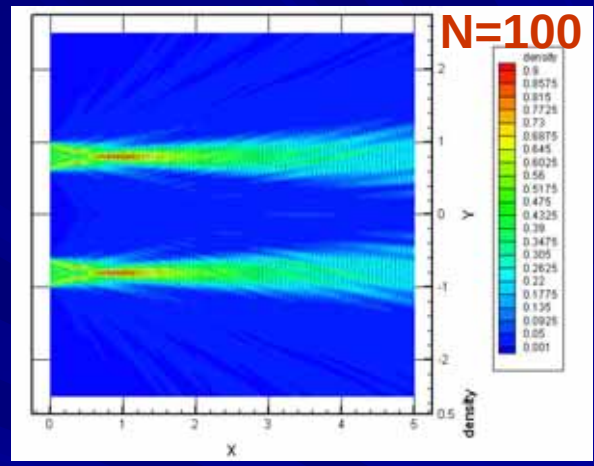

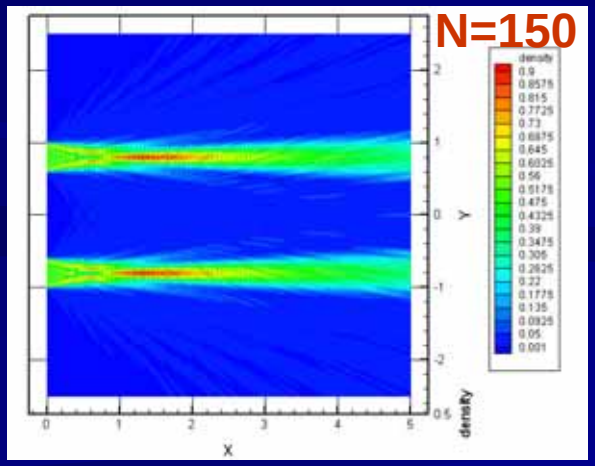

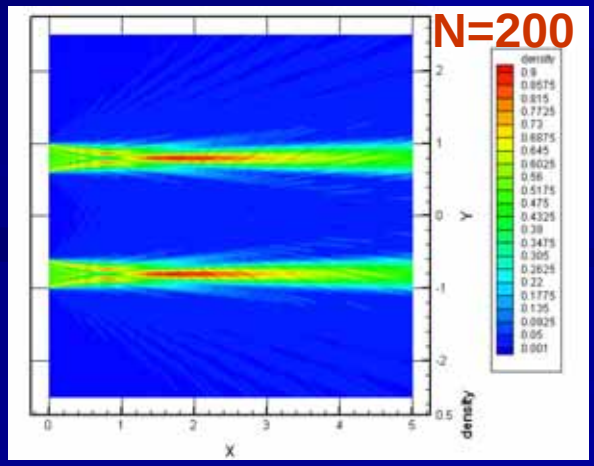

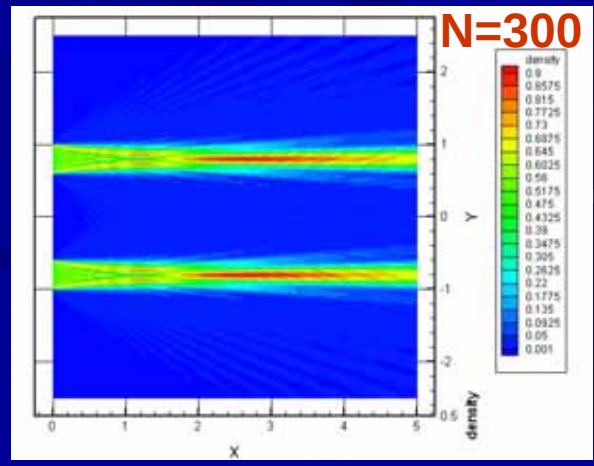

Quantum nanojet Fresnel structural complexities

-Quantum branching and clustering-

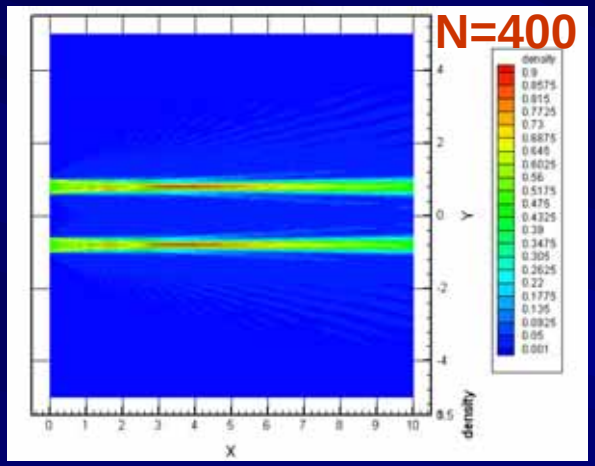

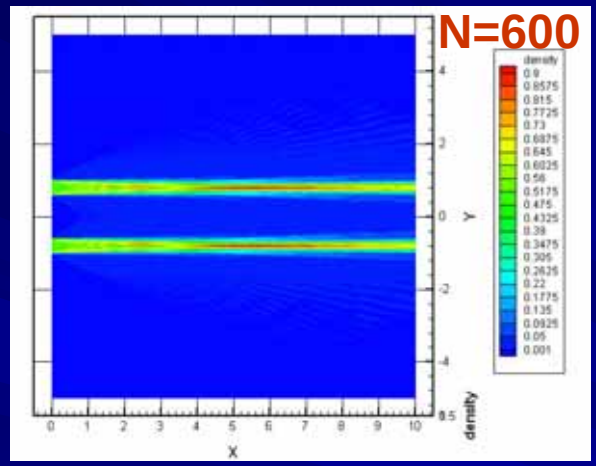

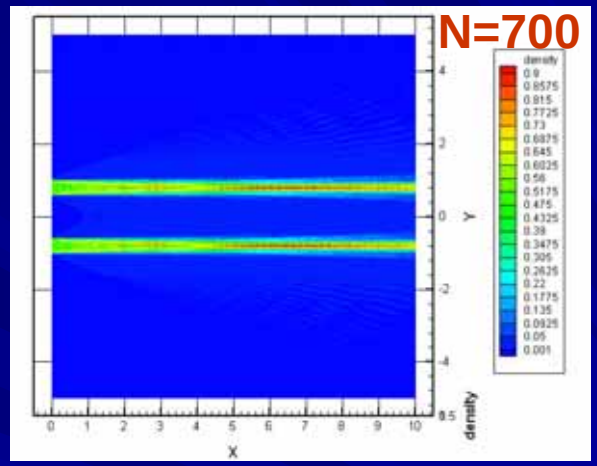

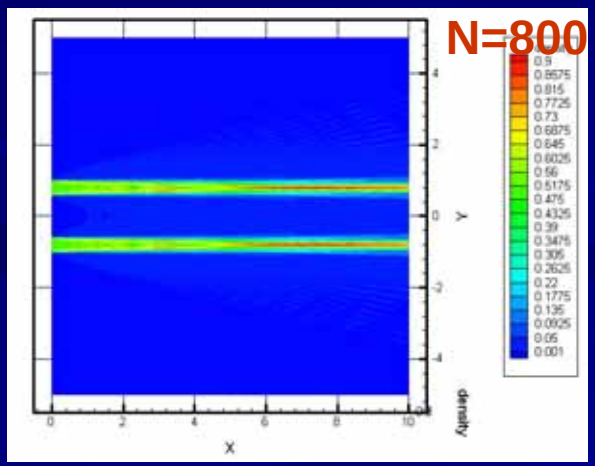

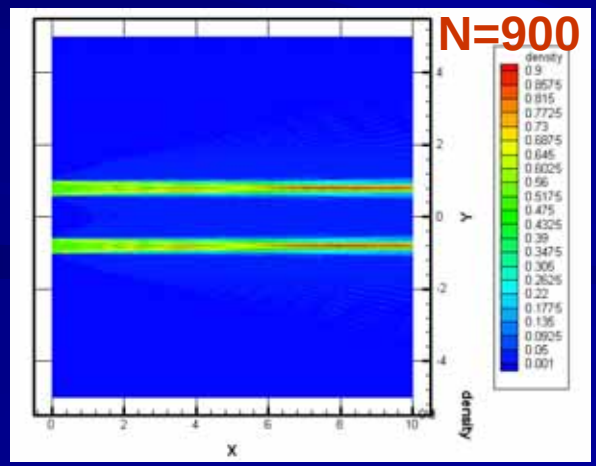

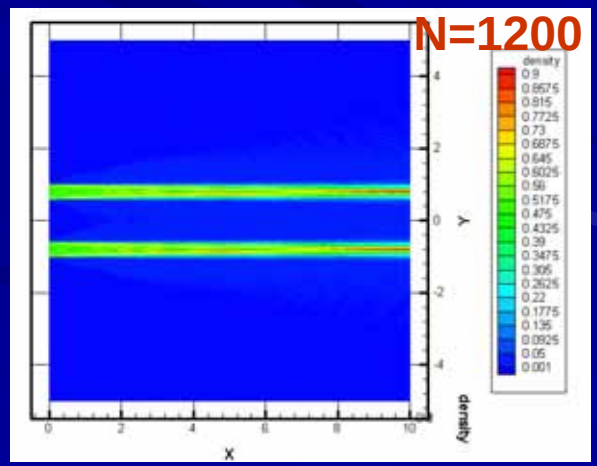

Density-Velocity Structures 1

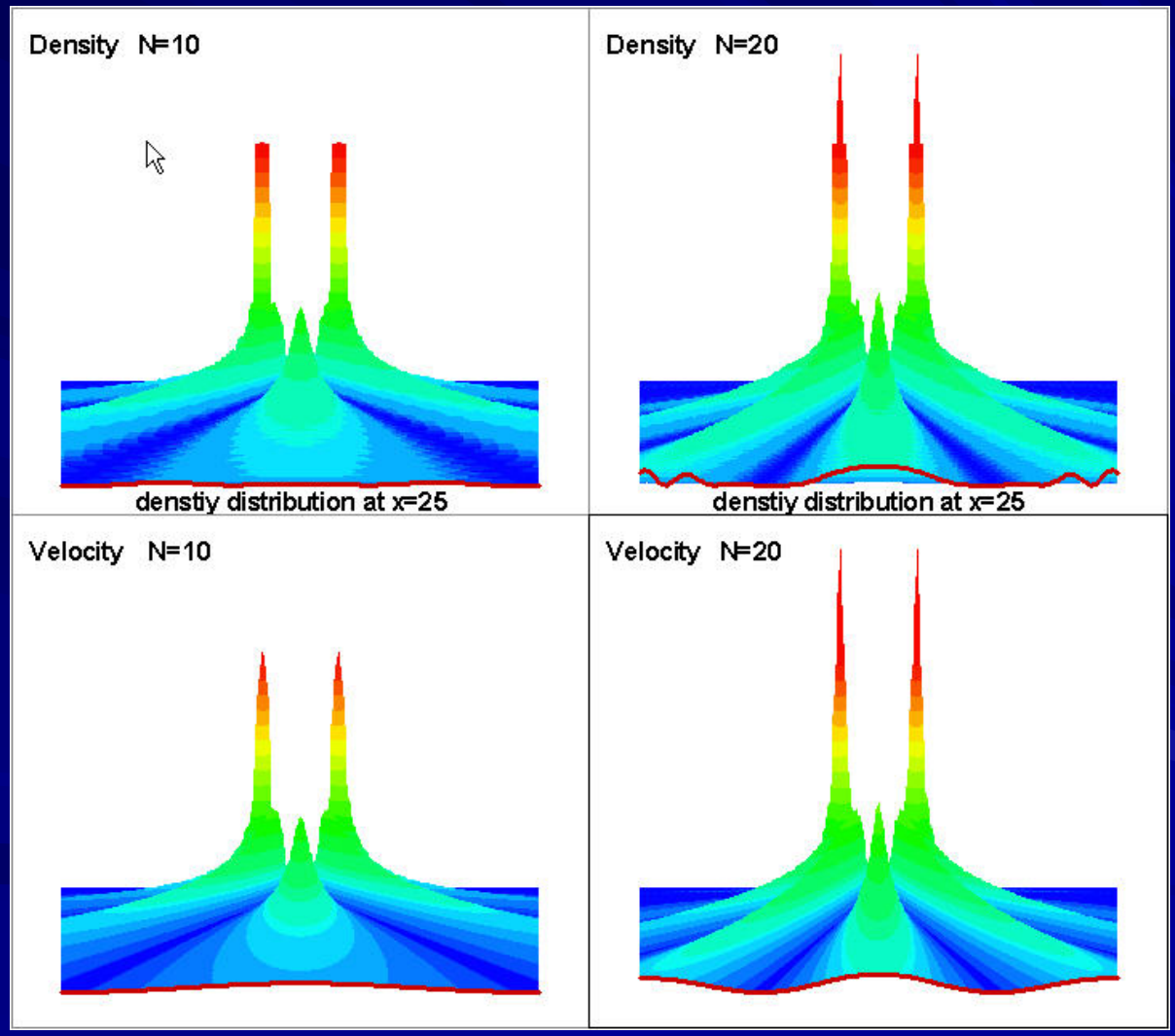

density and velocity distributions viewed from toward upstream

Density-Velocity Structures 2

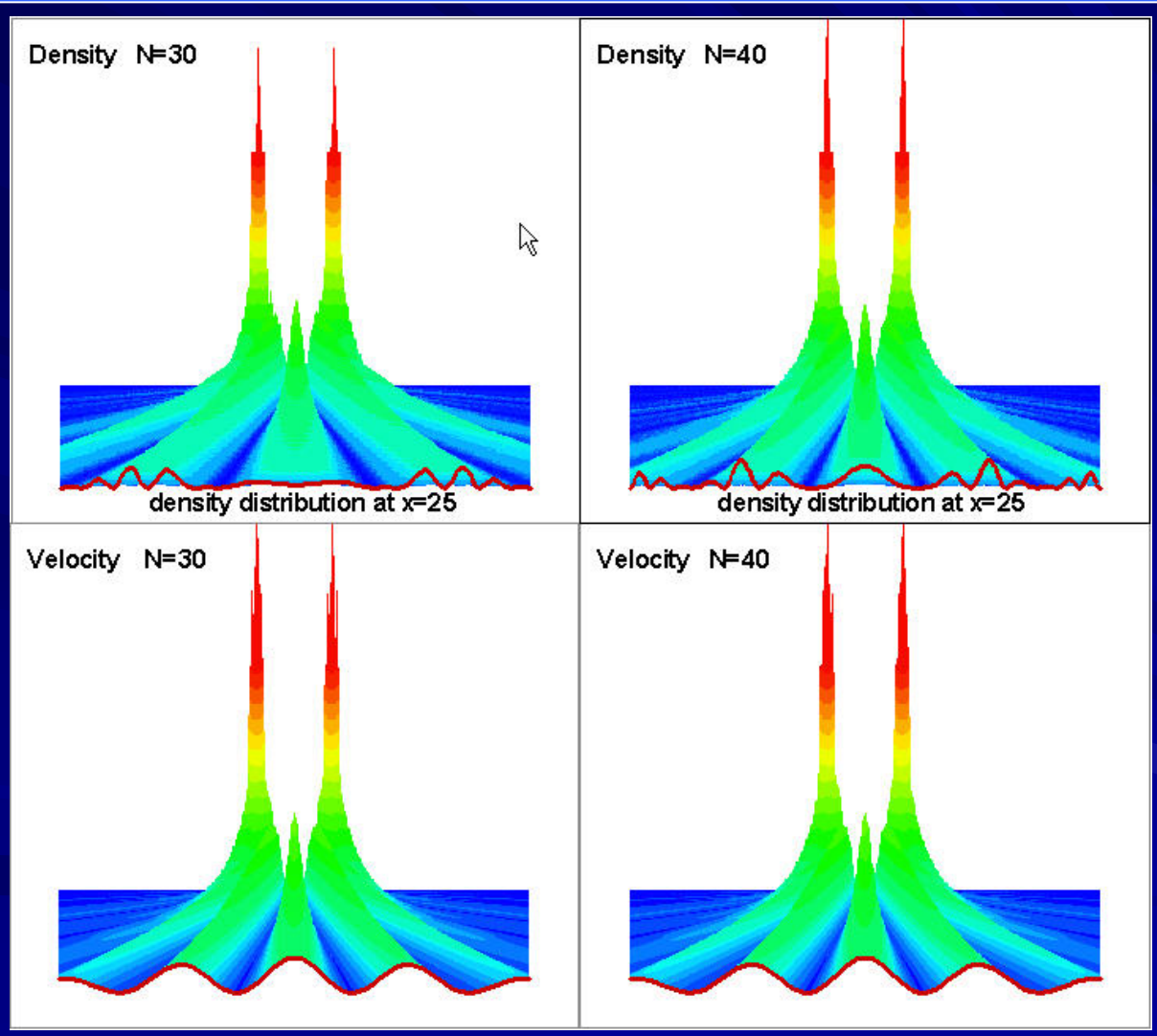

density and velocity distributions viewed from toward upstream

Axial Jet Structure 1

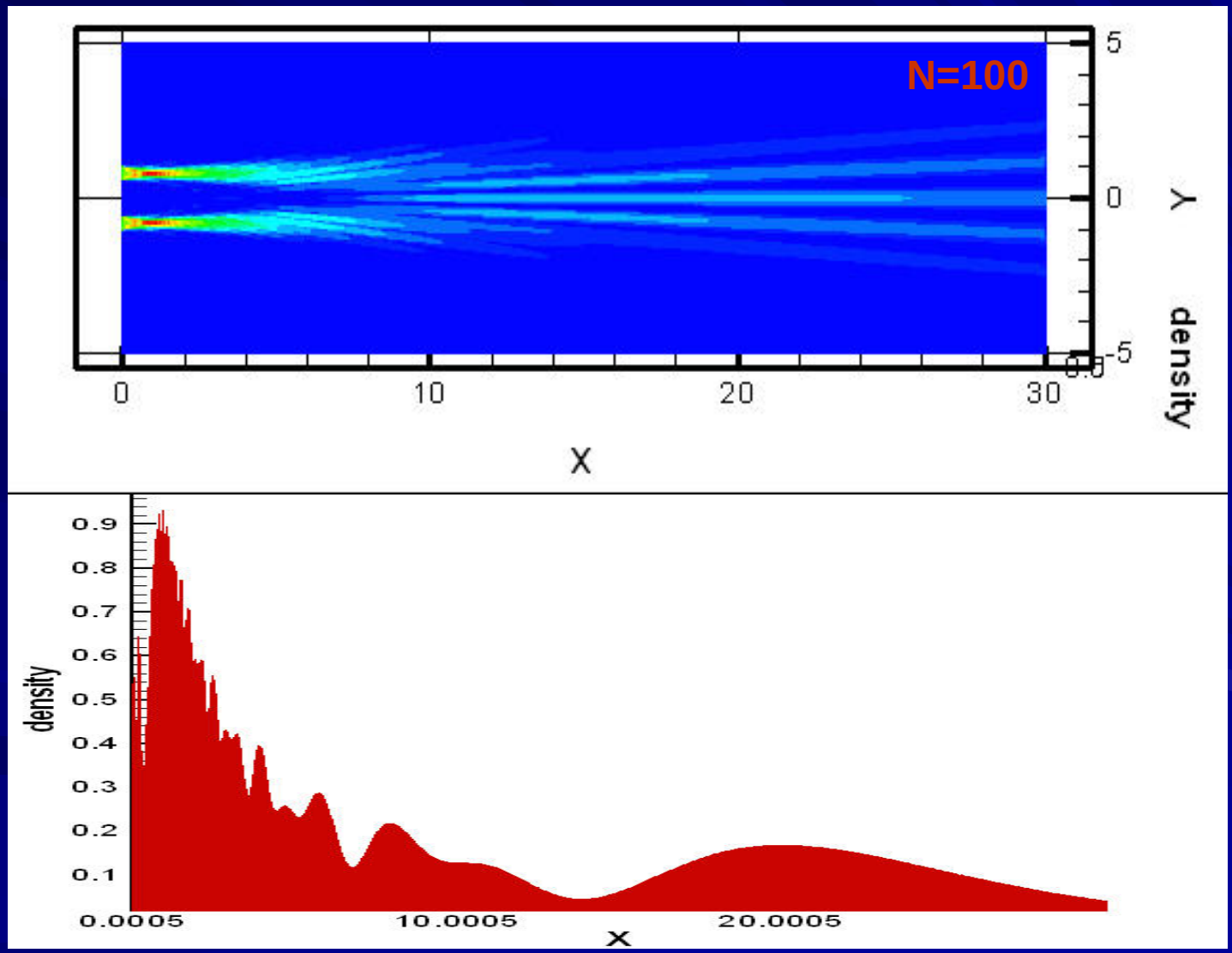

Axial Jet Structure 2

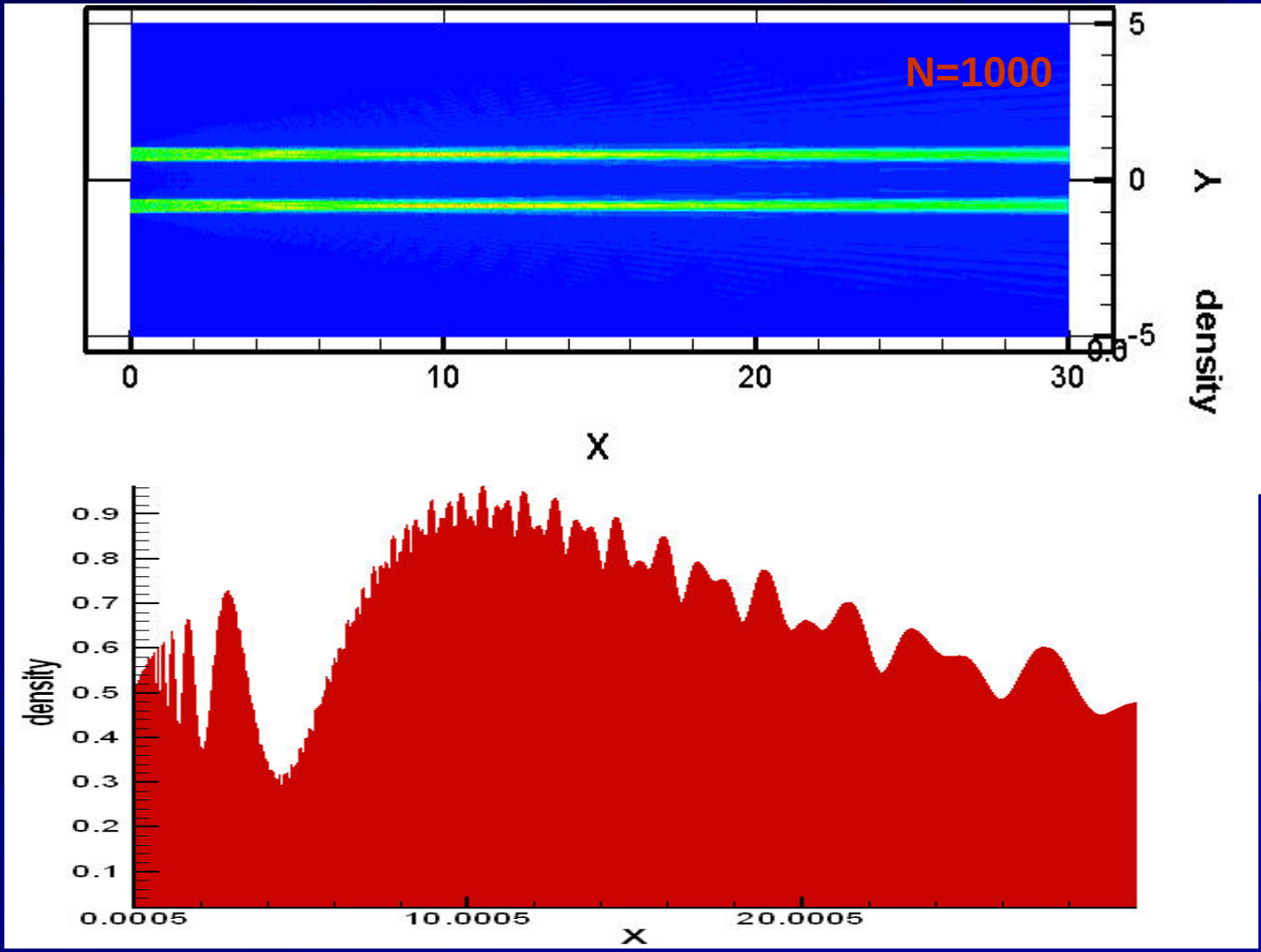

Interference fringe complexities

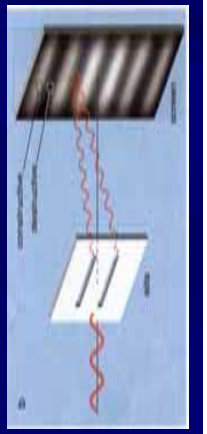

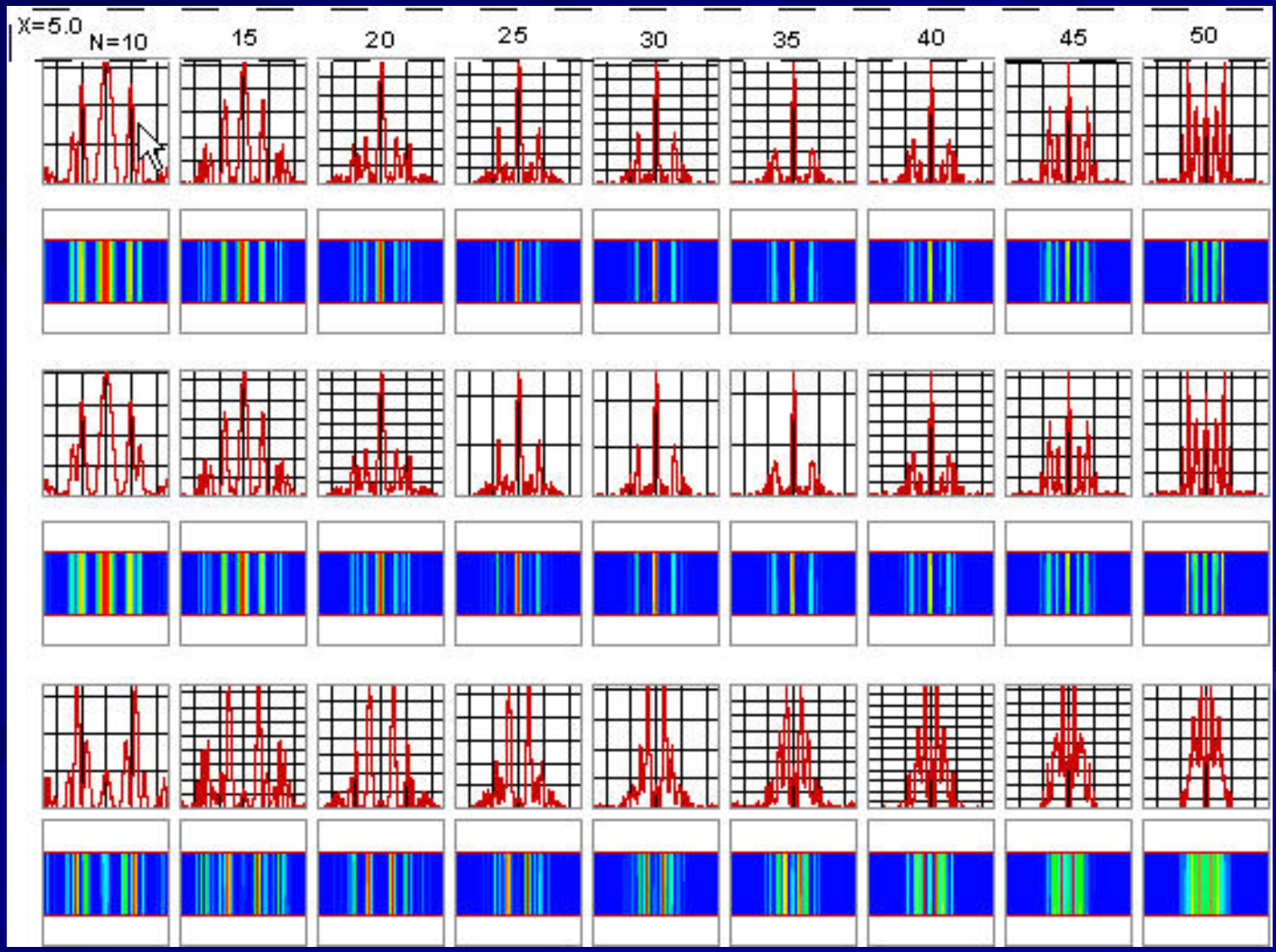

Interference fringe complexities

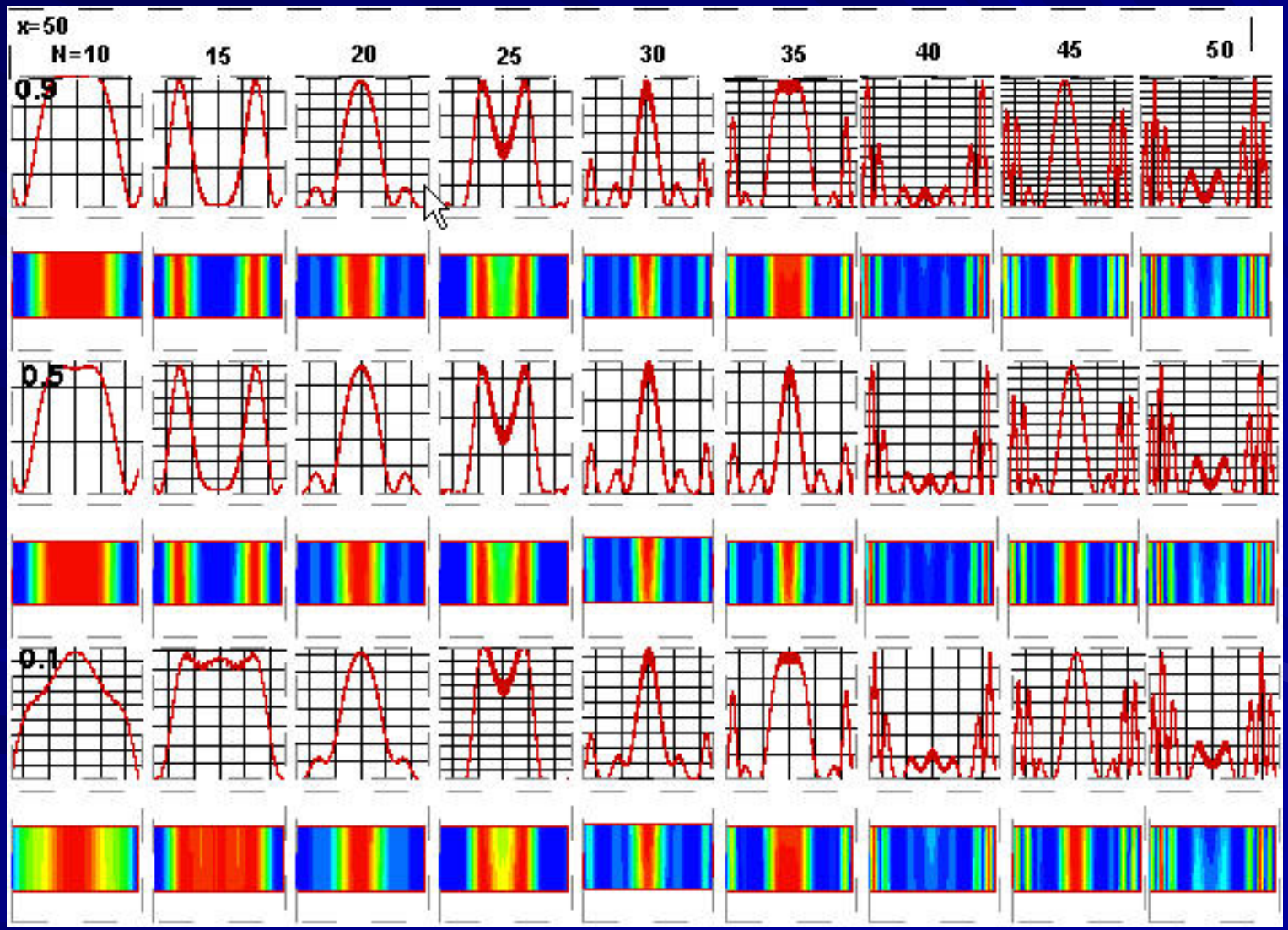

Axial Jet Structure 1

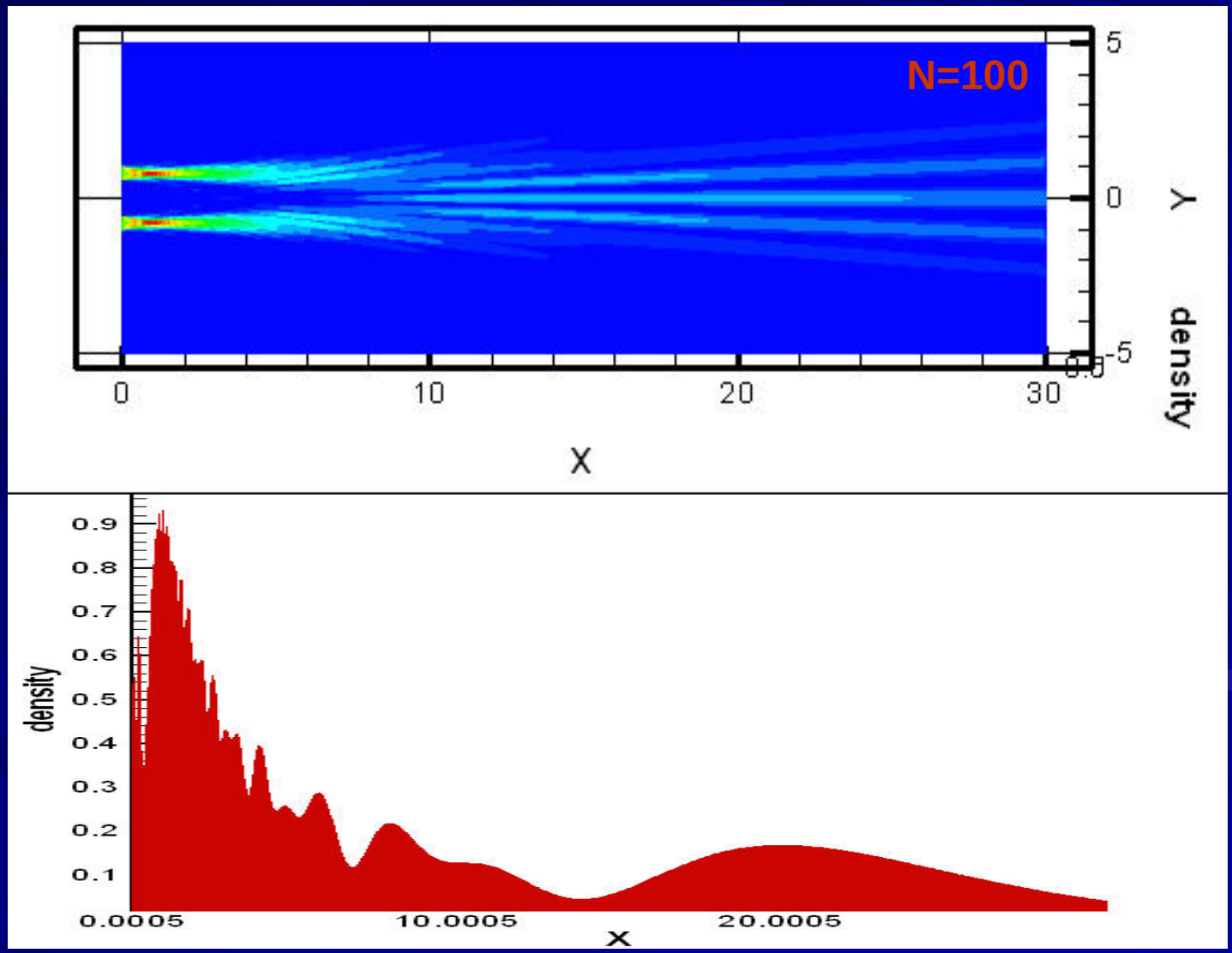

Quantum nanojet cluster core structure

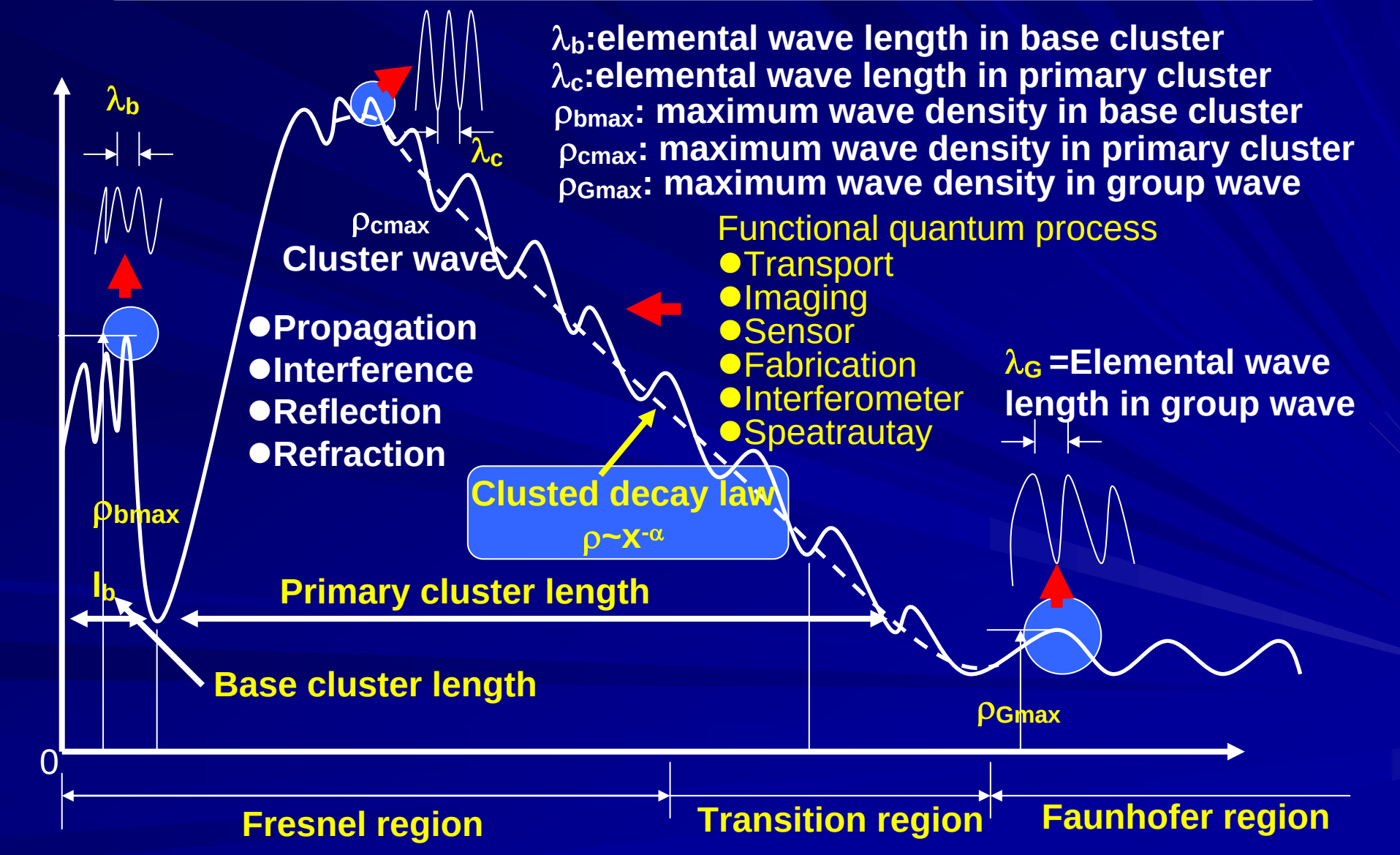

Quantum Cluster Correlations

$l_{mc}=l_{oc}+a_{mc}N^{S_{mc}}$ **location of cluster length**

$l_h=l_{oh}+a_hN^{S_h}$ **cluster length**

$l_b=l_{ob}+a_bN^{S_b}$ **base of cluster**

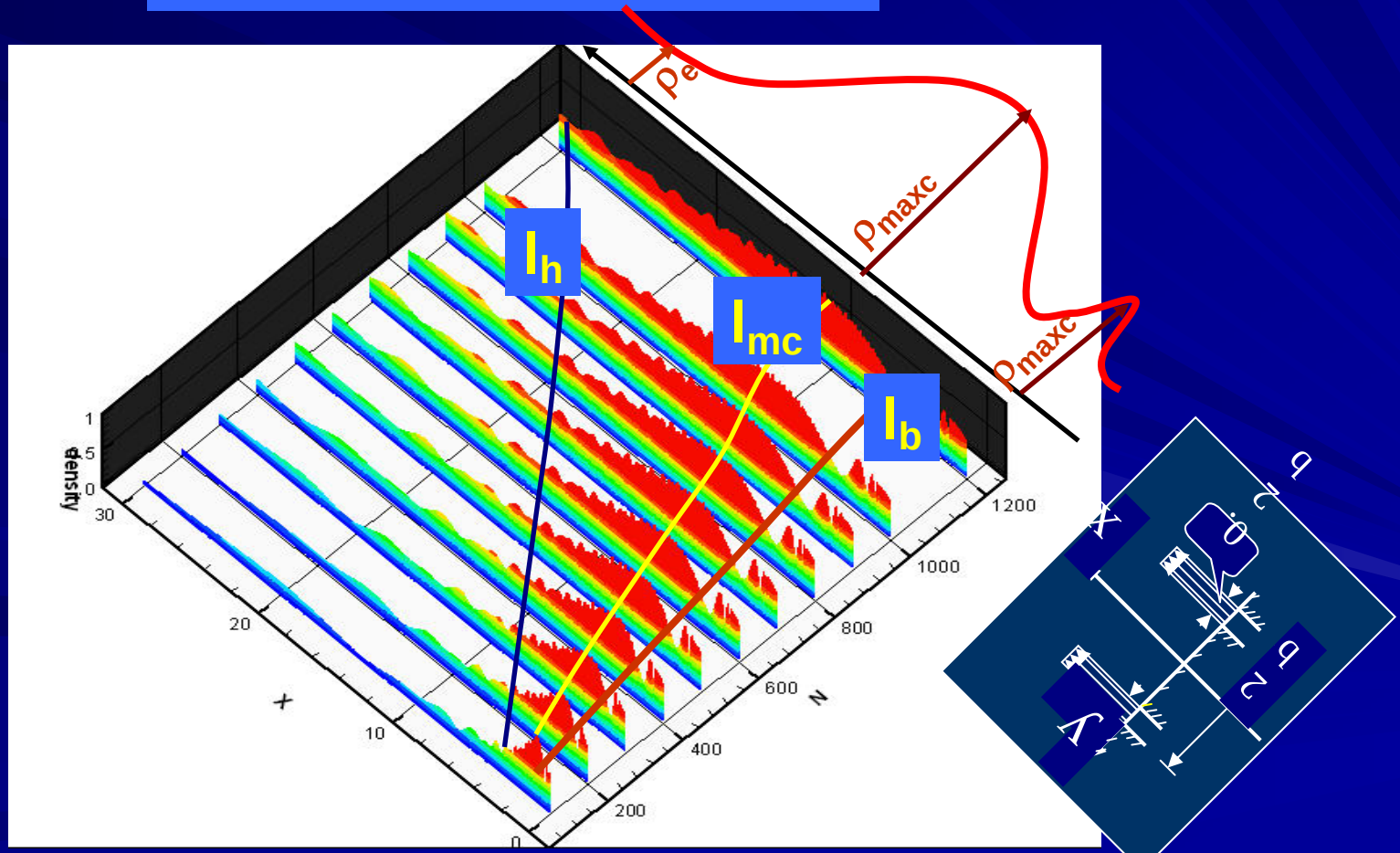

Quantum branching ,clustering and quantum-quasi-classical state transition

Double-slit electron jet

N=quantum Reynolds number

N_{cr}=critical number for state transtion

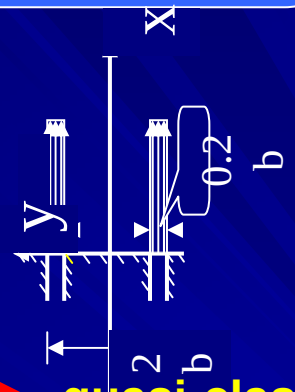

Quantum state → quantum state-qusiclassical → quasi-classical

Wave propagation, tunneling, reflection, retraction

Convection, diffusion

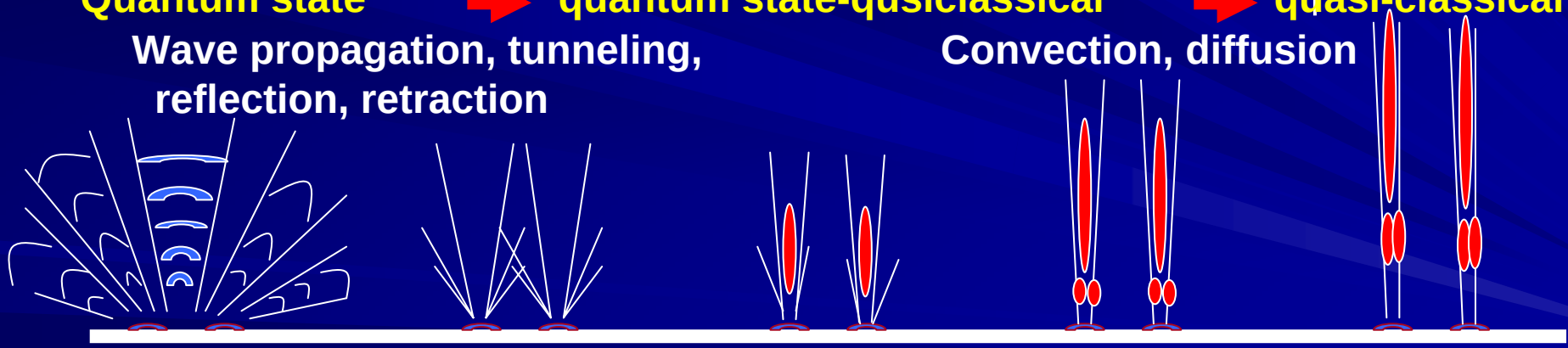

Fan-shaped multi-branch jet	Multi-subbranch jet	Two primary branches with substreams and clustering	Two primary branches and clustering	Two primary branches and clustering

Quantum-quasi-classical transition criterion

Processes characteristic time

- Quantum diffusion time: $\tau_d=R/v_d=R/\rho D$
- Convection time: L/u

Quantum diffusion was introduced by Chiu as follows

$v_d=-\rho\nabla\ln\rho$ $D=h/2m$

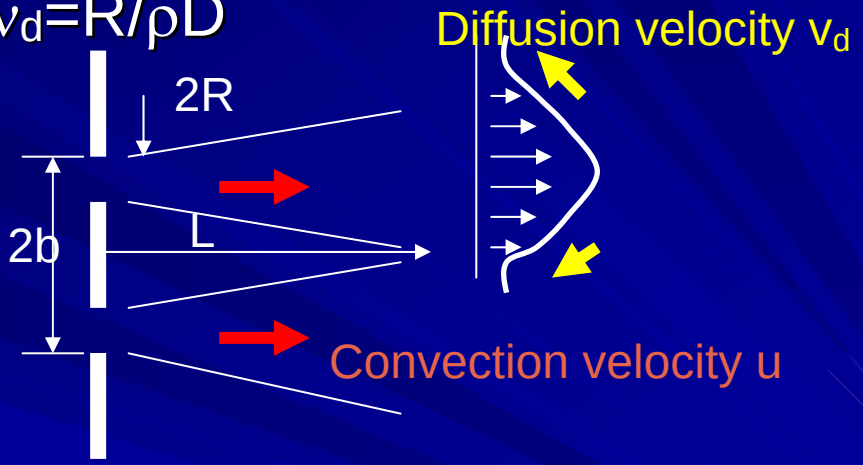

Nanojet behaviors

Quantum behavior: $\tau_d<<\tau_c$ $R/v<<L/u$, $N<<L/R$

Classical convection: $\tau_d>>\tau_c$ $R/v>>L/u$, $N>>L/R$

$$N=\frac{\sqrt{2mE}}{\hbar}\frac{b}{\pi}=\frac{u}{v_d}=\frac{u_b}{D}$$

Quantum-quasi-classical transition

Critical state: $\tau_d=\tau_c$ $R/v=L/u$, $N=N_{cr}=L/R=2b/R$

Functional quantum processes of quantum nanojets

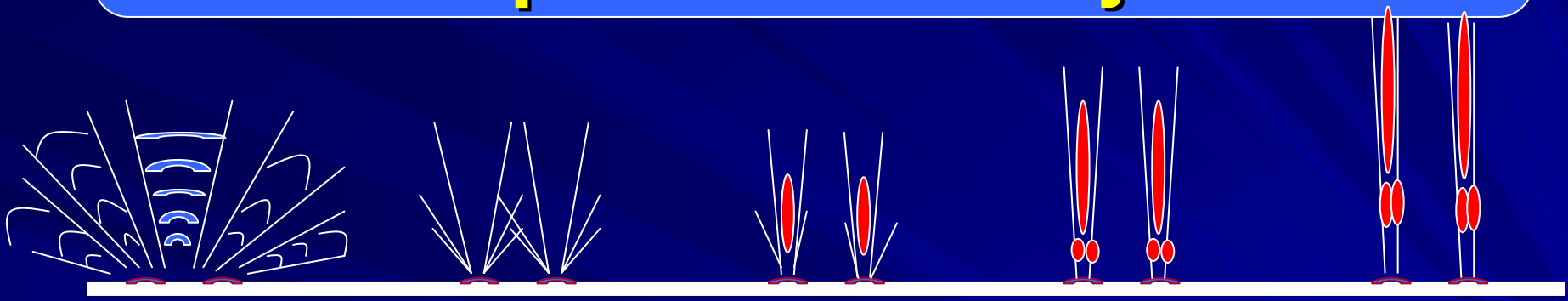

State o f nanojet

Quantum	Quantum-quasi classical	Quasi-quantum Quasi-classical	Quasi-classical	Quasi-classical
N<<Nc	N<Nc	N~Nc	N>Nc	N>>Nc

"*Functional quantum processes*" and quantum devices applications

Interferometer →	inteferometer	Electron lithography
Scanning tunnel microscope		Ion beam, Molecular beam
Nanoelectronics →		Nanoelectronics
Imaging →		Imaging
Spectrometer →		Spectrometer
	Nanofabrication	Nanofabrication

Quantum nanojet similarity law

- Two nanojets, 1 and 2, with the same slit geometry and inlet profiles, i.e., wave function and its derivative in x direction, are similar if the following condition is satisfied:

  $N_1 = N_2$

  where, N is the quantum Reynolds number, $N = mUb/hp$.

  Let b is fixed, then $N \propto mU$, thus the similarity condition is

  $U_2/U_1 = m_1/m_2$

- Example, for the same slit geometry, the structure of hydrogen atom jet, (ionized) is similar to that of electron.

  For H atom and electron we have Ue /UH = 1380

  For electron N=100=mUb/hp, m=9.1095x10^{-31}kg , b=200x10-9

  h = 1.05 x 10^{-34} , p = 3.14

  The electron velocity is Ue = 100x3.14x 1.05 x 10^{-34} /(9.1x10^{-31})x2x 10^{-7} = 1.8 x10^{4} m/sec

  The ionized hydrogen with velocity of UH = 1400m/sec will have similar jet structure.

Conclusions

Quantum nanojets **are the** ***smallest particle jets*****, which exhibit the fundamental quantum structural and dynamic complexities, and offer broad applications in quantum nanodevices.**

I. Quantum nanojets structural and dynamic complexities

Quantum behaviors:

Quantum branching**: multi-branches and two-branches (dual- slit nanojets).**

Quantum clustering**: Base cluster and primary cluster.**

Quantum-quasi-classical modes and transition

Quantum mode: $N < Ncr = S/R$

Quasi-classical jet mode $N > Ncr = S/R$

Quantum branching:

Multi-branches **are formed by the intersecting** ***right-and left running quantum waves*** **created in the** ***global jet field*****.**

Quantum clustering:

Clusters **are formed by the interacting** ***right-and-left quantum waves*** **at the axis of each** ***primary jet*****.**

Clusters **are characterized by the** ***location, cluster sizes*****,** ***density peak*** **and the** ***laws of growth*** **and** ***decay*****.**

Conclusions

II. Nanojet applications

Functional quantum process based applications

- •Cluster based applications:

  Mass spectrometer: determination of atomic weight

  (Concept is proposed, need experimental validation)

  Imaging, sensor, lithography, nanoelectronics.

  Multi-and two-branch based applications:

  Mass spectrometry: determination of molecular weights. (Concept has been proposed, need experimental validation).

  Interferometer and mass spectrometer (Concept has been proposed, experimental validation is needed.)

III.Areas of future research

Controlled nanojet, by active and passive controls, for optimum *functional quantum processes,* at steady state and/or time dependent is for broader applications.

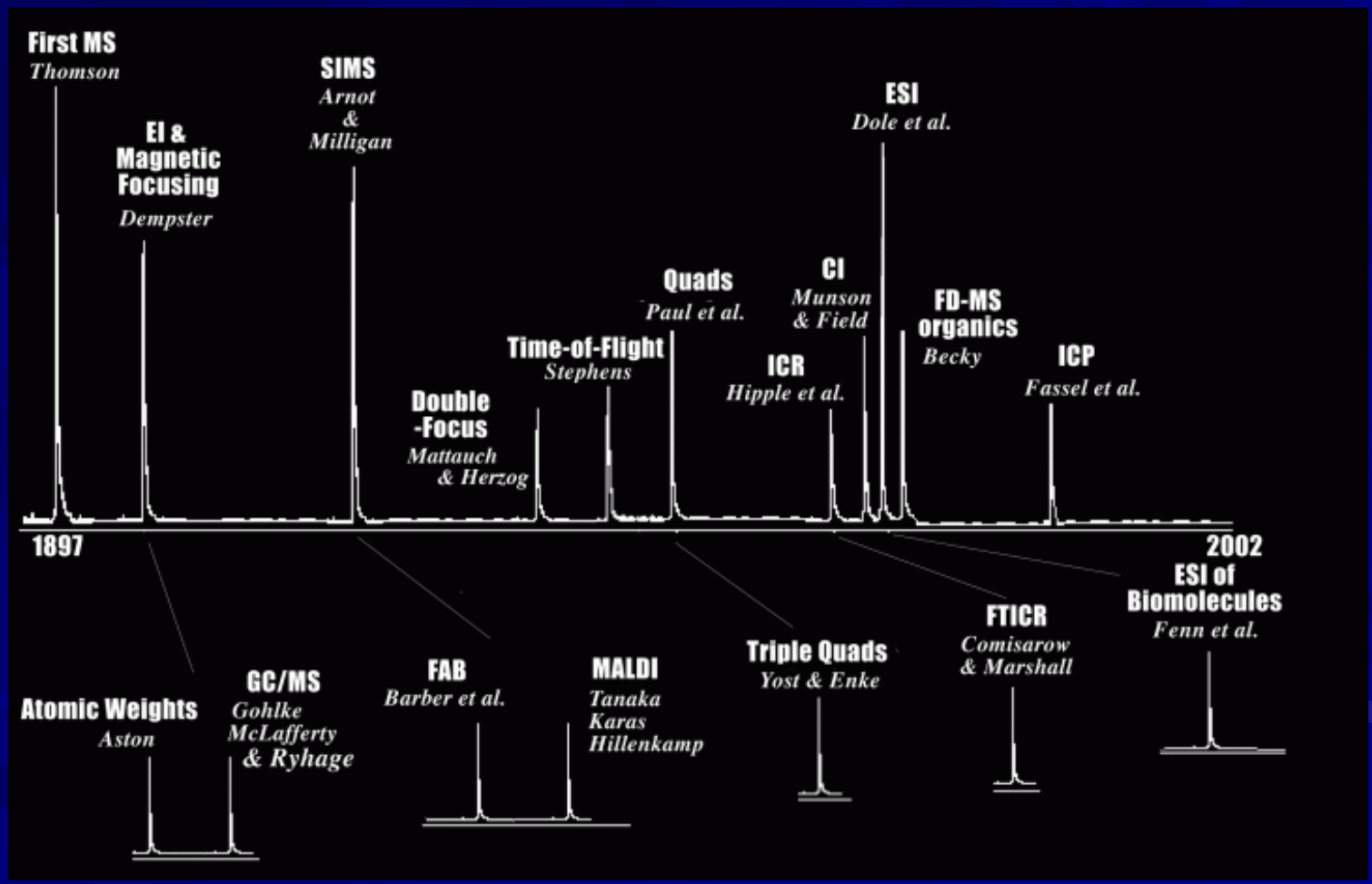
First MS
Thomson
SIMS
Arnot
&
Milligan
ESI
Dole et al.
EI &
Magnetic
Focusing
Dempster
Quads
Paul et al.
CI
Munson
& Field
FD-MS
organics
Becky
Time-of-Flight
Stephens
ICR
Hipple et al.
ICP
Fassel et al.
Double
-Focus
Mattauch
& Herzog
1897
2002
ESI of
Biomolecules
Fenn et al.
FTICR
Comisarow
& Marshall
Triple Quads
Yost & Enke
MALDI
Tanaka
Karas
Hillenkamp
FAB
Barber et al.
GC/MS
Gohlke
McLafferty
& Ryhage
Atomic Weights
Aston

Developments of quantum nanojet based new mass spectrometer/energy sensor

- New types of quantum nanojet-based diagnostic devices*:* mass spectrometer and energy sensor, each of which determines the mass of the particle, and the energy of the particle of the nanojet respectively.

Theoretical basis of quantum nanojet diagnostic devices:

A cluster parameter, C, given as function of the quantum Reynolds number N, by

$$L = G + K\,N(\gamma)$$

Mass spectrometer :

$$m = (p\hbar/2Eb)[(L - G)/K](1/\gamma)$$

Energy sensor :

$$E = (p\hbar/2mb)[(L - G)/K](1/\gamma)$$

- The concepts described above have not been experimentally validated. Further studies including the experimental studies for the validations and the test of accuracy of these devices must be carried out.

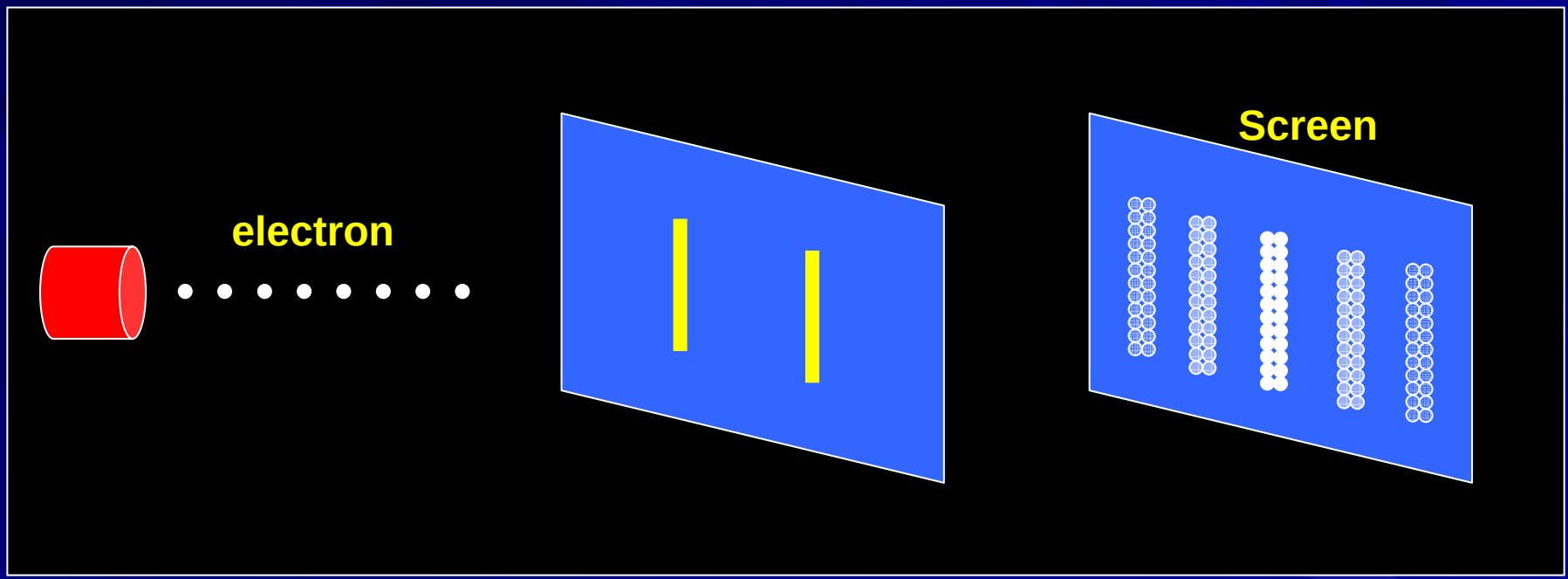
electron
Screen

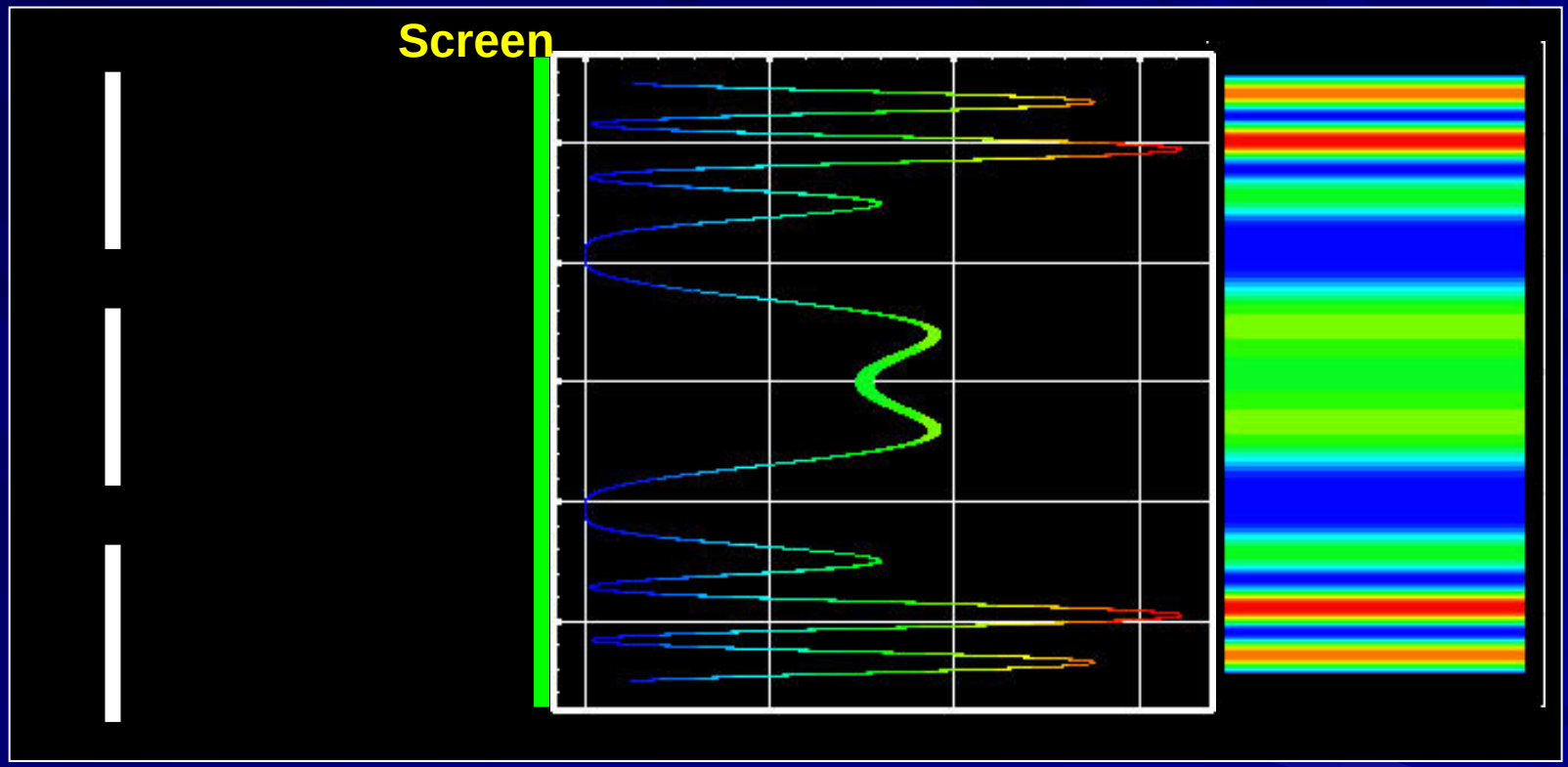
Screen

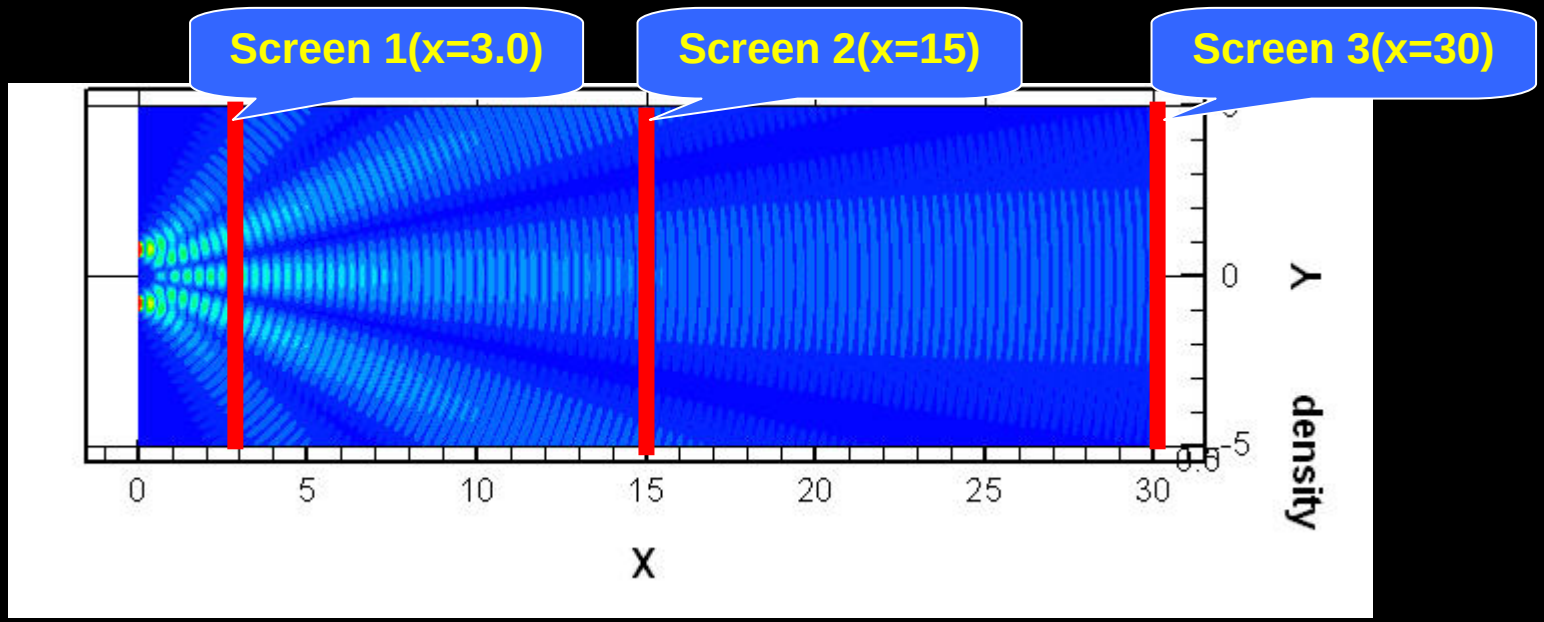
Screen 1(x=3.0)
Screen 2(x=15)
Screen 3(x=30)
0
5
10
15
20
25
30
X
0
-5
Y
density

Developments of Quantum Nanojet-Based Nanodevices

H.H. Chiu[1], C.T Lin, S.Y. Lin and T.C. Hung
Space Science and Technology &
Institute of Aeronautics and Astronautics
National Cheng Kung University
Tainan, Taiwan 701
[1]Email: hhchiu@htind1.iaa.ncku.edu.twT

F.L. Madarasz
U.S. Air Force Office of Scientific Research
and
University of Alabama in Huntsville
Huntsville, Alabama 35899

Abstract

Nano-jets of atoms, molecules or charged particles are anticipated to play new and important roles in the nanoengineering: nano- fabrication, electronics, and avionics; molecular assembling; micro- and nano-propulsion systems; atomic optics and interferometery; lithography; drug delivery systems; and quantum sensors. The objective of this paper is to understand the fundamentals driving the quantum dynamics and structural characteristics of nano-jets. The ultimate goal is to establish nano-jet design and control guidelines for specific applications. We've conducted extensive numerical simulations based on Schrödinger's equation, which simulate a double slit particle jet under various jet inlet conditions. The simulations are characterized by the quantum a Reynolds number, defined as the ratio of the inertia force to quantum force, N = mUb/h, where m is the mass of particle, U is the inlet velocity, b is the characteristic jet size, and h is the Planck constant. With the slit separation and widths fixed at of 200 nm and 20 nm, respectively, we conducted parametric studies varying the range of *N* from 10 to 1000, corresponding to the electron initial velocity of 10^6 to 10^8 m/s, to investigate the nature of the dynamic and structural variations of the jet streams. At lower Reynolds number, $0 < N < 100$, or $0 < U < 10^7$ m/s, the dual-slit jet reveals *multi-branching configurations*. For example, when N=10, Fig.1a, *quantum branching* is observed at a distance from a vertical plane passing through the jet nozzles that is comparable to the separation width of the slits. Branching is a result of the generation of higher harmonic probability density waves within the stream. The center, or forward propagating branch, is a result of the interaction of the streams effusing from each slit. Branching, as expected, has reflection symmetry through a horizontal plane dividing the two slits. As N increases the number of branches increases and their angular displacement with respect to the plane of symmetry decreases. Moreover, the center branch is generated at greater and greater distances from the jet nozzle(s). By the time the Reynolds number reaches 1000 the center branch occurs at infinity and the angular displacements of the side branches have converged on each other producing two distinct forward propagating beams of particles (See Fig. 1). A uniquely interesting phenomenon, which we call *quantum clustering*, is found over a broad range of Reynolds numbers. When N = 100 the probability density in the region of $0.5 \leq x \leq 1.7$, or 50 nm $\leq x \leq$ 170 nm, increases to the maximum value of 0.9. This is twice its value found at the plane of the jet nozzles and is an example of the quantum clustering of the probability current density. The detailed structures of these clusters vary as function of Reynolds number. Clustering is characterized by an initial axial growth in the probability density immediately after the two branches intersect on the reflection plane of symmetry. and thus constitutes the major self-interference of a jet. The first cluster, or *base cluster*, decays rapidly but is followed immediately by another rapid compression to peak density to form a *primary cluster,* which has a larger amplitude than the base cluster. The primary cluster decays exponentially due to a quantum tunneling process, which is a diffusion transport process associated with the low linear momentum of the beam particles in the forward direction. The region dominated by group wave propagation with long group wavelength as shown in Fig. 1, follows the primary cluster. The wavelength of the wavelet in the base and primary cluster and the group wave propagation region are approximately equal. The structural variation of a single-slit nanojet with respect to the quantum Reynolds number is also presented in Fig.2. Numerical simulations for the low, and intermediate energy ranges reveal profoundly complex structural variations of the interference fringe, quantum potential, and velocity distributions as shown in Fig. 3. Finally, we conclude that nanojets in a broad range of Reynolds number lend themselves to various nanodevices applications, depicted in Fig.4. Here N* is the critical Reynolds number at which the system transitions from a quantum to a classical regime.

Acknowledgements

The authors wish to extend their appreciation for the supports awarded by US Air Force Office of Scientific Research under the contract AOARD-03-4039.

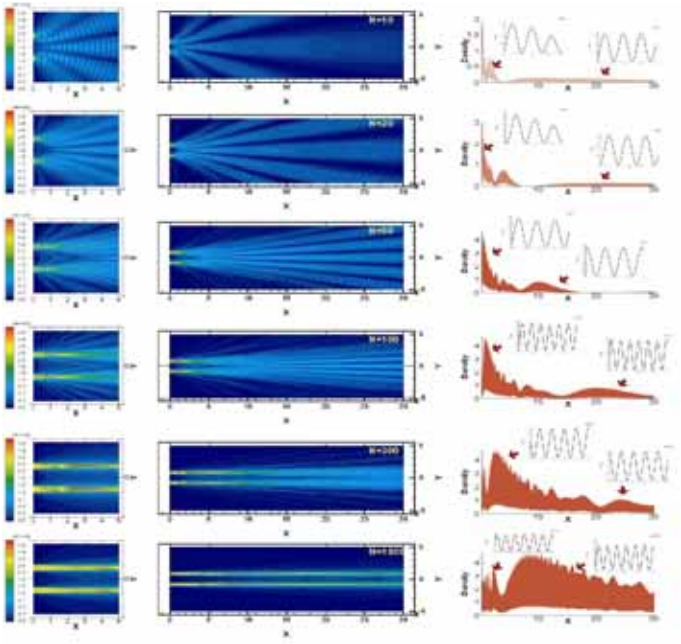

Fig1. Dual-slit nanojet structure

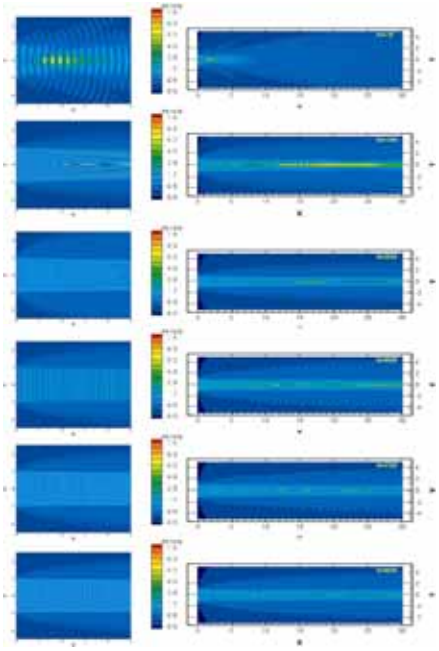

Fig2. Single-slit nanojet structure

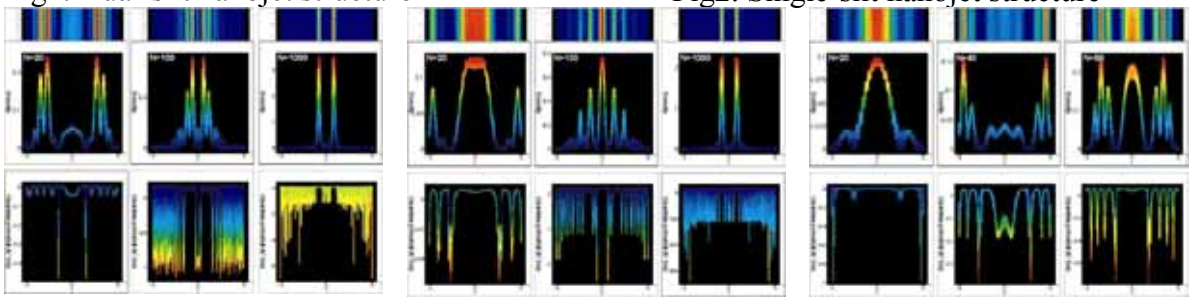

Fig 3. Interference fringes, quantum potentials and velocity distributions at various N

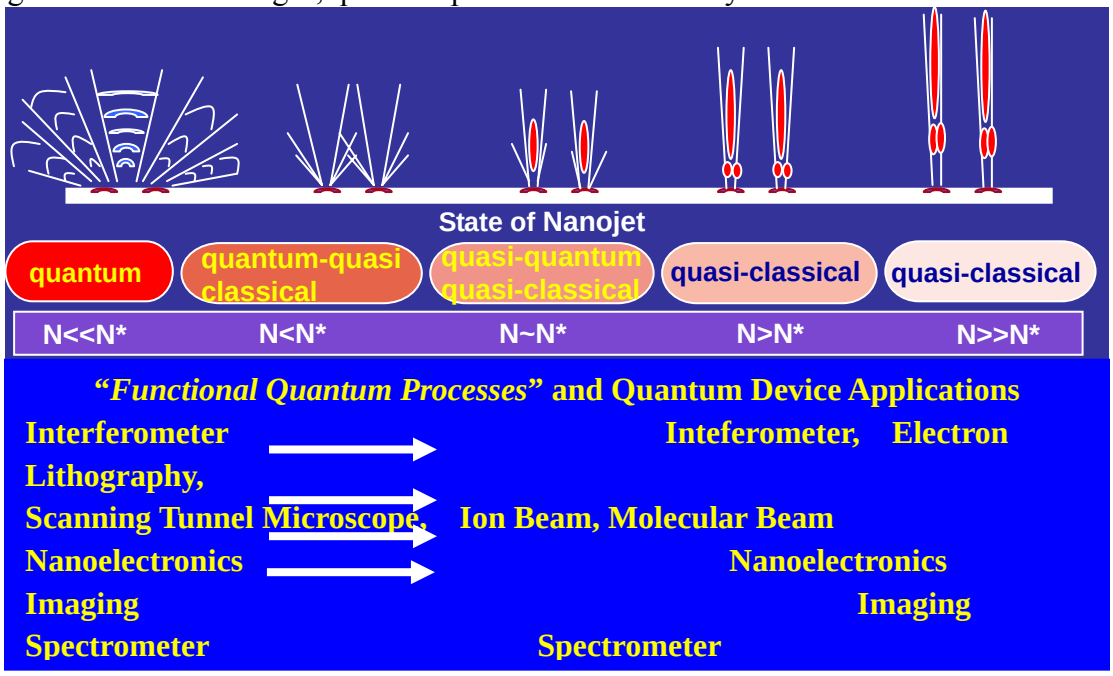

Fig 4. Application of nanojets in nanodevices